APPLICATIONS OF X-RAY CRYSTALLOGRAPHY: STUDIES INTO THE STRUCTURAL PERTURBATIONS OF *PERI*-SUBSTITUTED NAPHTHALENE DERIVATIVES

Amy L. Fuller

A Thesis Submitted for the Degree of PhD
at the
University of St. Andrews

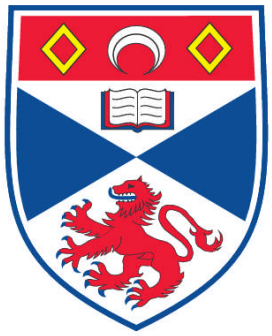

2009

APPLICATIONS OF X-RAY CRYSTALLOGRAPHY: STUDIES INTO THE STRUCTURAL PERTURBATIONS OF *PERI*-SUBSTITUTED NAPHTHALENE DERIVATIVES

by

Amy L. Fuller

A thesis submitted in partial fulfillment for the award of

DOCTOR OF PHILOSOPHY

School of Chemistry
University of St Andrews
North Haugh
St Andrews
Fife
KY16 9ST

14 September, 2009

DECLARATION

I, Amy L. Fuller, hereby certify that this thesis, which is approximately 33,001 words in length, has been written by me, that it is the record of work carried out by me and that it has not been submitted in any previous application for a higher degree.

I was admitted as a research student in September 2006 and as a candidate for the degree of PhD in July 2007; the higher study for which this is a record was carried out in the University of St Andrews between 2006 and 2009.
Date _____Signature of Candidate _____

I hereby certify that the candidate has fulfilled the conditions of the Resolution and Regulations appropriate for the degree of PhD in the University of St Andrews and that the candidate is qualified to submit this thesis in application for that degree.
Date _____Signature of Supervisor _____

In submitting this thesis to the University of St Andrews we understand that we are giving permission for it to be made available for use in accordance with the regulations of the University Library for the time being in force, subject to any copyright vested in the work not being affected thereby. We also understand that the title and the abstract will be published, and that a copy of the work may be made and supplied to any bona fide library or research worker, that my thesis will be electronically accessible for personal or research use unless exempt by award of an embargo as requested below, and that the library has the right to migrate my thesis into new electronic forms as required to ensure continued access to the thesis. We have obtained any third-party copyright permissions that may be required in order to allow such access and migration, or have requested the appropriate embargo below.

The following is an agreed request by candidate and supervisor regarding the electronic publication of this thesis:

Access to Printed copy and electronic publication of thesis through the University of St Andrews.

Date _____Signature of Candidate _____

Signature of Supervisor _____

ABSTRACT

The majority of research in this thesis uses X-ray crystallography to investigate the structural features of *peri*-substituted naphthalene compounds. X-ray crystallography is introduced in chapter one, followed by a discussion on modes of distortion *peri*-substituted naphthalene derivatives can undergo, in chapter two.

In chapter three, compounds having non-bonded -SPh and -EPh (E = S, Se, or Te) *peri*-substituents are compared. These similar compounds react differently when oxidized with bromine. The oxidation products are used to discuss a recently proposed mechanism and a more specific mechanism is suggested.

In chapter four, a one-pot synthesis for naphtho[1,8-*c,d*]-1,2-diselenole (Se_2naph) is reported. Substituents were added to Se_2naph to form two new naphthalene compounds. The substituents are found to distort the Se-Se bond and influence packing.

In chapter five, several diselenium-containing compounds are used as ligands in platinum(II)-bisdiphosphine complexes. The preference for platinum(II) to stay square planar dictates the geometry around the metal center, not the rigidity of the naphthalene backbone.

Chapter six introduces (8-phenylsulfanylnaphth-1-yl)diphenylphosphine, a *peri*-substituted naphthalene containing -SPh and -PPh_2 substituents, and several derivatives. This ligand is used in a variety of complexes containing platinum(II), ruthenium(II), and copper(I) metal halides, whose coordination geometries are discussed in chapter 7. The naphthalene-based ligands in Cu(I) and Ru(II) seem to determine the geometry around the metal, whereas the metal center *d*-orbitals dominate in the Pt(II) examples.

Chapters eight and nine deviate from the naphthalene theme. In chapter eight, X-ray analysis of sulfoxide compounds is used to discuss the structural environment around the sulfur. Various intra- and inter-molecular interactions were discovered in crystal packing.

Finally, chapter 9 uses STANDARD (St ANDrews Automated Robotic Diffractometer) to statistically analyze numerous E_2Ph_2 (E = S, Se, or Te) crystals to determine chirality. It is intriguing that Te_2Ph_2 shows a preference for one enantiomer over the other.

ACKNOWLEDGMENTS

My three years in St. Andrews has been full of adventures and new challenges. Certainly the biggest challenge has been to undertake the chemistry research detailed in this report.

I would most like to thank my supervising Professors, Alex Slawin, and J. Derek Woollins, who has served as a co-supervisor to me during my time here. Without Alex's patience and explanations and Derek's problem solving and advice, I wouldn't have come as far as I have. Thank you to both of them.

A big thank you goes to my co-postgrad Fergus Knight, who has been key in the development of my skills as a crystallographer. Without him and his continually growing supply of crystals, this thesis would be seriously lacking (Compounds **3.1**-**3.6**, **4.2**, **6.1**-**6.11**, **6.13**, **6.14**, and **7.1**-**7.8**).

Other members of the Woollins/Slawin/Killian research groups have been instrumental in my research. They have endlessly given me crystals to experiment on to help me grow as a crystallographer. I would like to thank Dr. Sahrah Parveen (**6.12**), Vit Matuska, Paul Waddell, Upulani Somisara, Dr. Petr Kilian, Dr. Piotr Wawrzyniak, Conor Fleming, Brian Morton, Ken Armstrong, Brian Surgenor, Fiona Rudolf, Dr. Dipak Dutta, and especially Dr Hua for all of his encouragement and support. They all have helped me grow as a person.

I can't go without mentioning my flatmate Lindesay Scott-Hayward for helping me with the statistics and Prof. Michael Bühl for the calculations in chapter 9, the AU staff for giving me a second home, and the girls' on my basketball team, volleyball team, and sand volleyball club for keeping me busy and in shape. Thank you all!

I also need to thank Dr. Tim Humphry. He has done more than anyone to help me with this degree. He has proofread page after page, encouraged me when things got rough, and listened when things were going well.

Finally, I would like to acknowledge the support of my family and friends. My family has been my rock of encouragement and love. Thank you for all you have done. Also, if there is anyone else I've forgotten, Thank you!

CONTENTS

LIST OF FIGURES

LIST OF TABLES

LIST OF SCHEMES

ABBREVIATIONS

Ph	Phenyl
S_2naph	Naphtho[1,8-*c,d*]-1,2-dithiole
Se_2naph	Naphtho[1,8-*c,d*]-1,2-diselenole
TMEDA	Tetramethylethylenediamine
dibenzSe_2	Dibenzo[*ce*]-1,2-diselenide
n-Bu	*n*-Butyl
mt-Se_2naph	2-mono-*tert*-butylnaptho[1,8-*c*,*d*][1,2]diselenole
Et	Ethyl
Me	Methyl
E.N.	Electronegativity
CSD	Cambridge Structural Database
p-Cy	*para*-cymene
etdmp	$Me_2PCH_2CH_2SEt$
dppte	1,2-bis-S-[20-(diphenylphosphino)benzoyl]dithioethane
$SOPh_2$	diphenyl sulfoxide
E_2Ph_2	diphenyl dichalcogenide

CHAPTER 1
AN INTRODUCTION TO CRYSTALLOGRAPHY

1.1. Introduction

Crystallography is the science concerned with the structure of and properties of the crystalline state. A crystallographer is a scientist in this discipline who uses X-ray or neutron diffraction to build pictorial representations (or models) of a crystalline solid. Each individual crystal in a crystalline solid is composed of a single arrangement of atoms that repeats, like building blocks, throughout three-dimensional space, where the smallest repeating pattern is called the unit cell (this is also referred to as the asymmetric unit). The symmetry of the repeating pattern in the crystal is in turn described by the space group of the crystal. A space group is a way of describing the arrangement of the repeating patterns in a crystal using a standardized system of notation. Because X-ray structure determination is so useful, it is almost always a principal goal of an experimental chemist to obtain a crystal structure (i.e. a structural representation) of every compound.

The science of determining crystal structure models (crystallography) has grown significantly over the past 100 years. Since the solving of the first crystal structure ($CuSO_4$), crystallography has been used to study the structural features of simple inorganic compound to enhance an understanding of basic inorganic principles. This introduction will focus on the science of crystallography.

1.2. Background

X-ray beams have a wavelength (with those generated using molybdenum at 0.71073 Å and copper at 1.54184 Å), which is an appropriate length to be diffracted by (i.e. bounce off) the electron cloud(s) in the crystal and produce useful information about the atomic arrangement.[1] As X-ray beams enter a crystal, they come in contact with all the various electron clouds in the crystal and get redirected, based on *Bragg's Law* (see section 1.1.2), to form a diffraction pattern of spots recorded as images (Figure 1-1[2]).[1]

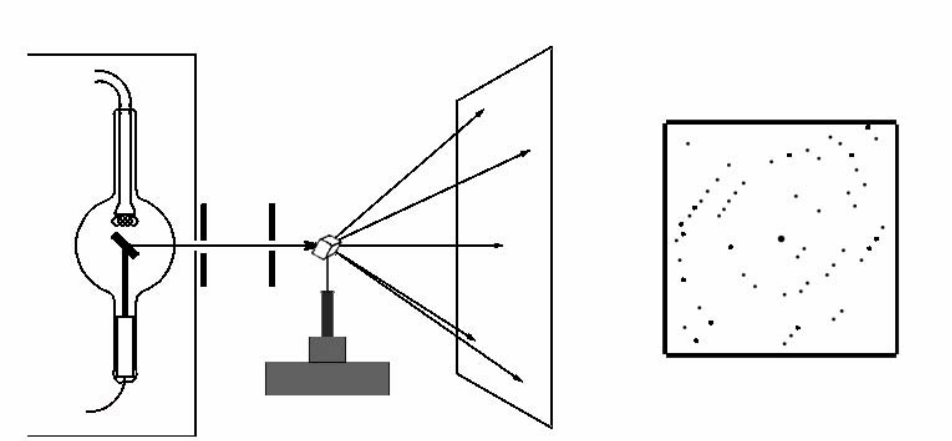

Figure 1-1. Schematic of an X-ray beam entering a crystal. The diffracted X-rays produce a diffraction pattern.[2]

The position and intensity of each reflection (spot) in a diffraction pattern, relative to the angle at which it entered the crystal, is used to reveal structural information about the atomic arrangement, such as atom positions, bond lengths and angles, torsion angles, non-bonded distances, and other important molecular features.

In order to know everything there is to know about the positions of the atoms in a crystal, a crystallographer needs to know three things: the unit cell parameters, the space group, and the coordinates of the atoms in the asymmetric unit. Knowing this information gives the crystallographer an opportunity to create a pictorial representation of the crystal. Such a representation is vital to experimental chemists who have synthesized an unknown compound or who want an accurate, detailed geometry to help them understand observed chemical or physical properties.

1.2.1. A Crystal

A crystal is compromised of a pattern, e.g. molecules, that repeat through out three dimensional space. Using two dimensions, Donald Sands describes a good way to visualize this concept, which is shown in Figure 1-2.[3] In this visualization, a ladybug stands in the interior of a crystal, at a point, called x. She looks around at the atoms that surround her and then starts crawling through the crystal. After walking in a straight line, she will eventually arrive at another point that is completely analogous to x. When the ladybug looks around the new location; it is completely indistinguishable from the starting point. She continues on to the next point, but finds the same thing. Of course, at the surface of a real crystal, this won't hold true, since the ladybug would walk out of the crystal, but the analogy works for the interior.

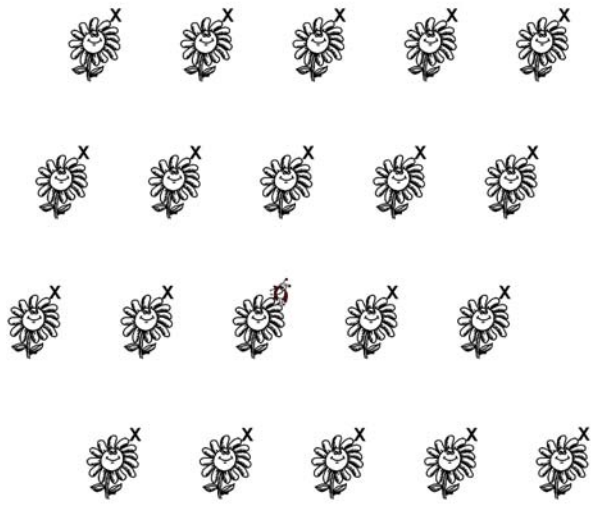

Figure 1-2. Depiction of a Ladybug walking through a crystal to indistinguishable points, x.

Continuing with the two-dimensional analogy, four identical points can be connected to make a unit cell, which is simply a "box" that contains one complete unit of the crystal. Every individual crystal is made up of the unit cells stacked in every direction. Figure 1-3 shows examples of three possible two dimensional unit

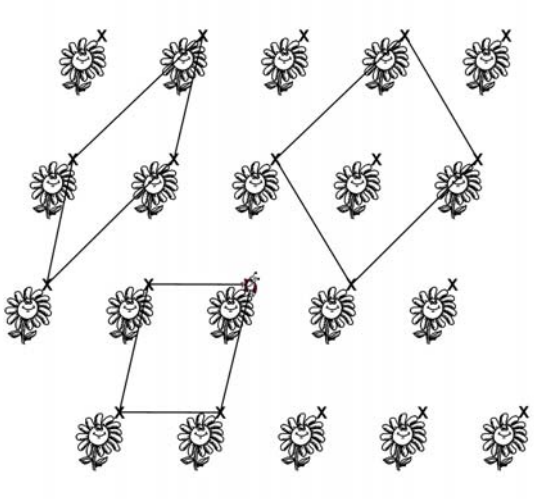

Figure 1-3. Three possible two dimensional unit cells.

cells. Even though any of the identical points can be chosen, a unit cell is generally chosen to include the highest degree of symmetry that can be found in the cell. For example, it is easier to calculate bond distances if the angles around the corner point are 90° or if the axes of the unit cell have equal lengths.[3]

There are seven basic unit cell geometries, shown in Table 1-1. These are called crystal systems. The most commonly seen crystal systems are triclinic, monoclinic, and orthorhombic, which are shown in Figure 1-4.[2]

The symmetry of the individual molecules within the unit cell is described by one of the 230 unique space groups. There are two types of symmetry that can exist in a crystal: symmetry of a point and symmetry of space (related to two

Table 1-1. The Seven Crystal Systems

Crystal System	Lattice Centring	Axial Lengths	Axial Angles
Triclinic	P	$a \neq b \neq c$	$\alpha, \beta, \gamma \neq 90°$
Monoclinic	P C	$a \neq b \neq c$	$\beta \neq 90°$ and $\alpha, \gamma = 90°$
Orthorhombic	P I C F	$a \neq b \neq c$	$\alpha, \beta, \gamma = 90°$
Hexagonal	P	$a = b \neq c$	$\alpha = \beta = 90°$ and $\gamma = 120°$
Trigonal	P R	$a = b = c$	$\alpha = \beta = \gamma \neq 90°$
Tetragonal	P I	$a = b \neq c$	$\alpha, \beta, \gamma = 90°$
Cubic	P I F	$a = b = c$	$\alpha, \beta, \gamma = 90°$

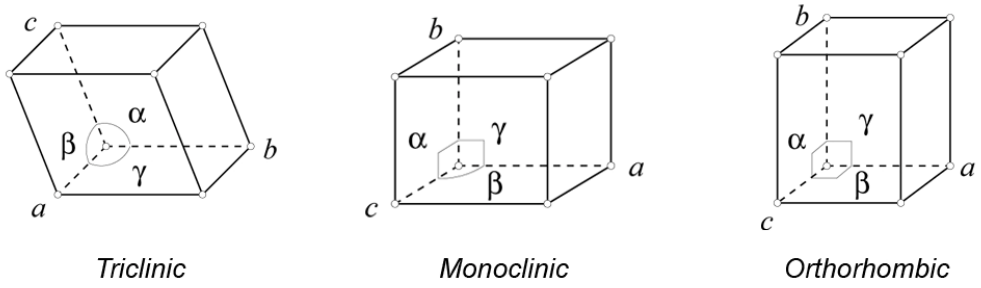

Figure 1-4. Examples of the most common unit cell geometries.

points).[1] Point symmetry includes operations such as inversion centres (-1), two-fold axes (2), or mirror planes (*m*). Space symmetry includes unit cell lattice centring (*P*, primitive; *C*, side-centered; *I*, body-centered; or *F*, face-centered), screw axes (2_1), and glide planes (*a*, *b*, *c*, or *n*). Every crystal structure is assigned a space group based on the symmetry within the crystal, which can have any combination of these symmetry operations. The symbol used to designate the space group describes the symmetry in the unit cell. For example, a monoclinic crystal with a space group of $P2_1/c$, has a **P**rimitive unit cell with a screw axis ($\mathbf{2_1}$) along the principle axis (axis b in Figure 1-4) with a ***c***-glide perpendicular to the principle axis. Another example, an orthorhombic crystal with the with the space group P*nma*, has a **P**rimitive unit cell with an ***n***-glide perpendicular to a, an ***m***-plane perpendicular to b, and an ***a***-glide perpendicular to c.

The three-dimensional images (the spot locations and their intensities) collected in the course of an X-ray diffraction experiment contain a geometric pattern of peaks that derive directly from the lattice and the unit cell geometry of the crystal system. The position of the peaks (or their absence) is used to determine the symmetry of the unit cell. "Systematic absences" in the image are locations of missing h, k, l reflections that are absent due to destructive wave interference.[4] These missing reflections are especially important when assigning the space group because when certain space symmetry exists in a crystal, specific reflections will be missing. The most common systematic absences are listed in

Table 1-2. For example, in the $P2_12_12_1$ space group the h00, 0k0, and 00l reflections will be missing when h, k, or l is odd (Figure 1-5). In a precession

Table 1-2. Most Common Systematic Absences

Symmetry Element	Affected Reflection		Condition
2-fold Screw (2_1)			
	a	*h00*	*h* = odd
	b	*0k0*	*k* = odd
	c	*00l*	*l* = odd
Glide Planes*			
b/2 (*b* glide)	*a*	*0kl*	*k* = odd
c/2 (*c* glide)			*l* = odd
b/2 + c/2 (*n* glide)			*k* + *l* = odd
a/2 (*a* glide)	*b*	*h0l*	*h* = odd
c/2 (*c* glide)			*l* = odd
a/2 + c/2 (*n* glide)			*h* + *l* = odd
a/2 (*a* glide)	*c*	*hk0*	*h* = odd
b/2 (*b* glide)			*k* = odd
a/2 + b/2 (*n* glide)			*h* + *k* = odd
Lattice Centering			
Primitive (**P**)		—	—
C-centered (**C**)		*hkl*	*h* + *k* = odd

* Glide planes are perpendicular to the listed translation

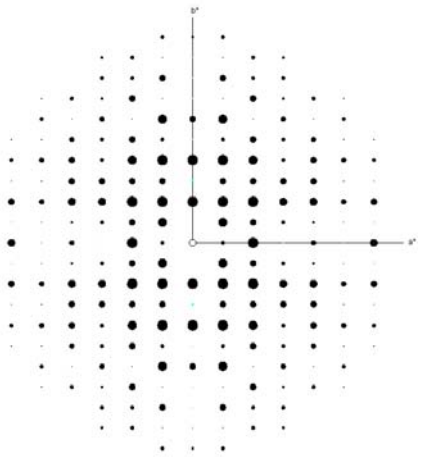

Figure 1-5. A computer generated precession photo in the hk0 plane from a crystal in the $P2_12_12_1$ space group.

photograph, the reflections are placed in a horizontal plane and it is then easily seen which reflections are missing (or very weak) in those instances.

1.2.2. *The Bragg Equation*

Because of the molecular patterns that exist in a crystal, it is possible to draw imaginary planes that run parallel to each other. These "lattice planes" are equally spaced and are separated by some distance, expressed as $d_{h,k,l}$.[3] Each plane overlaps an identical atomic arrangement (Figure 1-6).

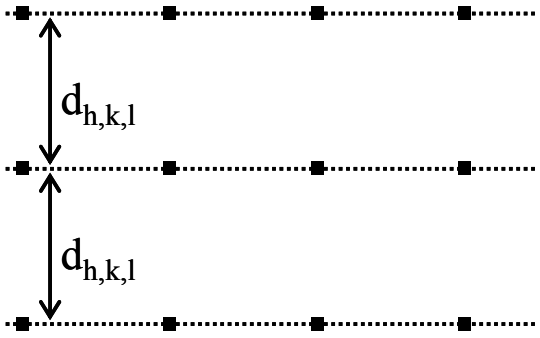

Figure 1-6. Lattice planes in a crystal are separated by some distance, $d_{h,k,l}$.

When an incoming X-ray wave hits the electron cloud of an atom, the waves re-radiate a portion of their energy as a spherical wave. These scattered waves will add constructively only in the directions where the path length difference, $2d_{h,k,l} \cdot \sin\theta$, is equal to an integer multiple of the wavelength ($n\lambda$).[3] This is related by the Bragg Equation shown in Equation 1-1.

$$n\lambda = 2d_{h,k,l} \cdot \sin\theta \qquad \text{Eqn. 1-1.}$$

When scattered waves interfere constructively and create peaks, the term $n\lambda$ essentially corresponds to the number of wavelengths that "fit" in between the lattice planes in the crystal. These peaks can only be obtained for allowed d

values, which are determined by the molecular arrangement in the crystal (Figure 1-7).[1]

As a three-dimensional crystal diffracts X-rays that are coming in at a precisely known angle, the diffracted beams will create a specific diffraction pattern, depending on the type and location of the atoms in the unit cell. Using equation 1-1, each observed spot can be labelled with three indices (h, k, l) based on the lattice planes present in the crystal. In this way, the Bragg Law forms the foundation of X-ray diffraction.[1]

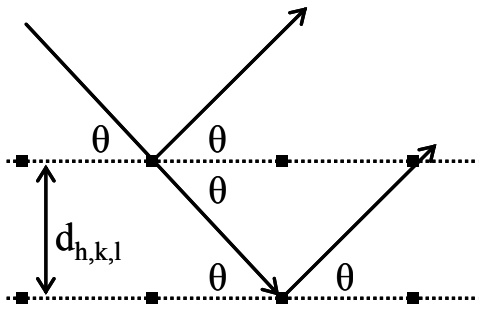

Figure 1-7. Incoming X-ray beam being scattered constructively by lattice planes, the theory is based on Bragg's Law.

1.3. Obtaining a Crystal Structure

There are four steps in obtaining an X-ray crystal structure. The first step is usually performed by the experimental chemist: grow an X-ray quality crystal. The following steps are preformed by a crystallographer: collect the data, create an initial structure, and finally solve the structure (Figure 1-8). In the following sections, these steps will be explained in more detail.

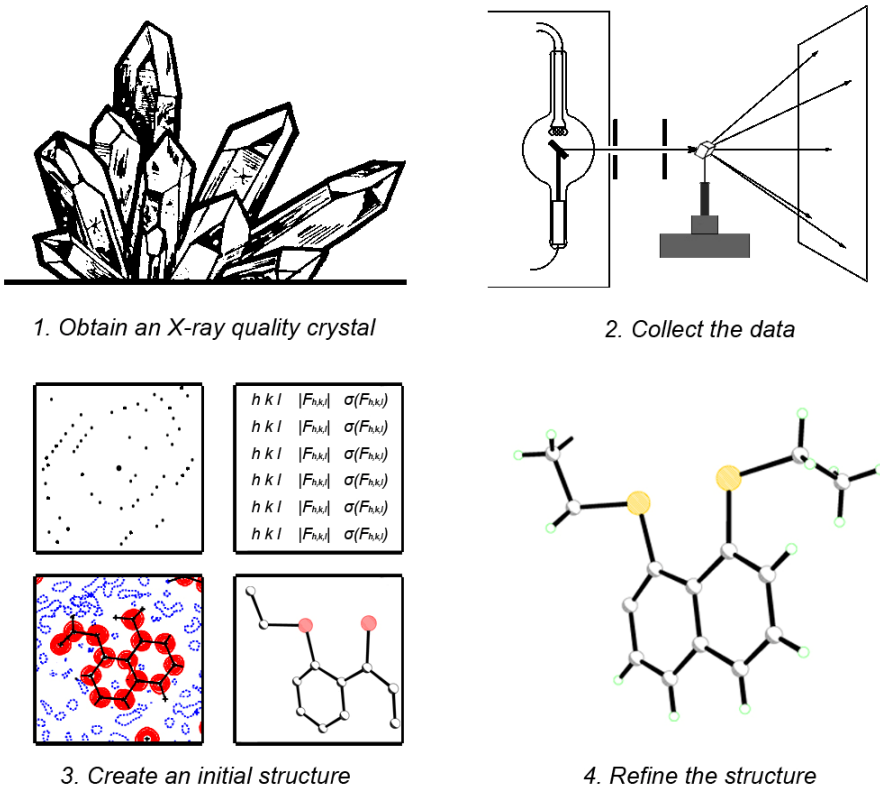

Figure 1-8. Steps in obtaining an X-ray crystal structure.

1.3.1. STEP 1 – Growing Crystals

Growing an X-ray quality crystal, more often than not, is much easier said then done. Preferably grown from a homogeneous solution, crystals form when the molecular units stack or pack together based on interactions or repulsions among them. When packing happens slowly, the molecules will fit together until a crystal, a three-dimensional repeating unit, is formed.

The growing of crystals can be deemed an art, as concentration, solubility, temperature, and luck all factor into the result. There are several techniques used in crystal growing, including, but not limited to: vapour diffusion, evaporation, solvent layering, and seeding. For clarity, solvent A is any solvent that can dissolve the sample to form a solution and solvent B cannot dissolve the sample (Figure 1-9).

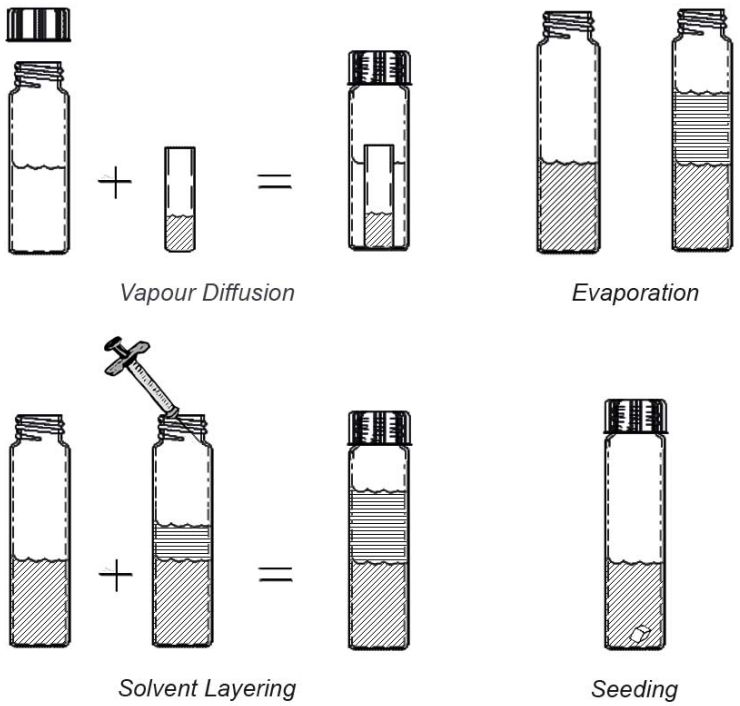

Figure 1-9. Graphic of crystal growing techniques.

Vapour diffusion occurs in a closed system. A small vial with a near-saturated solution of the sample in solvent A is placed into a larger outer vial containing solvent B. As the outer solvent evaporates, it will diffuse into the inner solution. Solvent B is chosen so it mixes well with solvent A and has a lower temperature of vaporization than does solvent A. Hopefully, this process will decrease the solubility of the compound in solution enough so that crystals will slowly form.

There are many evaporation techniques that can be used to produce X-ray quality crystals. For example, in one, a solution of the sample in solvent A is prepared and then is left open to slowly evaporate. As the solvent evaporates, the solution gets more and more concentrated, and the number of solute molecules that solvent A can hold decreases. If the rate of evaporation is slow, then molecules can pack slowly and effectively and a crystalline solid will fall out of solution. Another clever evaporation technique is making a solution where

solvents A and B work together. The solute of interest is dissolved in a minimal amount of solvent A, then solvent B is added to precipitate out the sample, and finally more of solvent A is added to redissolve the solid. When the vial is left open, solvent A should evaporate more readily than solvent B, which results in a gradient in the remaining solution. The compound of interest becomes more and more insoluble and, hopefully, crystallizes out of solution.

Solvent layering can be a very tricky technique to learn, but once mastered, is very useful. It is like vapour diffusion but with a quicker diffusion. In solvent layering, a near-saturated solution of the sample in solvent A is placed in a vial. Solvent B is chosen so it is miscible with and slightly less dense than solvent A. Solvent B is then, VERY slowly, placed (layered) on top of the solution. This process is typically done using an extremely small-bore needle in order to disrupt the solution/solvent interface as little as possible.

The final technique can be used in conjunction with any of the other techniques or by itself. Seeding is a process in which a nucleation point is introduced into a vial containing the sample solution. Usually, this “seed” is a crystal of the desired substance, but it could also be a grain of sand. Sometimes simply scratching the inside of the vial with a spatula creates grooves in the vial or chips of glass that can act as nucleation points. Any way it is done, the goal in seeding is to provide a starting point for the crystal to grow on.

Even for a chemist who has mastered these techniques, X-ray quality crystals can be quite difficult to grow. One of the biggest problems is a lack of patience. Once a crystallization vial is set up, it is best left alone, often for days or weeks, but sometimes it takes years for the crystals to grow.

1.3.2. STEP 2 – Collecting Data

After obtaining a suitable crystal for an X-ray experiment, an X-ray diffractometer is used to collect crystal data. This instrument is designed to aim X-ray beams through a crystal and record where the beams diffract and the intensity of the reflection. A schematic of a typical diffractometer can be seen in Figure 1-10. In an experiment, a precisely oriented X-ray beam is focused through a crystal positioned on a goniometer head. A beam stop, placed between the crystal and the detector, keeps non-diffracted X-rays from directly hitting the detector. The detector records the location and intensity of the diffracted X-ray beams. A video camera is used to magnify the crystal to help center the crystal in the X-ray beam. Finally, a stream of cooled N_2 surrounds the crystal in order to lower the thermal vibrations of the atoms and stabilize air sensitive crystals or minimize solvent diffusion out of the crystal during the experiment.

To collect a data set, the chosen crystal is coated with a sticky, amorphous oil. This oil is used to stick (or mount) the crystal on a very small nylon or plastic loop. The loop is located at the end of a metal rod attached to a magnetic base (Figure 1-11). The base will magnetically attach to the goniometer head of the diffractometer and the crystal can then be centered in the path of the X-ray beam.

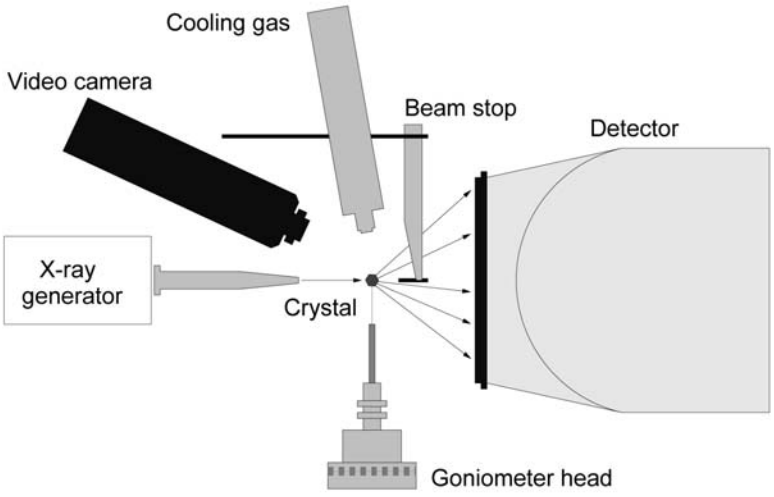

Figure 1-10. Schematic of an X-ray diffractometer.[2]

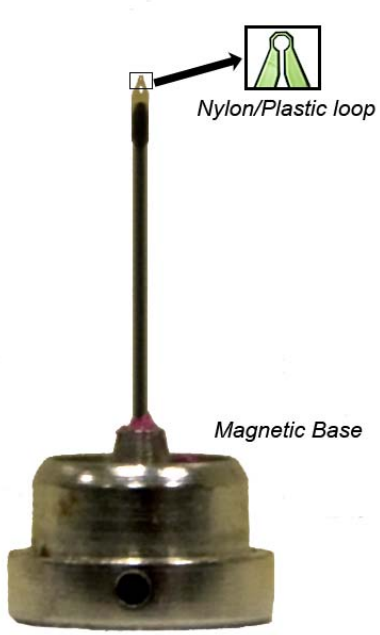

Figure 1-11. Photograph of a loop.

After the crystal is centered, the shutter is opened and the crystal is irradiated with a monochromatic X-ray beam. When the beam hits the crystal, the atoms in the crystal scatter the waves into a very specific diffraction pattern based on *Bragg's Equation* (Eqn 1-1).[1] The diffracted X-rays are recorded on a charge-coupled device (CCD) area detector in the form of images. Each image contains spots of varying sizes called reflections. An amorphous or polycrystalline material will produce dark rings in the image instead of spots (Figure 1-12).

Exposure time, atom size, and atom position all factor into the observed intensity of the reflections. The longer the exposure time or the bigger the atom will produce more intense reflections. The position and relative intensities of the reflections are then used to determine the identity and arrangement of the atoms in the crystal.

A single image is only a small slice of crystal data. In order to create a three dimensional picture of the crystal, a full data set needs to be recorded. Depending on the X-ray diffractometer, this is done by recording images as the

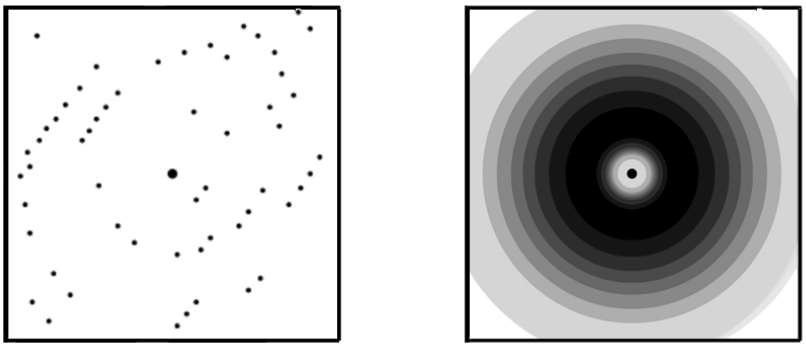

Single Crystal *Amorphous Material*

Figure 1-12. Images of a single crystal and an amorphous material.

crystal is rotated stepwise through various orientations around three rotational angles; Ω, X, and Φ. The Ω angle is rotation around an axis perpendicular to the beam; the X angle is rotation about an axis typically 50° to the Ω axis; and the Φ angle is rotation about the loop axis (Figure 1-13).[1] As the crystal is incrementally rotated through 180° on each axis, hundreds of images are recorded. The more internal symmetry a crystal has, less images need to be taken.

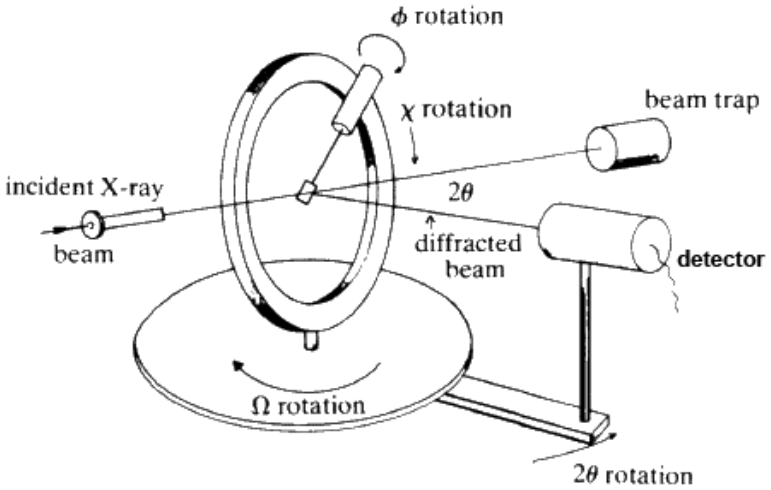

Figure 1-13. For a full data collection, the crystal rotates through various orientations around three rotational angles; Ω, X, and Φ.[5]

A full data collection can take hours to complete, but it is possible to identify the crystal system and the unit cell parameters after a few initial images. Knowing this information is vital to the data collection. If the parameters don't make sense, or if they match a known compound, then it is possible to stop the experiment and correct any problems before time is wasted on a full data collection. For example, if the unit cell is unusual, it may be necessary to change variables in the experiment (e.g. exposure time), re-center the crystal in the X-ray beam, or even choose a different crystal.

Even if some information about the crystal can be determined after a few images, the intensity for each individual reflection still needs to be measured in order to calculate atom positions, which requires a full data collection.

1.3.3. STEP 3 – Create an Initial Structure

Step three describes much of the computer work carried out by the crystallographer. Once data collection is finished, the positions of the reflections are converted into h, k, l indices and the intensities of the reflections into amplitudes. These values make it possible to create an electron density map, which then leads to the creation of an initial (incomplete) structure (Figure 1-14). This section will describe the creation of the initial structure in more detail.

1.3.3.1. Images

In data collection, hundreds of images are recorded. Every image contains many, many reflections (spots). Each reflection has two numerical values associated with it the amplitude, |F|, and phase, ø, of the diffracted wave.

The amplitude is equal to the height of the wave and the phase is equal to a horizontal shift of the original wave by a displacement factor (Figure 1-15).[1] These values are represented by vectors and then ultimately converted into h, k, l coordinates (related by the Pythagorean Theorem; Figure 1-15). The ideas and equations shown in Figure 1-15 are for one wave with one phase. The creation of an electron density map of the molecule from a diffraction pattern involves the addition of numerous waves with their correct relative amplitudes and phases.

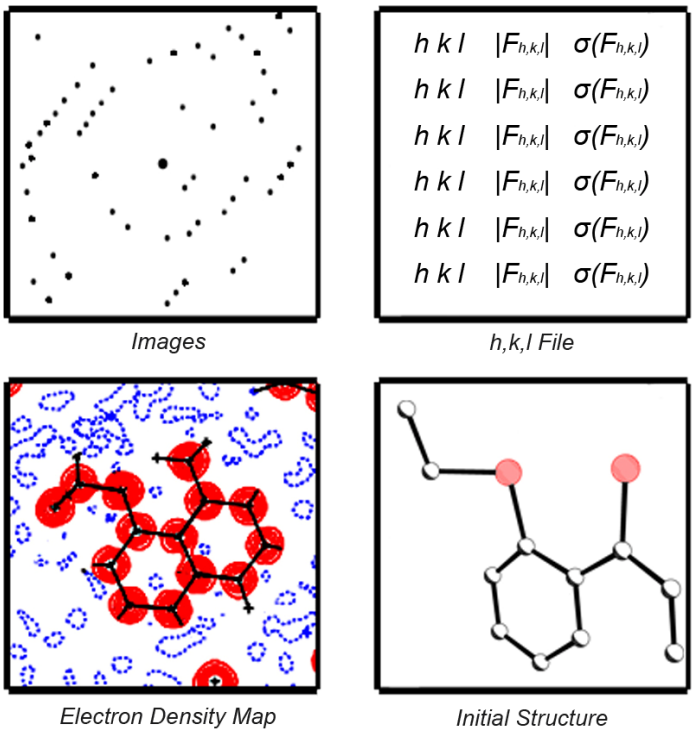

Figure 1-14. Depictions of the processes in step 3.

For each reflection, the intensity of the diffracted X-ray beam at each h, k, l position can be measured. The intensity ($I_{h,k,l}$) of each measured spot is proportional to the structure factor (**F**) (Equation 1-2). The calculation for the structure factor is shown in Equation 1-3, which is a complex number calculated

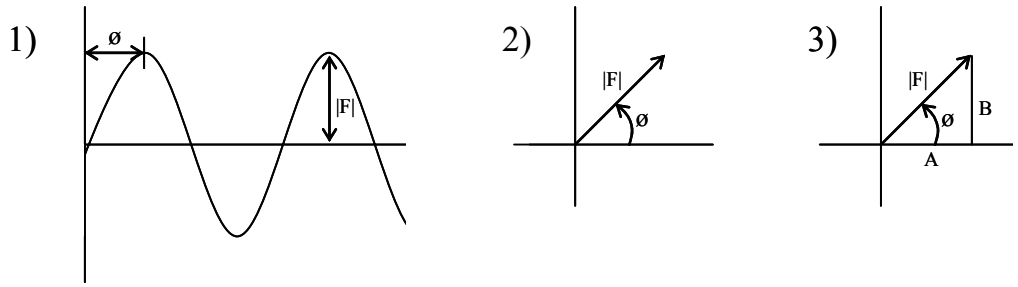

Figure 1-15. Depictions of how waves can be converted into Cartesian coordinates. 1) The wave amplitude, |F|, and the phase, ø, of a wave. 2) In vector form, |F| is the length and ø is the direction of the vector. 3) Using Pythagoras Theorem, $|F|^2 = A^2 + B^2$ and the tan ø = B/A. Therefore, A = |F| cos ø and B = |F| sin ø.[1]

$$I_{h,k,l} \propto (\boldsymbol{F}_{h,k,l})^2 \qquad \text{Eqn. 1-2.}$$

$$\boldsymbol{F} = |F| \cdot e^{i\phi} \qquad \text{Eqn. 1-3.}$$

from the amplitudes (|F|) and phases ($e^{i\phi}$) of the diffracted wave.[1,3] Because of the various experimental factors that alter the intensity, (i.e. geometric and absorption), the data obtained from the images is usually in a crude format.

1.3.3.2. Data Reduction

Data reduction is the process that corrects for the crudeness of the acquired data. Geometrical corrections can include changes in the incident X-ray beam intensity, the scattering power of the crystal, or Lorenz-polarization, in which the reflected radiation is partially polarized.[1] There are several different types of absorption corrections that can be made, with most of them based on the size and dimensions of the crystal and the calculation of path lengths.

The data reduction process also includes the merging and averaging of repeated and symmetry-equivalent measurements. This process will produce a unique, corrected, and scaled data set. A statistical analysis of the complete unique data set can provide an indication of the presence or absence of some symmetry elements.

Prior to the area detectors in use today, selected portions of the diffracted pattern needed to be recorded separately on different photographic films. This output style allowed for h, k, l indices to be assigned to individual reflections by counting along obvious rows of spots.[1] Figure 1-16 displays an example of a precession photograph where crystal information was taken by counting rows of reflections. Since the development of area detectors, it is no longer necessary to have all of the reflections in a horizontal plane and finding the h, k, l indices has become more of a computer "black box" process.

Data reduction produces a list of h, k, l indices with their corresponding observed structure amplitude, $|F_{h,k,l}|$, and the error, $\sigma(F_{h,k,l})$, associated with the

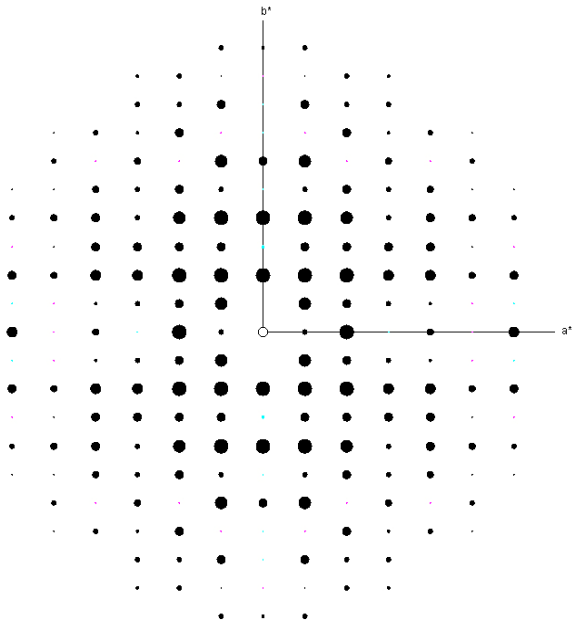

Figure 1-16. Computer generated precession photo in the hk0 plane from a crystal in the $P2_12_12_1$ space group.

amplitude (or these values will be squared, $F^2_{h,k,l}$ and $\sigma(F^2_{h,k,l})$, so information isn't lost when using the absolute value function on negative intensities).[1]

1.3.3.3. Electron Density Map

Using the list of h, k, l positions with the corresponding observed structure amplitude, $|F_{h,k,l}|$, and the error, $\sigma(F_{h,k,l})$, an electron density map can be created (Figure 1-17).

Converting the list of h, k, l reflection positions into atom positions in x, y, z coordinates can be performed using Equation 1-4.[1] The electron density, $\rho_{x,y,z}$ in electrons per $Å^3$ is equal to the summation of the observed structure amplitudes (1) multiplied by the phases of the waves (2) from all of the reflections (h,k,l), multiplied by an extra phase correction (3). The amplitudes (1) are measured and the phase correction (3) can be calculated, but the phase (2) can not be directly

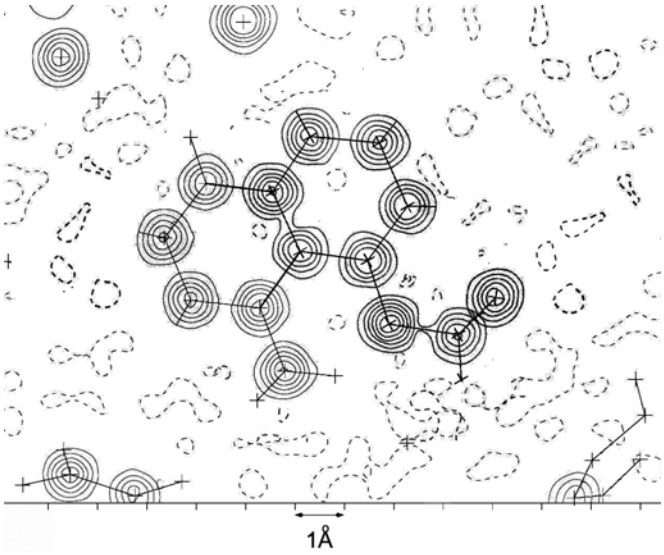

Figure 1-17. Pictorial representation of an electron density map.

$$\rho_{x,y,z} = \frac{1}{V}\sum_{h,k,l}\left|F_{h,k,l}\right| \cdot e^{(i\phi_{h,k,l})} \cdot e^{[-2\pi i(hx+ky+lz)]} \qquad \text{Eqn. 1-4.}$$

recorded during the experiment and cannot be calculated using the information obtained in the data collection.

Without the phase contribution, Equation 1-4 is useless. This is known as the "phase problem".[1] A trial-and-error method of guessing the phase of thousands of individual waves would be difficult to say the least, so several methods have been developed to solve the phase problem. Of the developed methods, direct methods and Patterson methods, are the two most commonly used to solve small molecule (< 1,000 atoms) crystal structures. However, direct methods are by far the most extensively used methods.

The basis for the Patterson methods is to set all phases equal to zero (treating the reflections as though all waves are in phase, where $e^0 = 1$) and square the phase amplitudes (Equation 1-5).[1] This new equation is similar to Equation 1-4, only without the problematic phase term (2).

Equation 1-5 consists of the summation of the squared amplitudes (1) multiplied by the extra phase correction (3). Patterson methods work best for

$$\rho_{x,y,z} = \frac{1}{V}\sum_{h,k,l}\left|F_{h,k,l}\right|^2 \cdot e^{[-2\pi i(hx+ky+lz)]} \qquad \text{Eqn. 1-5.}$$

1 3

structures containing heavy atoms. A Patterson map shows where atoms lie relative to each other, but not where they lie relative to the unit cell. When using this method, the results may look like an electron density map, but it is actually a map of vectors between atoms.

Direct methods, also known as *Ab initio* phasing, is the most popular method used for molecules with "equal atom" structures. The name "direct method" encompasses any method that obtains the reflection phases straight from the measured intensities.

Obtaining phases from the measured intensities can be done because an electron density map contains only positive or zero density concentrated into compact regions.[1] Regions cannot have negative density and therefore waves can be added together in order to build up and concentrate positive regions and cancel out negative ones. This puts considerable restrictions on the relationships among the phases of different reflections, especially the most intense ones, which contribute most to the sum. The individual phase relationships are still not certain and have to be expressed in terms of probabilities, which depend on their relative intensities.

In essence, direct methods are performed by selecting the most intense reflections and working out the probable relationships between their phases. When the relationship probabilities are known, then all of the different possible phases are tried to see how well the probabilities are satisfied. For the most promising combinations, Fourier transformation calculations are performed from the observed amplitude. Trial phases are then examined for recognizable molecular features. This method has been developed over many years and involves a considerable amount of computing. For many regular users, it is treated as a 'black box'.[1] A successful trial is when the method locates most of, if not all of the non-hydrogen atoms in a structure.

Almost all small molecule X-ray crystal structures are solved by using either the direct methods or Patterson methods.[1] There is no "correct" method for solving a particular structure. Once the right solution has been found, it can be further refined. If one method doesn't work other methods can be tried until one is successful. After all, the object is to beat the "phase problem", and exactly how this is done is not important.

1.3.3.4. Initial model

After using either direct methods or Patterson methods, only estimates for the phases are acquired. This allows for an initial structural model to be built by fitting atoms where the electron density appears. In an initial model, it is not always possible for all of the atoms to be located. Some atoms can be missing because of disorder, weak electron density, or size (e.g. hydrogen atoms) (Figure 1-18). There can be many things wrong with an initial model, which can make solving for the real structure more difficult.

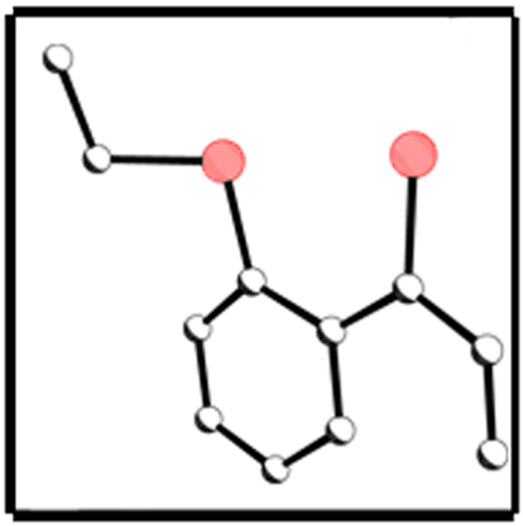

Figure 1-18. An initial image is most likely missing atoms and will need to be completed.

1.3.4. STEP 4 – Refining the Structure

In order to create a more complete model of the crystal, the initial estimated phases need to be refined. By adding or deleting atoms, altering the element choice, or accounting for thermal vibrations, each process will, hopefully, produce a better model. This process is called refinement and it is done to bring the model closer to the actual structure.

Each refinement cycle of the model produces a new set of calculated phases. Each time, these phases are used to produce a calculated diffraction pattern, which hopefully gets closer and closer to the actual measured diffraction pattern. The more refined the phases become, the better the calculated data fits the observed diffraction data.

The residual factor, or *R*-factor, is a parameter used to measure the fit of the model to the diffraction data. It is analogous to a simple percent error calculation, and as such is usually reported as a percent. The lower the R-factor is, the better the model. Calculating the R-factor involves using the structure factor (**F**), shown in Equation 1-3.[1] Equation 1-6 shows how the R-factor is calculated. This calculation involves the summation of the observed structure factors ($\mathbf{F_o}$) minus the calculated structure factors ($\mathbf{F_c}$), divided by the summation of the observed structure factors ($\mathbf{F_o}$).

$$\mathbf{R} = \frac{\sum \left| |\mathbf{F}_o| - |\mathbf{F}_c| \right|}{\sum |\mathbf{F}_o|} \qquad \text{Eqn. 1-6.}$$

When the crystallographer is satisfied with the set of phases that produce a suitable model, a crystallographic information file (.cif) is written. This is a simple text file that contains all of the parameters used in the experiment, along with atom positions, distances, and angles between atoms. The .cif file is how scientists communicate their structural model to the rest of the world.

1.4. References

(1) Clegg, W. (2006) *Crystal Structure Determination.* New York:Oxford University Press

(2) Kooijman, H. (2005) *Interpretation of Crystal Structure Determinations version 2.3* Utrecht University:Undergraduate course notes.

(3) Sands, D. E. (1969) *Introduction to Crystallography.* New York:W. A. Benjamin, Inc.

(4) Hammond, C. (2008) *The Basics of Crystallography and Diffraction;* New York:Oxford University Press: 2001.

(5) Image Retrieved on 22 November, 2008, from The Science Education Resource Center (SERC) website: http://serc.carleton.edu/images/research_education/geochemsheets/techniques/IUCrimg69.v2.gif

CHAPTER 2
INTRODUCTION TO *PERI*-SUBSTITUTED NAPHTHALENE

2.1. Introduction

X-ray crystallography is used to investigate structural features in crystalline compounds. One subject of interest in this thesis is *peri*-substituted naphthalene. Naphthalene ($C_{10}H_8$) is a very rigid, planar aromatic hydrocarbon consisting of two fused benzene rings. Historically, by convention, the *peri*-positions are defined as the 1, 8- positions (Figure 2-1).[1] The oldest *peri*-substituted naphthalene found in the Cambridge Structural Database (CSD) (version 5.30, updated May 2009) is a naphthalene molecule with a methine carbon in each *peri*- position, where there is a double bond between the two carbon atoms. This structure was reported in 1932[2], but it wasn't until the 1960s and later that extensive attention was focused on the *peri*-positions. In this thesis, I utilize X-ray crystallography to probe structural perturbations that occur in *peri*-disubstituted naphthalene compounds.

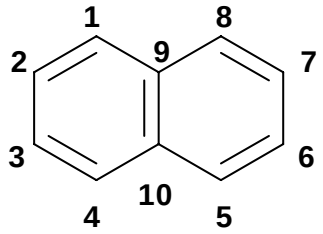

Figure 2-1. Historic numbering scheme of naphthalene.

2.2. *Peri*-Substitution

When the *peri*-positions are occupied by hydrogen atoms, the distance between the hydrogen atoms is 2.45(1) Å.[3] This proximity means that if any atom other than hydrogen is placed in these positions, they will be closer together than the sum of their Van der Waals radii.[4]

In fact, *peri*-substituted naphthalene forces its substituents closer than does any other type of disubtituted organic backbone. For example, in benzene the ortho positions are 3 to 4 Å apart; however the bay positions in phenanthrene come close to challenging naphthalene for substituent proximity (Figure 2-2). When the bay positions are occupied by hydrogen or fluorine atoms, they are actually closer than in naphthalene (H, *peri*- distance 2.45 Å vs. bay distance 2.04 Å)[5]. However, when larger halide atoms (Cl or Br) are substituted, the halides are further apart than substituents in the *peri*-positions in naphthalene (Cl, *peri*-distance 2.98 Å vs. bay distance 3.10 Å) (Figure 2-2).[5] This discovery was given two possible explanations: either it takes less energy for the non-bonded atoms to sit parallel than it does for them to sit head to head as in phenanthrene, or the naphthalene rings are more rigid than the phenanthrene backbone, forcing larger substituents closer together.[5]

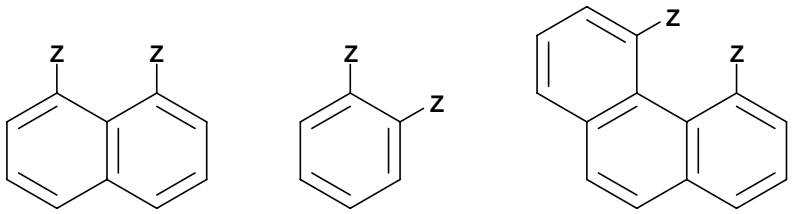

Figure 2-2. *Peri*-positions in naphthalene (a), ortho-positions in benzene (b), and the bay region in phenanthrene (c).

The naphthalene backbone certainly prefers not to distort. A CSD search of *peri*-disubstituted naphthalene compounds (1912 results) showed the mean torsion angle across the bridge head carbons is 179.99° (a planar torsion angle is 180°), suggesting that most of the di-substituted naphthalene compounds have a tendency to stay quite planar. These compounds have a torsion angle range (across the bridgehead carbons) of -159.9° to 163.3°. Substituted naphthalene rings do not show easily discernible patterns of distortion. For example, despite having only two extra chloride substituents, octachloronaphthalene is very

buckled (torsion angle (161.9°), whereas 1,2,4,5,6,8-hexachloronapthalene is planar (torsion 180.0°) (Figure 2-3).[6,7]

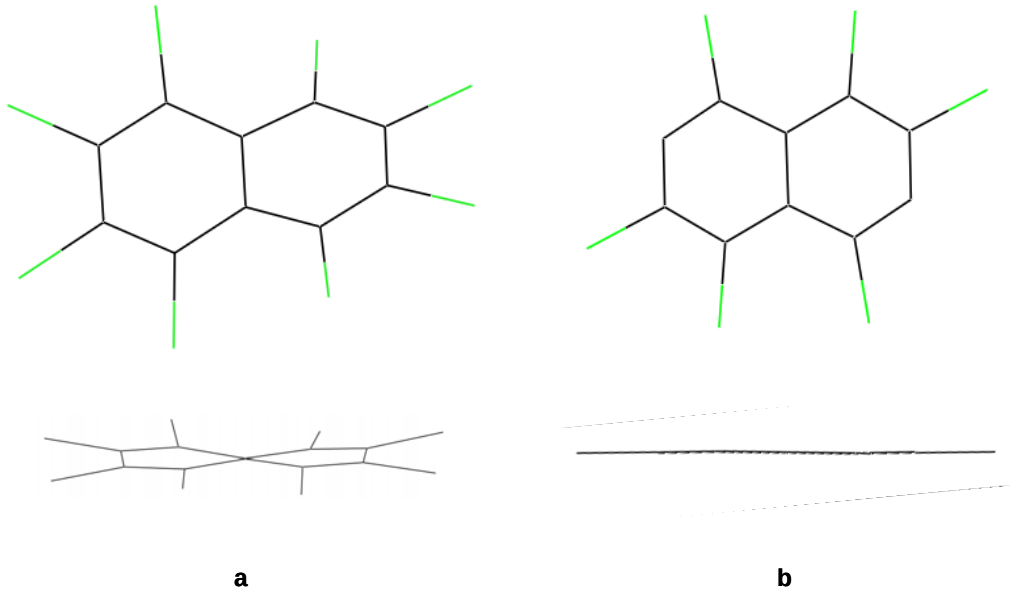

Figure 2-3. Line diagrams (top) of octachloronapthalene (a) and 1,2,4,5,6,8-hexachloronapthalene (b) and their side views (bottom).

The close proximity of the *peri*-positions and lack of flexibility of the backbone mean that substituents at those positions experience considerable sterically imposed interactions with each other that are not present in any other aromatic hydrocarbon, not even phenanthrene. The close contact means that steric strain from the substituents and resonance energy from the naphthalene ring compete against each other in *peri*-substituted naphthalene compounds. As the naphthalene molecule distorts, steric strain between the two substituents decreases. This being the case, the molecule could continue distorting to relieve all of the negative effects caused by steric interactions, except as it distorts, there is a loss of resonance stabilization because the naphthalene rings must remain planar in order to benefit from resonance stabilization. These competing influences engage in a continual tug-o'-war to produce the overall lowest energy structure for *peri*-substituted naphthalene molecules.

There are extremes in the different types of *peri*-substitution that can occur. In one extreme, the substituents can form a strong bond; the other extreme is the substituents have a very unfavorable interaction. A search of the CSD of *peri*-substituted naphthalene compounds showed a *peri*-distance range of 1.22 Å to 3.86 Å.[8,9] The smallest distance comes from a naphthalene having a double bond between two carbon *peri*-substituents (Figure 2-4a) and the largest distance belongs to a naphthalene substituted with two -$Sn(CH_3)_3$ substituents (Figure 2-4b).

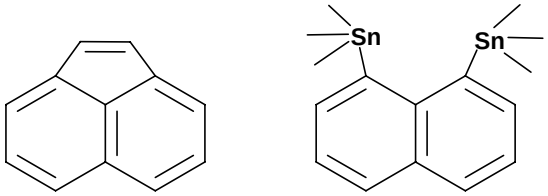

a b

Figure 2-4. Two types of *peri*-substituted naphthalene compounds, with the shortest (a) and longest (b) *peri*-distance.

Substituted naphthalene molecules, then, can display unique effects that result from trying to maintain planarity in the naphthalene rings while overcoming steric interactions introduced by *peri*- substitution. For example, if the substituents are bonded to one another, less strain will be placed on the backbone than if the substituents are non-bonded. However, there can still be strain on the molecule in a bonded situation, since even bound substituents will often need to lean towards or away from each other in order to have an optimal covalent bond length.

2.3. Relieving Steric Strain

There are four possible ways that steric strain can be relieved in a naphthalene ring system: lengthening the carbon-carbon or carbon-substituent (C-Z) bonds, in-plane deflection of the substituents, out-of-plane deflection of the substituents, or distortion of the naphthalene ring. Even the slightest molecular distortions can create a large amount of steric relief in the molecule.

2.3.1. Lengthening of C-Z Bond

It appears that bonds are very rarely stretched in order to relieve steric strain, since there is a large energy barrier to overcome in order for even a small perturbation in bond length to occur.[1] In order to focus more closely on the distortion of the C-Z bond, a CSD search was narrowed to *peri*-substituted naphthalene compounds where one substituent is a selenium atom and the other can be any atom except hydrogen (Figure 2-5). The search resulted in 28 hits, in which the C-Se bond length ranged from 1.90 Å to 1.99 Å (mean 1.94 Å) (Figure 2-6).[10,11] The compounds with the longest C-Se lengths and the shortest lengths are shown in Figure 2.7. Since the bond lengths in these compounds are only 0.1

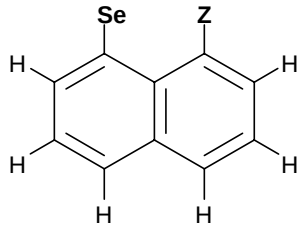

Figure 2-5. CSD search critera for narrowing *peri*-substituted naphthelene results; one selenium atom in the *peri*-position and any atom except hydrogen in the other position.

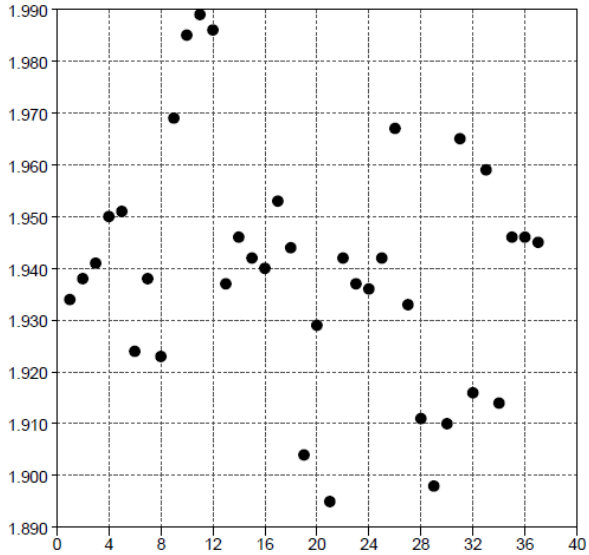

Figure 2-6. Graph of the C-Se bond length (Å) vs. compound number from the (narrow) CSD search.

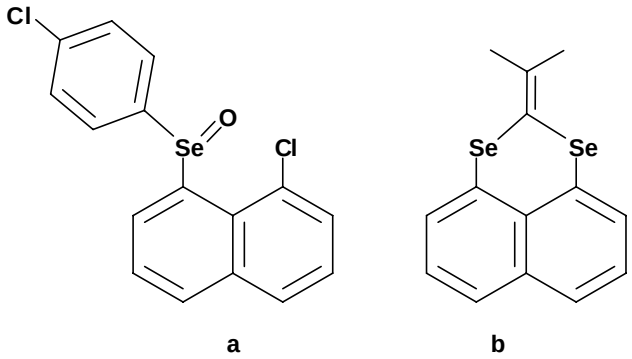

Figure 2-7. Search results for the longest C-Se bond length (a) and the shortest C-Se bond length (b) in *peri*-substituted naphthalene.

Å different (~5%), it seems as if the other three distortions are needed to relieve strain on the backbone.

2.3.2. In-Plane Deflection

In-plane deflections of *peri*-substituents on naphthalene can be determined by considering the angles centered on C(1) and C(8) (Figure 2-8). In order to determine the magnitude of in-plane distortions, it needs to be established how far the angles are distorted from the ideal 120° trigonal planar bond angles. For example, in an "unsubstituted" naphthalene molecule in the solid phase at 100 K (i.e. with hydrogen atoms in the *peri*- positions), the three angles around C(1) and C(8) are 121.0(1)° (outer), 118.3(1)° (inner), and 120.6(1)° (inside the ring).[3] Figure 2-8 shows examples of possible in-plane distortions around these carbon atoms: the substituents can bend inward, be geometrically ideal or close to ideal, or lean outward.

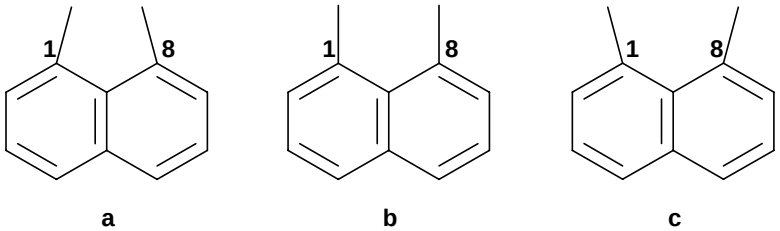

Figure 2-8. Possible in-plane distortions of the substituents centered on carbon atoms 1 and 8: inward bend (a), ideal system (b), and outward splay (c).

The narrowed CSD search (Figure 2-5) of *peri*-substituted naphthalene compounds containing one *peri*- selenium atom was used to look at the inner angle around the naphthalene carbon atom attached to the selenium. The smallest angle (113.9°) was found on the naphthalene derivative with -Se-I and -NMe_2 substituents, where the largest angle (128.9°), unsurprisingly, was found on a diselenium naphthalene ligand, which was bound to a platinum(II) metal center (Figure 2-9).[12,13] These results, compared to unsubstituted naphthalene (118.3(1)°), show that very large in-plane deflections are possible.

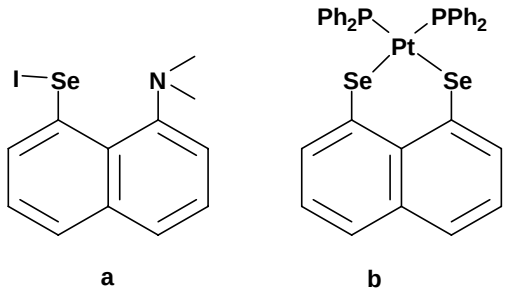

Figure 2-9. The smallest (a) and largest (b) in-plane distortions in *peri*-substituted selenium naphthalene derivatives.

2.3.3. Out-of-Plane Deflection

Out-of-plane deflection is calculated by measuring how far the substituents deviate from the ideal naphthalene plane. Of the 28 *peri*-substituted naphthalene compounds with at least one selenium substituent (narrow CSD search, Figure 2-5), the range of selenium deviation from the plane is 0.00 Å to 0.48 Å.[13,14] The compounds with the smallest and largest deviations are shown in Figure 2-10. It is interesting that the compound with the most severe out of plane deviation, [(Se_2naph)Pt(PPh_3)$_2$], also has the largest in-plane distortion of all of the compounds in the narrowed search. This likely indicates some unusually severe stress present in this compound.

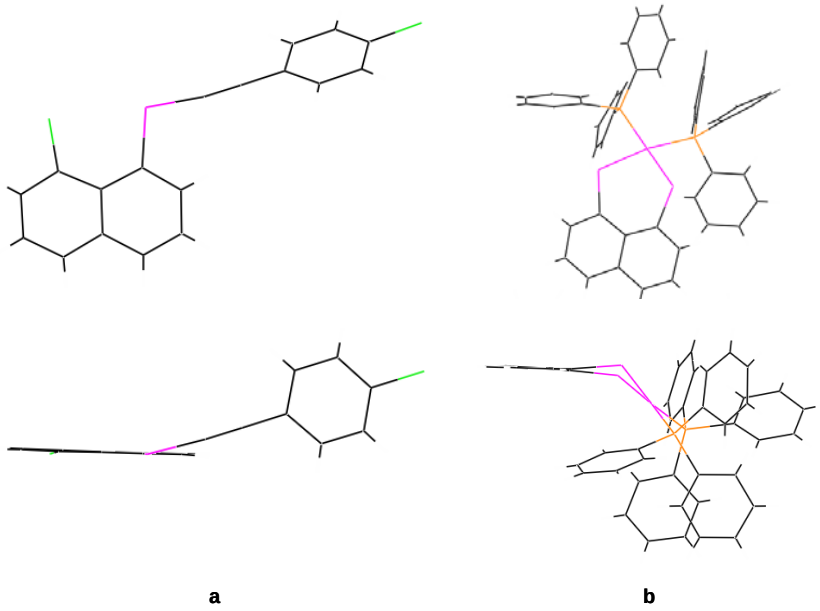

Figure 2-10. Wire drawings of the smallest (a, top) and largest (b, top) out-of-plane distortion of the Se atom from compounds in the CSD (narrowed) search. The bottom pictures shows the top view (a) and side view (b) of these compounds.

2.3.4. Distortion of the Naphthalene Backbone

Despite the above-mentioned tendency to stay planar and take advantage of resonance stabilization energy, some slight distorting or buckling of the backbone rings does often occur when *peri*-substituted naphthalene tries to relieve strain introduced by the substituents. The distortion of the naphthalene plane can be quantified by comparing the torsion angles that run through the central bridging carbon atoms to the same angles in an ideal planar system, in which they would either be 0° or 180° degrees (Figure 2-11).

The (narrowed) CSD search resulted in the torsion angle **a** (Figure 2-11) ranging from -6.7° to 5.4°. The two extreme distortions are from compounds with large *peri*-substituents (Figure 2-12).[15,16] The torsion angle that runs across the bridgehead carbons (**b**, Figure 2-11) ranged from -173.9° to 173.7°, another 12° range, again straddling linearity (180°). The compounds with the most distorted torsion angle (**b**, Figure 2-11) are a in Figure 2-12 and [(Se_2naph)Pt(PPh_3)$_2$].[13,15] It

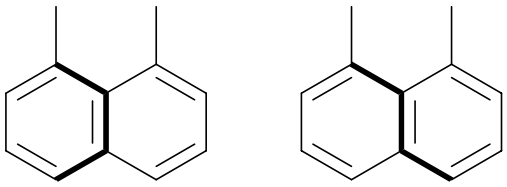

Figure 2-11. Torsion angles in bold, run through the bridgehead carbons. Ideally these angles are: a = 0° and b = 180°.

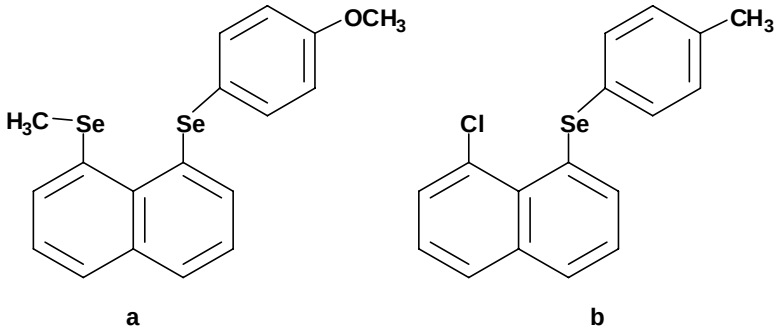

Figure 2-12. The largest **a** torsion angle from the (narrowed) CSD search are present in these two compounds a = -6.7° and b = 5.4°.

is interesting to note that the compound with the smallest out-of-plane distortion also has the most planar naphthalene ring (a in Figure 2-10).[14]

2.4. Hypervalency

Recently investigations have been conducted using naphthalene molecules in which the *peri*-positions contain heavier substituents, like the chalcogens or halides. It has been suggested that the *peri*-positions in the naphthalene backbone are a good environment for three atoms to precisely align, in close proximity, in order to form hypervalent interactions having a three center-four electron (3c-4e) system, as shown in Figure 2-13.[17,18] This type of interaction requires linearity on the part of the three atoms and that the atoms lie within the sum of their Van der Waals radii from one another.[17,18] There is much debate on this topic, both as to whether a hypervalent interaction is formed and how strong the interaction actually is.[19-23] If a hypervalent interaction can and does form, then it could

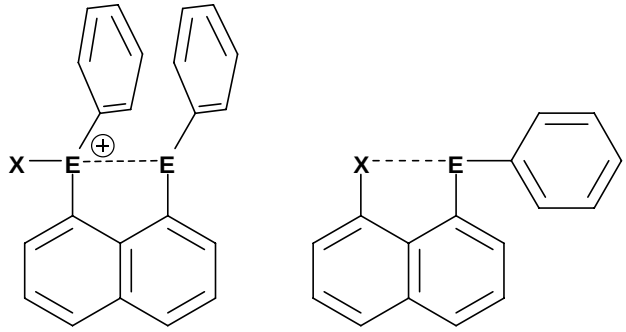

Figure 2-13. Examples of linear, weak hypervalent 3c-4e type interactions, X-E…E (left) and X…E-C (right), where X is a halide and E is a chalcogen.

explain several recently observed strange geometries of disubstituted naphthalene molecules reported in later chapters of this thesis.

2.5. Conclusions

In summary, much work has been done to try to understand the structural deviations that occur when naphthalene carries *peri*-substituents.[1] When the substituents interact, either favorably or not, the tendency for the rings to stay planar to take advantage of resonance stabilization energy creates steric strain in the molecule. There are four types of distortions: bond lengthening, in-plane and out-of-plane deflections, and naphthalene ring distortions that occur with *peri*-substituents. More often than not, a molecule will use combinations of more than one type of distortion to different degrees to relieve the steric interactions at the *peri*-positions.

For example, [(Se_2naph)Pt(PPh_3)$_2$] is an extreme outlier for more than one type of distortion (Figure 2-14).[13] This compound, out of the 28 results from the (narrow) CSD search, had the largest *peri*-distance (3.37 Å), the largest in-plane distortion (113.9°), the largest out-of-plane distortion of the selenium atom (0.48 Å), and the most buckled naphthalene ring (-174.9° across the bridgehead carbons). Although this example is an extreme case, it clearly shows that *peri*-

substituted naphthalene compounds can use all four modes of distortion and that they can be quite severe.

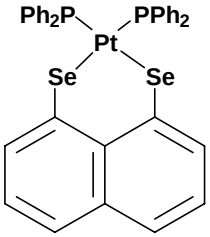

Figure 2-14. Line drawing of [(Se_2Naph)Pt(PPh_3)$_2$.

2.6. References

1. V. Balasubramaniyan, *Chem. Rev.*, 1966, 66, 567-641.
2. Schneider, *Z. Phys. Chem. -Leipzig*, 1932, B16, 460.
3. J. Oddershede and S. Larsen, *J. Phys. Chem. A*, 2004, 108, 1057-1063.
4. A. Bondi, *J. Phys. Chem.*, 1964, 68, 441-452.
5. R. Cosmo, T. W. Hambley and S. Stermhell, *Tetrahedron Lett.*, 1987, 28, 6239-6240.
6. E. Jakobsson, C. Lonnberg and L. Eriksson, *Acta Chem. Scand.*, 1994, 48, 891-898.
7. F. H. Herbstein, *Acta Cryst. B*, 35, 1661-1670.
8. T. R. Welberry, *Proc. R. Soc. London, Ser. A*, 1973, 334, 19-48.
9. J. F. Blount, F. Cozzi, J. R. Damewood, L. D. Iroff, U. Sjostrand and K. Mislow, *J. Am. Chem. Soc.*, 1980, 102, 99-103.
10. K. Kobayashi, S. Shinhara, M. Moriyama, T. Fujii, E. Horn, A. Yabe and N. Furukawa, *Tetrahedron Lett.*, 1999, 40, 5211-5214.
11. S. Hayashi, H. Wada, T. Ueno and W. Nakanishi, *J. Org. Chem.*, 2006, 71, 5574-5585.
12. A. Panda, G. Mugesh, H. B. Singh and R. J. Butcher, *Organometallics*, 1999, 18, 1986-1993.

13. S. M. Aucott, H. L. Milton, S. D. Robertson, A. M. Z. Slawin, G. D. Walker and J. D. Woollins, *Chem. Eur. J.*, 2004, 10, 1666-1676.

14. K. Yamane, S. Hayashi, W. Nakanishi, T. Sasamori and N. Tokitoh, *Polyhedron*, 2008, 27, 3557-3566.

15. W. Nakanishi, S. Hayashi and T. Uehara, *J. Phys. Chem. A*, 1999, 103, 9906-9912.

16. W. Nakanishi and S. Hayashi, *J. Org. Chem.*, 2002, 67, 38-48.

17. W. Nakanishi in *Handbook of Chalcogen Chemistry, New Perspectives in Sulfur, Selenium and Tellurium*, ed. F. A. Devillanova, 2006, 644-668.

18. W. Nakanishi, S. Hayashi and S. Toyota, *J. Org. Chem.*, 1998, 63, 8790-8800.

19. P. Nagy, D. Szabó, I. Kapovits, Á. Kucsman, G. Argay and A. Kálmán, *J. Mol. Struct.*, 2002, 606, 61-76.

20. R. J. Gillespie and E. A. Robinson, *Inorg. Chem.*, 1995, 34, 978-979.

21. S. Hayashi and W. Nakanishi, *Bull. Chem. Soc. Jpn.*, 2008, 81, 1605--1615.

22. G. P. Schiemenz, *Z. Natur. B*, 2007, 62, 2, 235-243.

23. G. P. Schiemenz, *Z. Natur. B*, 2004, 59, 7, 807-816.

CHAPTER 3

NON-BONDED -SPh AND -EPh (E = S, Se, OR Te) *PERI*-SUBSTITUTED NAPHTHALENE COMPOUNDS AND THE OXIDATIVE ADDITION OF BROMINE

3.1. Introduction

This chapter focuses on the structural deviations that occur in *peri*-substituted naphthalene molecules when the substituents do not form a covalent bond with each other. The compounds in this chapter comprise a structural series that have *peri*-substituents from group 16. In each compound, one substituent is -SPh and the other is -EPh, where E = S (**3.1**), Se (**3.2**), and Te (**3.3**) (Figure 3-1). Beyond their inherent structural differences, these compounds, **3.1**-**3.3,** were observed to react with Br_2 to form three very different products, which can be seen in Figure 3-1.

First, this chapter will focus on the structural deviations that occur in the base compounds **3.1**-**3.3** by comparing *peri*-distances, in-plane deflections, out-of-plane deflections, and naphthalene ring distortions. Next follows a discussion on

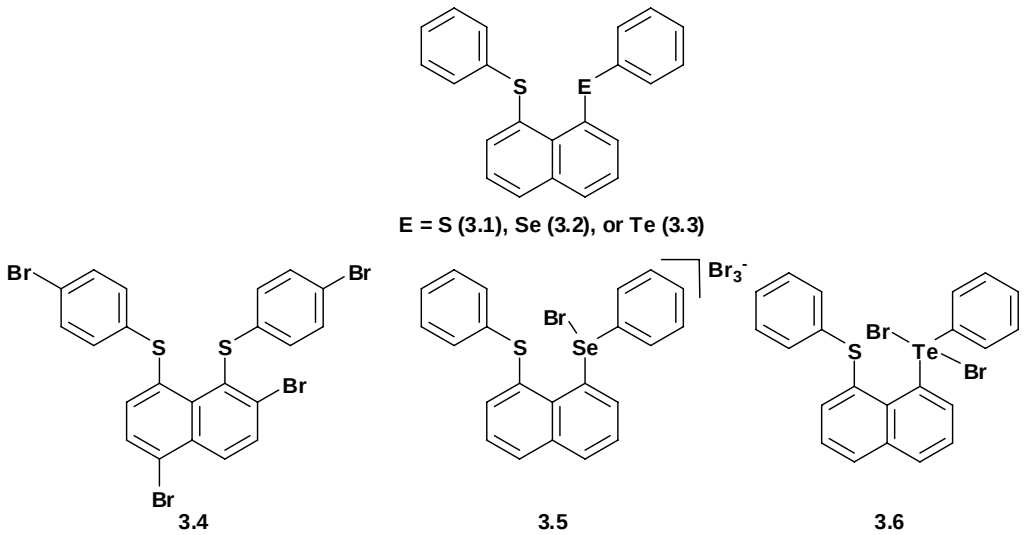

Figure 3-1. Compounds **3.1**-**3.6**, which will be discussed in this chapter.

the mechanism of oxidative addition of dibromine to organochalcogens. This discussion focuses on **3.4-3.6**, which result from the bromination of **3.1-3.3**.

3.2. Crystal Structure Data

(1,8-diphenylsulfanyl)naphthalene (**3.1**) is a *peri*-substituted naphthalene derivative that displays non-bonding interactions between the two -SPh groups (Figure 3-2). This molecule crystallizes in the $P2_1/c$ space group (R_1 = 6.58%). The selenium derivative, **3.2**, contains the *peri*-substituents -SPh and -SePh. These substituents also appear to be non-bonded and the molecule crystallizes in the $Pca2_1$ space group (R_1 = 5.93%). Compound **3.3** is the tellurium derivative, with the *peri*-substituents -SPh and -TePh, which, as in the other examples, are non-bonded. Compound **3.3** crystallizes in the P-1 space group (R_1 = 5.66%) with two independent molecules (**3.3a** and **3.3b**) in the unit cell (Figure 3-3). Refinement data for **3.1-3.3** can be found in Appendix 1.

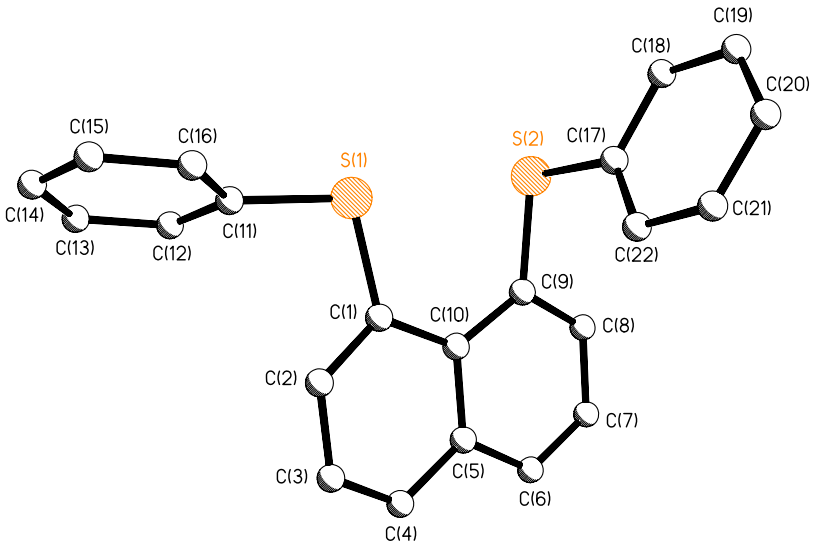

Figure 3-2. Structural representation of (1,8-diphenylsulfuryl)napthalene (**3.1**).

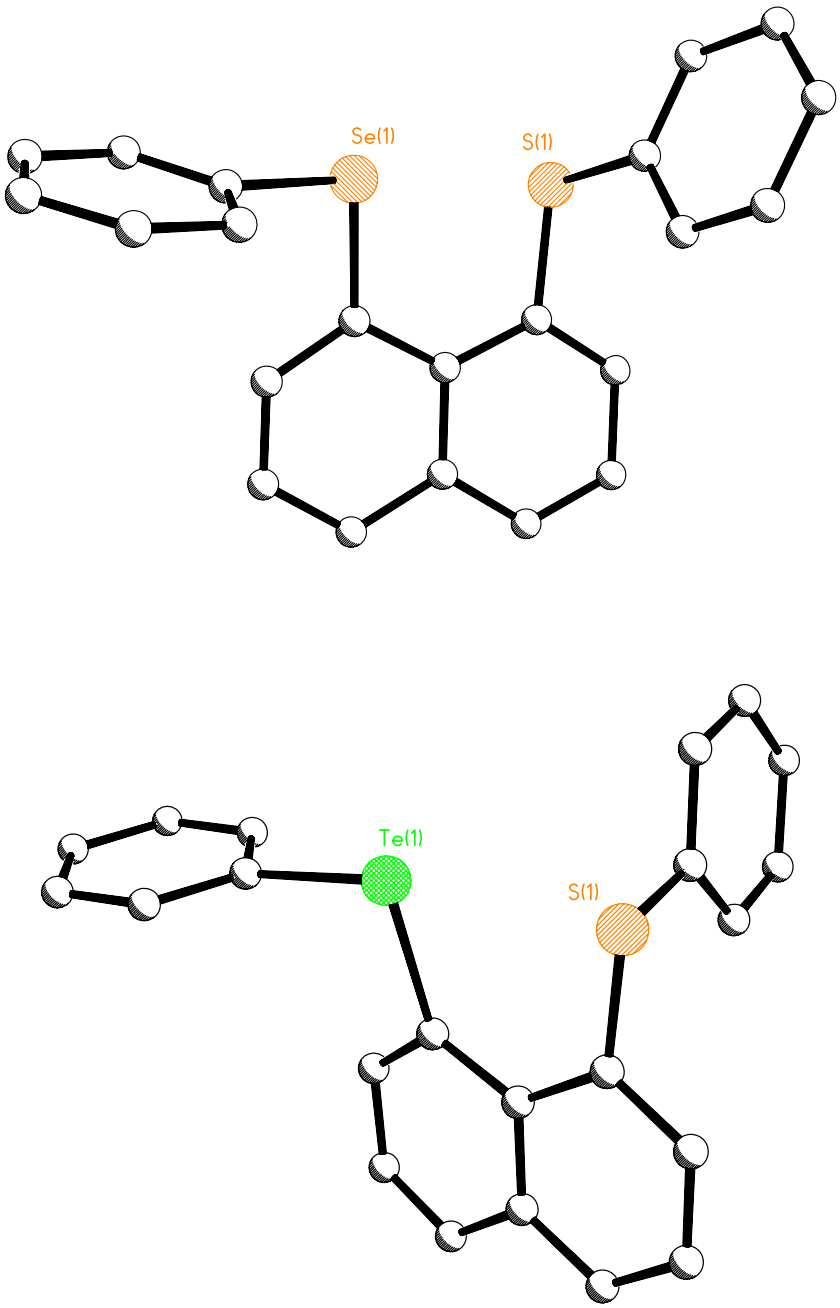

Figure 3-3. Structural representations of **3.2** (top) and **3.3a** (bottom).

3.2.1. Structural Similarities

The structural similarities and differences in **3.1**-**3.3** can best be described by comparing the C-E bond lengths and *peri*-distances, in-plane deflections of the substituents, out-of-plane deflections of the substituents, and naphthalene ring distortions. Table 3-1 contains selected bond lengths and angles for **3.1**-**3.3**.

As might be expected, the E-C(1) bond length increases as the size of E increases, from 1.783(4):1.794(3) Å (**3.1**), to 1.907(9) Å (**3.2**), to 2.100(5) Å (**3.3b**), to 2.141(5) Å (**3.3a**). The S-C(9) bond lengths are all similar, ranging from 1.770(5) Å to 1.813(8) Å. The E…E *peri*-distance in all of the compounds are very similar, at 3.0036(13) Å (**3.1**), 3.063(2) Å (**3.2**), 3.0684(13) Å (**3.3a**) and 3.0984(11) Å in (**3.3b**), increasing only slightly as the chalcogen atom gets bigger.

The in-plane deflections of the *peri*-substituents are very similar across all

Table 3-1. Selected bond lengths (Å) and angles (°) for **3.1**-**3.3**.

	3.1	**3.2**	**3.3a**	**3.3b**
S(1)…E[1]	3.0036(13)	3.063(2)	3.0684(13)	3.0984(11)
E[1] - C(1)	1.794(3)	1.907(9)	2.141(5)	2.100(5)
S - C(9)	1.783(4)	1.813(8)	1.770(5)	1.771(5)
C(1)-E[1]-C(11)	102.01(17)	98.1(3)	95.1(2)	94.7(2)
E[1]-C(1)-C(2)	118.2(2)	119.9(6)	117.2(4)	117.2(3)
E[1]-C(1)-C(10)	121.8(2)	122.3(6)	122.9(3)	123.2(4)
C(9)-S-C(17)	102.56(17)	102.1(4)	103.2(2)	101.0(3)
S-C(9)-C(8)	115.1(2)	113.8(7)	116.4(3)	116.0(4)
S-C(9)-C(10)	124.5(2)	122.3(6)	122.8(4)	122.9(3)
C(2)-C(1)-C(10)	120.0(3)	117.7(8)	119.6(4)	119.5(4)
C(10)-C(9)-C(8)	120.4(3)	123.5(8)	120.7(4)	120.8(5)
C(1)-C(10)-C(9)	126.8(3)	127.8(7)	126.1(4)	126.1(5)
C(4)-C(5)-C(10)-C(1)	-2.3(5)	7.4(13)	4.3(9)	-5.2(9)
C(6)-C(5)-C(10)-C(9)	-1.9(5)	2.9(13)	4.3(9)	-4.3(9)
C(4)-C(5)-C(10)-C(9)	177.2(3)	-174.5(8)	-174.6(6)	173.8(5)
C(6)-C(5)-C(10)-C(1)	178.6(3)	-175.2(8)	-176.9(6)	176.7(6)
Mean Plane Deviations				
S	-0.162(4)	-0.32(11)	0.146(7)	0.449(7)
E[1]	0.270(4)	0.43(11)	-0.565(7)	-0.406(7)

[1]E = S for **3.1**, Se for **3.2**, or Se for **3.3**.

the molecules. The E-C(1)-C(2) angles range from 117.2(4)° to 119.9(6)° and the E-C(1)-C(10) angles range from 121.8(2)° to 123.2(4)°. At the *peri*-position occupied by sulfur, the S-C(9)-C(8) angles range from 113.8(7)° to 116.4(3)° and the S-C(9)-C(10) angles range from 122.3(6)° to 124.5(2)°. At both *peri*-positions in all the molecules, the outer angles are smaller than the inner angles, indicating that the chalcogen atoms are leaning outward, away from each other. The angle C(9)-S-C(17) (C_{Ph}-S-C_{Naph} or phenyl-sufur-*peri*-carbon) is nearly the same in all of the -SPh substituents, which range from 101.0(3)° to 103.2(2)°. Both the high and low angles are in **3.3** (**a** and **b**, respectively). This might suggest that this distortion is a result of crystal packing effects, since **3.3a** and **3.3b** have the same structure. The C(1)-Se-C(11) angle is 98.1(3)° and the C(1)-Te-C(11) angles are 95.1(2)° to 94.7(2)°.

Very minor out-of-plane deflections of the *peri*-substituents occur in **3.1**-**3.3**. In all of them, the substituents deviate to different sides of the naphthalene plane. Both the smallest and the largest deviations occur in **3.3a**, in which the deviations are 0.146(7) Å and -0.565(7) Å.

The distortions in the naphthalene ring can be compared using the angles around the *peri*-positions (where the ideal angle is 120°) and the torsion angles containing the bridgehead carbons (where the ideal is 0° or 180°). The C(2)-C(1)-C(10) and C(10)-C(9)-C(8) angles are very similar in the sulfur and tellurium analogs (very close to 120° for both), but are ~3° different in the selenium analog (117.7(8)° and 123.5(8)°, respectively). The C(1)-C(10)-C(9) angle is similar in all of the compounds. The distortions in the torsion angles are smallest in the disulfur compound **3.1**, increase in the tellurium analog **3.3**, and further increase in the selenium analog **3.2**.

The above discussion illustrates that, despite the differences in the sizes of the chalcogen atom, **3.1**-**3.3** aren't structurally very different from one another. The selenium analog, **3.2**, seems to have more distortion in the naphthalene ring, especially the C(4)-C(5)-C(10)-C(9) angle, than in the other two compounds, but not by a large degree compared to the others. The only other noticeable difference is in the C_{Naph}-E-C_{Ph} angle, which decreases as the size of the chalcogen increases.

This alters the geometry around the E atom from an ideal "bent" geometry (bond angle ~110°). The possibility of a hypervalent interaction between *peri*-substituents could be forcing the geometry away from ideal, since the alteration of the C_{Naph}-E-C_{Ph} angle brings S(1)-E-C_{Ph} into an approximately linear configuration well within the Van der Waals radii of the two *peri*-substituents.[1] There are several examples where *peri*-substituted chalcogen naphthalene compounds form linear hypervalent three center four electron (3c-4e) systems (Figure 3-4).[2]

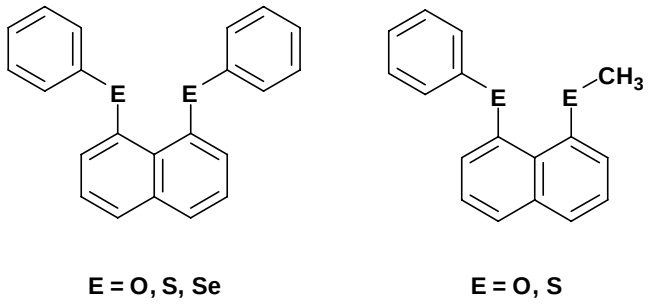

Figure 3-4. Examples of *peri*-substituted naphthalene compounds, which have been reported to have 3c-4e hypervalent interactions between E…E-C.[2]

3.3. Reaction with Br_2

It is intriguing that, despite their structural similarities, compounds **3.1**-**3.3** respond very differently to the introduction of multiple equivalents of elemental bromine (Figure 3-5). Reaction of Br_2 with **3.1** results in the poly-brominated product **3.4**, the addition of Br_2 to **3.2** formed **3.5**, an ionic compound with a bromine-substituted selenium atom on a naphthalene-based cation and a Br_3^- counter ion. Finally, the addition of excess Br_2 to **3.3** gives **3.6**, where the Te atom has simply inserted into the Br-Br bond. The crystal structures of **3.4**-**3.6** have been solved and the refinement data can be found in Appendix 1.

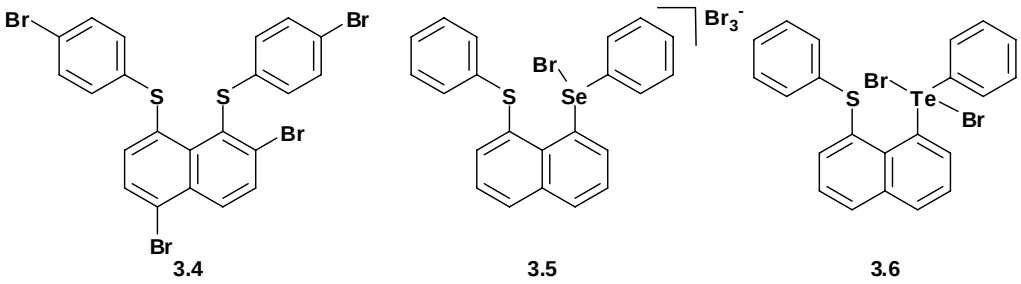

Figure 3-5. Products of the reaction of **3.1**, **3.2**, and **3.3** with Br_2 forming **3.4** (left), **3.5** (middle), and **3.6** (right), respectively.

While initially surprising, these results are consistent with the literature. A study published in 2007 found ~150 structurally characterized compounds containing the Br-E-Br motif, where E is S, Se, or Te.[3] The most common compounds contain tellurium, followed by selenium, and then sulfur. Refining the search (CSD, version 5.30, updated May 2009) by forcing E to also be attached to two carbon atoms resulted in fewer hits: 28 tellurium adducts, 13 selenium, and no sulfur compounds. Sulfur, rather than adding one or both bromine atoms, usually forms linear charge-transfer compounds. There is only one known diorganosulfur compound with an S-Br-Br motif (Figure 3-6), while the S-I-I motif is more common (17 compounds).[4] The selenium and tellurium compounds in the search have all formed oxidative addition products with the formula Br-E-Br and *quasi*-linear Br-E-Br angles (Br-Se-Br angles range from 169.9° to 180.0° and Br-Te-Br angles range from 171.1° to 179.4°).[5, 6]

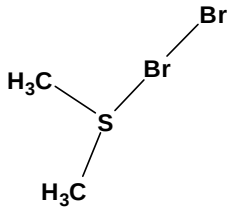

Figure 3-6. The only known S-Br-Br diorganochalcogen compound.

*3.3.1. Compound **3.4***

Elemental bromine does not react with benzene without a catalyst present. However, in the reaction of bromine with phenol, the -OH group acts as an *ortho*/*para* director and activates the aromatic ring towards electrophilic attack. When an excess of Br_2 is added to phenol, three sequential electrophilic substitution reactions occur (Scheme 3-1). The generally accepted mechanism of an electrophilic aromatic substitution at the *para*- and *ortho*- positions in phenol is shown in Scheme 3-2.[7]

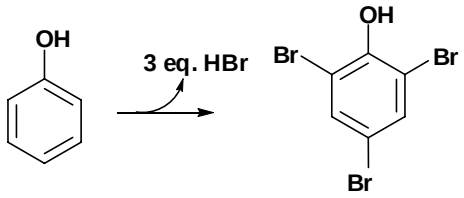

Scheme 3-1. Reaction of excess Br_2 addition to phenol.

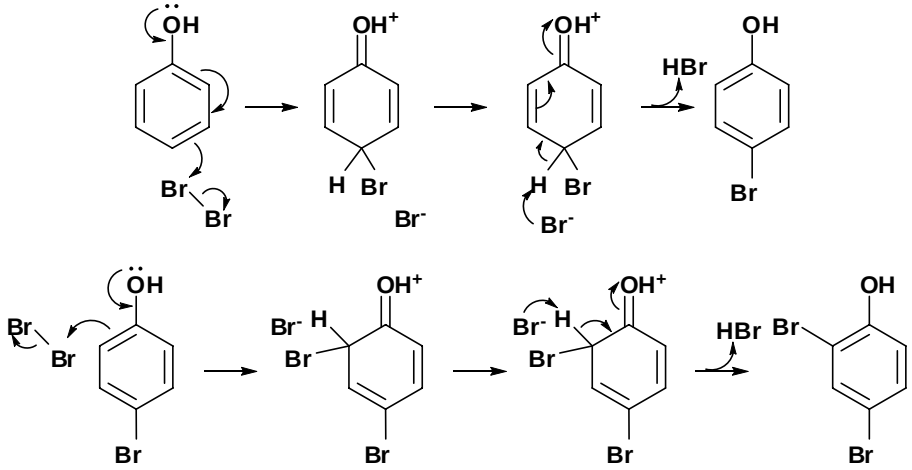

Scheme 3-2. Mechanism for Br_2 addition at the *para*- and *ortho*- positions in phenol.

Compound **3.1**, when reacted with Br_2, shows the same sort of behavior as phenol and forms **3.4**. Compound **3.4** crystallizes in the *C*2/*c* space group with R_1 = 8.66% (Figure 3-7). The pattern of substitution suggests that the thioether groups are activating the phenyl ring in the *para*-position and the naphthalene rings in one *para*- and one *ortho*-position, allowing electrophilic substitution of bromine on all of the aromatic rings to occur. It may be that further substitution did not occur due to the steric restrictions imposed on the molecule.

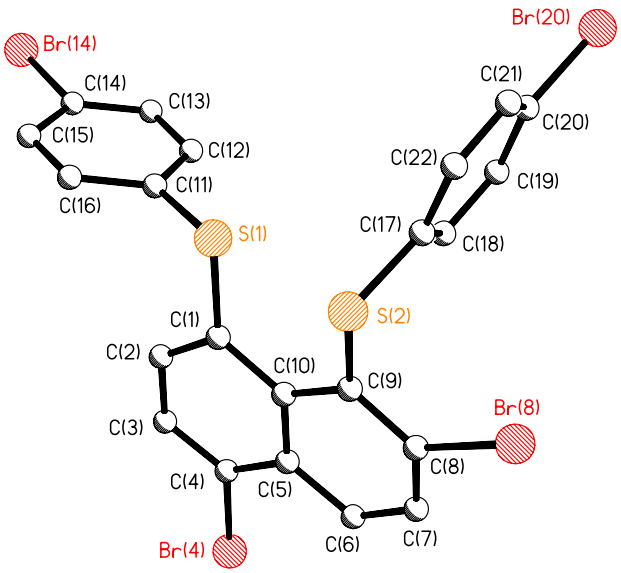

Figure 3-7. Structural representation of **3.4**.

The two *peri*-substituted disulfur naphthalene derivatives **3.1** and **3.4** are structurally very similar despite the bromine substituents on **3.4**. Table 3-2 shows selected bond distances and angles of both the starting material **3.1** and the brominated product **3.4**. Most of the angles and bond lengths are the same within error, with only a few slight differences: the S(1)…S(2) distance is slightly shorter in **3.4** (2.935(4) Å) than in **3.1** (3.0036(13) Å), the S(1) and S(2) atoms lie slightly further from the plane in **3.4**, and the naphthalene ring (perhaps because of the

Table 3-2. Selected bond lengths (Å) and angles (°) for **3.4** and **3.1**.

	3.4	**3.1**
S(1)…S(2)	2.935(4)	3.0036(13)
S(1) - C(1)	1.787(11)	1.794(3)
S(2) - C(9)	1.780(11)	1.783(4)
C(1)-S(1)-C(11)	101.5(5)	102.01(17)
S(1)-C(1)-C(2)	118.9(8)	118.2(2)
S(1)-C(1)-C(10)	122.3(8)	121.8(2)
C(9)-S-C(17)	102.3(5)	102.56(17)
S(2)-C(9)-C(8)	117.7(8)	115.1(2)
S(2)-C(9)-C(10)	121.6(8)	124.5(2)
C(2)-C(1)-C(10)	118.8(10)	120.0(3)
C(10)-C(9)-C(8)	120.3(9)	120.4(3)
C(1)-C(10)-C(9)	126.0(10)	126.8(3)
C(4)-C(5)-C(10)-C(1)	-4.9(15)	-2.3(5)
C(6)-C(5)-C(10)-C(9)	-2.8(15)	-1.9(5)
C(4)-C(5)-C(10)-C(9)	176.2(9)	177.2(3)
C(6)-C(5)-C(10)-C(1)	176.1(10)	178.6(3)
Mean Plane Deviations		
S(2)	-0.343(13)	-0.163(4)
S(1)	0.343(13)	0.270(4)

two bromo-substituents along with the two -SPh substituents) is more distorted in **3.4**, approximately 2° in all four torsion angles.

*3.3.2. Compound **3.5***

A series of pathways have been proposed by Detty *et al*. for the mechanism of oxidative addition of Br_2 to a selenium or tellurium atom in a diorganochalcogen (Scheme 3-3).[8] We can address the proposed mechanisms using **3.5**, plus an additional structure (**3.7**) will be introduced.

The first step in any of the possible mechanisms in Scheme 3-3 is the association of Br_2 with the chalcogen to form a charge-transfer complex. Bromine can either interact with the chalcogen "side on" as an η^2-complex (**a**) or "end on" as an η^1-complex (**b**). If Br_2 forms an η^1-complex with the chalcogen atom, the

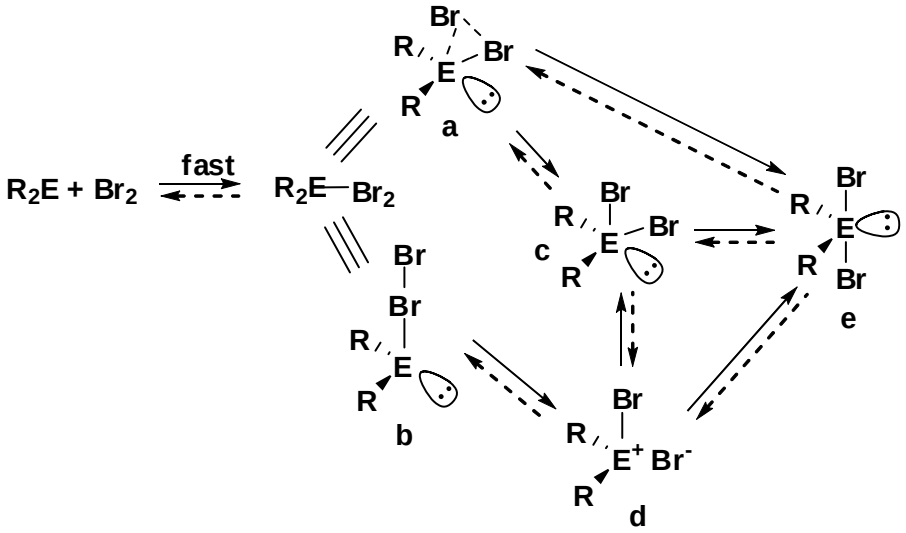

Scheme 3-3. Proposed mechanism for the oxidative addition of Br_2 to ER_2, where E = Se or Te, adapted from Detty *et al*. The initial fast reaction is association of Br_2 with the heteroatom, either in an η^1 or η^2 fashion. Concerted associative oxidative addition across an edge of the η^2-complex might lead directly to the final product **e**, or to *cis*-dibromide ligands, as in **c**, before proceeding to **e**. Alternatively, a dissociative mechanism starting from the η^1 complex would lead an ionic intermediate **d**, which would then collapse to *trans*-diaxial **e** and/or *cis*-chalcogen dibromide **c**.

interaction polarizes the bromine-bromine bond for further reaction. Although there are no discreet "end on" dibromine-chalcogen complexes known, there are two "extended charge transfer networks" that utilize Br_n bridges and six η^1 diiodine-selenium complexes that have been reported.[6,9-15] All of these I_2-selenium charge-transfer complexes utilize a selenium atom attached to an aliphatic backbone (Figure 3-8). The Se-I and I-I bond lengths range from 2.734(1)-2.829(4) Å and 2.870(3)-2.956(3) Å, respectively, and all of the Se-I-I bond angles are nearly linear (range from 174.3° to 179.3°).[9-14]

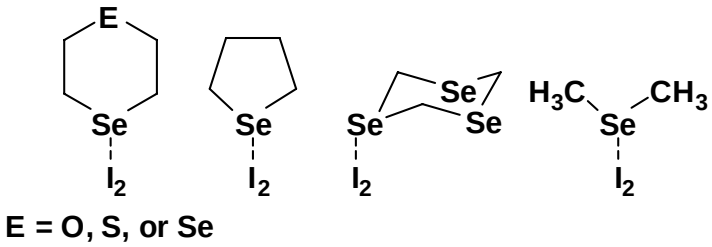

Figure 3-8. Known examples of selenium-iodide charge transfer complexes.

Compound **3.7**, depicted in Figure 3-9, is a discreet, η^1-diiodine-selenium naphthalene complex. To our knowledge, this is the first selenium-diiodine charge-transfer complex with an aromatic backbone (i.e. with electron withdrawing substituents attached to the selenium atom). Since the substituents dictate the electronic environment of the selenium, they directly affect the Se-I and I-I bond distances. Therefore, this naphthalene derivative has the longest Se-I bond distance (2.9795(8) Å) and the shortest I-I distance (2.7987(6) Å) of any of the end-on diiodine-selenium complexes in the literature. The long Se(1)-I(1) and

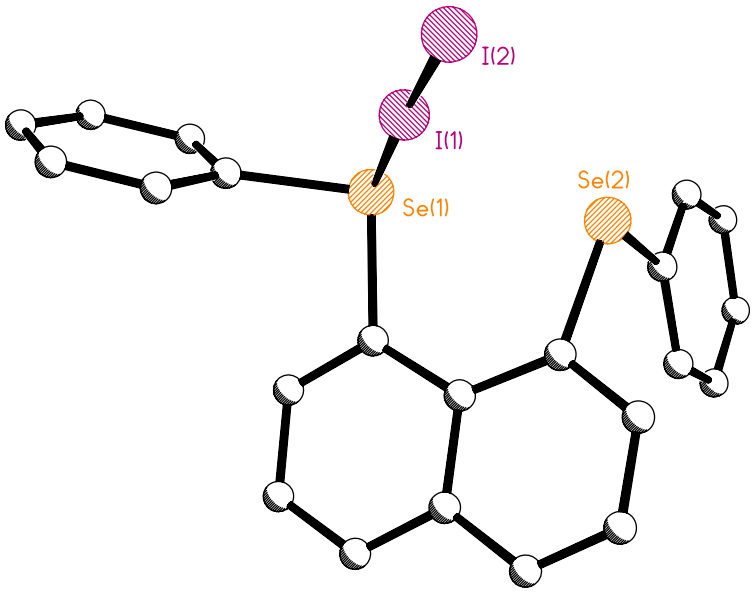

Figure 3-9. Structural representation of **3.7**.

short I(1)-I(2) bond lengths (in the naphthalene derivative) suggest that, logically enough, given the more electron-withdrawing substituents, the selenium in **3.7** is a weaker electron donor to I_2 than is the selenium atom in the aliphatic diorganoselenides.

Compound **3.7** is an analog of **b** in Scheme 3-3. While it is not certain why **3.7** does not react further, reasons can be suggested. Since there are a number of dibrominated diorganoselenium compounds in the literature, but no η^1- Se-Br_2 complexes (*e.g.* **b** in Scheme 3-3) known, it may mean that either **3.7** is thermodynamically more stable than the I^- disassociation product (analogous to **d** in Scheme 3-3) would be, or that Br_2 can from a stronger interaction in the charge transfer intermediate. A stronger interaction would more strongly polarize the Br-Br bond, which would promote Br-Br bond cleavage on the path toward a *trans*-dibrominated product. Regardless, the η^1- coordination of elemental iodine to the selenium atom is proof that this sort of interaction is possible in naphthalene based organochalcogens.

If cleavage of the Br-Br bond occurs, an ionic intermediate like compound **d** in scheme 3-3 is formed. In **d**, the cation has one bromine atom bound to the chalcogen atom and the other bromide serving as a counter ion. We have observed that addition of Br_2 to **3.2** resulted in the formation of the cationic mono-brominated compound (**3.5**) with a Br_3^- counter ion. Compound **3.5** crystallizes in the $P2_1/c$ space group with R_1 = 6.99% (Figure 3-10). Since selenium usually proceeds to *trans*-dibromination, the structure of **3.5** is highly unusual. The only other known example of a diorganoselenobromium cation has a tin hexachloride anion (Scheme 3-4).[16]

Given the unusual structure of **3.5** and its similarity to **d** in Scheme 3-3, we propose that it could be a trapped intermediate in the oxidative addition mechanism. The inability of **3.5** to further react with the bromide could be due to three reasons: either the selenium is too sterically hindered to accept another bromide (fairly self-explanatory due to the bulky phenyl, naphthalene ring, and bromine already attached), the hypervalent Br_3^- anion is too stable to further react, or the sulfur could donate electron density to the positively charged selenium

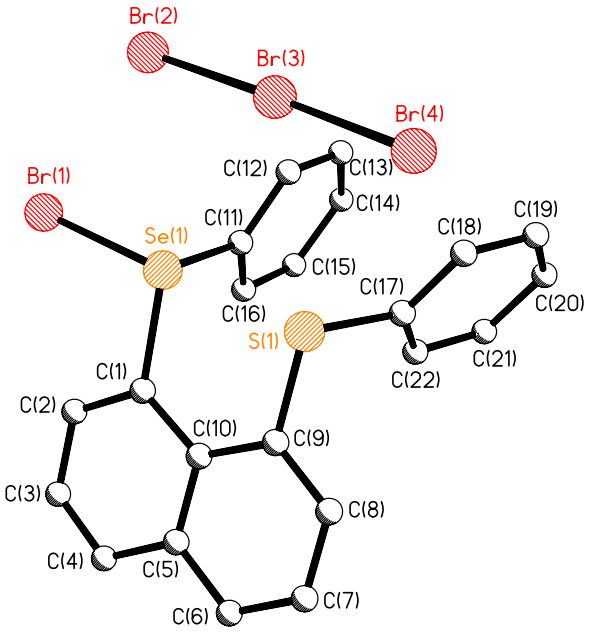

Figure 3-10. Structural representation of **3.5**.

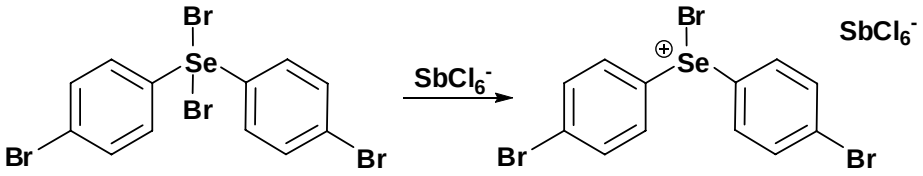

Scheme 3-4. Reaction producing a selenobromium cation.

atom, reducing its electrophilicity by way of a weak hypervalent Br-Se…S interaction. This would reduce the electrophilicity of the monobrominated selenium such that it does not want the electron density offered by a bromide anion.

The idea of electron donation from sulfur to selenium is not contradicted by the crystal structure of compound **3.5**. A CDS (version 5.30, updated May 2009) search of complexes containing an assigned Se-S single bond resulted in 19

compounds having Se-S bond lengths that range from 2.158(4) Å to 2.291(1) Å.[17, 18] When Se and S are in the *peri*-positions of a rigid naphthalene ring, an S-Se bond has a distance of 2.2442(1) Å.[19] In **3.5**, the Se(1)…S(1) distance is 2.721(2) Å, which is slightly shorter than the non-bonded Se(1)…S(1) distance in precursor **3.2** (3.063(2) Å), but much longer than any of the formal Se-S single bond distances found in the CSD search. This leaves room for the possibility of a positive interaction weaker than a formal single bond.

Based on the crystal structure, there does not appear to be any other reason for the sulfur and selenium to be forced closer toward each other besides a favorable interaction between them. Table 3-3 contains selected bond distances and angles for **3.2** and for the mono-brominated product, **3.5**. The largest structural difference in the backbone lies in the inner *peri*-angle, Se(1)-C(1)-C(10)

Table 3-3. Selected bond lengths (Å) and angles (°) for **3.5** and **3.2**.

	3.5	**3.2**
S(1)…Se(1)	2.721(2)	3.063(2)
Se(1) - C(1)	1.955(8)	1.907(9)
S(1) - C(9)	1.796(9)	1.813(8)
C(1)-Se(1) -C(11)	101.9(3)	98.1(3)
Se(1)-C(1)-C(2)	119.2(7)	119.9(6)
Se(1) -C(1)-C(10)	119.5(6)	122.3(6)
C(9)-S(1)-C(17)	102.7(4)	102.1(4)
S(1)-C(9)-C(8)	118.3(7)	113.8(7)
S(1)-C(9)-C(10)	119.8(7)	122.3(6)
C(2)-C(1)-C(10)	121.2(8)	117.7(8)
C(10)-C(9)-C(8)	121.7(8)	123.5(8)
C(1)-C(10)-C(9)	126.0(8)	127.8(7)
C(4)-C(5)-C(10)-C(1)	0.0(11)	7.4(13)
C(6)-C(5)-C(10)-C(9)	0.1(10)	2.9(13)
C(4)-C(5)-C(10)-C(9)	-179.2(8)	-174.5(8)
C(6)-C(5)-C(10)-C(1)	179.3(8)	-175.2(8)
Mean Plane Deviations		
S(1)	0.139(11)	-0.320(11)
Se(1)	0.112(11)	0.432(11)

and the outer *peri*-angle S(1)-C(9)-C(8). These angles suggest that both the Se(1) substituent and the S(1) substituent lean in toward each other in **3.5**. Another difference lies in the torsion angles, where **3.5** is quite planar compared to **3.2**. The planarity of the entire naphthalene-substituent system in **3.5** suggests the possibility of system-wide resonance in the molecule, including all of the carbon atoms, both of the *peri*-substituents, and the bromine atom bound to the selenium. The two phenyl rings in **3.5** are not in the plane of the rest of the atoms and therefore not part of such a system.

In hypervalent interactions involving three centers, four electrons are shared between the three centers- two bonding and two non-bonding. Hypervalency is suggested when the central atom in the set bears more electrons than an octet within its valence shell in a Lewis-dot structure (a classic example of this is the Br_3^- ion also present in **3.5**). In order for hypervalency to occur, a linear orientation between the three centers is required.[20] Correspondingly, the structure of **3.5** shows a very linear arrangement of the bromine, selenium, and sulfur atoms (176.33(6)°). In fact, the *peri*-positions in naphthalene seem to provide a particularly good environment for three atoms to precisely align in close proximity and form a three center four electron (3c-4e) system, as shown in Figure 3-11. Some possible resonance contributors to **3.5** are shown in Figure 3-12. Structures **A** and **B** are examples of hypervalency; however, due to the long

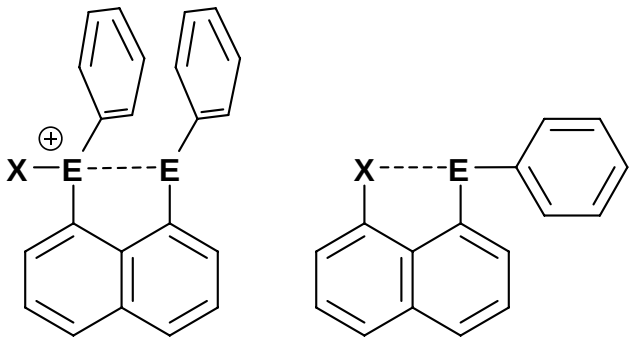

Figure 3-11. Examples of linear, weak hypervalent 3c-4e type interactions, X-E…E (left) and X…E-C (right).

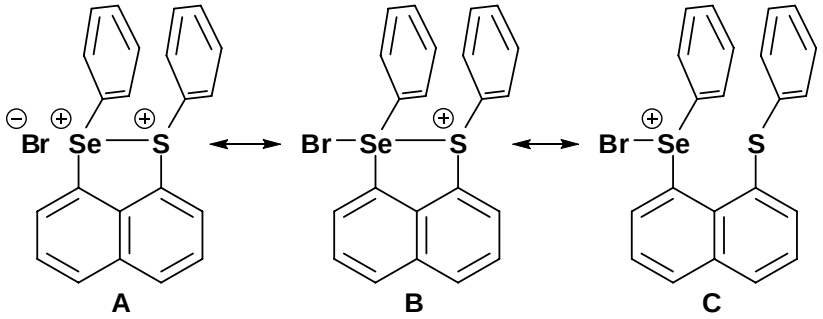

Figure 3-12. Possible resonance structures of **3.5**.

Se(1)…S(1) distance, we believe structure **C**, with no Se-S bond interaction, is a greater contributor than the other two.

*3.3.3. Compound **3.6***

The third *peri*-substituted naphthalene, a tellurium analog, is **3.3**. Reaction of Br_2 with this compound results in the *trans*-dibrominated product **3.6**. Compound **3.6** crystallizes in the *C*2/*c* space group with R_1 = 6.96% (Figure 3-13). Table 3-4 lists selected bond distances and angles for **3.6** and **3.3**.

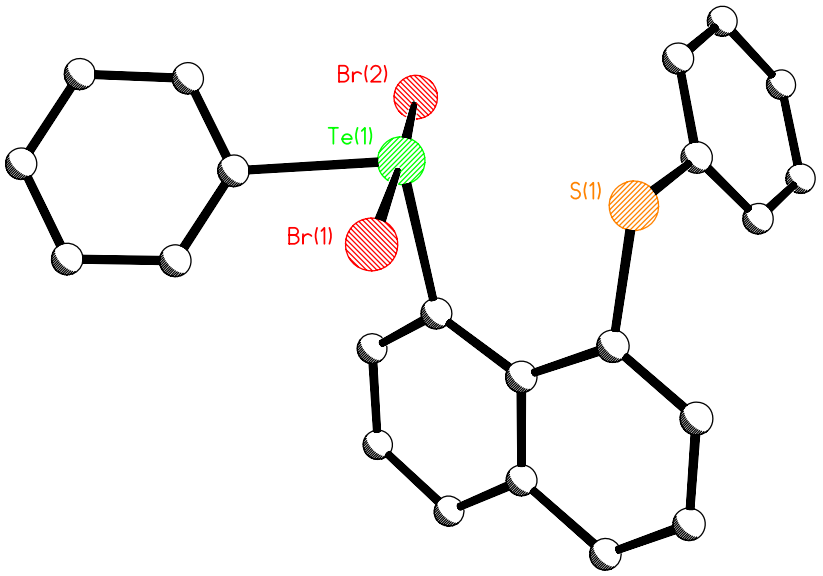

Figure 3-13. Structural representation of **3.6**.

Table 3-4. Selected bond lengths (Å) and angles (°) for **3.6**, **3.3a**, and **3.3b**.

	3.6	**3.3a**	**3.3b**[1]
S(1)…Te(1)	3.075(2)	3.0684(13)	3.0984(11)
Te(1) - C(1)	2.124(10)	2.141(5)	2.100(5)
S(1) - C(9)	1.782(11)	1.770(5)	1.771(5)
C(1)-Te(1)-C(11)	97.2(3)	95.1(2)	94.7(2)
Te(1)-C(1)-C(2)	116.0(7)	117.2(4)	117.2(3)
Te(1) -C(1)-C(10)	123.1(7)	122.9(3)	123.2(4)
C(9)-S(1)-C(17)	102.6(4)	103.2(2)	101.0(3)
S(1)-C(9)-C(8)	116.6(8)	116.4(3)	116.0(4)
S(1)-C(9)-C(10)	121.3(7)	122.8(4)	122.9(3)
C(2)-C(1)-C(10)	120.9(19)	119.6(4)	119.5(4)
C(10)-C(9)-C(8)	121.8(10)	120.7(4)	120.8(5)
C(1)-C(10)-C(9)	127.6(9)	126.1(4)	126.1(5)
C(4)-C(5)-C(10)-C(1)	4.3(13)	4.3(9)	-5.2(9)
C(6)-C(5)-C(10)-C(9)	2.3(12)	4.3(9)	-4.3(9)
C(4)-C(5)-C(10)-C(9)	-174.3(8)	-174.6(6)	173.8(5)
C(6)-C(5)-C(10)-C(1)	-179.1(8)	-176.9(6)	176.7(6)
Mean Plane Deviations			
S(1)	0.250(12)	0.146(7)	0.449(7)
Te(1)	-0.401(12)	-0.565(7)	-0.406(7)

[1]The analogous numbering scheme.

It is interesting that even with the addition of two bulky bromine atoms, the structural features of **3.6** and **3.3** are very similar. The torsion angles C(6)-C(5)-C(10)-C(9) and C(6)-C(5)-C(10)-C(1) are slightly more distorted and the S(1) atom lies further from the naphthalene plane in **3.6**, but both differences are very small. The sulfur deviation, at least, is likely due to the need to make room for one of the bromine atoms. The Br-Te-Br angle in **3.6** of 176.67(4)° is similar to those in previously reported R_2TeBr_2 complexes.[21-23] The Te(1)-Br(1) (2.702(11) Å) and Te(1)-Br(2) (2.6688(12) Å) distances are quite similar, with the Br-Te-Br axis turned so that one Br atom sits closer to the sulfur than does the other Br atom. In the solid state, an inversion center between two molecules of **3.6** creates a Te(1)…Br(1)' distance and Te(1)'…Br(1) distance of 3.69 Å (Figure 3-

14). From the molecular structure, it certainly seems that **3.6** is simply the product of the complete oxidative addition of one molecule of elemental bromine to the tellurium atom (**e** in Scheme 3-3).

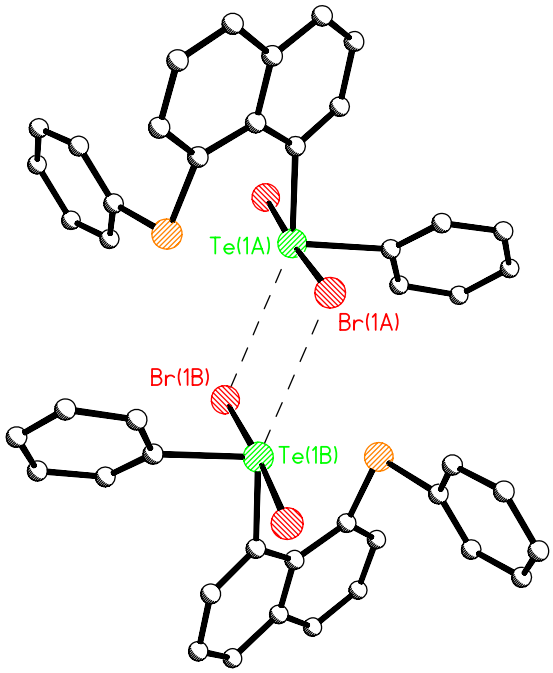

Figure 3-14. Packing interactions in **3.6**.

3.4. Conclusion

Three *peri*-substituted naphthalene compounds containing -SPh and -EPh (where E = S (**3.1**), Se (**3.2**), and Te (**3.3**)) as substituents have been crystallized and their crystal structures reported. Despite the size difference in the chalcogen atom at the *peri*-position, these three compounds are structurally very similar. However, when these compounds are reacted with bromine, they form quite different products.

In **3.1**, the sulfur atoms act to activate the various aromatic rings for oxidative addition of the bromine at the *para*- and *ortho*-positions to form **3.4**. This may be because disubstituted sulfur simply holds its electron density too close to interact with the dihalogen molecule, or perhaps the sulfur atom is too small and the naphthalene and phenyl rings too bulky, to fit one or more additional substituents on the sulfur.

Of the compounds presented in this chapter, the selenium-diiodine compound **3.7**, the monobrominated selenium compound **3.5**, and the dibrominated tellurium compound **3.6** are relevant to the mechanism of oxidative addition of dihalogen to organochalcogen atoms presented by Detty *et al*. and reproduced in Scheme 3-3.[8] While compound **3.6** is the product of dihalogen addition no matter which mechanism in Scheme 3-3 is taken, **3.7** and **3.5** are believed to potentially be trapped intermediates. These structures (and ones from the literature) cast doubt as to whether "side-on" association of a dihalogen to a chalcogen atom occurs and also on formation of the *cis*-disubstituted product (**a** or **c** in Scheme 3-3). Quite simply, there are not any η^2 dihalogen-chalcogen complexes known, and also, no *cis* disubstituted chalcogens. Compound **3.5**, in particular, is potentially a trapped intermediate in the oxidation pathway, analogous to structure **d** in Scheme 3-3. This is in part evidenced by its uniqueness in the literature.

Given this evidence, we can suggest that the oxidation of diorganochalcogen compounds proceeds through a pathway such as that shown in Scheme 3-5. In this pathway, there is no need for a *cis*-dihalogen complex (**c** in Scheme 3-3) to form, as it will be less stable than the *trans*-substituted product.

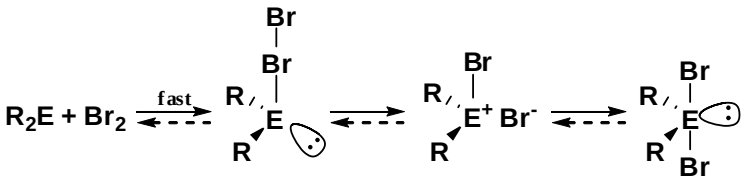

Scheme 3-5. Proposed mechanism for the oxidative addition of Br_2 to ER_2.

Additionally, since it seems that dihalogens do not associate side-on with disubstituted chalcogen atoms, a *cis*-intermediate does not need to form on the way to product. Therefore, it is most straightforward for the oxidative addition to proceed from end-on association to an ionic intermediate, and from there to a di-substituted product. While this research does not definitively answer the question of mechanism, we think it does make a start.

3.5. References

1. A. Bondi, *J. Phys. Chem.,* 1964, 68, 441-452.

2. S. Hayashi and W. Nakanishi, *Bull. Chem. Soc. Jpn.,* 2008, 81, 1605-1615.

3. M. C. Aragoni, M. Arca, F. A. Devillanova, A. Garau, F. Isaia, V. Lippolis and A. M. Mancini, *Bioinorg. Chem. Appl.,* 2007, 2007, 1-46.

4. B. Regelmann, K. W. Klinkhammer and A. Schmidt, *Z. Anorg. Allg. Chem.,* 1997, 623, 1633-1638.

5. J. D. McCullough and G. Hamburger, *J. Am. Chem. Soc.,* 1941, 63, 803-807.

6. W. Nakanishi, S. Hayashi, S. Yamaguchi and K. Tamao, *Chem. Commun.,* 2004, 140-141.

7. J. Clayden, N. Greeves, S. Warren and P. Wothers, *Organic Chemistry*, New York:Oxford University Press, 2001.

8. M. R. Detty, A. E. Friedman and M. McMillan, *Organometallics,* 1994, 13, 3338-3345.

9. G. Y. Chao and J. D. McCullough, *Acta Cryst.,* 1961, 14, 940-945.

10. H. Maddox and J. D. McCullough, *Inorg. Chem.,* 1966, 5, 522-526.

11. S. M. Godfrey, C. A. McAuliffe, R. G. Pritchard and S. Sarwar, *J. Chem. Soc, Dalton Trans.,* 1997, 1031-1036.

12. M. Arca, F. Cristiani, F. A. Devillanova, A. Garau, F. Isaia, V. Lippolis, G. Verani and F. Demartin, *Polyhedron,* 1997, 16, 1983-1991.

13. H. Hope and J. D. McCullough, *Acta Cryst.,* 1962, 15, 806-807.

14. H. Hope and J. D. McCullough, *Acta Cryst.,* 1964, 17, 712-718.

15. P. D. Boyle and S. M. Godfrey, *Coord. Chem. Rev.,* 2001, 223, 265-299.

16. A. Jung and G. Wolmershauser, *Z. Naturforsch.,* 1997, 52b, 345-350.

17. G. Rabe, J. Sundermeyer, H. W. Roesky, H. Schmidt and M. Noltemeyer, *Chem. Ber.,* 1990, 123, 691-696.

18. M. Kulcsar, A. Silvestru, C. Silvestru, J. E. Drake, C. L. B. Macdonald, M. B. Hursthouse and M. E. Light, *J. Organomet. Chem.,* 2005, 690, 3217-3228.

19. J. Meinwald, D. Dauplaise and J. Clardy, *J. Am. Chem. Soc.,* 1977, 99, 7743-7744.

20. W. Nakanishi in *Handbook of Chalcogen Chemistry, New Perspectives in Sulfur, Selenium and Tellurium*, ed. F. A. Devillanova, 2006, 644-668.

21. A. Chauhan, A. Kumar, R. Srivastava and R. Butcher, *Struct. Chem.,* 2007, 18, 181-186.

22. M. Asahara, S. Taomoto, M. Tanaka, T. Erabi and M. Wada, *Dalton Trans.,* 2003, 973-979.

23. A. K. S. Chauhan, P. Singh, A. Kumar, R. C. Srivastava, R. J. Butcher and A. Duthie, *Organometallics,* 2007, 26, 1955-1959.

CHAPTER 4

A ONE-POT SYNTHESIS OF NAPHTHO[1,8-*c,d*]-1,2-DISELENOLE AND A NEW SYNTHESIS OF ITS ALKYLATED COUNTERPARTS

4.1. Introduction

The first synthesis of naphtho[1,8-*c,d*]-1,2-diselenole (Se_2naph) was reported in 1977 by Meinwald *et al.* (Figure 4-1).[1] In their work, Se_2naph was synthesized by adding two equivalents of selenium powder to dilithionaphthalene and then exposing the reaction mixture to air to obtain the desired product in 18-22% yield. Today this preparation is still the most referenced procedure for making this compound.[1] In 1988, Yui *et al* reported a different synthetic route for Se_2naph, which involves the addition of sodium diselenide (Na_2Se_2) to 1,8-dichloronaphthalene, producing Se_2naph in a 69% yield.[2]

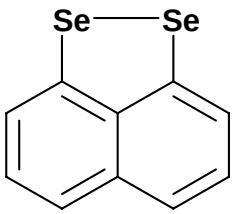

Figure 4-1. Naphtho[1,8-*c,d*]-1,2-diselenole (Se_2naph).

Both of these procedures are in reality quite lengthy and present a number of synthetic hurdles. For example, the experimental details reported by Meinwald *et al* are sparse and contain essentially no directions on how to expose the reaction mixture to air, which usually results in low yields. Others have reported synthesizing dilithionaphthalene from 1,8-dibromonaphthalene.[3,4] This compound, like the 1,8-dichloronaphthalene used in Yui's synthesis, is itself difficult to make and is usually obtained in low yield.[5] Another problem with Yui's method is the use of Na_2Se_2, which is dangerous to synthesize due to the handling of elemental sodium and selenium, and ammonia gas.[2] For an inexperienced chemist, the

"easiest" synthetic route to follow in order to produce Se_2naph is Meinwald's. However, the product is obtained in yields as low as 3%.

In 1994, a new synthesis for the sulfur analog, naphtho[1,8-*c,d*]-1,2-dithiole (S_2naph), was published.[6] Most interestingly, the procedure revealed that unsubstituted naphthalene can be used as a starting material and can be directly dilithiated using butyllithium to form 1,8-dilithium naphthalene. Following addition of elemental sulfur to the reaction, and work up, a 51% yield of S_2naph was reported. To date, this one-pot procedure is the simplest synthetic route reported for S_2naph.

We have now extended the above synthesis to the heavier chalcogen atom selenium. After a few minor modifications to the reported procedure, including changing the equivalents of reagents, Se_2naph has been successfully synthesized with a much healthier yield than previous efforts.

Se_2naph itself is an interesting molecule, especially when compared to other molecules. The crystal structure of Se_2naph has previously been reported, along with several other compounds having an Se-Se bond,[7] such as dibenzo[*ce*]-1,2-diselenide and diphenyl diselenide (Figure 4-2).[7, 8] Similar backbones in each of these compounds produce similar chemical environments for the selenium atoms. Each selenium atom forms two covalent bonds- one bond with the neighboring selenium atom and the other with a carbon from an aromatic ring system. Although the compounds are structurally similar around the selenium atoms, there are major differences in the conformation that the backbone forces on

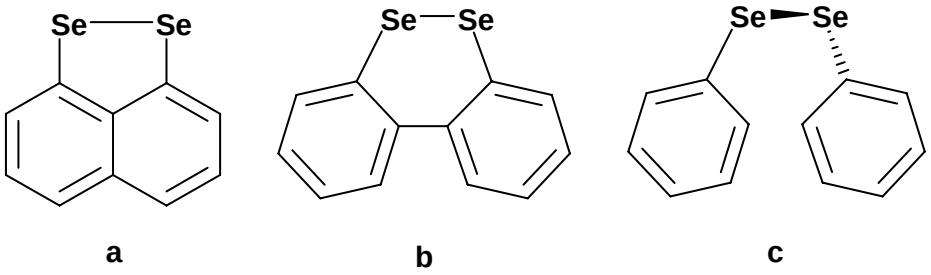

Figure 4-2. a) Se_2naph, b) dibenzo[*ce*]-1,2-diselenide, and c) diphenyl diselenide.

the selenium substituents. As a result, the Se-Se bond distance varies as a function of the flexibility of the di-aryl backbone. Se_2naph has the longest Se-Se bond distance at 2.36 Å, followed by dibenzo[*ce*]-1,2-diselenide (2.32 Å), and then diphenyl diselenide (2.29Å). The direct relationship that can be drawn is the more rigid the backbone, the longer the Se-Se bond.

Recently, the synthesis for di-*tert*-butylnaphtho[1,8-*c*,*d*][1,2]disulfide has been reported (Figure 4-3).[9,10] To examine how *tert*-butyl groups on the naphthalene backbone change the chalcogen-chalcogen bond, we decided to synthesize the selenium analog. The addition of the bulky, electron-donating groups could increase the electron density at the selenium atoms and thereby change the electronic environment of the selenium-selenium bond.

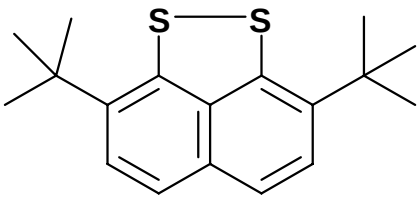

Figure 4-3. 2,7-di-*tert*-butylnaphtho[1,8-*c*,*d*][1,2]disulfide.

In order to make this comparison, two new compounds, 2,7-di-*tert*-butylnaphtho[1,8-*c*,*d*][1,2]diselenole (**4.1**) and 2-mono-*tert*-butylnaphtho[1,8-*c*,*d*][1,2]diselenole (**4.2**), have been synthesized and characterized by ^{1}H, ^{13}C, and ^{77}Se NMR and mass spectrometry (Figure 4-4). Exposure of **4.2** to bromine resulted in a third compound 4,7-di-bromo-2-mono-*tert*-butylnaphtho[1,8-*c*,*d*][1,2]diselenole (**4.3**) (Figure 4-5).

Here we report the details of the more efficient one-pot reaction for Se_2naph, and describe the synthetic procedure for **4.1** and **4.2**. The crystal structure of **4.1** and **4.3** are reported and compared. The crystal structures of several diselenide complexes will also be compared.

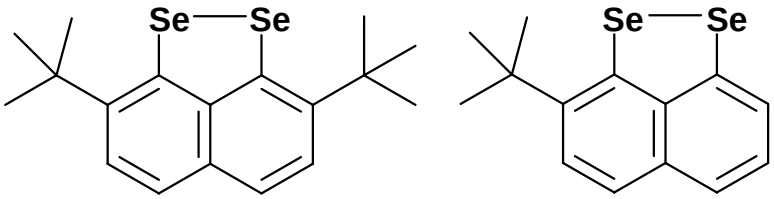

Figure 4-4. 2,7-di-*tert*-butylnaphtho[1,8-*c*,*d*][1,2]diselenole (**4.1**) and 2-mono-*tert*-butylnaphtho[1,8-*c*,*d*][1,2]diselenole (**4.2**).

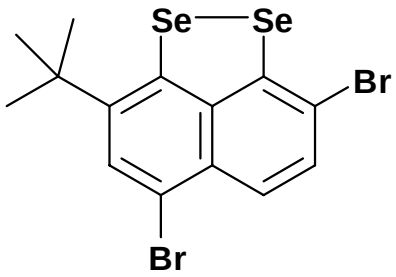

Figure 4-5. 4,7-di-bromo-2-mono-*tert*-butylnaphtho[1,8-*c*,*d*][1,2]diselenole (**4.3**)

4.2. Synthesis, Results, and Discussion

4.2.1. Synthesis

Se_2naph was synthesized using a slight modification of the 1994 one-pot synthesis reported by Ashe *et al* for S_2naph.[6] Under N_2, butyllithium (2.5 eq.) and then tetramethylethylenediamine (TMEDA) (2.5 eq.) were added to crystalline naphthalene. The solution was refluxed for three hours, then cooled to -78°C and Se powder (3 eq.) was added. After stirring overnight under N_2, hexane and water were added. The crude product was extracted, purified by column chromatography, and recrystallized from methylene chloride/pentane to give purple needle crystals in 26% yield (Scheme 4-1).

In addition to Se_2naph, the *tert*-butyl-substituted derivatives, **4.1** and **4.2**, have also been synthesized. The addition of *tert*-butyl groups on the naphthalene ring was accomplished using the synthesis reported for di-*tert*-butyl naphtho[1,8-

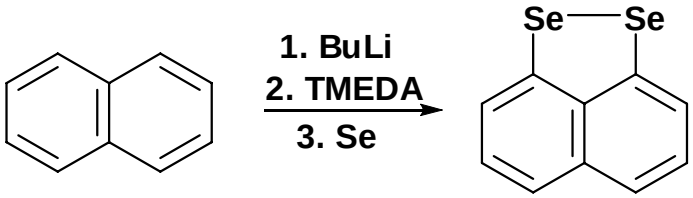

Scheme 4-1. New synthesis of naphtho[1,8-*c*,*d*]-1,2-diselenole (Se_2naph).

c,*d*][1,2]disulfide.[9,10] This reaction proceeds via a standard Friedel-Crafts alkylation wherein two molar equivalents of $AlCl_3$ are added to a mixture of Se_2naph and 3 eq. of *t*-butyl chloride in CH_3NO_2 at 80°C. The solution was then heated at ~80°C for two hours. Distilled water was added and the aqueous solution was extracted with methylene chloride. The organic layer was dried over $MgSO_4$, filtered, and the solvent was removed via rotary evaporation. The resultant solid, containing a mixture of mono- and di-substituted compounds, was purified by chromatography on a silica gel column with elution using hexane. The **4.1** eluted first, followed by **4.2**, then, finally, the starting material.

Compound **4.2**, a dark, red oil, was obtained in a 23% yield. The proton NMR spectrum of **4.2** has a multiplet ranging from 7.5-7.2 ppm corresponding to the aromatic protons of the molecule and a large singlet at 1.6 ppm arising from the *tert*-butyl group. The ^{77}Se NMR spectrum contains two major signals (Figure 4-6). The compound being observed in the selenium NMR is made up of ^{77}SeSe, Se^{77}Se, and ^{77}Se^{77}Se isotopomers. (Any selenium sample is a mixture of several stable isotopes, but only ^{77}Se, natural abundance of 7%, is NMR active.) The first two isotopomers give rise to singlets centered at 413.6 and 360.1 (Figure 4-6), whilst the latter gives an AX spectrum with $J_{Se\text{-}Se}$ = 345 Hz. The peak at 360.1 ppm corresponds to the selenium atom closest to the *tert*-butyl group, based on comparison to the ^{77}Se spectra of Se_2naph and **4.1**.

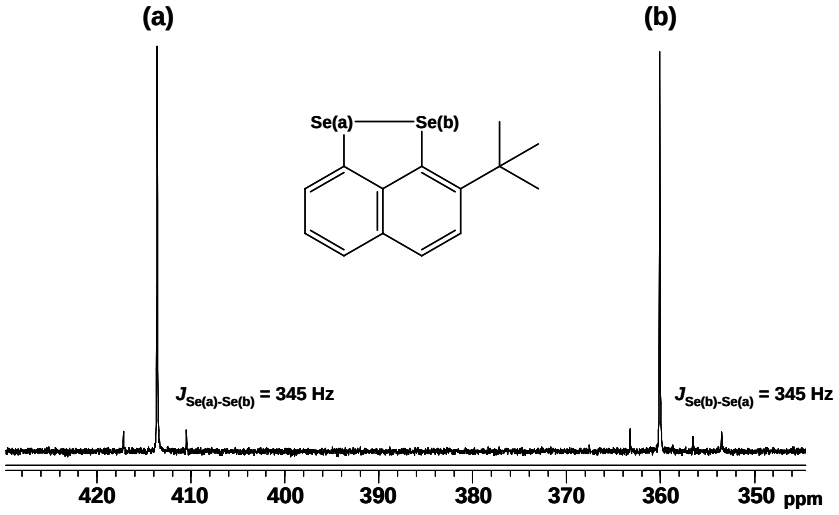

Figure 4-6. The ^{77}Se NMR for **4.2**, peaks a) 413.6 ppm and b) 360.1 ppm.

Eleven out of twelve possible peaks are seen in the ^{13}C NMR spectrum of **4.2**. Relative peak intensities, however, suggest the possibility of an overlapped signal at 126.8 ppm. The mass spectrum mirrors the calculated spectrum with molecular ion peaks at 339 [^{78}Se, ^{80}Se] and 341 [^{80}Se, ^{80}Se].

Compound **4.1** was crystallized by slow evaporation of a pentane solution to give orange blocks for a final 3% yield. The proton NMR spectrum reveals a multiplet from 7.5-7.4 ppm (J_{H-H} = 8, 21 Hz) with a large singlet at 1.56 ppm. The ^{77}Se NMR spectrum has a singlet at 352.71 ppm. Eight peaks are expected and seen in the ^{13}C NMR spectrum. The experimental mass spectrum mirrors the calculated spectrum with molecular ion peaks of 396 [^{78}Se, ^{80}Se] and 398 [^{80}Se, ^{80}Se].

4.2.2. X-ray Crystallography

Crystal structures were obtained for most of the compounds in this chapter. Compound **4.2** is a persistent oil and could not be crystallized; however its brominated counterpart could be crystallized, so the X-ray crystal structures for **4.1** and **4.3** were solved (Figure 4-7). Compound **4.1** crystallizes in the *Pcca* space group (R_1 = 4.44%), where half of the molecule is solved as half an independent

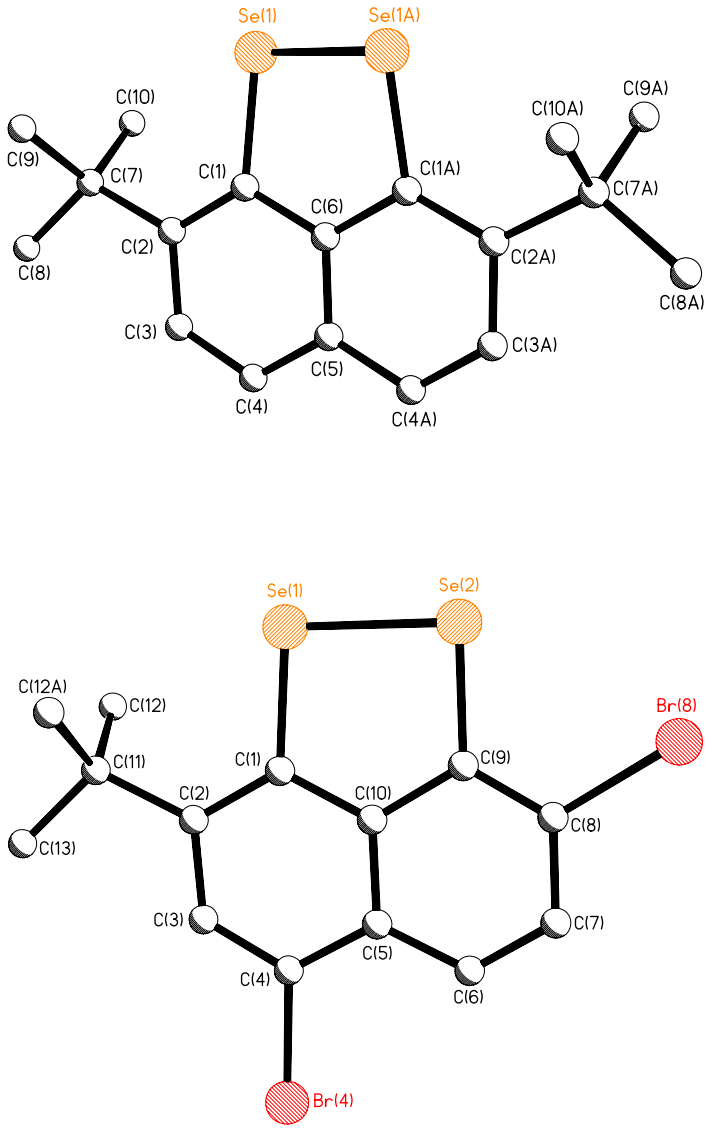

Figure 4-7. Molecular representation of **4.1** (top) and **4.3** (bottom).

molecule and then is expanded by symmetry to reveal the full molecule. Compound **4.3** crystallizes in the $P2_1/m$ space group (R_1 = 4.99%). This compound too must be expanded by symmetry. There is a plane of symmetry in **4.3** that runs along the naphthalene plane, leading to expansion to reveal the full *t*-butyl group. The parameters from the X-ray collection and refinement of all structures are in Appendix 1. Table 4-1 contains selected bond lengths and angles.

Table 4-1. Selected bond angles (°) for **4.1** and **4.3**.

	4.1[a]	**4.3**
Se(1)-Se(2)	2.3383(5)	2.3388(14)
Se(1)-C(1)	1.934(3)	1.935(9)
Se(2)-C(9)		1.888(9)
Se(1)-Se(2)-C(9)		90.9(3)
Se(2)-Se(1)-C(1)	93.16(10)	93.9(2)
Se(1)-C(1)-C(2)	122.4(2)	122.0(7)
Se(1)-C(1)-C(10)	113.2(2)	114.4(6)
Se(2)-C(9)-C(8)		121.6(7)
Se(2)-C(9)-C(10)		119.1(7)
C(2)-C(1)-C(10)	124.3(3)	123.6(8)
C(10)-C(9)-C(8)		119.3(8)
C(1)-C(10)-C(9)	124.8(3)	121.7(8)
C(4)-C(5)-C(10)-C(1)	-0.9(2)	-1.0(5)
C(6)-C(5)-C(10)-C(9)	-0.9(2)	-1.0(5)
C(4)-C(5)-C(10)-C(9)	179.1(2)	180.0(10)
C(6)-C(5)-C(10)-C(1)	179.1(2)	180.0(10)
Mean Plane Deviations		
Se(1)	-0.199(6)	-3.245(4)
Se(2)		-3.302(4)

[a]Se(2) is Se(1A), C(10) is C(6), C(9) is C(5), and C(6) is C(4A)

With the synthesis, characterization, and X-ray crystallography of **4.1** and **4.3** completed, a structural comparison between these compounds and other diselenide compounds could be made (Figure 4-2). Table 4-2 contains a list of Se-Se and Se-C bond lengths for diphenyl diselenide, dibenzo[*ce*]-1,2-diselenide, and Se_2naph.[11-13] The Se-Se bond length in **4.1** is 2.3383(5) Å, which is similar to **4.3** (2.3388(14) Å). Both of these compounds have shorter Se-Se bond lengths than in

Table 4-2. Bond lengths (Å)

	diphenyl diselenide[11]	dibenzo[*ce*]-1,2-diselenide[12,b]	Se_2naph[13]
Se-Se	2.29(1)	2.323(2)	2.3639(5)
Se-C_{ph}	1.93(5)	1.907(6), 1.912(7)	1.914(3)

[b]One of the three independent molecules.

Se_2naph, (2.3639(5) Å), but longer than in diphenyl diselenide (2.29(1) Å) and dibenzo[*ce*]-1,2-diselenide (2.323(2) Å). The Se-C bond lengths in **4.3** are asymmetric. Their environments are asymmetric as well. Se(1) is trans to Br(4), and *ortho*- to the *t*-butyl group on C(2). In contrast, the Se(2) atom is *ortho*- to Br(8). Correspondingly, the Se(1)-C(1) bond length is 1.953(9) Å, whilst the Se(2)-C(9) bond length is much shorter at 1.888(9) Å. The Se-C bond lengths in the rest of the molecules are all similar to, if not slightly smaller than, the Se(1)-C(1) bond length in **4.3**. The Se-C bond lengths of **4.1** are 1.934(3) Å, which is the same as the Se-C bond length of diphenyl diselenide (1.93(5) Å), and longer than the Se-C bonds in Se_2naph (1.914(3) Å) and dibenzo[*ce*]-1,2-diselenide (1.907(6) Å and 1.912(7) Å).

There is a shortened Se-Se bond in **4.1** and **4.3** compared to Se_2naph. The electronic environment of **4.1** seems to be similar to that of diphenyl diselenide, due to the similarity in length between the Se-C bonds. However, the Se-Se bond length of **4.1** is longer than in the diphenyl diselenide case; this is probably due to the rigid naphthalene backbone, which will not allow the selenium atoms to come closer together. The selenium atom environment of **4.3** is unsymmetric compared to the selenium atoms in the other compounds. The Se(1)-C(1) bond is very similar to **4.1**, but the Se(2)-C(9) bond distance is the shortest of the series at 1.888(9) Å.

To see how the substitution of the naphthalene ring affects the selenium-naphthalene ring interaction, comparisons between Se_2naph, **4.1**, and **4.3** made by looking at in-plane distortions and out-of-plane deflections of the substituents and by looking at the buckling of the naphthalene ring are useful.

In-plane distortions of the substituents are determined by looking at the bond angles (a, b, c, and d in Figure 4-8) around the *peri*-carbon atoms (Se-C-C). In Se_2naph, these angles range from 121.0(2)° to 121.9(2)° (ideal trigonal planar geometry is 120°). However, in **4.1**, the outer angles (a and d) are 122.4(2)° and the inner angles (b and c) are much smaller at 113.2(2)°. In **4.3**, the angles a and b are similar to **4.1**, probably due to having the same *ortho*-substituent. However, angles c and d on the carbon with an *ortho*-bromide are 119.1(7)° and 123.6(8)°,

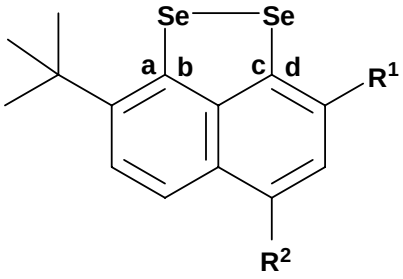

R^1 = *t*-butyl, R^2 = H

R^1 and R^2 = Br

Figure 4-8. Angles (a, b, c, d) can be used to describe the in-plane distortions of the substituents in **4.1** (R^1 = t-butyl, R^2 = H) and **4.3** (R^1 = R^2 = Br).

respectively. These two angles are much closer to ideal, suggesting that the *ortho*-*t*-butyl group is influencing in-plane distortion of the selenium atom on one side of the naphthalene ring while the smaller bromide on the other side is not forcing the selenium to shift. The Se-Se-C bond angles also show distortion on the *t*-butyl side of the ring. The ideal angle is 90°, and in Se_2naph, the Se-Se-C angles are 91.5(3)° and 92.4(3)°. The angle increases in **4.1**, in which both Se-Se-C angles are 93.16(10)°, meaning that the selenium atoms are leaning towards one another a little bit more. In **4.3**, these angles are very different from each other. The Se(1)-Se(2)-C(9) angle (on the bromide side) is 90.9(3)° and the Se(2)-Se(1)-C(1) angle (on the *t*-butyl side) is 93.16(10)°.

Out-of-plane deflections are determined by measuring the distance that the selenium atoms deviate from the naphthalene plane. While Se_2naph and **4.3** are almost perfectly planar, in **4.1**, both selenium atoms bifurcate ~0.1989(57) Å from the naphthalene plane, one Se on each side. This deflection can be best visualized by looking at the end-on view of a molecular wire drawing. For comparison, the end-on views of Se_2naph, **4.1**, and **4.3** are shown in Figure 4-9.

The short Se-Se bond in **4.1** brings the Se atoms closer compared to Se_2naph, forcing the selenium atoms out of the plane. However, this doesn't occur in Se_2naph or **4.3**, which may suggest that there is a significant amount of resonance being present in the five-membered ring of these two structures.

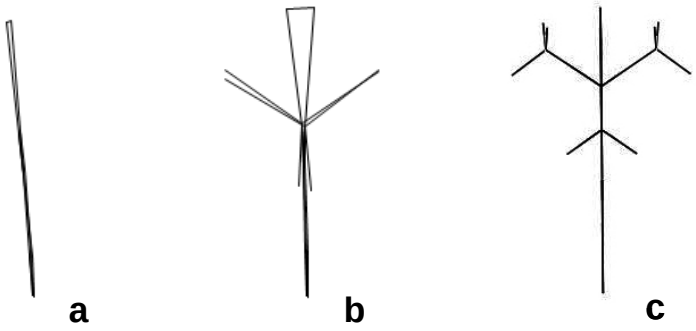

Figure 4-9. Out-of-plane deflections of a) Se_2naph, b) **4.1**, and c) **4.3**.

Distortions of the naphthalene rings themselves caused by the additional substituents can be determined by comparing the torsion angles around the bridgehead carbon atoms of the backbone. In Se_2naph, these torsion angles are 1.1(13)° and 0.6(12)° (for both rings as in Figure 4-10(a)) and 178.7(9)° and 179.6(8)° (across the ring as in (b)).[13] In **4.1**, the torsion angles are 0.9(2)° and 179.1(2)°, and the angles are just as flat in **4.3** at -1.0(5)° and 180.0(10)°. Since the distortion in the naphthalene ring is so small, the amount of it caused by the substituents is certainly very small.

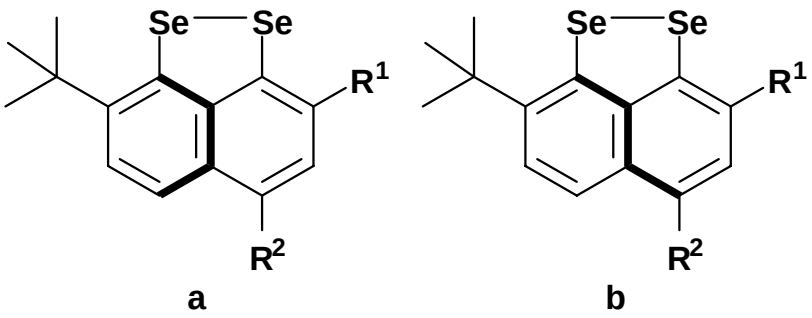

Figure 4-10. Torsion angles, in bold, run through the bridgehead carbons of **4.1** (R^1 = t-butyl, R^2 = H) and **4.3** (R^1 = R^2 = Br). Ideally, these angles are: a = 0° and b = 180°.

Contrary to many of the angle comparisons, comparison of the crystal packing in Se_2naph, **4.1**, and **4.3** shows vast differences. Se_2naph crystallizes in the monoclinic, $P2_1/n$ space group, **4.1** crystallizes in the orthorhombic *Pcca* space group, and **4.3** crystallizes in $P2_1/m$. It has been reported that in the solid state, Se_2naph displays some "interesting" packing effects attributed to the high polarizability of the selenium atom.[13] This is because Se_2naph forms herringbone π-stacks that are linked by an Se…Se interaction, with a π-π distance between naphthalene rings on separate molecules of 3.81 Å. However, likely due to the bulky *t*-butyl arms, there are no inter-molecular interactions between Se atoms in the crystal packing of **4.1**. The packing based on glide planes is shown along the b-axis (Figure 4-11) and the a-axis (Figure 4-12).

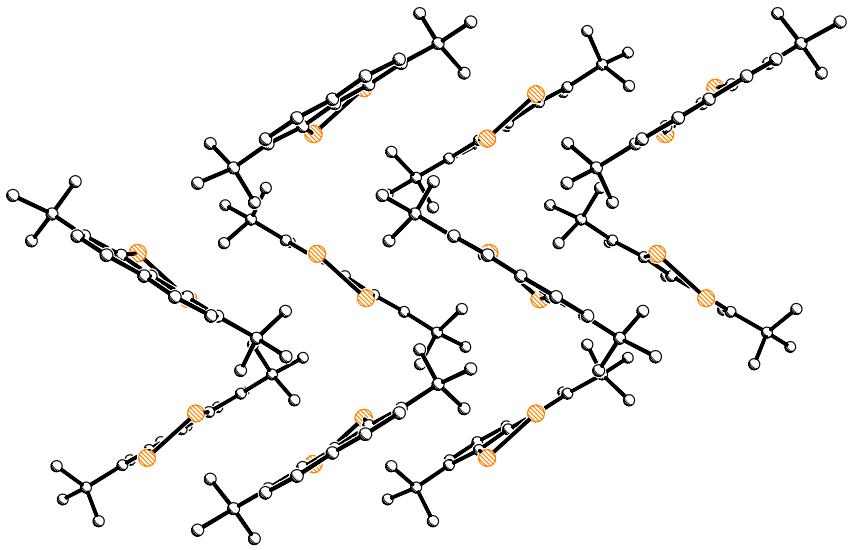

Figure 4-11. View of crystal packing in **4.1** along the b-axis.

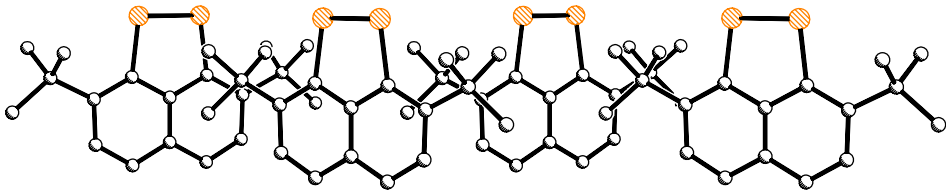

Figure 4-12. View of crystal packing in **4.1** along the a-axis.

In **4.3**, there is evidently no intermolecular Se…Se interaction, however, there is close contact between the Br(4) atom of one molecule and the Br(8)' atom of another molecule. The intermolecular Br(4)…Br(8)' distance is 3.4790(13) Å. This interaction and the resulting packing, is illustrated in Figure 4-13.

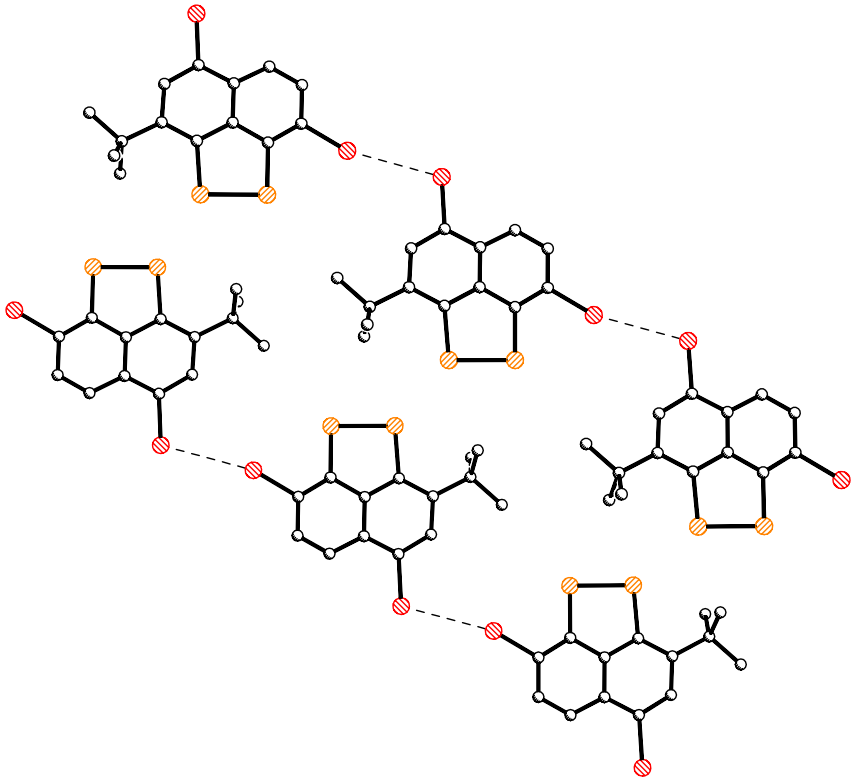

Figure 4-13. View of crystal packing in **4.3** along the b-axis.

4.3. Conclusion

A new, efficient one-pot synthesis of Se_2naph has been reported. Also, Friedel-Crafts alkylation has been utilized in the synthesis of **4.1** and **4.2**. These new compounds have been synthesized and characterized by ^{1}H, ^{13}C, and ^{77}Se NMR and mass spectrometry. Additionally, bromine was added to **4.2** to form **4.3**. Both **4.1** and **4.3** have been crystallographically characterized.

A structural comparison of **4.1**, **4.3**, and Se_2naph has been presented, along with comparisons of the Se-Se and Se-C bonds of several other aromatic compounds containing an Se-Se bond. It seems that the addition of bulky, electron-donating *tert*-butyl substituents or the bromide substituents on the naphthalene ring enriches the electronic environment around the selenium atoms, resulting in a decrease in the Se-Se bond length. This decrease in bond length is accompanied by an out-of-plane deflection in the **4.1** molecule. This deflection is not seen in **4.3**. In fact, the molecule is very planar, suggesting that there could be a significant amount of resonance in the five-membered ring involving the selenium atoms. In-plane distortion and buckling of the naphthalene plane are minor in both **4.3** and **4.1**, although, **4.3** shows some asymmetry in the angles around and the bond lengths of the two *peri*-positions. The bulky substituents do disrupt the "interesting" packing effects that are present in Se_2naph leaving the bromide-bromide interactions as the main feature of the packing in **4.3**.

4.4. Experimental

4.4.1. General Remarks

All synthetic procedures were performed under nitrogen using standard Schlenk techniques unless otherwise stated. Reagents were obtained from commercial sources and used as received. Dry solvents were collected from an MBraun solvent system. ^{1}H, ^{13}C, and ^{77}Se spectra were recorded on a Jeol DELTA GSX270 spectrometer. Chemical shifts are reported in ppm and are referenced to $CDCl_3$. Coupling constants (J) are given in Hz.

4.4.2. Synthesis of Naphtho[1,8-c,d]-1,2-diselenole (Se_2naph)

Crystalline naphthalene (6.10 g, 47.6 mmol) was added to a 500 mL round bottom Schlenk flask. The flask was evacuated and purged with nitrogen. Butyllithium (BuLi) (46.8 mL of 2.5 M in THF, 117 mmol) was added dropwise via syringe with stirring, followed by the slow addition of TMEDA (17.7 mL, 117 mmol). Upon addition, the flask became slightly warm and a white precipitate (pcc) formed. The pcc dissolved as the solution yellowed and then became increasingly darker until it was dark reddish in color. A reflux condenser was added to the flask, which was then warmed to ~70°C for two hours. The mixture was allowed to cool to room temperature, at which time the reflux condenser was replaced by a septum. The mixture was then further cooled to -70°C using a dry ice/acetone bath. Tetrahydrofuran (THF) (~150 mL) was added dropwise via syringe. Selenium powder (11.1 g, 141 mmol) was then added at once. The reaction mixture was allowed to slowly warm to room temperature and was stirred overnight under nitrogen. *Caution!* As the mixture warms to room temperature, the flask becomes slightly pressurized. Make sure the stopper is clipped and the flask is opened to nitrogen.

The next day, the flask was opened and the mixture was poured into a 2 L separatory funnel where ~500 mL of distilled water and ~300 mL of hexane was then added. It was difficult to see the separation line, but as the water layer was removed the line became more evident. The hexane layer, a clear purple solution, was collected. Silica gel was added to the organic layer and the solvent was evaporated. The silica gel/product was placed on top of a silica column and the product was eluted with hexane. The purple band was collected and the solvent evaporated. The purple solid was dissolved in a minimal amount of methylene chloride. The solution was then layered with hexane and placed in the freezer for recrystallization. Yield 3.544 g, 26%. ^{1}H and ^{77}Se NMR matched those of the previous reported samples.[1]

*4.4.3. Synthesis of 2,7-di-tert-butylnaphtho[1,8-c,d][1,2]diselenole (**4.1**) and 2-mono-tert-butylnaphtho[1,8-c,d][1,2]diselenole (**4.2**)*

2,7-di-*tert*-butylnaphtho[1,8-*c*,*d*][1,2]diselenole (**4.1**) and 2-mono-*tert*-butylnaphtho[1,8-*c*,*d*][1,2]diselenole (**4.2**) were prepared by methods reported for the thiol analogues.[9, 10] Se_2naph (0.38 g, 1.3 mmol), *t*-butyl chloride (0.43 mL, 4.1 mmol), and CH_3NO_2(~7 mL), were added to a 100 mL round bottom Schlenk flask. The reaction was heated with stirring to ~80°C and $AlCl_3$ (36 mg, 0.27 mmol) was added. The mixture continued to heat at ~80°C for one hour. After the reaction cooled to room temperature, distilled water was added, which then was extracted with methylene chloride. The organic layer was removed, dried over $MgSO_4$, filtered, and the solvent was evaporated. These compounds were purified by column chromatography on silica gel elution using hexane, with **4.1** eluting first, then **4.2**, followed by starting material. **4.1** was crystallized by slow evaporation of a pentane solution to give orange blocks (17 mg, 3 %). **4.2** is a dark red oil (104 mg, 23 %), and finally 81 mg (21 %) of the starting material was recovered.

4.1: ^{1}HNMR ($CDCl_3$) 7.52-7.44 (m, 4H, $J_{H\text{-}H}$ = 8, 21 Hz), 1.56 (s, 18H); ^{77}SeNMR ($CDCl_3$) 352.71 (s); ^{13}CNMR ($CDCl_3$) (8 peaks expected) 144.05, 140.37, 136.99, 134.98, 125.82, 124.37, 36.66, 29.10. MS (TOF MS CI): *m/z* 396 [^{78}Se, ^{80}Se], 398 [^{80}Se].

4.2: ^{1}HNMR ($CDCl_3$) 7.52-7.17 (m, 5H), 1.53 (s, 13H); ^{77}SeNMR ($CDCl_3$) 413.61(s), 413.61 (d, $J_{Se\text{-}Se}$ = 345 Hz), 360.07 (s), 360.07 (d, $J_{Se\text{-}Se}$ = 345 Hz); ^{13}CNMR ($CDCl_3$) 144.31, 139.53, 138.77, 138.29, 136.49, 126.77, 124.81, 123.30, 121.97, 36.51, 29.16. MS (TOF MS CI): *m/z* 339 [^{78}Se, ^{80}Se], 341 [^{80}Se].

4.5. References

1. J. Meinwald, D. Dauplaise, F. Wudl and J. J. Hauser, *J. Am. Chem. Soc.,* 1977, 99, 255-257.

2. K. Yui, Y. Aso, T. Otsubo and F. Ogura, *Bull. Chem. Soc. Jpn.,* 1988, 61, 953-959.

3. D. Dauplaise, J. Meinwald, J. C. Scott, H. Temkin and J. Clardy, *Ann. N. Y. Acad. Sci.,* 1978, 313, 382-394.

4. J. L. Kice, Y. Kang and M. B. Manek, *J. Org. Chem.,* 1988, 53, 2435-2439.

5. S. Vyskocil, L. Meca, I. Tislerova, I. Cisarova, M. Polasek, S. R. Harutyunyan, Y. N. Belokon, M. J. Stead Russel, L. Farrugia, S. C. Lockhart, W. L. Mitchell and P. Kocovsky, *Chem. Eur. J.,* 2002, 8, 4633-4648.

6. A. J. Ashe III, J. W. Kampf and P. M. Savla, *Heteroat. Chem.,* 1994, 5, 113-119.

7. S. Murata, T. Suzuki, A. Yanagisawa and S. Suga, *J. Heterocycl. Chem.,* 1991, 28, 433-438.

8. R. E. Marsh, *Acta Cryst.,* 1952, 5, 458-462.

9. M. Tesmer and H. Vahrenkamp, *Eur. J. Inorg. Chem.,* 2001, 1183-1188.

10. S. M. Aucott, H. L. Milton, S. D. Robertson, A. M. Z. Slawin and J. D. Woollins, *Dalton Trans.,* 2004, 3347-3352.

11. J. D. Lee and M. W. R. Bryant, *Acta Cryst.,* 1969, 25, 2094-2101.

12. M. R. Bryce, A. Chesney, A. K. Lay, A. S. Batsanov and J. A. K. Howard, *J. Chem. Soc. Perkin Trans. 1,* 1996, 2451-2459.

13. S. M. Aucott, H. L. Milton, S. D. Robertson, A. M. Z. Slawin and J. D. Woollins, *Heteroat. Chem.,* 2004, 15, 530-542.

CHAPTER 5

STRUCTURAL STUDIES FOCUSED ON THE DISELENIDE LIGANDS OF FOUR-COORDINATE MONO- AND DI-NUCLEAR PLATINUM(II)-BISPHOSPHINE COMPLEXES

5.1. Introduction

The nature of the organic backbone in diselenide compounds can influence the Se-Se bond. A comparison of the Se-Se bonds in the organodiselenide compounds Se_2naph, dibenzo[*ce*]-1,2-diselenide, diphenyl diselenide, and 2,-di-*tert*-butylnaphtho[1,8-*cd*][1,2]diselenide suggested that the more rigid the organic backbone, the longer the Se-Se bond (Figure 5-1). By chelating these ligands to a metal center, we hope to better understand the effects that the organic backbone has upon complexation and the distortions that can occur in the various backbones.

There are very few metal complexes that have either Se_2naph (or any naphthalene derivative) or dibenzSe as a ligand. These are limited to the platinum(II) bisphosphine complexes, [Pt(Se_2naph)(PPh_3)$_2$],

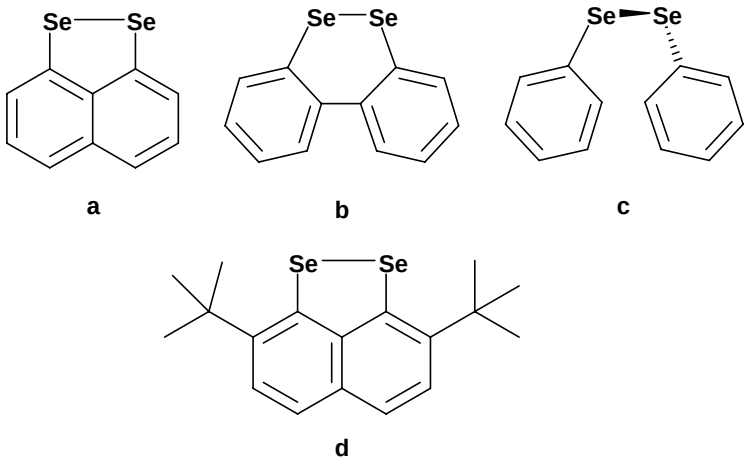

Figure 5-1. Line drawings of a) naphtha[1,8-*c*,*d*]-1,2-diselenide, b) dibenzo[*ce*]-1,2-diselenide, c) diphenyl diselenide, and d) 2,-di-tert-butylnaphtho[1,8-*cd*][1,2]diselenide.

[Pt(Se_2naph)(PMe_3)$_2$], and [Pt(dibenzSe_2)(PPh_3)$_2$].[1,2] In addition, there are only a few reported mononuclear square planar complexes having two -SePh ligands. These include *cis*- and *trans*-[Pt(SePh)$_2$(PPh_3)$_2$], *trans*-[Pt(SePh)$_2$(P(*n*-Bu)$_3$)$_2$], and *trans*-[Pt(SePh)$_2$(PEt_3)$_2$], and some mononuclear germanium complexes, including: [Ge(SePh)$_2$(R)$_2$], where R = Me, Et, *n*-Pr, *n*-Bu, and Ph) and [Ge(SePh)$_2$(R)], where R = -$(CH_2)_4$- or -$(CH_2)_5$-.[3-6] The only reported crystal structure of the germanium complexes is that of [Ge(SePh)$_2$((-CH_2-)$_4$)], while the crystal structures of several platinum complexes are known.[7]

In contrast to the above mononuclear platinum and germanium examples, the vast majority of complexes synthesized with -SePh ligands are dinuclear. These complexes have the -SePh moieties bridging two metal centers forming a diamond core structure as in Figure 5-2, which shows a few examples of known complexes with bridging -SePh ligands.[8-11]

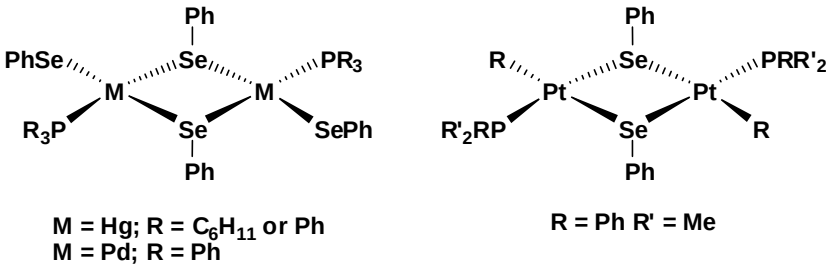

Figure 5-2. Known complexes with a diamond core structure.

To date, there is only one reported series. This series contains platinum bis-triphenylphosphine complexes containing like selenium ligands with the general formula LPt(PPh_3)$_2$, where L is Se_2naph, dibenzo[*ce*]-1,2-diselenide, or diphenyl diselenide (Figure 5-3). These complexes were not synthesized as a series in a single laboratory, but have been reported independently by several groups. In those reports, the syntheses of [Pt(PPh_3)$_2$(Se_2naph)], [Pt(PPh_3)$_2$(dibenzSe_2)], and *cis*-[Pt(PPh_3)$_2$(SePh)$_2$] were obtained via an oxidative addition reaction with [Pt(PPh_3)$_4$] and the respective neutral diselenide.[1,3,12] It has further been reported that [Pt(PPh_3)$_2$(Se_2naph)] and *cis*-[Pt(PPh_3)$_2$(SePh)$_2$] have

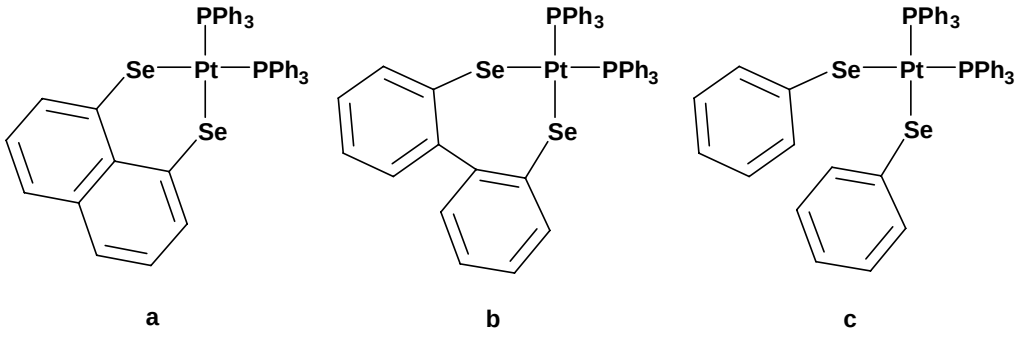

Figure 5-3. a) $[Pt(PPh_3)_2(Se_2naph)]$, b) $[Pt(PPh_3)_2(dibenzSe_2)]$, and c) *cis*-$[Pt(PPh_3)_2(SePh)_2]$.

been synthesized by first reducing the Se-Se bond followed by addition of the reduced diselenide to a solution of *cis*-$[PtCl_2(PPh_3)_2]$.

In order to expand the number of diselenide complexes and to obtain a series of diselenide platinum complexes from which to draw structural insights, we have synthesized and characterized a new series of complexes produced by reactions using *cis*-$[PtCl_2(P(OPh)_3)_2]$ as a starting material. The ligands naphtha[1,8-*c*,*d*]-1,2-diselenide (Se_2naph), 2-mono-*tert*-butylnaphtho[1,8-*c*,*d*][1,2]diselenole (mt-Se_2naph) dibenzo[*ce*]-1,2-diselenide ($dibenzSe_2$), and diphenyl diselenide have been used as ligands for the resulting four-coordinate mono- and di-nuclear platinum(II) bisphosphine complexes are $[Pt(Se_2naph)(P(OPh)_3)_2]$ (**5.1**), $[Pt(mt\text{-}Se_2naph)(P(OPh)_3)_2]$ (**5.2**), $[Pt_2(dibenzSe_2)_2(P(OPh)_3)_2]$ (**5.3**), *cis*-$[Pt(SePh)_2(P(OPh)_3)_2]$ (**5.4**), and *trans*-$[Pt_2(SePh)_4(P(OPh)_3)_2]$ (**5.5**) (Figure 5-4). The X-ray structures of these compounds are reported along with a detailed comparison of their structures focussing on the geometry about the selenide ligands.

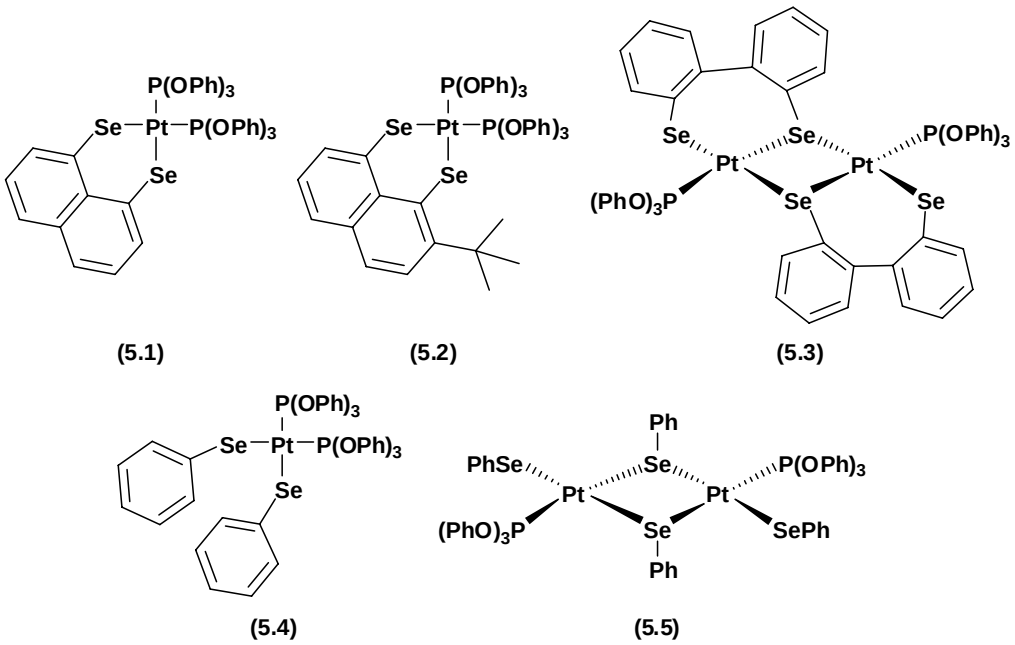

Figure 5-4. [Pt(Se_2naph)($P(OPh)_3$)$_2$] (**5.1**), [Pt(mt-Se_2naph)($P(OPh)_3$)$_2$] (**5.2**), [Pt_2(dibenzSe_2)$_2$($P(OPh)_3$)$_2$] (**5.3**), *cis*-[Pt($SePh)_2$($P(OPh)_3$)$_2$] (**5.4**), and *trans*-[Pt_2($SePh)_4$($P(OPh)_3$)$_2$] (**5.5**).

5.2. Results and Discussion

5.2.1. Synthesis and Characterization

Complexes **5.1**-**5.5** were synthesized under nitrogen by first creating a lithium selenide salt by addition of $LiBEt_3H$ to a dry THF solution of the appropriate ligand. Then, *cis*-[$PtCl_2$($P(OPh)_3$)$_2$] was added to the mixture. After stirring overnight, silica gel was added to the reaction mixture and the solvent was removed under vacuum. Purification was performed by column chromatography via the addition of the silica/product solid to a silica gel column followed by elution of impurities with hexane. The product was then eluted from the column using dichloromethane. X-ray quality crystals were obtained for complexes **5.1**-**5.5** by pentane diffusion into a dichloromethane solution. The synthetic scheme is shown in Scheme 5-1.

Of this series of complexes, not all have been fully characterized, but all have yielded molecular structures through X-ray crystallography. Complexes **5.1**

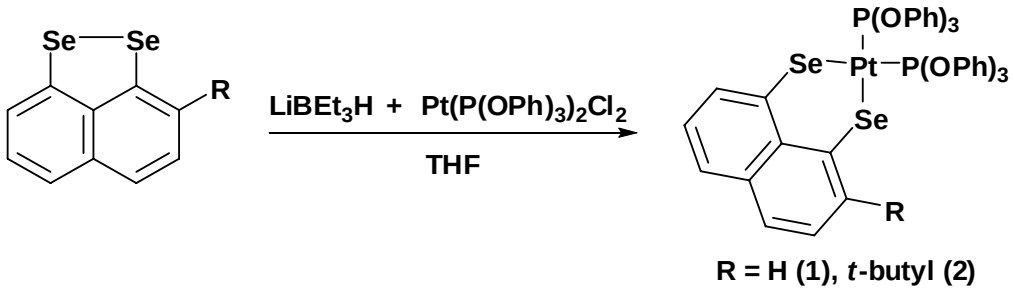

Scheme 5-1. Synthesis of **5.1** and **5.2**.

and **5.2** have been fully characterized by EA, MS, IR, Raman, and ^{1}H, ^{13}C, ^{31}P, ^{77}Se, and ^{195}Pt NMR. Complex **5.1** was synthesized in a 53% yield. The calculated elemental analysis (EA) data for **5.1** best fits the experimental data for the complex plus one molecule of dichloromethane. Mass spectrometry data show a molecular ion peak at 1100 corresponding to the desired M^+ value. Complex **5.2** was crystallized in a 50% yield. Calculated EA data fit the experimental data with a trace amount of dichloromethane. Mass spectrometry showed a molecular ion peak at 1156 corresponding to the desired M^+. We were unable to isolate bulk samples of complexes **5.3**, **5.4**, and **5.5**, so their degree of characterization is less. Only their X-ray structures have accurately been determined, along with some multi-nuclear NMR data. The mass spectrometry for the samples containing **5.3** and **5.4**/**5.5** showed a desired peak at 1631 and 1635.6, respectively that matches the theoretical isotope profile for M^+; however, there are higher molecular ion peaks in both spectra.

5.2.2. NMR Characterization

The ^{31}P, ^{77}Se, and ^{195}Pt NMR spectral data for **5.1-5.5** are shown in Table 5-1. Spectra were recorded on crystalline sample dissolved in $CDCl_3$.

In the ^{31}P NMR spectrum, **5.1** displays a signal at 87.4 ppm, and both platinum ($J_{P\text{-}Pt}$ = 4711 Hz) and selenium ($J_{P\text{-}Se}$ = 28 Hz) coupling are visible in the spectrum. The ^{77}Se NMR contains a triplet at 139.5 ppm with $J_{Se\text{-}P}$ = 28 Hz and

Table 5-1. Values from NMR[a] spectra for complexes **5.1-5.5**.

	5.1	**5.2**[b]	**5.2**[c]	**5.3**	**5.4/5.5**
^{31}P NMR (ppm)	87.4	89.3	86.3	85.3	84.5
J_{P-P} (Hz)		68	68		
J_{P-Pt} (Hz)	4711	4686	4669	4685	4724
J_{P-Se} (Hz)	28	12,28	34	21	
^{77}Se NMR (ppm)	139.5	138.4	258.4(d)	222.78-226.9(m)	221.4-222.5(m)
J_{Se-P} (Hz)	28	7, 29	19, 36		
J_{Se-Pt} (Hz)	205	327	327		
^{195}Pt NMR(ppm)	-4711.0(dd)	-4574.9(dd)		-4569.7(dd)	-4074.9(dd)
J_{Pt-P} (Hz)	4711	4979		4685	4707
J_{Pt-Se} (Hz)	203			183	

[a]All NMR samples were prepared from crystalline samples in $CDCl_3$. [b,c]In complex **5.2**, two signals result from the ^{77}Se atom present in one of two inequivalent positions, either the position closest to or furthest away from the substituted *tert*-butyl arm. At this time, based on comparisons to complex **5.1**, it is thought that the ^{77}Se peak at 138.4 ppm corresponds to the ^{77}Se atom furthest from the *tert*-butyl substituent.

J_{Se-Pt} = 205 Hz. The ^{195}Pt NMR displays a triplet at -4711.0 ppm (J_{Pt-P} = 4711 Hz) (J_{Pt-Se} = 203 Hz).

The asymmetry of the ligand (mt-Se_2naph) makes the NMR spectrum of **5.2** more complicated than that of **5.1**. In the ^{31}P NMR spectra of **5.2**, there is an AX type splitting pattern with both platinum and selenium satellites. This complex splitting pattern is due to the ^{31}P being *trans* to inequivalent ^{77}Se atoms from the mt-Se_2naph ligand. Two phosphorus signals are present, at 89.3 ppm (J_{P-P} = 68 Hz), (J_{P-Pt} = 4686 Hz), (J_{P-Se} = 19, 28) and 86.3 ppm (J_{P-P} = 68 Hz), (J_{P-Pt} = 4669 Hz), (J_{P-Se} = 34) as displayed in Figure 5-5. The ^{77}Se NMR of complex **5.2** consists of two signals, each split once by phosphorus and once by platinum, resulting in a doublet-of-doublets-like appearance for each signal. These signals are centered at 258.4 ppm (J_{Se-P} = 36, 19 Hz) (J_{Se-Pt} = 327 Hz) and 138.4 ppm (J_{Se-P} = 7, 29 Hz) (J_{Se-Pt} = 212 Hz). The peak at 138.4 ppm has been assigned to the ^{77}Se furthest from the *tert*-butyl arm based on comparison to **5.1**. The ^{195}Pt NMR of **5.2** is a triplet centered at -4574.9 ppm (J_{Pt-P} = 4679 Hz).

The ^{31}P NMR data for complex **5.3** displays a single signal centered at 85.3 ppm with a J_{P-Pt} = 4685 Hz. The ^{77}Se NMR consists of a complicated

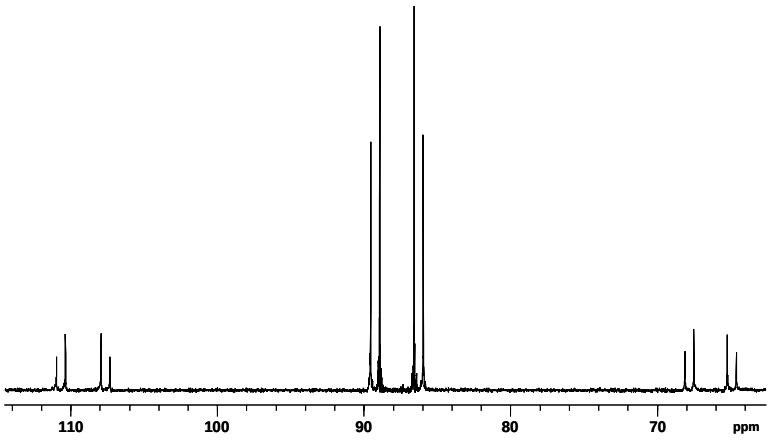

Figure 5-5. The ^{31}P NMR spectrum for complex **5.2**.

multiplet ranging from 222.8-226.9 ppm, and the ^{195}Pt NMR displays a triplet centered at -4569.6 ppm ($J_{Pt\text{-}P}$ = 4685 Hz) along with ^{77}Se satellites ($J_{Pt\text{-}Se}$ = 183 Hz).

The ^{31}P, ^{77}Se, and ^{195}Pt NMR spectra for **5.4** and **5.5** were measured using a sample that contained crystalline material containing at least some crystals of both complexes, as determined by X-ray studies. The NMR data, however, is indicative of either a single species in solution, or, if both complexes are actually present, then of precisely overlapping signals. The ^{31}P spectrum has a single signal at 84.5 ppm with platinum satellites ($J_{P\text{-}Pt}$ = 4724 Hz). As in **5.3**, the ^{77}Se NMR spectrum of **5.4/5.5** has a complicated multiplet ranging from 221.4-222.5 ppm. The ^{195}Pt NMR spectrum displays a triplet centered at -4074.9 ppm ($J_{Pt\text{-}P}$ = 4707 Hz).

5.2.2. X-ray crystallography

Molecular representations of the X-ray crystal structures of **5.1**, **5.2**, and **5.4a** are shown in Figure 5-6, while Figure 5-7 shows **5.3** and **5.5**. The summary of X-ray collection and refinement for **5.1-5.5** can be found in Appendix 1. The X-ray analyses show that in every complex, the platinum center lies in a distorted square-planar coordination environment.

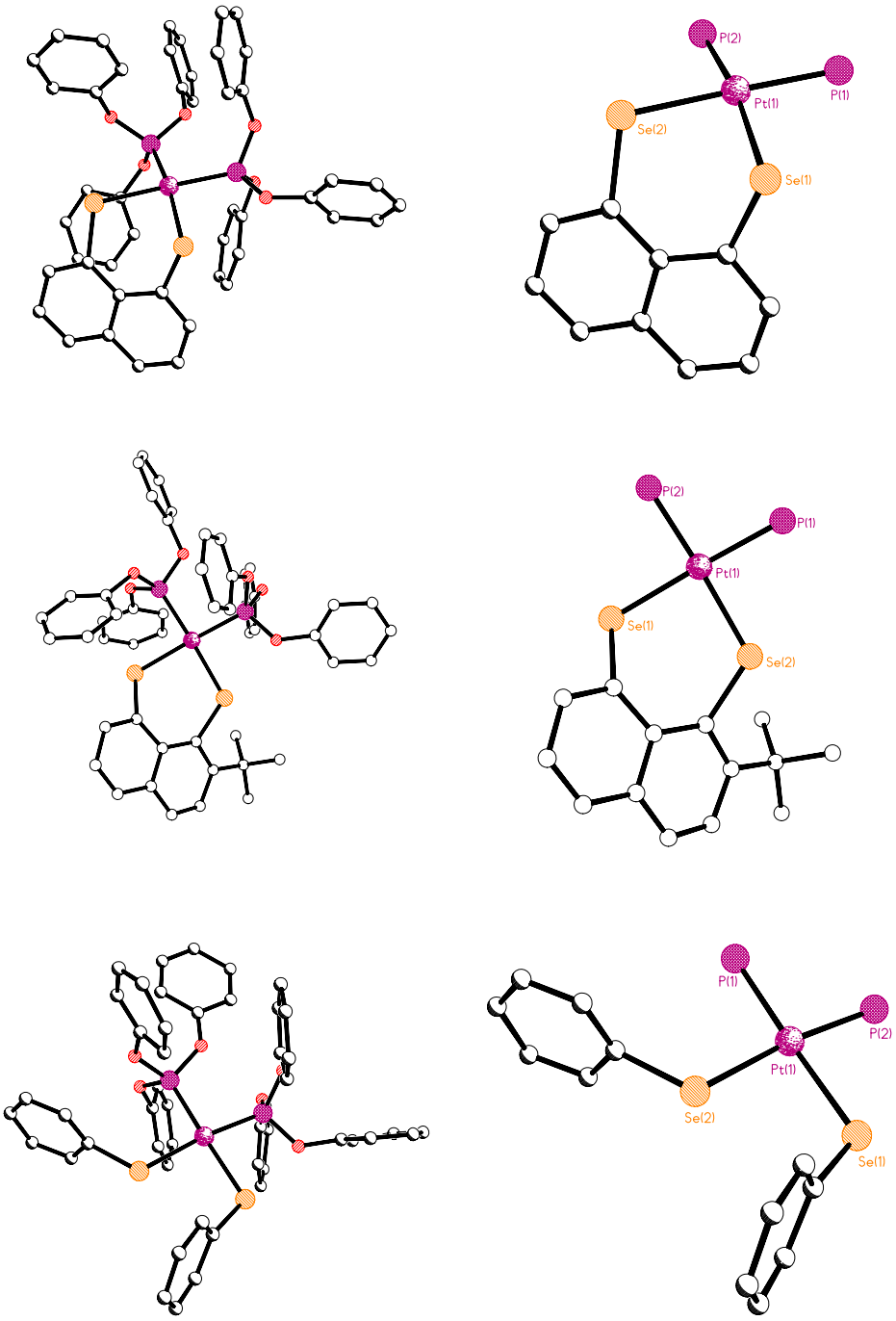

Figure 5-6. Molecular representations of full structures of **5.1** (left-top), **5.2** (left-middle), and one molecule of **5.4a** (left-bottom), along with the enlargement of the metal center (right) showing selected atoms.

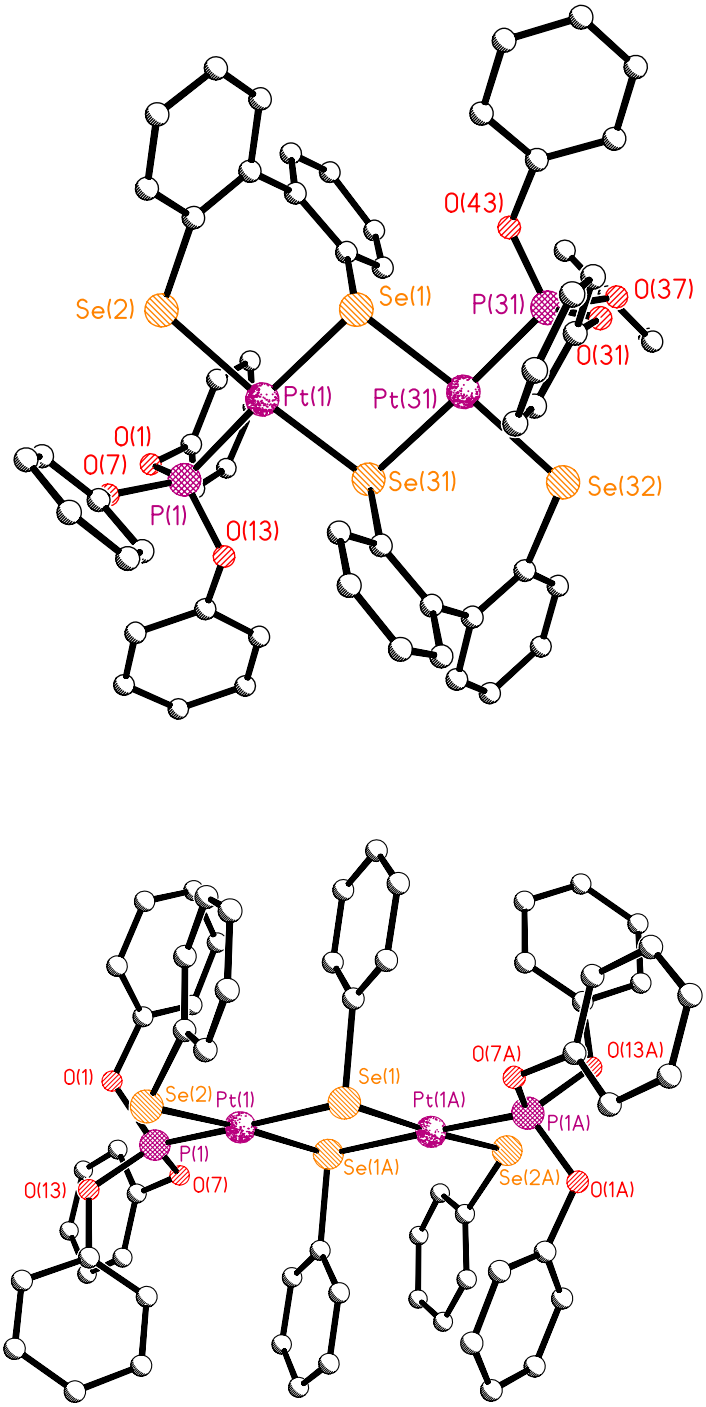

Figure 5-7. Molecular representations of complex **5.3** (top) and complex **5.5** (bottom).

The differing molecular structures of **5.4** and **5.5** were quite unexpected. As described above, the ^{31}P NMR clearly suggested that one species was present in the solution after synthesis and purification of the reaction mixture. Crystallization using pentane diffusion into a dichloromethane solution produced orange block crystals, which were characterized by X-ray crystallography, revealing the monomeric structure of **5.4**. The data refined in the C_2/c space group and the final refinement had three independent molecules and two solvent (CH_2Cl_2) molecules when symmetrically expanded (one and a half molecules, along with a solvent molecule exist in the asymmetric unit, R_1 = 12.50%). Only one full molecule (**5.4a**) in the asymmetric unit is shown in Figure 5.5 (bottom).

A week after the initial X-ray experiments, a data collection on a second crystal was performed. This revealed the structure of dimeric **5.5**. Complex **5.5** crystallizes in a *P-1* unit cell with two half molecules in the asymmetric unit, which is then symmetrically expanded to make two whole molecules.

Complexes **5.1**, **5.2**, and **5.4** have strong similarities. Each of these complexes is monomeric, containing a four-coordinate Pt(II) center having two -$P(OPh)_3$ ligands and two selenium ions from one or more selenide ligands. Complex **5.1** is coordinated by Se_2naph, **5.2** is coordinated by mt-Se_2naph, and **5.4** is coordinated by two -SePh ligands. A list of selected bond lengths and angles for the three complexes is given in Tables 5-2 and 5-3. A comparison of bond lengths within this series of mononuclear complexes shows that all of these complexes have very similar Pt-P bond lengths ranging from 2.2232(13) Å to 2.2390(16) Å, with complex **5.2** having the shortest Pt-P bond length. The Pt-Se bond lengths have a larger difference. The Pt-Se bond distances are longest in **5.4** ranging from 2.481(2) Å to 2.463(2) Å, slightly shorter in **5.1** at 2.4600(7) Å and 2.4527(7) Å, and yet shorter in **5.2** at 2.4356(5) Å and 2.4256(5) Å. The short Pt-Se distances in **5.2** is possibly an effect of the electron donating *tert*-butyl arm on the naphthalene ring.

Table 5-2. Selected bond lengths (Å) for complexes **5.1**, **5.2**, and **5.4**.

	5.1	**5.2**	**5.4a**	**5.4b**[1]
Pt(1)-Se(1)	2.4600(7)	2.4356(5)	2.474(2)	2.481(2)
Pt(1)-Se(2)	2.4527(7)	2.4256(5)	2.463(2)	2.481(2)
Pt(1)-P(1)	2.2390(16)	2.2232(13)	2.229(5)	2.235(5)
Pt(1)-P(2)	2.2324(14)	2.2385(14)	2.224(4)	2.235(5)
Se(1)-C(1)	1.921(6)	1.914(5)	1.85(2)	1.87(2)
Se(2)-C	1.924(6)	1.930(4)	1.94(2)	

[1]Analgous atom to numbering scheme.

Table 5-3. Selected bond angles (°) for complexes **5.1**, **5.2**, and **5.4**.

	5.1	**5.2**	**5.4a**	**5.4b**[1]
Se(1)-Pt(1)-Se(2)	85.55(2)	89.885(17)	87.47(7)	89.43(8)
Se(1)-Pt(1)-P(1)	91.19(4)	86.94(3)	177.85(13)	171.09(14)
Se(2)-Pt(1)-P(2)	88.80(4)	88.02(4)	173.70(14)	171.09(14)
P(1)-Pt(1)-P(2)	94.67(6)	95.29(4)	92.35(18)	99.3(2)
Se(1)-Pt(1)-P(2)	169.82(5)	176.93(3)	86.50(13)	86.11(15)
Se(2)-Pt(1)-P(1)	176.33(4)	175.08(3)	93.73(13)	86.11(15)
Pt(1)-Se(1)-C(1)	100.17(17)	107.59(13)	110.3(6)	105.0(6)
Pt(1)-Se(2)-C	107.63(18)	116.77(15)	112.8(5)	

[1]Analgous atom to numbering scheme.

The Se(1)-Pt(1)-Se(2) bond angles increase from 85.55(2)° in **5.1**, to 87.47(7)° in **5.4a**, to 89.43(8)° in **5.4b**, and finally to 89.885(17)° in **5.2**. It is interesting that the only difference between **5.1** (the smallest angle) and **5.2** (the largest angle) is the substitution of the *tert*-butyl substituent on the naphthalene ring. Also, the size of the Se(1)-Pt(1)-Se(2) bond angle in **5.4** falls in the middle of the series of complexes, despite not being restricted by the backbone, as in **5.1** and **5.2**. The similarity of the bond angle (only ~4° difference) amongst the complexes is likely not coincidental, even if the ligands have no strong geometric preferences, the geometry of the complex is still limited by the tendency of Pt(II) to be square planar. It could be possible that even the slightest differences in the strength of the selenium donor could be a factor in the geometry around the platinum center. Also, the fact that the two structures of complex **5.4** differ by

nearly 2^{o} despite having the same molecular connectivity implicates crystal packing rather than intrinsic structural differences in the variation in that bond angle in **5.4a** and **5.4b**.

The difference in bond angle between **5.2** and **5.1** likely arises from the presence of the *tert*-butyl group on the naphthalene ring *ortho* to one of the selenium atoms in **5.2**. The steric bulk of the *tert*-butyl group pushes the selenium atom nearest to it out of the plane of the naphthalene ring, rendering the Se-Pt-Se bond angle larger than in **5.1**, where the selenium atoms may be constrained by a need to stay in the plane of the rings to participate in π-resonance.

Compared to the 4^{o} variation in the Se-Pt-Se angles, the *cis*- bond angles Se-Pt-P in the three complexes are universally similar. The Se(1)-Pt(1)-P(1) bond angle in **5.4** is 85.81(11)° and the Se(2)-Pt(2)-P(2) bond angle is 93.22(9)°. These angles in **5.1** differ from 90° by about 2.3°, with the Se(1)-Pt(1)-P(1) bond angle being 91.19(4)° and the Se(2)-Pt(2)-P(2) bond angle being 88.80(4)°. The bond angle differences in **5.2** are similar to the other two complexes, with the Se(1)-Pt(1)-P(1) bond angle being 86.94(3)° and the Se(2)-Pt(2)-P(2) bond angle being 88.02(4)°. The two *trans* Se-Pt-P bond angles of the three complexes likewise differ from each other by only a few degrees. The difference between the two angles is 7.5° in **5.1**, 5.5° in **5.4** and 1.8° in **5.2**.

The smallest of the *trans* Se-Pt-P bond angles occurs in **5.1**, with an angle of 169.82(5)°. Other than a bond angle of 173.43(11)° in **5.4**, all the other *trans* bond angles in all three complexes are very close to 176°. Like all the other angles, the P(1)-Pt(1)-P(2) bond angles of **5.1**, **5.2**, and **5.4** are very similar, except in **5.4b**, where it is the largest by 4° at 99.3(2)°. Somewhat strangely, the steric strain presented by the *t*-butyl group in **5.2** and the greater degree of freedom allowed by the lack of a constraining background in **5.4** do not seem to cause much variation in the structure around the metal center. The metal center appears to be dictating the geometry and forcing the ligands to arrange themselves so that the complex has as close to a square planar motif it can.

Complexes **5.3** and **5.5** are different from the three just discussed, in that they each crystallize as a dinuclear complex with two four-coordinate Pt(II) metal

centers in a diamond core motif as shown in Figure 5-7. Each Pt(II) ion in both complexes is coordinated by three selenium ions and one -$P(OPh)_3$ ligand. A list of selected bond lengths and angles for **5.3** and **5.5** are shown in Table 5-4 and Table 5-5, respectively. The difference between the two coordination spheres is that **5.3** has bis-selenium ligands based on the biphenyl backbone, while the platinum centers in **5.5** are ligated by individual -SePh ligands. One of the selenium atoms on the biphenyl in **5.3** is in a bridging position, which forces the ligand to twist and strain in order for the platinum to coordinate the other selenium atom. In **5.5**, the bridging and terminal positions are occupied by the -SePh ligands instead.

Table 5-4. Selected bond lengths (Å) and angles (°) for complex **5.3**.

Pt(1)-P(1)	2.202(2)	Pt(31)-P(31)	2.200(2)
Pt(1)-Se(2)	2.4370(10)	Pt(31)-Se(32)	2.4449(11)
Pt(1)-Se(31)	2.4582(10)	Pt(31)-Se(31)	2.4544(10)
Pt(1)-Se(1)	2.4569(10)	Pt(31)-Se(1)	2.4628(10)
Se(1)-C(19)	1.928(9)		
Se(31)-C(49)	1.944(10)		
Se(32)-C(56)	1.960(9)		
Se(2)-C(26)	1.922(10)		
P(1)-Pt(1)-Se(2)	88.50(7)	P(31)-Pt(31)-Se(32)	88.72(7)
P(1)-Pt(1)-Se(31)	93.86(7)	P(31)-Pt(31)-Se(1)	94.00(7)
Se(2)-Pt(1)-Se(1)	93.64(3)	Se(32)-Pt(31)-Se(31)	93.44(4)
Se(31)-Pt(1)-Se(1)	83.89(3)	Se(31)-Pt(31)-Se(1)	83.85(3)
Se(2)-Pt(1)-Se(31)	173.11(4)	Se(32)-Pt(31)-Se(1)	172.28(4)
P(1)-Pt(1)-Se(1)	177.60(7)	P(31)-Pt(31)-Se(31)	177.84(7)
C(19)-Se(1)-Pt(1)	93.9(3)	C(49)-Se(31)-Pt(31)	93.2(3)
C(19)-Se(1)-Pt(31)	106.5(3)	C(49)-Se(31)-Pt(1)	107.1(3)
Pt(1)-Se(1)-Pt(31)	96.04(3)	Pt(31)-Se(31)-Pt(1)	96.22(3)
C(26)-Se(2)-Pt(1)	110.1(3)	C(56)-Se(32)-Pt(31)	110.6(3)

Table 5-5. Selected bond lengths (Å) and angles (°) for **5.5**.

Pt(1)-P(1)	2.186(2)	Pt(31)-P(31)	2.193(2)
Pt(1)-Se(2)	2.4493(9)	Pt(31)-Se(32)	2.4445(8)
Pt(1)-Se(1A)	2.4697(9)	Pt(31)-Se(3A)	2.4632(8)
Pt(1)-Se(1)	2.4771(8)	Pt(31)-Se(31)	2.4763(8)
Se(1)-Pt(1A)	2.4697(9)	Se(31)-Pt(3A)	2.4632(8)
Se(1)-C(19)	1.927(7)	Se(31)-C(49)	1.931(7)
Se(2)-C(25)	1.932(8)	Se(32)-C(55)	1.925(8)
P(1)-Pt(1)-Se(2)	85.83(6)	P(31)-Pt(31)-Se(32)	84.01(5)
P(1)-Pt(1)-Se(1A)	95.66(6)	P(31)-Pt(31)-Se(3A)	96.90(5)
Se(2)-Pt(1)-Se(1)	94.71(3)	Se(3A)-Pt(31)-Se(31)	84.07(3)
Se(1A)-Pt(1)-Se(1)	83.89(3)	Se(32)-Pt(31)-Se(31)	94.99(3)
Se(2)-Pt(1)-Se(1A)	175.74(3)	Se(32)-Pt(31)-Se(3A)	176.46(3)
P(1)-Pt(1)-Se(1)	178.57(5)	P(31)-Pt(31)-Se(31)	178.86(6)
C(19)-Se(1)-Pt(1A)	98.9(2)	C(49)-Se(31)-Pt(3A)	100.5(2)
C(19)-Se(1)-Pt(1)	104.2(2)	C(49)-Se(31)-Pt(31)	103.7(2)
Pt(1A)-Se(1)-Pt(1)	96.11(3)	Pt(3A)-Se(31)-Pt(31)	95.93(3)
C(25)-Se(2)-Pt(1)	106.6(2)	C(55)-Se(32)-Pt(31)	106.3(2)

Rather unsurprisingly, given their similar coordination spheres, the bond distances in **5.3** and **5.4** are very similar throughout the complexes. The Pt-P bond lengths are similar at ~2.20 Å in **5.3** and ~2.19 Å in **5.5**. The Pt-Se bonds in both complexes differ depending on whether they are coordinated in a terminal or bridging fashion, but are again markedly similar between the two complexes. In **5.3**, the terminal Pt-Se bond lengths are ~2.44 Å, whereas the bridging bond lengths are ~2.46 Å. In **5.5**, the terminal Pt-Se bond lengths are ~2.45 Å, and the bridging bond lengths are ~2.47 Å.

Like the bond distances, the bond angles in **5.3** and **5.5** are very similar. Complex **5.3** has two obtuse angles and two acute angles around the platinum centers, which form a flattened X with a platinum atom in the center. The Se-Pt-Se bond angle of the diamond core is 83.89(3)°, and the angle *trans* to this, across

the platinum center, is 88.50(7)°. The other two angles around the platinum center are ~94°. The Pt-Se-Pt bond bridging the diamond core is 96.04(3)°.

The bond angles in **5.5** track very closely to those in **5.3**. The Se-Pt-Se bond angle of the diamond core is 83.89(3)° and *trans* to this, the angle is 85.83(6)°. The other two angles around the platinum center are 94.71(3)° and 95.66(6)°. The bridging Pt-Se-Pt angles are both almost exactly 96°. From this data, it seems as though the visibly twisted biphenyl-based diselenium ligand is not responsible for the distortion of the geometry around the metal center in **5.3**, since the -SePh ligands in **5.5** end up giving the complex an extremely similar set of bond lengths and angles without the ligand imposing a geometric restriction.

5.3. Conclusions

The synthesis and partial characterization of a new series of selenide platinum(II) bisphosphine complexes has been reported. These complexes were synthesized by the addition of *cis*-$[PtCl_2(P(OPh)_3)_2]$ to a lithium selenide salt (made in situ). This synthesis resulted in the mononuclear complexes $[Pt(Se_2naph)(P(OPh)_3)_2]$ (**5.1**), $[Pt(mt\text{-}Se_2naph)(P(OPh)_3)_2]$ (**5.2**), and *cis*-$[Pt(SePh)_2(P(OPh)_3)_2]$ (**5.4**) and the dinuclear complexes $[Pt_2(dibenzSe_2)_2(P(OPh)_3)_2]$ (**5.3**) and *trans*-$[Pt_2(SePh)_4(P(OPh)_3)_2]$ (**5.5**). The X-ray structures of these compounds have been reported. It seems that the preference for platinum(II) to be square planar, and not the rigidity of the organic backbone, dictates the geometry of these complexes.

5.4. Experimental

5.4.1. General Remarks

All synthetic procedures were performed under nitrogen using standard Schlenk techniques unless otherwise stated, reagents were obtained from commercial sources and used as received. Dry solvents were collected from an MBraun solvent system. ^{1}H, ^{13}C, ^{31}P, and ^{77}Se spectra were recorded on a Jeol DELTA GSX270 spectrometer. ^{195}Pt spectra were obtained on a Bruker AVII400.

Chemical shifts are reported in ppm and coupling constants (*J*) are given in Hz. IR (KBr pellet) and Raman spectra (powder sample) were obtained on a Perkin-Elmer system 2000 Fourier Transform spectrometer. Elemental analysis was performed by the University of St. Andrews, School of Chemistry Service. Positive-ion FAB mass spectra were performed by the EPSRC National Mass Spectrometry Service, Swansea. Precious metals were provided by Ceimig Ltd.

5.4.2. Synthetic Remarks

The compound *cis*-[$Pt(P(OPh)_3)_2Cl_2$] (OPh = OC_6H_5) was prepared by adding two equivalents of $P(OPh)_3$ to *cis*-[$PtCl_2$(cod)] (cod = 1,5-cyclooctadiene) in dichloromethane at room temperature instead of by the reported proceedure.[13]

*5.4.3. Standard synthesis for [Pt(L)(P(OPh)$_3$)$_2$], L = Se$_2$naph (**5.1**) and mt-Se$_2$naph (**5.2**)*

In a Schlenk tube, ~10 mL of dry THF was added to 1 mol eq. of L, the resulting purple solution was stirred for 10 minutes, and then 2 mol eq. of a 1 M solution of $LiBEt_3H$ in THF was added dropwise via syringe. Upon addition, the solution turned bright yellow and gas evolution was observed. This solution was stirred ~15 min and [$Pt(P(OPh)_3)_2Cl_2$] was added. The solution turned an orange color and was stirred 12 hours, after which ~1g of silica gel was added and the solvent was evaporated under vacuum. The flask containing the orange solid was opened to the air and the solid was placed on a short hexane-packed silica gel column. The column was eluted with hexane to remove any unreacted starting material and then washed with CH_2Cl_2. The CH_2Cl_2 band was collected and the solvent was removed under vacuum. Orange crystals were obtained for **5.1** (98 mg, 53%) and **5.2** (109mg, 50%) after recrystallization from CH_2Cl_2 by pentane diffusion.

[$Pt(Se_2naph)(P(OPh)_3)_2$] (**5.1**): Se_2naph (47 mg, 165 mmol), 0.33 mL 1 M soln of $LiBEt_3H$ in THF, and [$Pt(P(OPh)_3)_2Cl_2$] (147 mg, 165 mmol). Yield: 97 mg (53%). Anal. Calc'd (%) for $PtSe_2P_2O_6C_{46}H_{36}\cdot CH_2Cl_2$: C, 47.60; H, 3.23. Found (%): C, 47.79; H, 3.10. FAB^+ MS: *m/z* 1100 [M^+]. IR (KBr) : υ max, cm^{-1}

= 1587, 1486, 1182, 1159, 918, 778, 757, 687, 596, 496. Raman, cm^{-1} = 30720, 1591, 1538, 1333, 1007, 851, 733, 530, 200. All NMR samples were prepared from crystalline samples in $CDCl_3$. ^{1}H NMR: 7.6 (d, J_{H-H} = 7 Hz), 7.5 (d, J_{H-H} = 7 Hz), 7.2-6.9 (m), 6.9 (t, J_{H-H} = 7 Hz). ^{13}C NMR: 150.9, 136.3, 135.1, 129.8, 126.9, 125.2, 124.7, 120.9. ^{31}P NMR: 87.4 ppm (J_{P-Pt} = 4711 Hz) (J_{P-Se} = 28 Hz). ^{77}Se NMR: 139.5 ppm (t, J_{Se-P} = 28 Hz) (J_{Se-Pt} = 205 Hz). ^{195}Pt NMR: -4711.0 ppm (t, J_{Pt-P} = 4711 Hz) (J_{Pt-Se} = 203 Hz).

[Pt(mt-Se_2naph)($P(OPh)_3)_2$] (**5.2**): mt-Se_2naph (64 mg, 187 mmol), 0.37 mL 1 M soln of $LiBEt_3H$ in THF, and [$Pt(P(OPh)_3)_2Cl_2$] (166 mg, 187 mmol). Yield: 109 mg (50%). Anal. Calc'd (%) for $PtSe_2P_2O_6C_{50}H_{44}\cdot 0.5CH_2Cl_2$: C, 50.50; H, 3.78. Found (%): C, 50.51; H, 3.49. FAB^+ MS: *m/z* 1156 [M^+]. IR (KBr) : υ max, cm^{-1} = 1588, 1488, 1186, 1160, 922, 776, 756, 686, 595, 497. Raman, cm^{-1} = 3066, 1595, 1586, 1515, 1340, 1007, 857, 733, 185. All NMR samples were prepared from crystalline samples in $CDCl_3$. ^{1}H NMR: 7.4-7.0 (m), 6.9 (t, J_{H-H} = 7 Hz).), 1.7(s) ^{13}C NMR: 151.0, 150.9, 147.0, 142.5, 132.9, 132.1, 131.9, 129.7, 129.6, 126.5, 125.5, 125.2, 125.0, 123.9, 123.2, 121.0, 120.9, 120.7, 120.6, 38.2, 31.6. ^{31}P NMR: 89.3 ppm (d, J_{P-P} = 68 Hz), (J_{P-Pt} = 4686 Hz) (J_{P-Se} = 19, 28) 86.3 ppm (d, J_{P-P} = 68 Hz), (J_{P-Pt} = 4669 Hz) (J_{P-Se} = 34). ^{77}Se NMR: 258.4 ppm (dd, J_{Se-P} = 36, 19 Hz) (J_{Se-Pt} = 327 Hz) 138.4 ppm (dd, J_{Se-P} = 7, 29 Hz) (J_{Se-Pt} = 212 Hz). ^{195}Pt NMR: -4574.9 ppm (t, J_{Pt-P} = 4679 Hz).

*5.4.4. Synthesis of [Pt_2(dibenz$Se_2)_2$($P(OPh)_3)_2$] (**5.3**)*

In a Schlenk tube, ~10 mL of dry THF was added to 1 mol eq. of dibenzSe_2, the resulting pale orange solution was stirred for 10 minutes and then 2 mol eq. of a 1 M solution of $LiBEt_3H$ in THF was added dropwise via syringe. Upon addition, the solution turned very pale yellow, then clear with gas evolution. This solution was stirred ~15 min and [$Pt(P(OPh)_3)_2Cl_2$] was added. The solution turned bright yellow in color and was stirred 12 hours, after which time ~1g of silica gel was added and the solvent was evaporated under vacuum. The flask containing the yellow solid was opened to the air and the solid was placed on top of a short hexane-packed silica gel column. The column was eluted with hexane to

remove any unreacted starting material and then washed with 2:1 CH_2Cl_2:hexane. The resulting bright yellow band was collected and the solvent was removed under vacuum. X-ray quality crystals were obtained for **3** after recrystallization from CH_2Cl_2 by pentane diffusion. FAB^+ MS: *m/z* 1631 [M^+] (matches theoretical isotope profile for **5.3**, but there are higher molecular ion peaks in the sample). IR (KBr) : υ max, cm^{-1} = 1588, 1486, 1184, 1160, 1025, 922, 765, 687, 595, 491. Raman, cm^{-1} = 3066, 1589, 1030, 1008. NMR samples were prepared from crystalline samples in $CDCl_3$. ^{31}P NMR: 85.3 ppm ($J_{P\text{-}Pt}$ = 4685 Hz) ($J_{P\text{-}Se}$ = 21). ^{77}Se NMR: 222.8 – 226.9 ppm (m). ^{195}Pt NMR: -4569.7 ppm (t, $J_{Pt\text{-}P}$ = 4685 Hz) ($J_{Pt\text{-}Se}$ = 183 Hz).

*5.4.5. Synthesis of cis-[Pt(SePh)$_2$(P(OPh)$_3$)$_2$] (**5.4**) and [Pt$_2$(SePh)$_4$(P(OPh)$_3$)$_2$] (**5.5**)*

In a Schlenk tube, ~10 mL of dry THF was added to 1 mol eq. of Se_2Ph_2, the resulting yellow solution was stirred for 10 minutes and then 2 mol eq. of a 1 M solution of $LiBEt_3H$ in THF was added dropwise via syringe. Upon addition, the solution turned pale yellow with gas evolution. This solution was stirred ~15 min and [$Pt(P(OPh)_3)_2Cl_2$] was added. The solution turned bright orange in color and was stirred 12 hours, after which time ~1g of silica gel was added and the solvent was evaporated. The flask containing the orange solid was opened to the air and the solid was placed on a small hexane silica gel column. The column was eluted with hexane to remove any unreacted starting material and then washed with 2:1 CH_2Cl_2:hexane. This orange band was collected and the solvent was removed under vacuum. Complexes **5.4** and **5.5** co-crystallized out of the same CH_2Cl_2 solution by pentane diffusion. Complex **5.4** was deep orange in color, almost red, whereas **5.5** was bright yellow. All data was obtained from crystalline solid that contained both **5.4** and **5.5**. Anal. Calc'd (%) for $PtSe_2P_2O_6C_{48}H_{40}$ (**5.5**): C, 51.12; H, 3.57 and for $Pt_2Se_4P_2O_6C_{60}H_{50}$ (**5.5**): C, 44.08; H, 3.08. Found (%): C, 44.62; H, 2.81. FAB^+ MS: *m/z* 1635 [M^+] (matches theoretical isotope profile for **5.5**, but there are higher molecular ion peaks in the sample). IR (KBr) : υ max, cm^{-1} = 1587, 1485, 1183, 1156, 919, 784, 686, 601, 488. Raman, cm^{-1} = 3063,

1597, 1576, 1220, 1169, 1071, 1001, 226, 178. NMR samples were prepared in $CDCl_3$. ^{31}P NMR: 84.51 ppm ($J_{P\text{-}Pt}$ = 4724 Hz). ^{77}Se NMR: 221.44-222.50 ppm (m). ^{195}Pt NMR: -4074.88 ppm (t, $J_{Pt\text{-}P}$ = 4707 Hz).

5.5. References

1. S. M. Aucott, H. L. Milton, S. D. Robertson, A. M. Z. Slawin, G. D. Walker and J. D. Woollins, *Chem. Eur. J.,* 2004, 10, 1666-1676.

2. S. M. Aucott, P. Kilian, S. D. Robertson, A. M. Z. Slawin and J. D. Woollins, *Chem. Eur. J.,* 2006, 12, 895-902.

3. V. P. Ananikov, I. P. Beletskaya, G. G. Aleksandrov and I. L. Eremenko, *Organometallics,* 2003, 22, 1414-1421.

4. C. P. Morley, C. A. Webster and M. D. Vaira, *J. Organomet. Chem.,* 2006, 691, 4244-4249.

5. M. Rudd and S. Lindeman, *J. Chem. Cryst.,* 2007, 37, 375-379.

6. M. S. Hannu, R. Oilunkaniemi, R. S. Laitinen and M. Ahlgén, *Inorg. Chem. Commun.,* 2000, 3, 397-399.

7. S. Tomoda, M. Shimoda, Y. Takeuchi and Y. Iitaka, *Chem. Lett.,* 1988, 17, 535-538.

8. R. Oilunkaniemi, R. S. Laitinen and M. Ahlgrén, *J. Organomet. Chem.,* 2001, 623, 168-175.

9. E. S. Lang, M. M. Dias, S. S. d. Santos, E. M. Vázquez-López and U. Abram, *Z. Anorg. Allg. Chem.,* 2004, 630, 462-465.

10. P. A. W. Dean and J. J. Vittal, *Main Group Metal Organ. Chem.,* 2002, 25, 697-698.

11. V. K. Jain, S. Kannan, R. J. Butcher and J. P. Jasinski, *J. Organomet. Chem.,* 1994, 468, 285-290.

12. S. M. Aucott, D. Duerden, Y. Li, A. M. Z. Slawin and J. D. Woollins, *Chem. Eur. J.,* 2006, 12, 5495-5504.

13. S. J. Sabounchei and A. Naghipour, *Molecules,* 2001, 6, 777-783.

CHAPTER 6

STRUCTURAL ANALYSIS OF *PERI*-SUBSTITUTED NAPHATHLENE WITH GROUPS 15 AND 16 SUBSTITUENTS

6.1. Introduction

This chapter focuses on the strain-induced structural variations that occur in *peri*-substituted naphthalene when the *peri*-substituents contain elements from groups 15 (P) and 16 (O, S or Se) and these *peri*-substituents are not covalently bound to each other. This chapter is divided into three sections, which will purely describe structural features, followed by a summary for comparative purposes. Section 1 describes the structural features of a crystallographically characterized parent molecule (8-phenylsulfanylnaphth-1-yl)diphenylphosphine (**6.1**) (Figure 6-1),[1] section 2 discusses the structural changes that occur in **6.1** when increased bulk is added to the phosphorus atom through oxygenation (-P(=O)Ph_2), sulfuration (-P(=S) Ph_2), or selenation (-P(=Se)Ph_2), and section 3 discusses compounds similar to **6.1**, but in which the size of the non-phosphorus-containing *peri*-substituent is varied (-SePh, -SEt, or -OMe) (Figure 6-2).

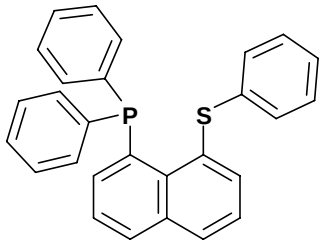

Figure 6-1. Line drawing of (8-phenylsulfanylnaphth-1-yl)diphenylphosphine (**6.1**).

6.2. Section 1

(8-phenylsulfanylnaphth-1-yl)diphenylphosphine (**6.1**, Figure 6-1) is a *peri*-substituted naphthalene derivative that displays non-bonding interactions between the -PPh_2 and -SPh substituents (Figure 6-3). This molecule crystallizes in the space group $P2_1/c$ (R_1 = 7.74%). Refinement data can be found in Appendix 1.

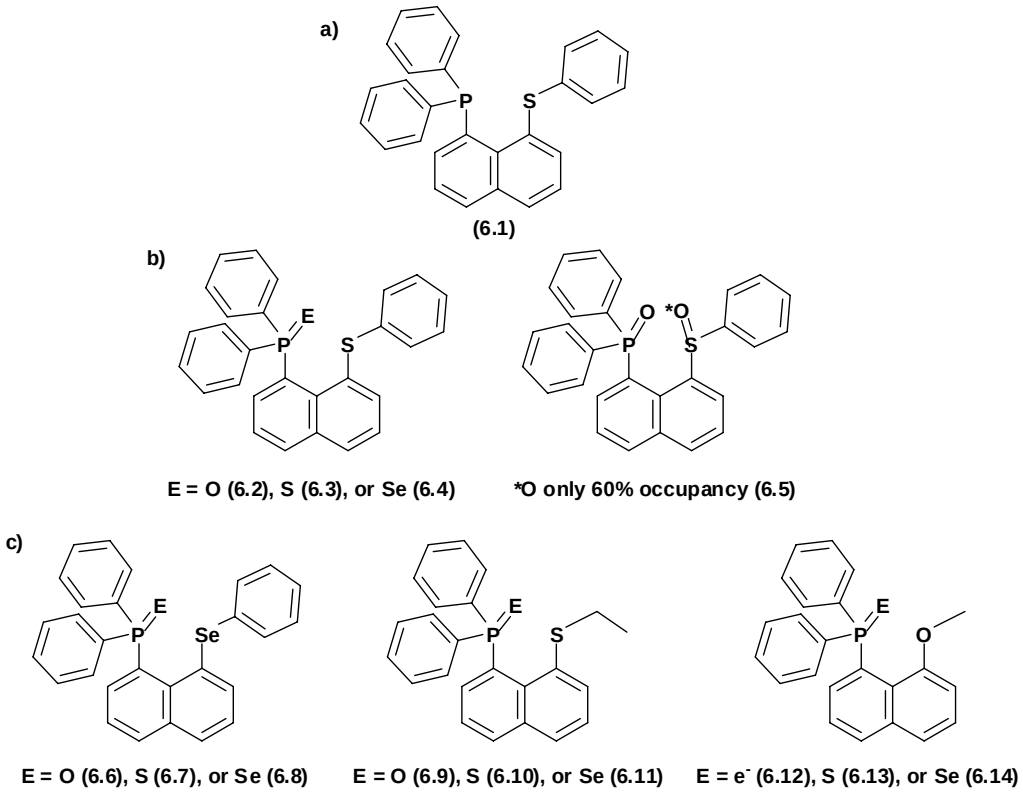

Figure 6-2. (8-phenylsulfanylnaphth-1-yl)diphenylphosphine (**6.1**) and its derivatives discussed in sections 2 and 3.

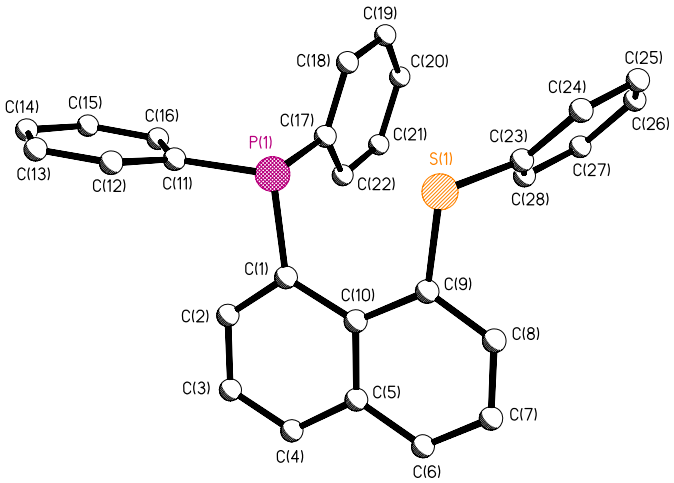

Figure 6-3. Molecular structure of **6.1**.

A structural comparison of **6.1** to unsubstituted naphthalene reveals the distortions used by **6.1** to reduce the steric strain created by the presence of bulky *peri*-substituents (Table 6-1).

Table 6-1. Selected bond lengths (Å) and angles (°) of naphthalene and **6.1**.

	Naphthalene[a]	**6.1**[b]
X(1)…X(2)	2.45(1)	3.0339(13)
X(1)-C(1)	1.08(1)	1.850(3)
X(2)-C(9)	1.08(1)	1.784(3)
X(1)-C(1)-C(2)	121.2(1)	118.0(2)
X(1)-C(1)-C(10)	118.3(1)	124.1(2)
X(2)-C(9)-C(8)	121.0(1)	115.1(2)
X(2)-C(9)-C(10)	118.5(1)	123.8(2)
C(2)-C(1)-C(10)	120.6(1)	117.8(3)
C(10)-C(9)-C(8)	120.5(1)	121.0(3)
C(1)-C(10)-C(9)	121.7(1)	126.4(3)
C(4)-C(5)-C(10)-C(1)	-0.05(1)	-1.2(4)
C(6)-C(5)-C(10)-C(9)	0.05(1)	0.1(3)
C(4)-C(5)-C(10)-C(9)	180.00(3)	-179.5(3)
C(6)-C(5)-C(10)-C(1)	180.00(3)	178.5(3)

[a] Measured at 100K. [2]
[a] X(1) and X(2) are both hydrogen atoms.
[b] X(1) is P(1) and X(2) is S(1).

In **6.1**, the P(1)-C(1) bond length is 1.850(3) Å and S(1)-C(9) bond length is 1.784(3) Å, whilst the non-bonding distance between the P(1) and S(1) atoms is 3.0339(13) Å. For comparison, in naphthalene[2], the distance between the *peri*-hydrogen atoms is 2.45(1) Å, i.e. much closer than the *peri*-substituents in **6.1**. A 3c-4e hypervalent interaction seems likely in **6.1** since the P(1)…S(1) distance is well within the sum of the Van der Waals radii of 3.60 Å and there is a quasi-linear arrangement of the S(1)…P(1)-C_{Ph} atoms (174.5(1)°).[3-5]

In-plane deflections are evident in **6.1**; the outer angles around the *peri*-positions, P(1)-C(1)-C(2) (118.0(2)°) and S(1)-C(9)-C(8) (115.1(2)°) are smaller than the similar outer angles (H-C-C) in naphthalene (~121°) and the inner angles P(1)-C(1)-C(10) (124.1(2)°) and S(1)-C(9)-C(10) (123.8(2)°) are larger than those

in naphthalene.[2] Also, in **6.1**, the out-of-plane deflections for P(1) is 0.0181(49) Å and 0.1359(48) Å for S(1).

The ring distortions around the *peri*-positions in the naphthalene backbone of **6.1** are 126.4(3)° for C(1)-C(10)-C(9), 121.0(3)° for C(10)-C(9)-C(8), and 117.8(3)° for C(2)-C(1)-C(10). In naphthalene, all three of these angles are roughly 121°.[2] Naphthalene is, for the most part, quite planar with central torsions angles close to 0° or ± 180°. The naphthalene backbone in **6.1** deviates slightly from planar, with the central torsion angles of C(4)-C(5)-C(10)-C(1) = -1.2(4)°, C(6)-C(5)-C(10)-C(9) = 0.1(3)°, C(4)-C(5)-C(10)-C(9) = -179.5(3)°, and C(6)-C(5)-C(10)-C(1) = 178.5(3)°.

Since the *peri*-substituents are the only difference between **6.1** and naphthalene, the presence and in particular the added bulk of the -PPh_2 and -SPh groups in **6.1** must be responsible for all four distortions relative to naphthalene. We speculated that increasing the bulk in the *peri*-positions of **6.1** would allow us to correlate which specific characteristics of the *peri*-substituents can cause specific structural distortions. The next section addresses compounds with added bulk (O, S, or Se) on the P(1) atom of **6.1**.

6.3. Section 2

The phosphorus atom in **6.1** may be oxidized to form a -$P(=O)Ph_2$ *peri*-substituted analog (**6.2**), a thiophosphonate analog (-$P(=S)Ph_2$ is **6.3**), or a selenophosphonate (-$P(=Se)Ph_2$ to give **6.4**). Further, the S(1) atom of **6.1** is (partially) oxidized, creating -$P(=O)Ph_2$ and -S(=O)Ph *peri*-substituents in **6.5**, (Figure 6-4). Since **6.1** used four modes of distortion to stabilize the -PPh_2 and -SPh substituents, we can compare their structures to understand how increased bulk around the *peri*-substituents affects the naphthalene backbone.

Compound **6.2** co-crystallizes with one molecule of CH_2Cl_2 in a triclinic (*P*-1) cell (R_1 = 5.08%). Compounds **6.3** and **6.4** are isomorphous and crystallize in $P2_1/n$ (R_1 = 5.82% and 4.27%, respectively) (Figure 6-5). Refinement data can be found in Appendix 1. Table 6-2 displays selected bond lengths and angles for **6.1**-**6.4**.

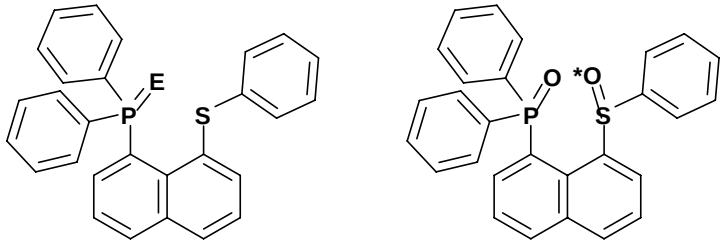

E = O (6.2), S (6.3), or Se (6.4) *O only 60% occupancy (6.5)

Figure 6-4. Line drawings of **6.2**, **6.3**, **6.4**, and **6.5**.

Unsurprisingly, the P=E distance in **6.2**, **6.3**, and **6.4** significantly increases as the chalcogen size increases; however the bonds remain typical of P=E bond distances. (Normal P=E bond distances for which E is O and S in C_3-**P=E** are 1.489(10) Å and 1.954(5) Å, respectively. Similarly, in X_3-**P=Se**, the P=Se bond length average is 2.093(19) Å.[6,7]) The P(1)-C(1) bond distances in **6.2**, **6.3**, and **6.4** are statistically invariant from each other, but they are all slightly shorter than the P(1)-C(1) distance in **6.1**. The S(1)-C(9) bond distance in **6.1**-**6.4** are indistinguishable within error.

The *peri*-distance increases in **6.2**, **6.3**, and **6.4** when compared to **6.1**. However, the distance does not increase reliably with increasing chalcogen size. The P(1)…S(1) distance in **6.2** is smaller than in **6.3** or in **6.4**, however this distance in **6.3** and **6.4** is almost identical. This is in accordance with their similar unit cell parameters, but seems counterintuitive because of the size difference of the P=S verses the P=Se moiety.

A 3c-4e hypervalent interaction seems likely in these compounds since the P(1)…S(1) distances are well within the sum of the Van der Waals radii of 3.60 Å and there is a quasi-linear arrangement of the S(1)…P(1)-C_{Ph} atoms (177.6(1)° for **6.2**, 174.0(1)° for **6.3**, and 173.8(1)° in **6.4**).[3-5]

Due to the shorter P(1)…S(1) distance and the increased linearity of the S(1)…P(1)-C_{Ph} bond angle in **6.2**, compared to **6.3** and **6.4**, it seems as though the oxidation of the phosphorus atom by the more electronegative oxygen atom forms a stronger hypervalent interaction between the sulfur and the pentavalent

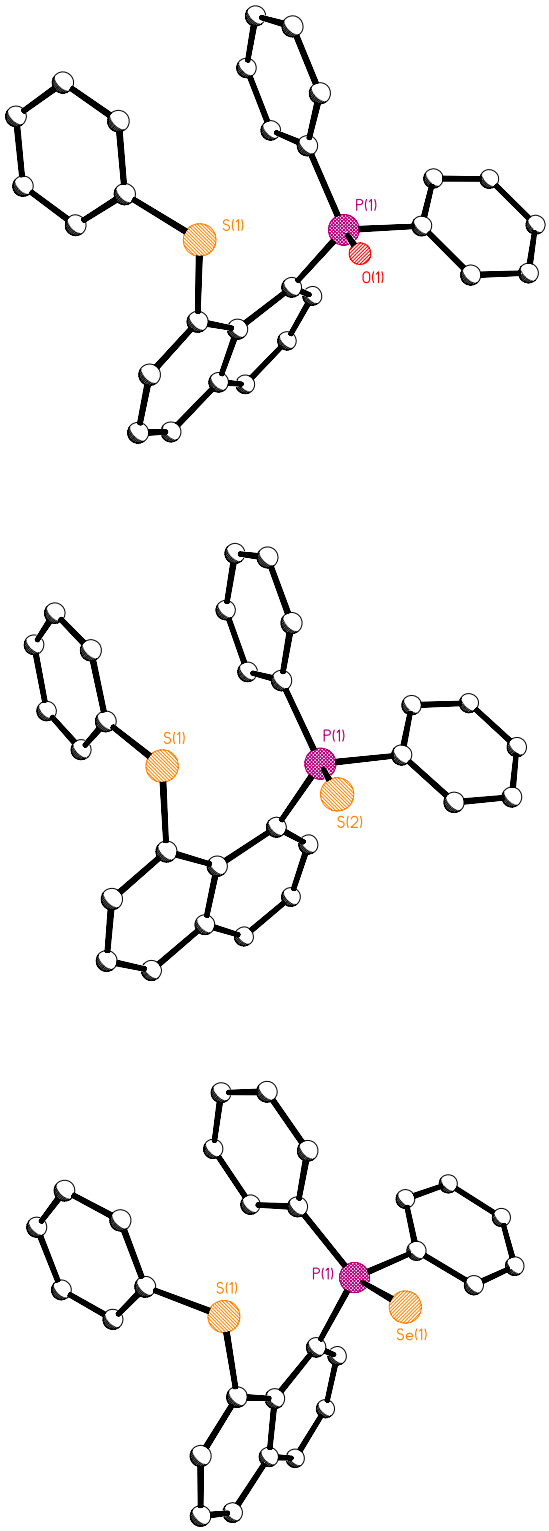

Figure 6-5. Structural representations of **6.2**, **6.3**, and **6.4**.

Table 6-2. Selected bond lengths (Å) and angles (°) for **6.1**-**6.4**.

	6.1[b]	**6.2**	**6.3**	**6.4**
P(1)…S(1)	3.0339(13)	3.1489(9)	3.1909(11)	3.1900(13)
S(1)…E[1]		2.9612(17)	3.3142(11)	3.3974(10)
P(1) - E[1]		1.492(2)	1.9585(12)	2.1181(11)
P(1) - C(1)	1.850(3)	1.835(3)	1.837(3)	1.836(4)
S(1) - C(9)	1.784(3)	1.777(3)	1.779(3)	1.782(4)
S(1)…P(1)-C_{Ph}	174.5(1)	177.6(1)	174.0(1)	173.8(1)
C(1) - P(1) - E[1]		114.34(14)	113.09(10)	112.29(12)
P(1)-C(1)-C(2)	118.0(2)	116.1(2)	116.0(2)	115.7(2)
P(1)-C(1)-C(10)	124.1(2)	124.6(2)	124.2(2)	125.0(3)
S(1)-C(9)-C(8)	115.1(2)	117.6(2)	116.3(2)	116.3(3)
S(1)-C(9)-C(10)	123.8(2)	121.6(2)	122.2(2)	122.5(3)
C(2)-C(1)-C(10)	117.8(3)	118.7(3)	118.8(3)	118.3(3)
C(10)-C(9)-C(8)	121.0(3)	120.7(3)	121.3(3)	121.0(3)
C(1)-C(10)-C(9)	126.4(3)	126.2(3)	127.3(3)	126.6(3)
C(4)-C(5)-C(10)-C(1)	-1.2(4)	-9.4(3)	-6.5(4)	-7.5(5)
C(6)-C(5)-C(10)-C(9)	0.1(3)	-8.6(3)	-6.4(4)	-4.0(5)
C(4)-C(5)-C(10)-C(9)	-179.5(3)	170.3(2)	173.4(2)	173.1(3)
C(6)-C(5)-C(10)-C(1)	178.5(3)	171.7(2)	173.7(2)	175.4(3)
Mean Plane Deviations				
P(1)	0.0181(49)	0.631(4)	0.633(4)	0.621(5)
S(1)	0.1359(48)	-0.582(4)	-0.451(4)	-0.433(5)
E[1]		1.623(5)	2.198(4)	2.346(5)

[1]E = O for **6.2**, S for **6.3**, or Se for **6.4**.

phosphorus. Though it is true that in all three cases the phosphorus atom is formally in the same oxidation state, when bound to sulfur (EN 2.5) or selenium (EN 2.4), phosphorus (EN 2.2), it will nonetheless be considerably more electron rich than when bound to oxygen (EN 3.5).[8] This would render the phosphorus in **6.2** substantially more electron deficient than the phosphorus in either **6.3** or in **6.4**, which would make it attract electron density from the lone pairs on the neighboring sulfur atom, leading to a shorter interatomic distance.

Unsurprisingly, because the P(1)…S(1) distance is increased, the outer angles, P(1)-C(1)-C(2) and S(1)-C(9)-C(8), are all less than 120° and the inner angles, P(1)-C(1)-C(10) and S(1)-C(9)-C(10), are all greater than 120°. The outer angles for **6.2**-**6.4** are smaller than those in **6.1**. The inner angles are similar (or

slightly smaller) in **6.2**-**6.4** than in **6.1**, suggesting that other structural deviations are used to accommodate the added bulk of the chalcogen atom on the phosphorus substituent in the *peri*-region.

It appears that **6.2**-**6.4** account for the added bulk in the *peri*-region through out-of-plane distortions. In **6.2**-**6.4**, the deviations of both P(1) and S(1) from the naphthalene plane are all similar and are all much larger than in **6.1**. In **6.2**, the S(1) atom deviates further from the plane than it does in **6.3** and **6.4**. In all of the compounds, P(1) deviates to one side of the plane and S(1) deviates to the other side. This type of split distortion should logically have an effect on the naphthalene backbone. Furthermore, the distance that E deviates from the naphthalene plane increases as the size of the chalcogen increases.

The distortions of the naphthalene ring are fairly severe in **6.2**-**6.4**. The inner ring torsion angles in the naphthalene ring are distorted ~ ± 9° from planar in **6.2** and ~ ± 7° in **6.3**. The ring in **6.4** is more twisted, as the four inner torsion angles are very different from each other; C(4)-C(5)-C(10)-C(1) is -7.5(5)°, C(6)-C(5)-C(10)-C(9) is -4.0(5)°, C(4)-C(5)-C(10)-C(9) is 173.1(3)°, and C(6)-C(5)-C(10)-C(1) is 175.4(3)°. The angles in the naphthalene backbone around the *peri*-substituents can be compared to unsubstituted naphthalene. The C(10)-C(9)-C(8) angle in **6.1**-**6.4** is very similar to that of naphthalene, but C(1)-C(10)-C(9) is much larger (by ~5°) and C(2)-C(1)-C(10) is slightly smaller (by ~3°) in the substituted compounds.

More bulk in the *peri*-region is introduced in a derivative of **6.2** (**6.5)**, where both P(1) and S(1) have been oxidized to form -P(=O)Ph_2 and -S(=O)Ph groups (Figure 6-6). Crystallographically, O(2) (of the S=O bond) is only a 60% occupant crystallizing in a triclinic (*P*-1) unit cell (R_1 = 5.61%). A comparison of selected bond angles and distances of **6.5** with **6.1** and **6.2** are shown in Table 6-3. The S(1)-O(2) distance of 1.468(3) Å appears slightly shorter than a typical S=O bond (1.497(13) Å), but that could be due to the partial occupancy of O(2).[6, 7] The addition of the oxygen atom on S(1) in **6.5** creates slightly different deviations compared to **6.2**. The S(1)-C(9) distance in **6.5** is slightly longer than in **6.2**, while the P(1)…S(1) distance is similar in these two compounds. The in-plane

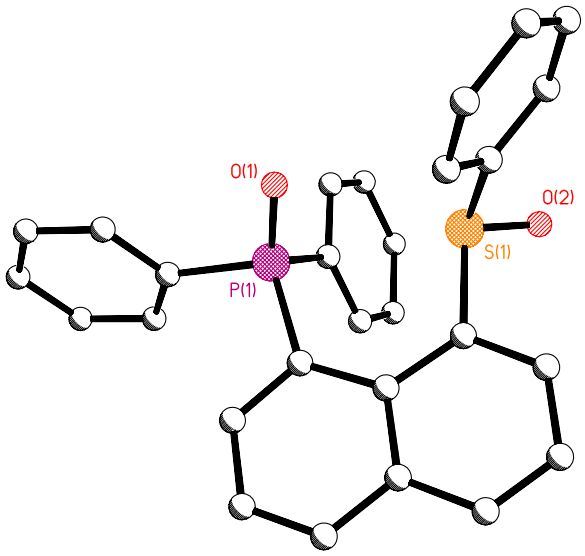

Figure 6-6. Structural representation of **6.5**, where O(2) is a 60% occupant.

distortions in **6.5** are more severe than in **6.2**, evidenced by larger (~3°) inner angles, smaller (~3°) outer angles, and close-to-linear torsion angles. The out-of-plane distortions in **6.5** are not as severe as in **6.2**, perhaps since the in-plane distortions are larger. In fact, the S(1) atom in **6.5** essentially rests in the naphthalene plane (-0.005(4) Å).

6.4. Section 3

The structural deviations available to **6.1** were further explored by altering the non-phosphorus containing *peri*-substituent. Described in this section are compounds similar to the oxidized, sulfurized, and selenized derivatives **6.2**-**6.4**, but with variation occurring at the -SPh *peri*-substituent (Figure 6-7). There are three modifications that replace the -SPh *peri*-substituent; a bulkier -SePh substituent, a smaller -SEt substituent, and an even smaller -OMe substituent (Figure 6-7). These three modifications will be individually discussed.

Table 6-3. Selected bond lengths (Å) and angles (°) for **6.1**, **6.2**, and **6.5**.

	6.1	**6.2**	**6.5**
P(1)…S(1)	3.0339(13)	3.1489(9)	3.1424(9)
S(1)…O(1)		2.9612(17)	3.079(2)
P(1)…O(2)			4.357(2)
S(1) - O(2)			1.468(3)
P(1) - O(1)		1.492(2)	1.4892(18)
P(1) - C(1)	1.850(3)	1.835(3)	1.832(3)
S(1) - C(9)	1.784(3)	1.777(3)	1.805(3)
S(1)…P(1)-C_{Ph}	174.5(1)	177.6(1)	169.5(1)
O(2) - S(1) - C(9)			107.78(17)
C(1) - P(1) - O(1)		114.34(14)	113.83(14)
P(1)-C(1)-C(2)	118.0(2)	116.1(2)	114.9(2)
P(1)-C(1)-C(10)	124.1(2)	124.6(2)	126.3(2)
S(1)-C(9)-C(8)	115.1(2)	117.6(2)	113.8(2)
S(1)-C(9)-C(10)	123.8(2)	121.6(2)	124.0(2)
C(2)-C(1)-C(10)	117.8(3)	118.7(3)	118.7(2)
C(10)-C(9)-C(8)	121.0(3)	120.7(3)	122.2(3)
C(1)-C(10)-C(9)	126.4(3)	126.2(3)	127.4(2)
C(4)-C(5)-C(10)-C(1)	-1.2(4)	-9.4(3)	-3.0(4)
C(6)-C(5)-C(10)-C(9)	0.1(3)	-8.6(3)	-1.9(4)
C(4)-C(5)-C(10)-C(9)	-179.5(3)	170.3(2)	177.0(2)
C(6)-C(5)-C(10)-C(1)	178.5(3)	171.7(2)	178.1(2)
Mean Plane Deviations			
P(1)	0.018(5)	0.631(4)	-0.78(4)
S(1)	0.136(5)	-0.582(4)	-0.005(4)
O(1)		1.623(5)	1.176(5)
O(2)			-0.899(5)

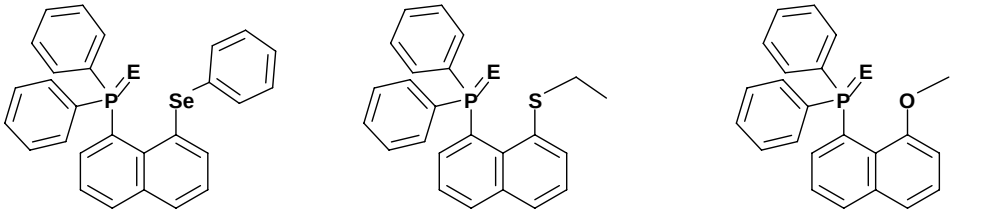

E = O (6.6), S (6.7), or Se (6.8) **E = O (6.9), S (6.10), or Se (6.11)** **E = e^- (6.12), S (6.13), or Se (6.14)**

Figure 6-7. Three types of compounds discussed in Section 3.

6.4.1. Modification 1

Compounds **6.6**, **6.7**, and **6.8** are similar to the versions of **6.1** where P(1) has been oxidized, sulfurized, and selenized, however, these compounds have a bulkier -SePh *peri*-substituent (instead of -SPh as seen in **6.1**) (Figure 6-7). Despite having the bulkier -SePh group, **6.7** and **6.8** are isomorphous with **6.3** and **6.4**, which contain the -SPh group. All four of these compounds crystallize in the $P2_1/n$ space group. Compounds **6.7** and **6.8** solved with R_1 = 4.31% and 5.53%, respectively. Unlike the other two compounds in the -SePh series, **6.6** crystallizes in the $P2_1$ space group with R_1 = 3.74% (Figure 6-8). Refinement data can be found in Appendix 1. Table 6-4 displays selected bond lengths and angles of **6.1** and **6.6**-**6.8**.

The P=E distance in **6.6**, **6.7**, and **6.8** increases as the chalcogen size increases, and the distances are typical of P=E bond distances.[6,7] Similar to the **6.2**-**6.4** series in section 2, the Se(1)…E distance is similar in the sulfur and selenium compounds, **6.7** and **6.8**, but much shorter in the oxygen compound **6.6**. The P(1)-C(1) bond distances are similar in **6.6**-**6.8**. The Se(1)-C(9) bond distance in **6.7** and **6.8** are very similar, but (surprisingly) the equivalent bond length in **6.6** is slightly longer. The addition of the bulkier -SePh *peri*-substituent has increased the *peri*-distance of these compounds compared to the -SPh analogs by ~0.08 Å. The P(1)…Se(1) distance in the -SePh analogs increases from 3.2152(15) Å (**6.6**) to 3.2776(16) Å (**6.8**) to 3.2803(8) Å (**6.7**). This means that, unlike **6.2**-**6.4**, increasing the size of the chalcogen on the phosphorus atom in these compounds does not lead to a proportional increase in the *peri*-distance.

In-plane distortions are evident since the outer angles are all less than 120° and the inner angles are all greater than 120°. The out-of-plane distortions of Se(1) and P(1) in **6.6**-**6.8** are similar to each other, but much larger than in **6.1**, which is unsurprising due to the increased size of the *peri*-substituents. The distance of E from the plane shows that while the deflection of **6.7** and **6.8** are similar, the O(1) atom in **6.6** lies much closer to the naphthalene plane. It is also interesting that there is a short Se(1)…O(1) distance (2.770(3) Å) in **6.6**.

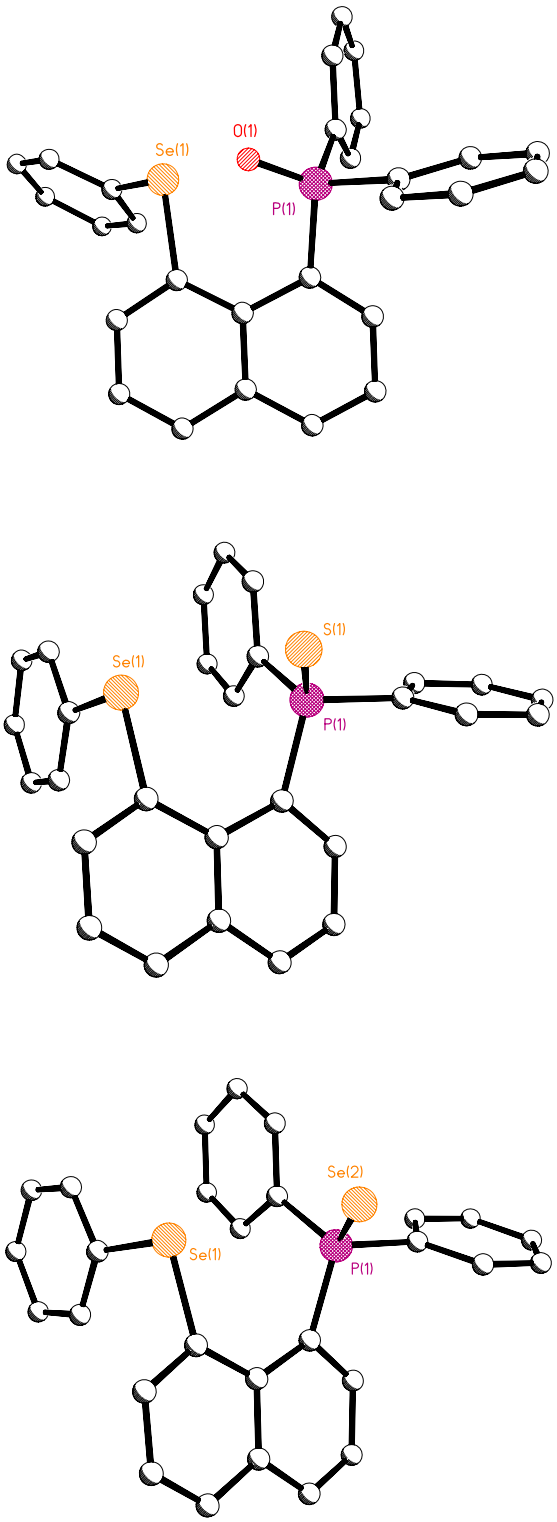

Figure 6-8. Structural representations of **6.6**, **6.7**, and **6.8**.

Table 6-4. Selected bond lengths (Å) and angles (°) for **6.1**, **6.6**, **6.7**, and **6.8**.

	6.1 [1]	**6.6**	**6.7**	**6.8**
P(1)…Se(1)	3.0339(13)	3.2152(15)	3.2803(8)	3.2776(16)
Se(1)…E[2]		2.770(3)	3.3490(7)	3.4217(8)
P(1) - E[2]		1.476(4)	1.9567(10)	2.1165(16)
P(1) - C(1)	1.850(3)	1.826(5)	1.837(3)	1.825(6)
Se(1) - C(9)	1.784(3)	1.937(4)	1.916(3)	1.917(6)
S(1)…P(1)-C_{Ph}	174.5(1)	167.9(1)	173.5(1)	172.9(1)
C(1) - P(1) - E[2]		113.0(2)	112.88(9)	112.52(19)
P(1)-C(1)-C(2)	118.0(2)	116.1(4)	115.5(2)	114.8(4)
P(1)-C(1)-C(10)	124.1(2)	123.6(3)	125.4(2)	126.5(4)
Se(1)-C(9)-C(8)	115.1(2)	114.0(3)	114.5(2)	114.5(4)
Se(1)-C(9)-C(10)	123.8(2)	125.1(3)	124.7(2)	124.5(4)
C(2)-C(1)-C(10)	117.8(3)	119.5(4)	118.2(2)	117.5(5)
C(10)-C(9)-C(8)	121.0(3)	120.9(4)	120.6(2)	120.8(6)
C(1)-C(10)-C(9)	126.4(3)	126.8(4)	126.7(2)	126.3(5)
C(4)-C(5)-C(10)-C(1)	-1.2(4)	-7.6(7)	-6.4(4)	-3.8(8)
C(6)-C(5)-C(10)-C(9)	0.1(3)	-7.6(8)	-5.2(3)	-5.4(5)
C(4)-C(5)-C(10)-C(9)	-179.5(3)	170.5(5)	173.6(2)	175.1(5)
C(6)-C(5)-C(10)-C(1)	178.5(3)	174.4(5)	174.9(2)	175.7(5)
Mean Plane Deviations				
P(1)	0.018(5)	-0.578(6)	0.601(3)	0.578(7)
Se(1)	0.1365	0.451(6)	-0.420(3)	-0.397(7)
E[2]		-1.458(8)	2.179(4)	2.314(8)

[1] S(1) is implied in this compound instead of Se(1).
[2] E = O for **6.6**, S for **6.7**, or Se for **6.8**.

As expected, the distortions of the inner torsion angles in the naphthalene backbone of **6.6-6.8** are more severe than in **6.1**. Surprisingly though, the distortions in the naphthalene backbone increase as the size of E decreases. The most severe distortions are seen in **6.6**. This could be either due to the O(1) atom being more in the naphthalene plane or it could be the reason why the O(1) atom can sit closer to the plane. The oxygen atom being in the plane, further, may be due to an oxygen-selenium interaction that is not as favored when the oxygen atom is replaced by sulfur or selenium.

6.4.2. Modification 2

Further modification of the *peri*-substituents has been made on the sulfurized and selenized derivatives of **6.1** by replacing the -SPh *peri*-substituent with the smaller -SEt group, forming **6.9**, **6.10**, and **6.11** (Figure 6-9). Compound **6.9** crystallizes in the *C*2/*c* space group with R_1 = 6.77%, whereas **6.10** crystallizes in a $P2_1/c$ space group with R_1 = 6.58%, and **6.11** crystallizes in the $P2_1/n$ space group with R_1 = 6.90% (Figure 6-10). Selected bond lengths and angles can be seen in Table 6-5. Refinement data is in Appendix 1.

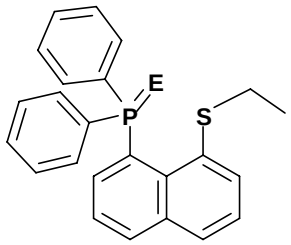

E = O (6.9), S (6.10), or Se (6.11)

Figure 6-9. Modification 2 of **6.1** where -SPh is replaced by an -SEt group.

The P=E bond distances are typical and, as expected, increase as the size of E increases.[6,7] The P(1)-C(1) bond distance and the S(1)-C(9) bond distance are similar **6.9**-**6.11**. The P(1)…S(1) distance slightly increase from 3.1346(13) Å (**6.9**) to 3.2083(14) Å (**6.10**) to 3.2283(19) Å (**6.11**). These distances are much shorter than the distances in the compounds containing the bulkier -SePh *peri*-substituents (**6.6**-**6.8**). Compounds **6.9**-**6.11**, like the others, display in-plane distortions where the outer angles are all less than 120°, the inner angles are all greater than 120°, and the angles in all three compounds are very similar to each other.

The out-of-plane distortions in **6.9**-**6.11** are more severe than in any of the other series, with **6.10** being the most distorted. S(1) and P(1) deviate on opposite sides of the plane. The distance of E from the plane in this series drastically increases by almost 0.3 Å as the size of E increases.

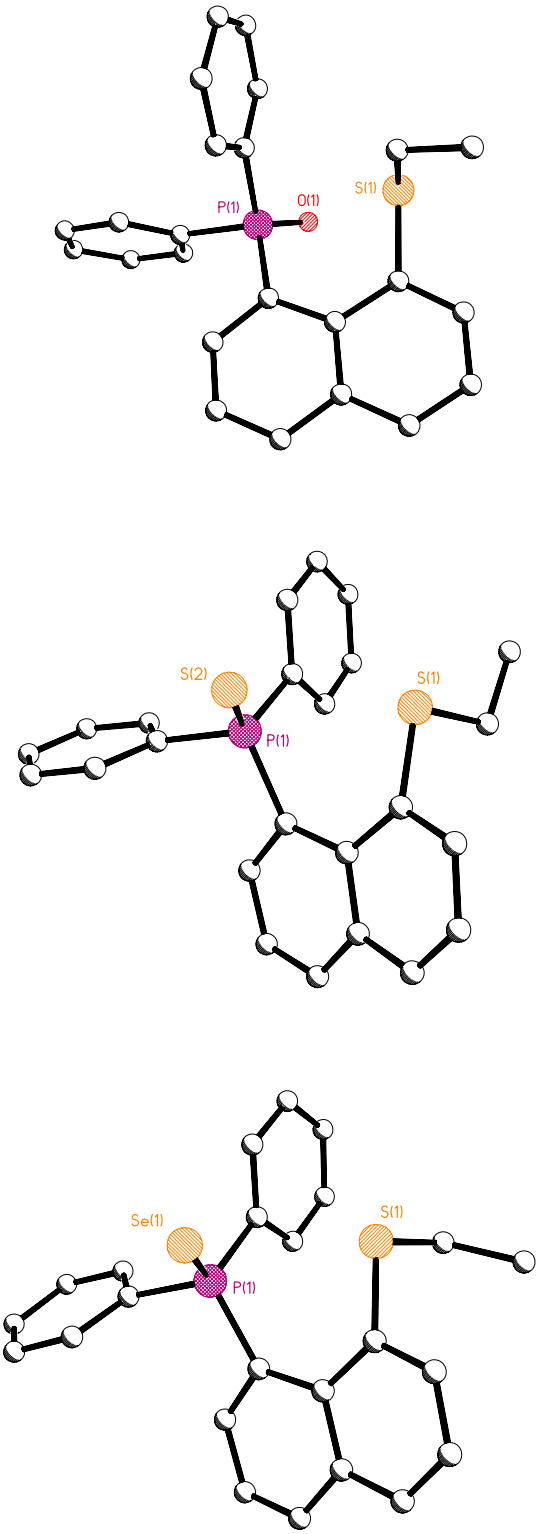

Figure 6-10. Structural representations of **6.9**, **6.10** and **6.11**.

Table 6-5. Selected bond lengths (Å) and angles (°) for **6.9**, **6.10**, and **6.11**.

	6.9	**6.10**	**6.11**
P(1)…S(1)	3.1349(13)	3.2083(14)	3.2283(19)
S(1)…E[1]	3.033(2)	3.2951(15)	3.4326(18)
P(1) - E[1]	1.487(2)	1.9550(14)	2.1103(17)
P(1) - C(1)	1.832(3)	1.837(3)	1.843(5)
S(1) - C(9)	1.772(3)	1.783(4)	1.771(6)
S(1)…P(1)-C_{Ph}	174.3(1)	175.4(1)	170.9(1)
C(1) - P(1) - E[1]	112.50(15)	114.17(12)	111.67(19)
P(1)-C(1)-C(2)	116.7(2)	115.5(2)	115.6(3)
P(1)-C(1)-C(10)	123.9(2)	124.5(2)	124.2(3)
S(1)-C(9)-C(8)	116.4(3)	117.5(3)	116.7(4)
S(1)-C(9)-C(10)	122.7(2)	121.4(2)	122.4(4)
C(2)-C(1)-C(10)	118.3(3)	119.2(3)	118.8(4)
C(10)-C(9)-C(8)	120.7(3)	120.3(3)	120.5(5)
C(1)-C(10)-C(9)	126.5(3)	126.0(3)	127.2(4)
C(4)-C(5)-C(10)-C(1)	-5.6(5)	10.4(5)	5.0(9)
C(6)-C(5)-C(10)-C(9)	-4.0(5)	10.3(5)	6.0(9)
C(4)-C(5)-C(10)-C(9)	175.0(3)	-171.0(3)	-175.3(6)
C(6)-C(5)-C(10)-C(1)	175.4(3)	-168.4(3)	-173.7(6)
Mean Plane Deviations			
P(1)	-0.566(4)	-0.620(4)	-0.599(7)
S(1)	0.404(4)	0.744(4)	0.527(6)
E[1]	-1.720(5)	-2.019(5)	-2.302(7)

[1]E = O for **6.9**, S for **6.10**, or Se for **6.11**.

The naphthalene backbone distortions seem fairly minor when comparing the distortions in the angles around the *peri*-substituents. While the C(10)-C(9)-C(8) angles are close to 120°, the C(1)-C(10)-C(9) angles are 126.5(3)° for **6.9**, 126.0(3)° for **6.10**, and 127.2(4)° for **6.11**. The C(2)-C(1)-C(10) angles are all ~119°. Despite these seemingly minor distortions in the angles around the *peri*-positions, the inner ring torsion angles display much distortion. These torsion angles in **6.10** are ~10° off linear, but are less distorted in **6.9** and **6.11**.

6.4.3. Modification 3

The final alteration made to **6.1** is the replacement of the -SPh substituent with an -OMe group (Figure 6-11). The -OMe group is the smallest of the *peri*-substituent series. Having an -OMe and a -PPh_2 group in the *peri*-positions, **6.12** crystallizes in the *P*-1 space group with R_1 = 6.31%. To form **6.13** or **6.14**, the phosphorus atom of **6.12** has been sulfurized or selenized, respectively (Figure 6-12). These derivatives, **6.13** and **6.14**, are isomorphous and crystallize in *P*-1 with two independent molecules in the asymmetric unit. Compound **6.13** gave R_1 = 7.88% and **6.14** gave R_1 = 3.86%. Selected bond distances and angles are displayed in Table 6-6.

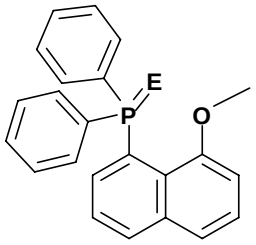

Figure 6-11. Modification 3 of **6.1** where -SPh is replaced by an -OMe group.

The P(1)…O(1) distance is the shortest in **6.12** and increases with addition of E. However, the distance between the *peri*-substituents in **6.12**-**6.14** does not increase as the chalcogen atom size increases. The P(1)-C(1) distance in **6.12** is 1.860(3) Å, and it shortens slightly with the addition of E to the phosphorus atom (**6.13a** (1.839(3) Å) and **6.13b** (1.832(4) Å). The O(1) - C(9) bond distance is similar in all three compounds.

In comparison to the other series in this chapter, **6.12**-**6.14** display unique in-plane distortions. In all of the other compounds, the P(1)-C(1)-C(2) outer angle is less than 120° and the inner P(1)-C(1)-C(10) angle is greater than 120°. Surprisingly, this is reversed for **6.12**-**6.14**, where the outer O(1)-C(9)-C(8) angle is greater than 120° and the inner O(1)-C(9)-C(10) angle is less than 120°. This means that in these compounds the -OMe group has in-plane distortions that make it lean towards the phosphorus substituent.

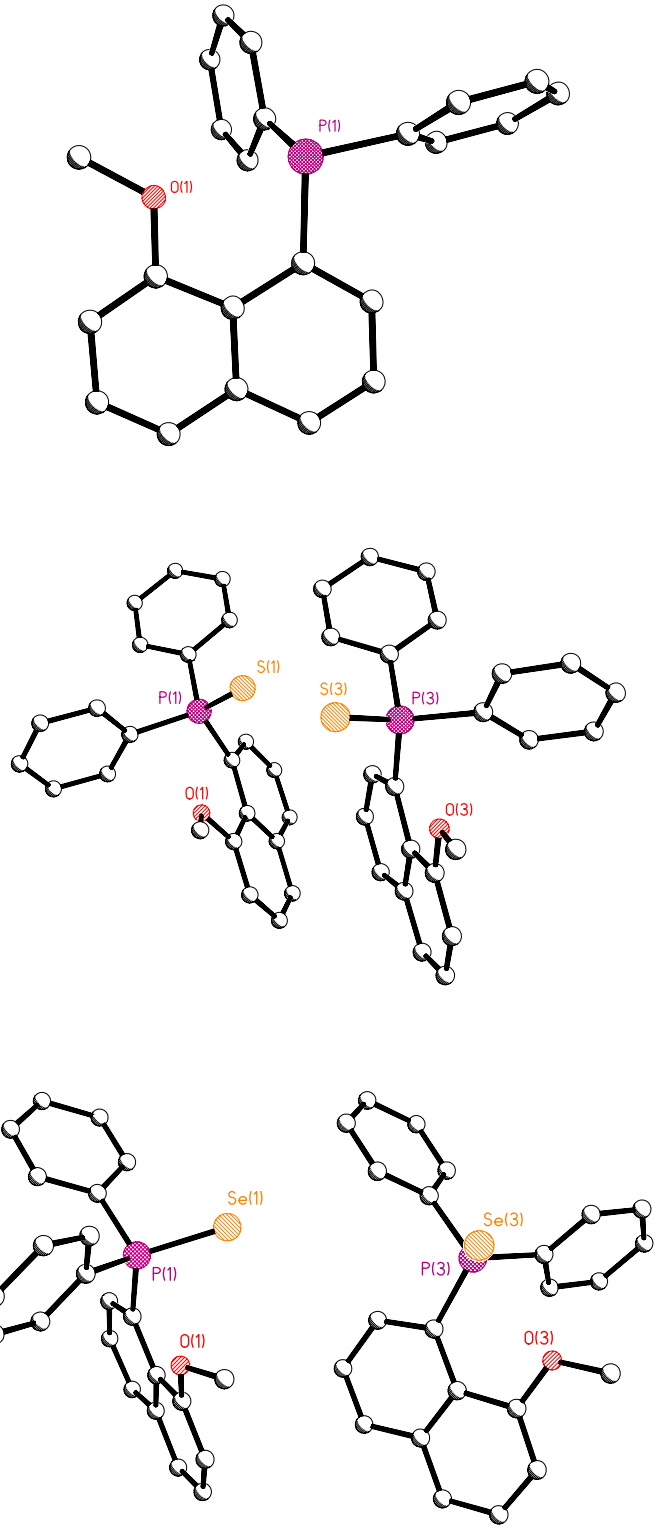

Figure 6-12. Structural representations of **6.12** and the two independent molecules of **6.13** and **6.14**.

Table 6-6. Selected bond lengths (Å) and angles (°) for **6.12**, **6.13,** and **6.14**.

	6.12	**6.13a**	**6.13b**[1]	**6.14a**	**6.14b**[1]
P(1)…O(1)	2.678(2)	2.819(3)	2.793(3)	2.827(3)	2.806(3)
O(1)…E(1)		3.165(3)	3.124(3)	3.247(3)	3.200(2)
P(1) - E(1)		1.9598(14)	1.9589(12)	2.1175(9)	2.1157(8)
P(1) - C(1)	1.860(3)	1.839(3)	1.832(4)	1.837(3)	1.837(3)
O(1) - C(9)	1.362(4)	1.362(4)	1.353(5)	1.356(3)	1.354(4)
S(1)…P(1)-C_{Ph}	170.5(1)	169.6(1)	170.1(1)	170.2(1)	170.1(1)
C(1) - P(1) - E(1)		114.53(12)	114.89(12)	114.82(11)	113.80(11)
P(1)-C(1)-C(2)	118.5(2)	115.5(3)	115.8(3)	115.6(3)	115.3(3)
P(1)-C(1)-C(10)	122.8(2)	125.4(2)	126.0(2)	125.6(2)	125.6(2)
O(1)-C(9)-C(8)	123.4(3)	122.7(3)	123.5(3)	122.9(3)	123.3(3)
O(1)-C(9)-C(10)	114.3(2)	115.5(3)	115.0(4)	116.0(3)	115.1(3)
C(2)-C(1)-C(10)	118.4(3)	118.8(3)	118.2(3)	118.5(3)	119.0(3)
C(10)-C(9)-C(8)	122.3(3)	121.9(3)	121.5(3)	121.1(2)	121.6(3)
C(1)-C(10)-C(9)	124.6(3)	125.4(3)	124.7(3)	124.8(2)	125.2(3)
C(4)-C(5)-C(10)-C(1)	0.8(3)	-0.1(4)	-3.1(4)	-0.9(5)	-3.0(4)
C(6)-C(5)-C(10)-C(9)	0.6(3)	0.3(4)	-3.1(4)	-0.3(5)	-2.8(4)
C(4)-C(5)-C(10)-C(9)	-178.1(2)	179.4(4)	177.2(3)	178.6(3)	177.3(3)
C(6)-C(5)-C(10)-C(1)	179.5(2)	-179.3(3)	176.6(3)	-179.8(3)	176.9(3)
Mean Plane Deviations					
P(1)	0.120(4)	-0.215(5)	-0.053(5)	-0.238(4)	-0.004(4)
O(1)	0.033(4)	0.038(5)	0.084(5)	0.079(4)	0.062(5)
E(1)		-1.937(5)	1.633(6)	-2.081(5)	1.847(5)

[1]Add 30 to all atom names C(1) = C(31).
E = e in **6.12**, S in **6.13**, and Se in **6.14**.

Looking at the out-of-plane distortions of P(1) and O(1) in **6.12**-**6.14** yields some very surprising observations. In **6.12**-**6.14** O(1) deviates only slightly from the naphthalene plane, but P(1) deviates rather drastically. In **6.12**, P(1) is 0.120(4) Å from the plane in the same direction as O(1). Surprisingly though, in **6.13** and **6.14** the deviation varies drastically between the two independent molecules in the unit cell. In **6.13a** P(1) lies -0.215(5) Å from the plane, where in **6.13b** it lies -0.053(5) Å from the plane. This phenomenon is also seen in **6.14**, where in **6.14a**, the P(1) atom lies -0.238(4) Å from the plane and in **6.14b**, it is very close to being in the plane of the ring (-0.004(4) Å).

Another novelty with **6.12**-**6.14** is the distance of E (as in P=E) from the plane, which is again similar between the two compounds, but different between the two independent molecules in the unit cell. In **6.13a**, S(1) deviates -1.937(6) Å in the same direction as P(1), while in **6.13b**, S(1) deviates 1.633(6) Å in the same direction as O(1). The same phenomenon is seen in **6.14** where Se(1) in **6.14a** deviates -2.081(5) Å from the plane in the same direction as P(1), but the Se(1) in **6.14b** deviates 1.847(5) Å toward O(1). It is notable that despite the varying size of chalcogen atom, the degree of deviation of S(1) or Se(1) are similar.

The distortions in the naphthalene backbone are similar between compounds **6.12**, **6.13a**, and **6.14a**, but again different between the two independent molecules in the unit cell. There are minor distortions of the inner ring torsion angles in **6.12**, **6.13a**, and **6.14a**, which are similar and very near linear. The distortions in **6.13b** and **6.14b**, however, are similar to each other, but much more severe than their in-cell counterparts. The angles near the *peri*-positions in the naphthalene ring are all very similar in **6.12**-**6.14**, with the C(10)-C(9)-C(8) angles ranging from 121.5(3)° to 122.3(3)°, the C(1)-C(10)-C(9) angles ranging from 124.6(3)° to 125.4(3)°, and the C(2)-C(1)-C(10) angles ranging from 118.2(3)° to 119.0(3)°.

6.5. Summary

Fourteen *peri*-substituted naphthalene compounds have been crystallographically characterized. It has been found that subtle changes in the *peri*-substituent can cause slightly different structural perturbations to occur.

In **6.1**-**6.14** the *peri*-distance, for the most part, increases as the size of the *peri*-substituent increases or as the phosphorus atom becomes oxidized (with O, S, or Se) (Figure 6-13). Therefore, the largest *peri*-distance (although not by much) occurs in compounds containing the -SePh moiety opposite the phosphorus substituent, and the smallest *peri*-distance occurs in the compounds containing the -OMe moiety. However, the -SPh and -SEt compounds have similar *peri*-distances.

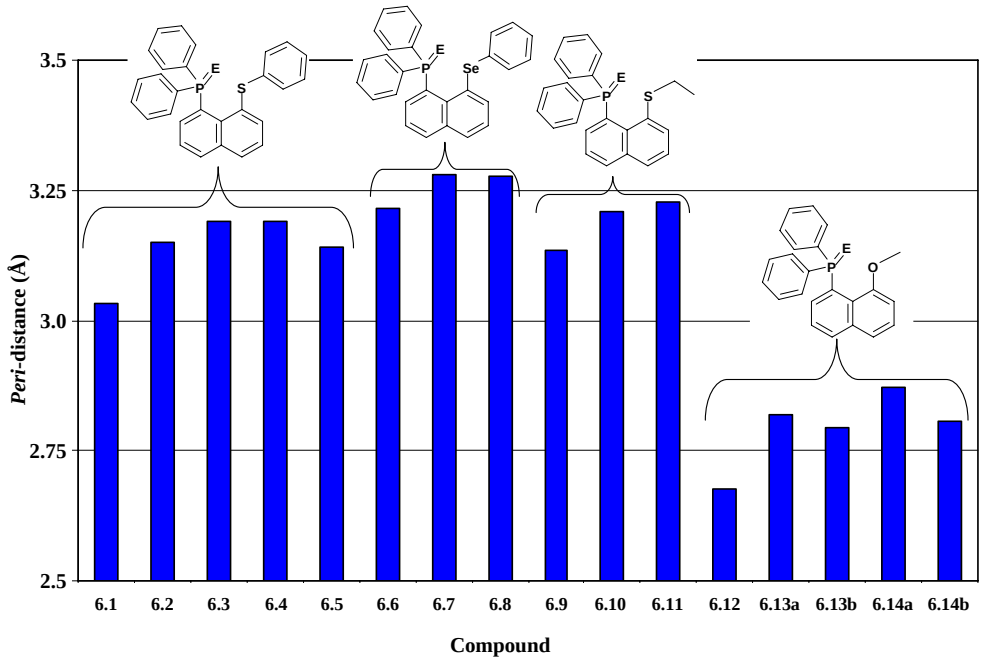

Figure 6-13. Graph of *peri*-distance (Å) for **6.1-6.14b**.

The distance of the *peri*-substituents from naphthalene, as might be expected, is dependant on atom size. For example, in the -SePh containing compounds, the Se(1)-C(9) bond distances range from 1.916(3) Å to 1.937(4) Å, where in the -SPh and -SEt containing compounds, the S(1)-C(9) bond distances range from 1.771(6) Å to 1.784(3) Å, followed by the -OMe compounds with the O(1)-C(9) bond distances ranging from 1.353(5) Å to 1.362(4) Å. The S(1)-C(9) distance in **6.5** is larger than in the other -SPh compounds (1.805(3) Å). This is most likely due to the oxidation of the sulfur atom. The P(1)-C(1) distances, in all of the compounds, are similar ranging from 1.825(6) Å in **6.8** to 1.860(3) Å in **6.12**. This small range means that, conversely to the S(1)-C(9) distance, the oxidation of the phosphorus atom does not effect the P(1)-C(1) bond length.

Compared to naphthalene, **6.1-6.14** all display in-plane deviations where the *peri*-substituents distort away from the ring. The -OMe compounds display the smallest E(1)-C(9)-C(10) inner angles (likely to do with the smaller substituent size), and in the -SPh, -SePh, and -SEt compounds, though larger, the angle is very similar across all of the compounds. The -SePh compounds have slightly

larger angles, but are within experimental error of the same angle in the other compounds. The P(1)-C(1)-C(10) inner angles in **6.1**-**6.14** seem to increase when the phosphorus atom is oxidized, but there doesn't seem to be a trend with increasing chalcogen atom size (Figure 6-14).

The out-of-plane distortions of P(1) and E(1) (E = S, Se, or O) for these compounds are shown in Figure 6-15. Most of the compounds display deviation where P(1) is on one side of the naphthalene ring and E(1) is on the other. There are a few cases, namely in **6.1**, **6.5**, and **6.12**, where both *peri*-substituents are distorted to the same side of the naphthalene ring. In **6.1**-**6.14** the out-of-plane distortions for both *peri*-atoms are most severe in **6.10**, where the P(1) atom deviates -0.620(4) Å from the plane and the S(1) atom deviates 0.744(4) Å on the other side of the plane. The most planar compound (least out-of plane distortion) is **6.14b**, where the P(1) is -0.004(4) Å from the plane and O(1) is 0.062(5) Å from the plane.

Comparing individual atom deviations, **6.5** has the furthest P(1) deviation, it is interesting that this compound also has the smallest S(1) deviation.

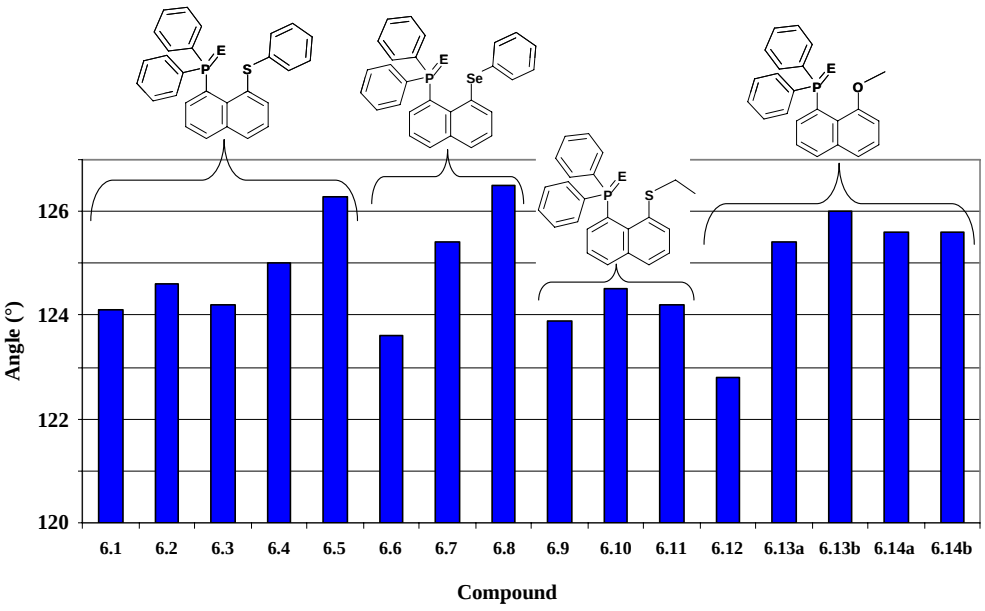

Figure 6-14. Graph of the P(1)-C(1)-C(10) angle for **6.1**-**6.14b**.

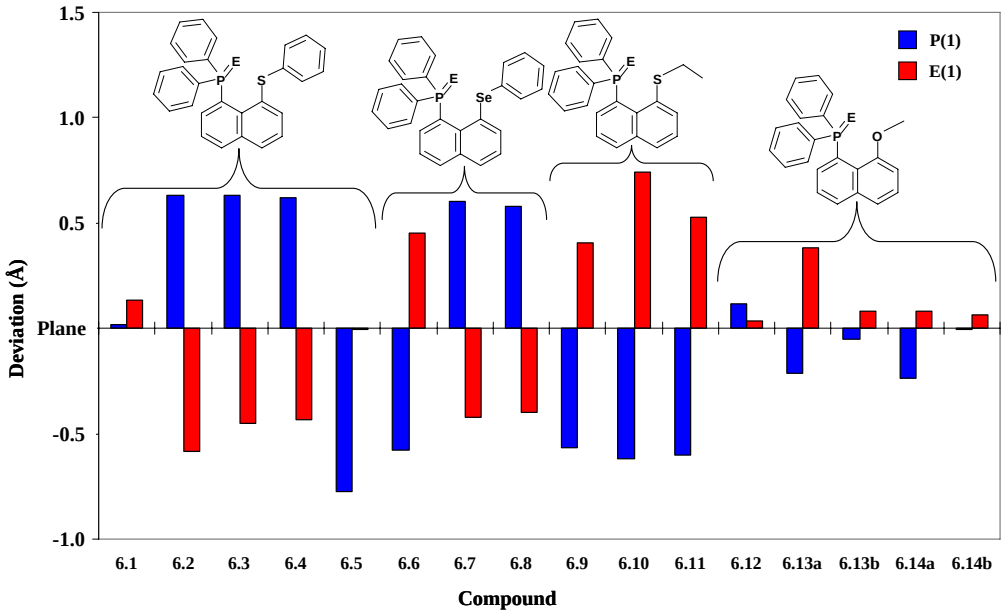

Figure 6-15. *Peri*-substituent deviation from the naphthalene plane for **6.1**-**6.14b**.

Compound **6.14b** has the smallest P(1) deviation. The largest S(1) deviation is in **6.10** (0.744(4) Å), which also has one of the largest P(1) deviations. Even though -SePh is sterically the largest group, the *peri*-Se(1) atom in **6.6**, **6.7**, and **6.8** does not deviate the farthest from the plane.

Unsurprisingly, the distance of E (as in P=E) from the naphthalene plane drastically increases as the size of the chalcogen atom increases, with the -OMe series having the shortest distance. Figure 6-16 shows the distance (absolute value) of E from the naphthalene plane, where a blue column represents E on the same side of the naphthalene plane as -PPh_2 and red represents the same side as E(1). In **6.5**, O(1) lies on the same side as the -PPh_2 group and O(2) lies on the side as -SPh. It is interesting to note that in all of the compounds, except **6.13b** and **6.14b**, the chalcogen atom lies on the same side of the naphthalene plane as the -PPh_2 group. Furthermore, the PhE…E=P distance for these compounds increase as the chalcogen atom (=E) increases, except in the -OMe series. These distances range from **6.6**, where the Se(1)…O(1) distance is 2.770(3) Å to the

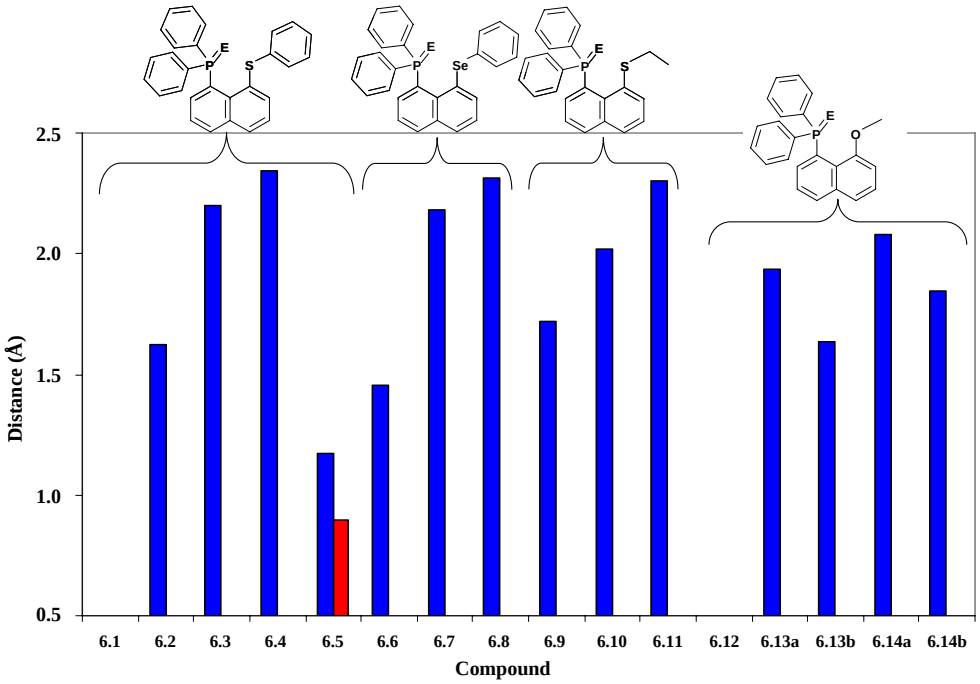

Figure 6-16. Graph of the distance of (=E) from the naphthalene plane in **6.1**-**6.14b**. The blue lines are when E lies on the same side of the plane as the phosphorus moiety and the red lines are when E lies on the same side as the -EPh moiety.

Se(2)…Se(1) distance of 3.4217(8) Å in **6.8**. It is interesting that the two extreme cases are in the -SePh series. The O(2)…P(1) distance in **6.5** is, by far, the largest distance at 4.357(2) Å.

Finally, the angles in the naphthalene backbone around the *peri*-substituents in these compounds display minor distortions (Table 6-7). The largest difference from naphthalene and these compounds lie in the bay region between the *peri*-positions, with angle C(1)-C(10)-C(9). In naphthalene, this angle is 121.7(1)°, but in all of the compounds, the angle is much larger ranging from 124.6(3)° to 127.4(2)°.

Table 6-7. Selected naphthalene backbone angles (°).

Angle	Naphthalene	6.1-6.14b
C(2)-C(1)-C(10)	120.6(1)	117.5(5) to 119.5(4)
C(10)-C(9)-C(8)	120.5(1)	120.3(3) to 122.3(3)
C(1)-C(10)-C(9)	121.7(1)	124.6(3) to 127.4(2)

A comparison of only one of the inner ring torsion angles in the naphthalene backbone of **6.1-6.14** can help summarize the deviations in the ring. Figure 6-17 displays a graph of the absolute value of the torsion angle C(6)-C(5)-C(10)-C(1). In naphthalene, this inner ring torsion angle is essentially planar (0.05(1)°). Surprisingly, in both the -SPh and -SePh compounds, increasing the size of the chalcogen atom on P(1) decreases the distortions in the naphthalene ring backbone. There seems to be no trend in the -SEt compounds and the -OMe substituted compounds all have very small inner ring distortions. That being said, in the -OMe case, **6.13a** and **6.14a** (the sulfur and selenium derivatives) have the most planar naphthalene ring distortions.

It is notable that **6.10** (the -SEt, -P(=S)Ph_2 derivative) has the largest deviation from naphthalene planarity in the whole series, not only in the C(6)-C(5)-C(10)-C(1) angle, but also in all of the inner ring torsion angles. (Figure 6-18) With this knowledge, it is unsurprising that in **6.10** S(1) and P(1) are in extreme positions on opposite sides of the plane. This could suggest an S(1)…S(2) interaction, sitting only 3.2951(15) Å apart, which could cause the major distortion of the naphthalene backbone. Also, there could be a possible

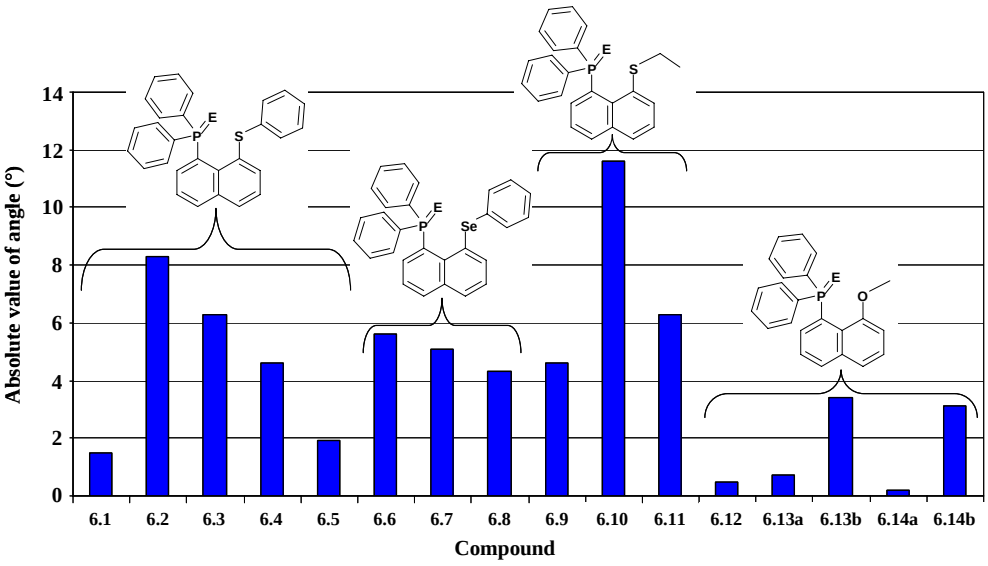

Figure 6-17. Graph of the absolute value of torsion angle C(6)-C(5)-C(10)-C(1). (**6.10**, **6.11**, **6.13a** and **6.14a** are negative).

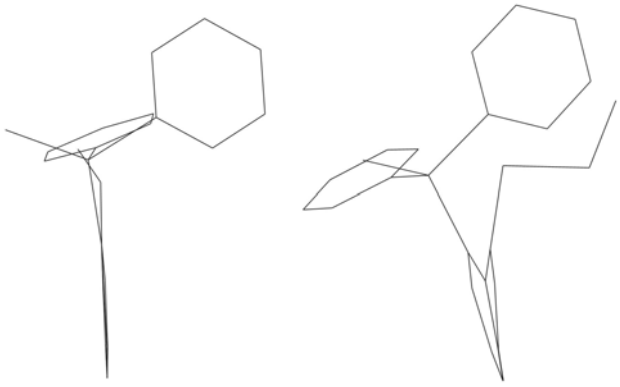

Figure 6-18. Side view wire diagrams showing the extreme cases of naphthalene backbone distortion from the flattest ring in **6.13** to the most distorted ring in **6.10**.

interaction between the ethyl group and phenyl group in **6.10** (distance is 4.041(1) Å) which does not occur in the other -SEt compounds.

6.6. References

1. S. C. Abrahams, J. M. Robertson and J. G. White, *Acta Cryst.*, 1949, 2, 233-238.

2. J. Oddershede and S. Larsen, *J. Phys. Chem. A*, 2004, 108, 1057-1063.

3. A. Bondi, *J. Phys. Chem.*, 1964, 68, 441-452.

4. S. Hayashi and W. Nakanishi, *Bull. Chem. Soc. Jpn.*, 2008, 81, 1605-1615.

5. W. Nakanishi in *Handbook of Chalcogen Chemistry, New Perspectives in Sulfur, Selenium and Tellurium*, ed. F. A. Devillanova, 2006, 644-678.

6. P. Mueller, R. Herbst-Irmer, A. L. Spek, T. R. Schneider and M. R. Sawaya, *Crystal Structure Refinement: A Crystallographer's Guide to SHELXL*, Oxford University Press, 2006.

7. F. H. Allen, O. Kennard, D. G. Watson, L. Brammer, A. G. Orpen and R. Tayor, *J. Chem. Soc. Perkin Trans. II*, 1987, S1-S19.

8. J. E. Huheey, E. A. Keiter and R. L. Keiter, *Inorganic Chemistry: Principles of Structure and Reactivity*, HarperCollins College Publishers, 1993.

CHAPTER 7
STRUCTURAL ANALYSIS OF METAL BOUND (8-PHENYLSULFANYLNAPHTH-1-YL)DIPHENYLPHOSPHINE

7.1. Introduction

A great deal of coordination chemistry and catalytic work has been done using complexes in which the metal centers have bidentate, hemilabile ligands.[1,2] These ligands are especially useful during catalysis because the chelate effect stabilizes the catalyst in the absence of a substrate, but during a chemical reaction, the weaker ligating atom from the ligand can be displaced, creating an open binding site for catalysis. Once the substrate is converted to product, the weak ligating atom can re-bind to the metal center to restore the resting state of the catalyst.

Bidentate ligands containing asymmetric, mixed donor groups are well known. However ligands containing both a phosphine donor ($-PR_3$) and a thioether ($-SR_2$) substituent are less recognized. This is despite the possibility of hemilabile characteristics from the soft/hard differences of the P/S atoms.[3] For example, when bidentate P/S ligands are coordinated to soft metals, like Pt(II), Ru(II), and Cu(I), the harder thioether donor is expected to be more labile than the softer phosphine donor.[4]

Altering the size and electronic effects of the backbone can drastically change the chelating properties of the ligand, which, in turn, can change the catalytic activity of the metal center. Bidentate, mixed phosphine-thioether donor ligands can have either a flexible aliphatic backbone or a rigid aromatic backbone, although some P/S ligands are known to contain both. The structural properties of the backbone determine the ring size and shape when bound to a metal center. Larger, aliphatic backbones allow for more flexibility in the ligand bite angle, where rigid, aromatic backbones can create destabilizing steric strain in the ligand or around the metal center.

The naphthalene-based compound (8-phenylsulfanylnaphth-1-yl)diphenylphosphine (**7.1**, reported in the previous chapter as **6.1**) has been used

as a ligand in a series of mononuclear platinum(II)-halide complexes (**7.2**-**7.4**), a mononuclear ruthenium(II)-Cl complex (**7.5**), and finally, in a series of binuclear copper(I)-halide complexes (**7.6**-**7.8**) (Figure 7-1). In each case, **7.1** is a bidentate ligand binding datively through the phosphorus and sulfur atoms. Therefore, when bound, it forms a six-membered ring with the metal center. All of the complexes reported here have been crystallographically characterized. In this chapter, their structural features will be discussed followed by a comparative summary of all of the compounds.

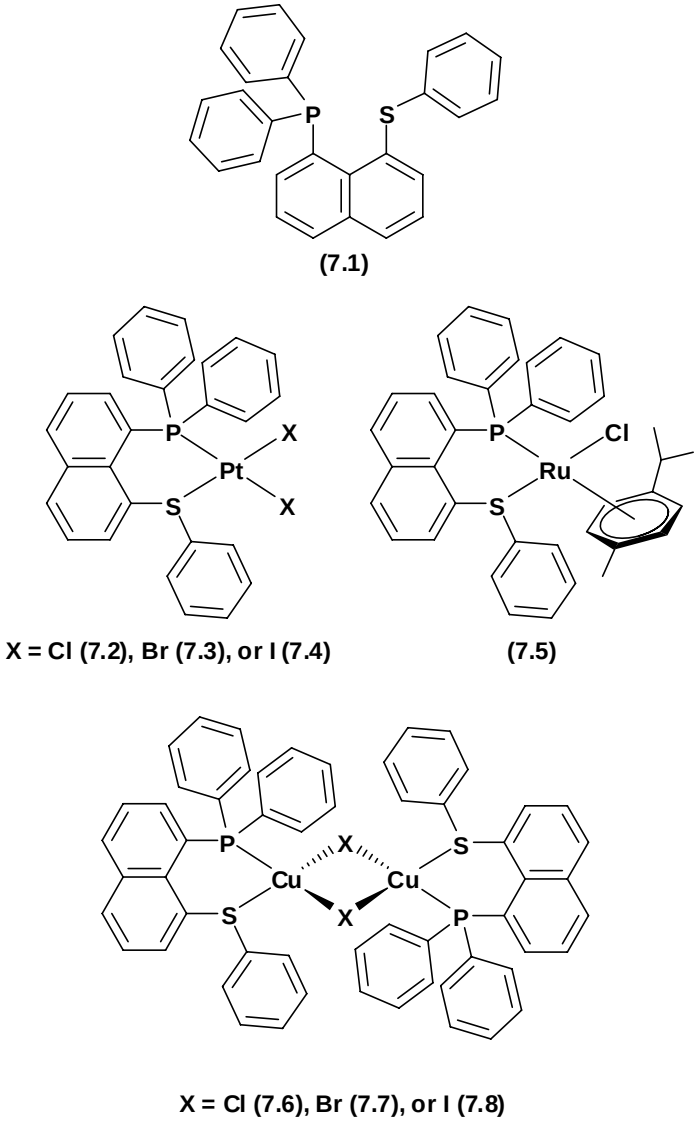

Figure 7-1. (8-phenylsulfanylnaphth-1-yl)diphenylphosphine (**7.1**) and the mononuclear and binuclear metal complexes involving it.

7.2. Platinum(II)-Halide Complexes

A wide variety of mononuclear Pt(II)-dihalide complexes, in which the metal atom is coordinated by both a phosphine and a thioether donor, are known. A search of the Cambridge Structural Database (version 5.30, May 2009) resulted in complexes having phosphine/thioether ligands with a range of backbones, including no backbone (i.e. two separate ligands), a flexible, aliphatic backbone, or (most commonly) a ferrocene-based backbone (Figure 7-2).[5-8] Other than the complexes discussed in this chapter, there is one Pt(II)-dichloride complex with a phosphine/thioether ligand based on a naphthalene backbone.[9] Chloride is the most common anion in this type of complex, with only a few complexes containing either bromide or iodide. In fact, there are no complete series, and only one partial series, shown in Figure 7-3.[6]

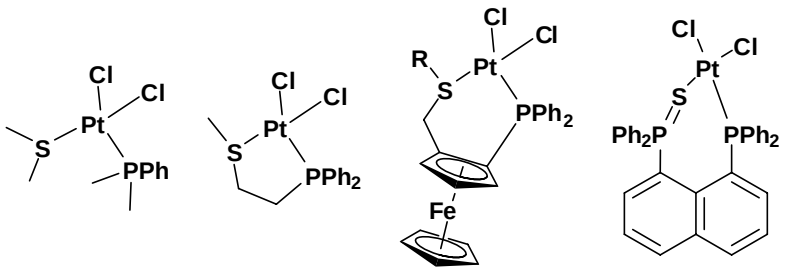

Figure 7-2. Examples of Pt(II)-dichloride complexes with thioether/phosphine ligands having various backbones, starting on the far left no backbone (i.e. two separate ligands), a flexible, aliphatic backbone, (most commonly) a ferrocene-based backbone, and a naphthalene based backbone.

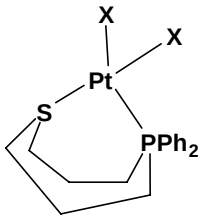

X = Cl or I

Figure 7-3. Only structurally characterized literature example of Pt(II)-dihalide partial series.

The Pt(II)-dihalide complexes of **7.1**, which have the general formula [Pt(**7.1**)X_2]; where (X = Cl (**7.2**), Br (**7.3**), and I (**7.4**)), are the only known series of Pt(II)-dihalide complexes containing a phosphine/thioether ligand. This gives the opportunity to compare how the halide ions affect the ligand environment around the metal center.

Complexes **7.2**-**7.4** display a mononuclear, four-coordinate platinum(II) metal center, which is ligated by two halide ions and one molecule of **7.1** (Figure 7-4). These complexes all crystallize in similar, but not identical, monoclinic unit cells. Complex **7.2** crystallizes in the $P2_1/n$ space group with one molecule of $CHCl_3$ in the unit cell, whereas **7.3** and **7.4** both crystallize in the space groups $P2_1/n$ and $P2_1/c$, respectively, each with one molecule of CH_2Cl_2 in the unit cell. These structures have been refined to R_1 equal to 9.87% in **7.2**, 6.77% in **7.3**, and 3.94% in **7.4**. Refinement data can be found in Appendix 1.

7.2.1. Metal Center Environment

In these compounds, the Pt(II) metal center is square planar with the X(1)-Pt(1)-X(2) angles and the P(1)-Pt(1)-S(1) angles all ~90°. The P(1)-Pt(1)-X(2) angles are slightly greater than 90° and the S(1)-Pt(1)-X(1) angles are ~3° less than 90°. The P(1)-Pt(1)-X(1) angles and the S(1)-Pt(1)-X(1) angles are ~5° less than 180°. The bonds and angles around the Pt(II) metal centers are shown in Table 7-1.

The Pt(1)-X distance increases as the size of the halide ion increases and it is interesting to note that in each case, the halide (X(1)) trans to P(1) is slightly longer than the halide (X(2)) trans to S(1). In each complex, the Pt(1)-P(1) distance is shorter than the Pt(1)-S(1) distance. In **7.2**, the Pt(1)-P(1) distance is 2.221(5) Å, which is somewhat less than that of **7.3** or **7.4**, whose distances are equal within standard error (2.232(2) Å and 2.2326(15) Å). Complex **7.3** has the

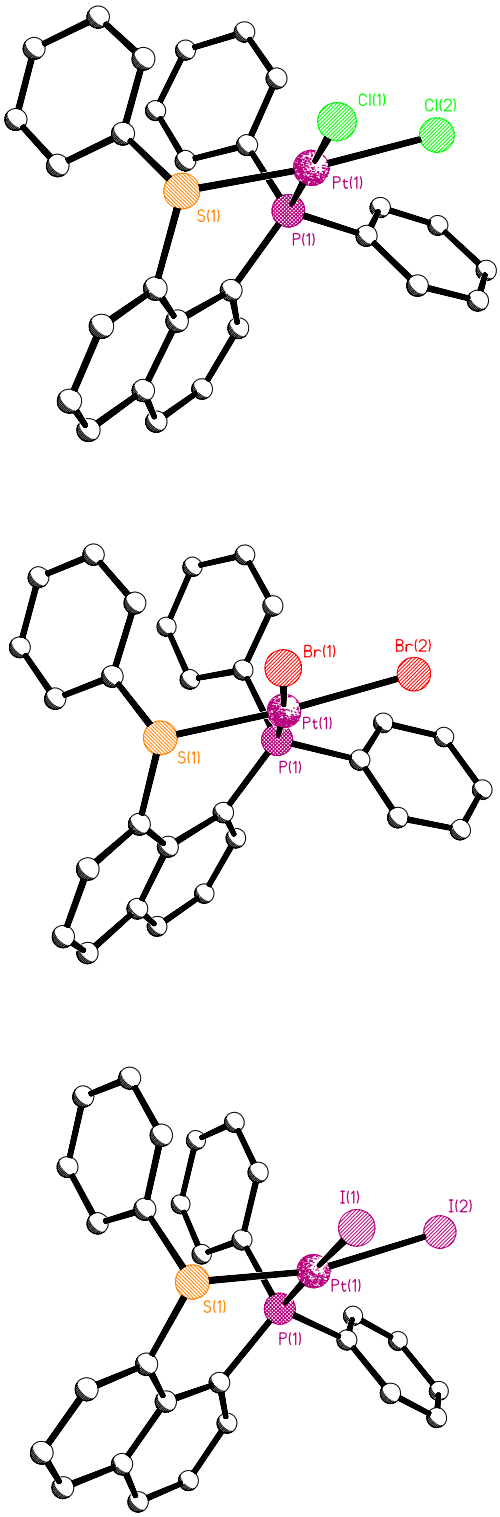

Figure 7-4. Structural representations of **7.2**, **7.3**, and **7.4**.

Table 7-1. Selected bond lengths (Å) and angles (°) for **7.1**, **7.2**, **7.3**, and **7.4**.

	7.1	**7.2**	**7.3**	**7.4**
Pt(1) - X(1)		2.377(5)	2.4817(14)	2.6553(4)
Pt(1) - X(2)		2.303(5)	2.4244(15)	2.6052(4)
Pt(1) - P(1)		2.221(5)	2.232(3)	2.2326(15)
Pt(1) - S(1)		2.262(5)	2.256(3)	2.2752(16)
X(1)-Pt(1)-X(2)		89.37(18)	90.09(4)	90.163(15)
P(1)-Pt(1)-X(1)		176.70(18)	175.93(8)	176.21(4)
P(1)-Pt(1)-X(2)		92.57(18)	92.92(8)	92.43(4)
S(1)-Pt(1)-X(1)		87.82(17)	86.26(8)	87.42(4)
S(1)-Pt(1)-X(2)		175.35(18)	175.58(8)	168.80(5)
P(1)-Pt(1)-S(1)		90.41(18)	90.61(11)	90.56(5)
Mean Plane Deviations				
P(1)	0.018(5)	0.21(2)	0.303(14)	-0.003(8)
S(1)	0.136(5)	-0.29(2)	-0.299(13)	-0.074(9)
Pt(1)		0.99(3)	0.996(17)	-1.054(11)

[1]X = Cl for **7.2**, Br for **7.3**, or I for **7.4**.

shortest Pt(1)-S(1) distance of 2.256(3) Å, which increases in **7.2** to 2.262(5) Å and further increases in **7.4** (2.2752(16) Å).

7.2.2. Ligand Environment

The changes that unbound ligand **7.1** undergoes when bound to Pt(II) metal centers can be compared. The bond lengths and angles of Pt(II)-bound and unbound ligand are shown in Table 7-2.

When **7.1** is bound to platinum, the nonbonding P(1)…S(1) distance slightly increases by ~0.1 Å from **7.2** < **7.3** < **7.4**. Conversely, the P(1)-C(1) distances in **7.2** and **7.3** are similar and are shorter than the P(1)-C(1) distance in **7.4**, which is shorter than the same distance in **7.1**. The S(1)-C(9) distances in **7.1** and **7.2**-**7.4** are all similar.

The increased P(1)…S(1) distance in these complexes occur in conjunction with changes in the in-plane distortions of the P and S atoms from the naphthalene rings. The outer P(1)-C(1)-C(2) angle is much larger in free **7.1** (118.5(3)°) than when it is bound to the metal center. The P(1)-C(1)-C(2) angle in

Table 7-2. Selected bond lengths (Å) and angles (°) for **7.1**, **7.2**, **7.3**, and **7.4**.

	7.1	**7.2**	**7.3**	**7.4**
P(1)…S(1)	3.0339(13)	3.182(6)	3.191(3)	3.203(2)
P(1) - C(1)	1.850(3)	1.80(2)	1.807(13)	1.837(6)
S(1) - C(9)	1.784(3)	1.76(2)	1.763(13)	1.770(7)
P(1)-C(1)-C(2)	118.0(2)	116.5(14)	116.2(9)	115.0(4)
P(1)-C(1)-C(10)	124.1(2)	128.5(14)	126.9(8)	125.9(4)
S(1)-C(9)-C(8)	115.1(2)	112.5(15)	113.7(8)	111.9(5)
S(1)-C(9)-C(10)	123.8(2)	124.0(14)	125.8(8)	126.2(4)
C(2)-C(1)-C(10)	117.8(3)	115.0(18)	116.9(11)	119.1(5)
C(10)-C(9)-C(8)	121.0(3)	123.1(19)	120.5(11)	121.9(6)
C(1)-C(10)-C(9)	126.4(3)	125.4(18)	125.6(11)	127.8(6)
C(4)-C(5)-C(10)-C(1)	-1.2(4)	-9(2)	-7.6(16)	3.1(11)
C(6)-C(5)-C(10)-C(9)	0.1(3)	1(2)	-6.9(16)	1.5(11)
C(4)-C(5)-C(10)-C(9)	-179.5(3)	176.9(16)	174.7(10)	-177.2(7)
C(6)-C(5)-C(10)-C(1)	178.5(3)	175.9(16)	170.8(10)	-178.2(7)
Mean Plane Deviations				
P(1)	0.018(5)	0.21(2)	0.303(14)	-0.003(8)
S(1)	0.136(5)	-0.29(2)	-0.299(13)	-0.074(9)
Pt(1)		0.99(3)	0.996(17)	-1.054(11)

[1]X = Cl for **7.2**, Br for **7.3**, or I for **7.4**.

7.2 and **7.3** are similar (116.5(14)° and (116.2(9)°)), while **7.4** has the smallest angle (115.0(4)°). The inner P(1)-C(1)-C(10) angle of the free ligand **7.1** (124.1(2)°) is less than in the complexes, where **7.4** (125.9(4)°) < **7.3** (126.9(8)°) < **7.2** (128.5(14)°). The outer S(1)-C(9)-C(8) angle is much larger in free **7.1** (115.1(2)°) than in **7.2**-**7.4**; where **7.4** is again the smallest of the complexes (111.9(5)°) < **7.2** (112.5(15)°) < **7.3** (113.7(8)°). The inner S(1)-C(9)-C(10) angle is similar in free **7.1** and when bound in **7.2**, but is larger in **7.3** and **7.4**.

In **7.1** and **7.4**, S(1) and P(1) are only slightly out of the naphthalene plane and, interestingly enough, in both compounds they are pushed off to the same side, with S(1) being further out of plane P(1). In **7.2** and **7.3**, P(1) and S(1) lie on opposite sides of the naphthalene plane. Of all the platinum complexes, **7.3** displays the furthest distortion (P(1); 0.303(14) Å and S(1); -0.299(13) Å). In **7.2**-**7.4**, Pt(1) lies almost 1 Å from the plane.

The C(2)-C(1)-C(10) angle in the naphthalene backbone is the most distorted in **7.4**, which is consistent with it having the largest S(1)…P(1) *peri*-distance. The C(1)-C(10)-C(9) angles in **7.2**-**7.4** are similar, with **7.4** being slightly larger. The C(10)-C(9)-C(8) angles increase **7.3** < **7.4** < **7.2**.

The naphthalene backbone is most severely distorted in **7.2**, where the C(4)-C(5)-C(10)-C(1) torsion angle is -9(2)°, whereas **7.3** has the most distorted C(6)-C(5)-C(10)-C(1) angle (170.8(10)°). In **7.4**, all of the inner ring torsion angles in the naphthalene backbone distort less than 3.1°.

7.3. Ruthenium(II)-Cl Complexes

Searching the CSD for Ru(II)-Cl complexes containing a phosphine/thioether ligand(s) resulted in numerous hits, but limiting the results so the metal center also contained a *para*-cymene (*p*-Cy) ligand resulted in just five complexes. Of the five complexes, there are three different backbones, which are shown in Figure 7-5.[10-13] This figure shows the cationic portions of the five known Ru(II)-Cl complexes with the general formula [(η^6-*p*-Cy)Ru(**L**)Cl]X. The ligand in **7.9** contains a dimethylene linker between the phosphine and thioether

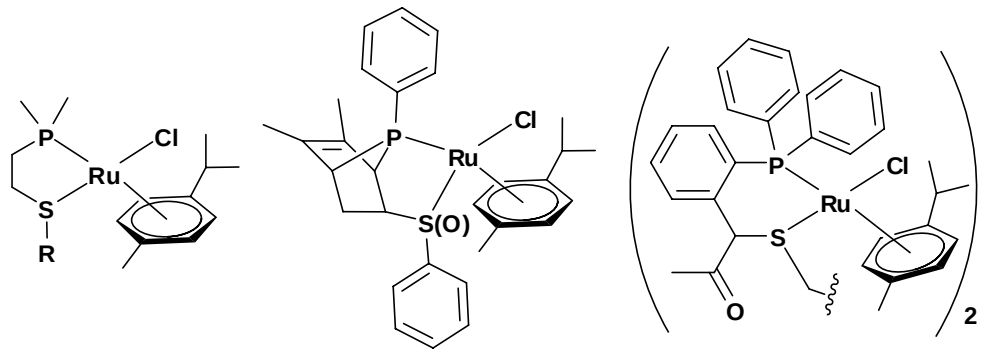

(7.9a, b) **(7.10a, b)** **(7.11)**

Figure 7-5. The cationic portions of five known Ru(II)-Cl complexes with the general formula [(η^6-*p*-Cy)Ru(**L**)Cl]X. On the left **7.9**, where **a**, R = Me and **b**, R = Et. In the center, **7.10**, where **a** contains a thioether and in **b**, the thioether is oxidized. On the right, only half of **7.11** is pictured, the complex contains two Ru(II) metal centers ligated by a single ligand.

(in **a**, R is a methyl group; in **b**, R is an ethyl group). The ligand in **7.10** contains a cyclohexene backbone (in **7.10b**, the thioether is oxidized). Only half of **7.11** is pictured. This complex contains two Ru(II) metal centers ligated by a single ligand. The ligand is linked by a dimethylene bridge linking two thioethers.

To add to this set, **7.5** has the formula [(η^6-*p*-Cy)Ru(**7.1**)Cl]Cl and consists of a mononuclear ruthenium(II) metal center ligated by a chloride ion, η^6-*para*-cymene (*p*-Cy), and **7.1**, with an outer-sphere chloride ion. The cationic portion of this complex is show in Figure 7-6. The complex crystallizes with one molecule of acetone ($OC(CH_3)_2$) in a monoclinic unit cell ($P2_1/n$, R_1 = 11.26%). Refinement details are contained in Appendix 1.

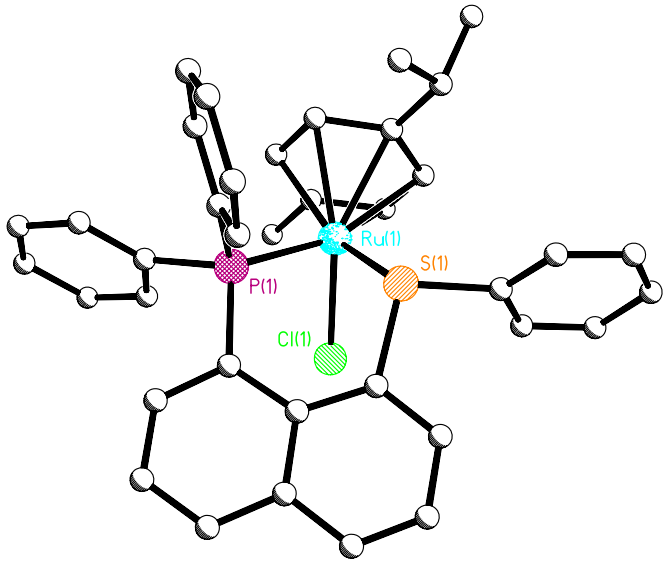

Figure 7-6. A structural representation of the cationic portion of **7.5**.

7.3.1. Metal Center Environment

Distinctive characteristics of the Ru(II) metal center can be found by comparing the crystal structure of **7.5** with those in compounds **7.9a** and **7.11**. All of the compounds have similar environments around the metal center of [(η^6-*p*-Cy)Ru(L)Cl]$^+$, where L = etdmp (**7.9a**) or dppte (**7.11**) (Figure 7-5).[10, 13]

The three ligands, **7.1**, etdmp, and dppte, have neutral phosphine and thioether donor atoms, however, etdmp has a slightly more flexible and smaller backbone. The flexible backbone of **7.9a** was used in a study to help understand the hemilability of bidentate P/S ligands.[10] Dppte, in **7.11**, has the same size ring as **7.1** upon coordination to the Ru(II) metal center, but the backbone is, again, slightly more flexible. It must also be noted that dppte has two coordination sites and ligates to two ruthenium(II) metal centers, but that both of these metal centers are effectively identical. The bond lengths and angles around the metal centers of **7.5**, **7.9a**, and **7.11** are shown in Table 7-3.

Table 7-3. Selected bond lengths (Å) and angles (°) for **7.5**, **7.9a**, and **7.11**.

	7.5	**7.9a**[10]	**7.11**[13]
Ru(1) - Cl(1)	2.396(2)	2.403(1)	2.3914(13)
Ru(1) - P(1)	2.319(2)	2.313(1)	2.3255(13)
Ru(1) - S(1)	2.356(2)	2.377(1)	2.3592(11)
Ru(1) - *p*-Cy	2.234(9)-2.275(8)	2.198(3)-2.273(3)	2.218(4)-2.282(5)
P(1)-Ru(1)-S(1)	80.22(8)	84.52(4)	80.80(4)
P(1)-Ru(1)-Cl(1)	89.03(9)	86.68(4)	87.74(4)
S(1)-Ru(1)-Cl(1)	89.61(8)	90.89(4)	89.59(4)

Each Ru(II) center forms a characteristic "piano stool" geometry by coordinating a chloride anion, a neutral η^6-*para*-cymene ligand, and a bidentate P/S donor ligand (**FKW99-0-3** (**7.5**), etdmp (**7.9a**), and dppte (**7.11**)). The Ru-Cl bond distances are similar and increase from 2.3914(13) Å in **7.11** to 2.396(2) Å in **7.5** to 2.403(1) Å in **7.9a** (Table 7-3). In each complex, the *p*-Cy ligand forms an η^6-bond with the metal center. The range of Ru(I)-(*p*-Cy) bond distances overlap in **7.5**, **7.9a**, and **7.11**.

The Ru(1)-P(1) bond distance is similar in **7.5** and **7.9a**, but is longer in **7.11**. The Ru(1)-S(1) distance is similar in **7.5** and **7.11**, but slightly longer in **7.9a**. In each case, however, the Ru(1)-P(1) distance is shorter than the Ru(1)-S(1) distance, likely caused by the differing soft/hard donor properties of the phosphine and thioether atoms.

Since the ligand backbones are of differing flexibilities, it is interesting to compare their bite angles. The P(1)-Ru(1)-S(1) angle in **7.5** (80.22(8)°) is very

similar to **7.11** (80.80(4)°), which is expected since the chelate ring is the same size. The same angle in **7.9a** (84.52(4)°) is the largest of the three complexes, which is interesting since **7.9a** has the smallest chelate ring; however, the etdmp ligand possesses the most flexible backbone of the three. The P(1)-Ru(1)-Cl(1) angle is the largest in **7.5** (89.03(9)°) and is the smallest in **7.9a** (86.52(4)°). In **7.11**, this angle is 87.74(4)°. The S(1)-Ru(1)-Cl(1) angle is close to 90° in all three complexes.

7.3.2. Ligand Environment

The structural distortions of **7.1**, when bound to a ruthenium(II) metal center (as in **7.5**), can also be compared (Table 7-4). The P(1)…S(1) distance is slightly shorter when bound in **7.5** (3.013(3) Å) than in the free ligand **7.1** (3.0339(13) Å). It is interesting to note that the P(1)…S(1) distance in **7.11** (3.04(1) Å) is most similar to **7.1** and, therefore, is slightly larger than the P…S

Table 7-4. Selected bond lengths (Å) and angles (°) for **7.1** and **7.5**.

	7.1	**7.5**
P(1)…S(1)	3.0339(13)	3.013(3)
P(1) - C(1)	1.850(3)	1.816(10)
S(1) - C(9)	1.784(3)	1.829(10)
P(1)-C(1)-C(2)	118.0(2)	116.4(7)
P(1)-C(1)-C(10)	124.1(2)	124.9(7)
S(1)-C(9)-C(8)	115.1(2)	115.5(7)
S(1)-C(9)-C(10)	123.8(2)	121.3(7)
C(2)-C(1)-C(10)	117.8(3)	118.7(9)
C(10)-C(9)-C(8)	121.0(3)	122.9(9)
C(1)-C(10)-C(9)	126.4(3)	127.7(9)
C(4)-C(5)-C(10)-C(1)	-1.2(4)	-0.1(9)
C(6)-C(5)-C(10)-C(9)	0.1(3)	-5.4(11)
C(4)-C(5)-C(10)-C(9)	-179.5(3)	177.5(7)
C(6)-C(5)-C(10)-C(1)	178.5(3)	176.9(7)
Mean Plane Deviations		
P(1)	0.018(5)	-0.096(11)
S(1)	0.136(5)	0.217(11)
Ru(1)		-1.284(14)

distance in **7.5**. This is surprising since the ligands form the same size chelate ring and have similar bite angles; however, the ligand in **7.11** is slightly more flexible and has more steric bulk in the dimer, which could cause it to distort more than **7.1** upon complexation. The P(1)…S(1) distance in **7.9a** (3.15(1) Å) is much larger than in the other three compounds. This is consistent with the larger observed P(1)-Ru(1)-S(1) angle and the more flexible backbone, however, it is counterintuitive since the chelate ring is smaller.

The P(1)-C(1) bond distance is smaller in **7.5** than in **7.1**. In contrast, the S(1)-C(9) bond distance is much smaller in **7.1** than in **7.5**.

The in-plane deviations of the outer P(1)-C(1)-C(2) angle in **7.5** is smaller than the same angle in **7.1**, where the S(1)-C(9)-C(8) angle is similar in both compounds. The inner P(1)-C(1)-C(10) angle is slightly bigger in **7.5** than in **7.1**, but the S(1)-C(9)-C(10) is much smaller in **7.5** than in **7.1**.

The out-of-plane deviations of P(1) and S(1) are larger in **7.5** than in **7.1**. Additionally, the ruthenium ion in **7.5** lies -1.2837(136) Å from the naphthalene plane. Lastly, the naphthalene ring distortions of the angles C(2)-C(1)-C(10), C(1)-C(10)-C(9) and C(10)-C(9)-C(8) are larger in **7.5** than in **7.1**. The large *p*-Cy ligand in **7.5** may be sterically crowding the bidentate ligand, causing some of these distortions

7.4. Copper(I)-Halide Complexes

A search of the CSD for dihalide copper complexes with phosphine/thioether ligand(s) resulted in 20 hits. Almost all of the results were binuclear copper complexes with bridging halide ions. Most of the complexes contained two separate ligand donors, triphenylphosphine (or a close derivative) and a thiourea alkyl chain ($S=C(NH_2)(NHR)$), of which most have been reported by Lobana *et al*. There is only one example where the phosphine/thioether donors are on a single backbone. It is a binuclear, dichloride-bridged complex with a ferrocene based backbone (Figure 7-7).[14,15]

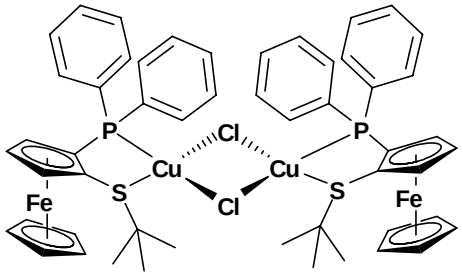

Figure 7-7. The only example of a Cu(I)-X_2 complex with a single P/S-containing ligand.

Of the 20 search results, there were four chloride, six bromide, and ten iodide complexes; however, there are only two halide series. The first example is a polymeric chain, which contains a bridging P/S ligand between the two copper metal centers, forming a six-membered (S-P-Cu) ring (Figure 7-8).[16] The second contains two separate phosphorus/sulfur ligands of triphenyl phosphine and acetophenone thiosemicarbazone (Figure 7-8).[17] The chloride and bromide complexes (with these ligands) are structurally identical, but in the iodide case, the sulfur ligand forms a third bridge between the metal centers.

We have used **7.1** as a ligand in a series of binuclear Cu(I)-halide complexes. These complexes have the standard formula [(**7.1**)Cu(μ-X)$_2$Cu(**7.1**)]; where X = Cl (**7.6**), Br (**7.7**), or I (**7.8**) (Figure 7-9). These copper complexes all

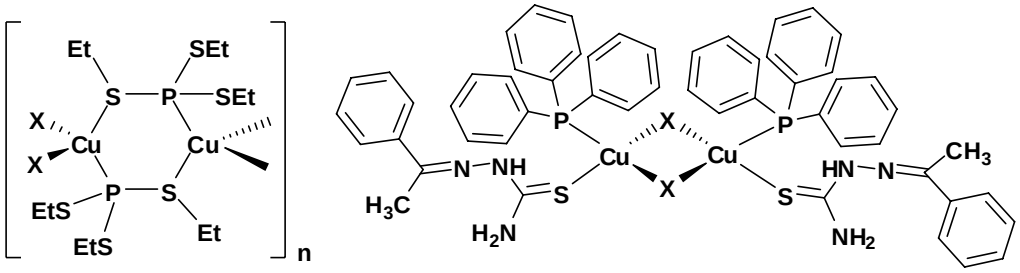

Figure 7-8. Examples of Cu(I)-dihalide series. Left drawing depicts a polymeric structure with a P/S bridging ligand (X = Cl, Br, or I). Right drawing depicts the ligands triphenyl phosphine and acetophenone thiosemicarbazone (X = Cl or Br).

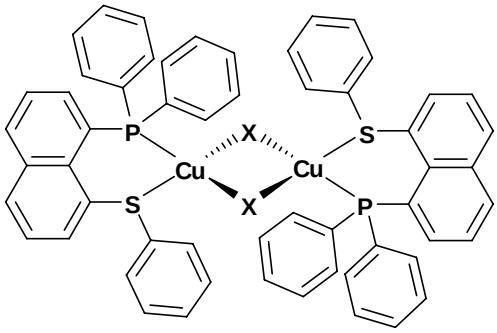

X = Cl (7.6), Br (7.7), or I (7.8)

Figure 7-9. Binuclear copper(I) complexes of **7.1**.

crystallize in very similar (*P*-1) triclinic unit cells with an inversion center that lies in the middle of the complex (Figure 7-10). The R_1 factors for **7.6**, **7.7**, and **7.8** are 8.57%, 8.58%, and 6.84%, respectively. Appendix 1 includes refinement data.

7.4.1. Metal Center Environment

Each Cu(I) metal center is pseudo-tetrahedral and is ligated by the bidentate P/S ligand (**7.1**) and two bridging halide anions. Table 7-5 shows bond distances and angles around the metal centers in these complexes. The overall binuclear complexes are formed by two Cu(I) metal ions each containing a ligand linked by the two bridging halogen anions.

Surprisingly, the Cu…Cu distance in these complexes decreases as the halide ion size increases. In **7.6**, the Cu(1)…Cu(1)' distance is 3.0037(13) Å, which is greater than **7.7** (2.9296(14) Å) > **7.8** (2.8568(11) Å). However, the X(1)…X(1)' distance increases as the halide ions increase. In **7.6**, this distance is 3.744(2) Å < **7.7** (3.9193(14) Å < **7.8** (4.3287(8) Å). The result of this is an elongation of the diamond-shaped core of the complexes along the X-X' axis as the size of the halogen ion increases.

As expected, the Cu(1)-X(1) and the Cu(1)-X(1)' bond distances increase as the halide size increases, however, there is some asymmetry, as the Cu(1)-X(1) distance is slightly shorter than the Cu(1)-X(1)' bond distance in all cases. The

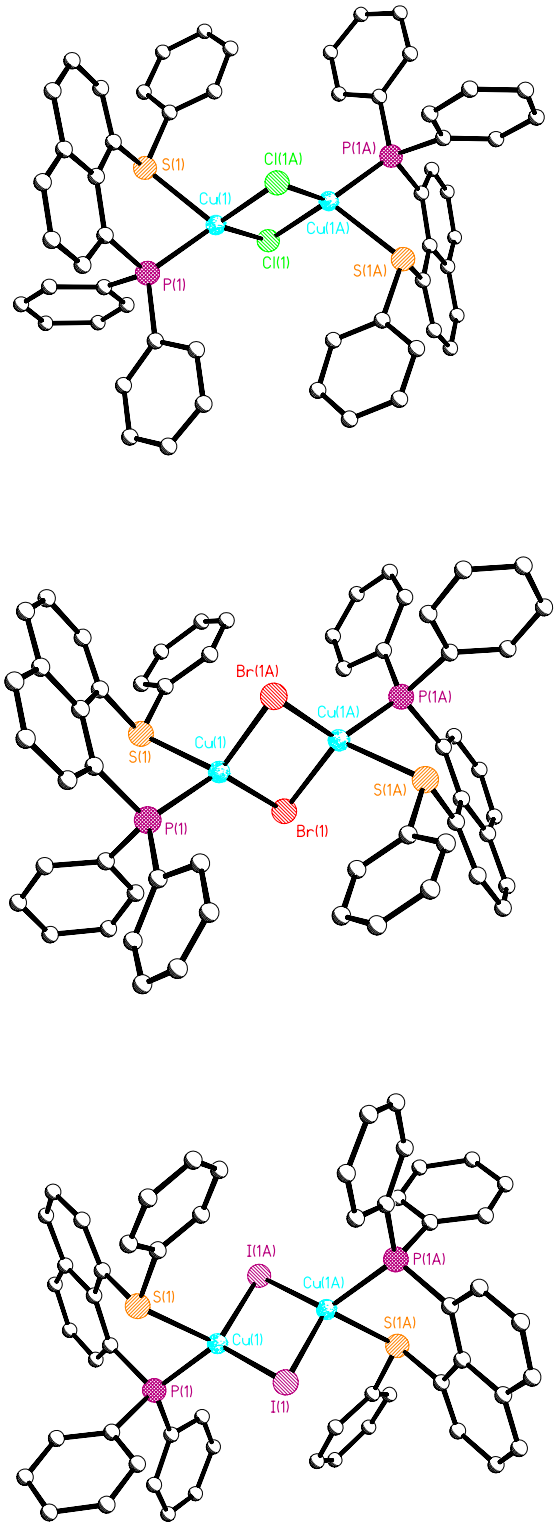

Figure 7-10. Structural representations of **7.6**, **7.7**, and **7.8**.

Table 7-5. Selected bond lengths (Å) and angles (°) for **7.1**, **7.6**, **7.7**, and **7.8**.

	7.1	**7.6**	**7.7**	**7.8**
Cu(1)…Cu(1)'		3.0037(13)	2.9296(14)	2.8568(11)
X(1)…X(1)'		3.744(2)	3.9193(14)	4.3287(8)
Cu(1) - X(1)		2.3889(17)	2.4301(14)	2.5809(11)
Cu(1) - X(1)'		2.411(2)	2.4630(16)	2.6055(12)
Cu(1) - P(1)		2.222(2)	2.217(2)	2.248(2)
Cu(1) - S(1)		2.487(2)	2.442(2)	2.444(2)
Cu(1)-X(1)-Cu(1)'		77.48(6)	73.55(4)	66.85(3)
X(1)-Cu(1)-X(1)'		102.52(6)	106.45(4)	113.15(3)
P(1)-Cu(1)-X(1)		127.97(7)	126.62(8)	125.01(7)
P(1)-Cu(1)-X(1)'		120.62(8)	116.52(9)	113.00(7)
S(1)-Cu(1)-X(1)		108.34(7)	108.47(7)	106.70(6)
S(1)-Cu(1)-X(1)'		113.14(6)	113.12(7)	112.15(6)
P(1)-Cu(1)-S(1)		81.51(7)	82.89(7)	81.52(7)
Mean Plane Deviations				
P(1)	0.018(5)	-0.199(9)	-0.196(10)	-0.090(9)
S(1)	0.136(5)	0.101(9)	0.112(10)	0.186(9)
Cu(1)		-1.616(11)	-1.566(12)	1.594(11)

[1]X = Cl for **7.6**, Br for **7.7**, or I for **7.8**.

Cu(1)-P(1) bond distances are similar ranging from 2.217(2) Å to 2.248(2) Å and the Cu(1)-S(1) distances are also similar and range from 2.442(2) Å to 2.487(2) Å.

As implied by the "elongating diamond" above, the Cu(1)-X(1)-Cu(1)' angle decreases as the halide ion size increases, so **7.6** (77.48(6)°) > **7.7** (73.55(4)°) > **7.8** (66.85(3)°). Correspondingly, the X(1)-Cu(1)-X(1)' angle distinctly increases from **7.6** (102.52(6)°) < **7.7** (106.45(4)°) < **7.8** (113.15(3)°). The P(1)-Cu(1)-S(1) bond angle is ~82° in all three complexes.

7.4.2. Ligand Environment

The P(1)…S(1) distance of **7.1**, when bound to the copper center, is larger than in uncoordinated **7.1**. Table 7.6 shows a comparison of bond distances and angles of the coordinated and uncoordinated ligand. The P(1)…S(1) distance in these complexes ranges from 3.067(2) Å (**7.8**) to 3.089(3) Å (**7.7**; **7.6** is 3.081(2) Å). Conversely, the P(1)-C(1) bond distances of **7.1** and **7.6**-**7.8** are identical

Table 7-6. Selected bond lengths (Å) and angles (°) for **7.1**, **7.6**, **7.7**, and **7.8**.

	7.1	**7.6**	**7.7**	**7.8**
P(1)…S(1)	3.0339(13)	3.081(2)	3.089(3)	3.067(2)
P(1) - C(1)	1.850(3)	1.844(7)	1.837(8)	1.847(8)
S(1) - C(9)	1.784(3)	1.796(8)	1.812(8)	1.805(8)
P(1)-C(1)-C(2)	118.0(2)	116.7(5)	116.6(5)	116.6(5)
P(1)-C(1)-C(10)	124.1(2)	124.7(5)	124.1(6)	124.1(6)
S(1)-C(9)-C(8)	115.1(2)	118.1(6)	116.9(6)	117.1(6)
S(1)-C(9)-C(10)	123.8(2)	121.9(5)	121.4(5)	121.1(5)
C(2)-C(1)-C(10)	117.8(3)	118.4(7)	119.1(7)	119.1(7)
C(10)-C(9)-C(8)	121.0(3)	119.8(7)	121.5(7)	121.8(7)
C(1)-C(10)-C(9)	126.4(3)	127.3(7)	129.0(7)	129.1(7)
C(4)-C(5)-C(10)-C(1)	-1.2(4)	1.6(11)	-0.6(12)	-0.2(8)
C(6)-C(5)-C(10)-C(9)	0.1(3)	-1.5(11)	-0.2(9)	0.3(8)
C(4)-C(5)-C(10)-C(9)	-179.5(3)	179.8(6)	179.7(7)	-179.0(7)
C(6)-C(5)-C(10)-C(1)	178.5(3)	-179.7(7)	179.4(8)	179.0(7)
Mean Plane Deviations				
P(1)	0.018(5)	-0.199(9)	-0.196(10)	-0.090(9)
S(1)	0.136(5)	0.101(9)	0.112(10)	0.186(9)
Cu(1)		-1.616(11)	-1.566(12)	1.594(11)

[1]X = Cl for **7.6**, Br for **7.7**, or I for **7.8**.

within error. Additionally, the S(1)-C(9) bond distances in **7.6**-**7.8** range from 1.796(8) Å to 1.812(8) Å, which is larger than **7.1** and increases with **7.6** < **7.8** < **7.7**.

The outer P(1)-C(1)-C(2) angle is ~1° smaller in **7.6**-**7.8** than in **7.1**, however the inner angle P(1)-C(1)-C(10) is almost identical in **7.1** and **7.6**-**7.8**. The outer S(1)-C(9)-C(8) angle increases through the range 116.9(6)° to 118.1(6)°, where **7.7** < **7.8** < **7.6**. The smallest of these angles is ~2° larger than in **7.1**. Finally, the inner S(1)-C(9)-C(10) angle in **7.1** (123.8(2)°) is larger than in **7.6** - **7.8** (~121°).

The out-of-plane deviations of P(1) are most distorted in **7.6** and **7.7**, being -0.199(9) Å and -0.196(10) Å from the naphthalene plane, respectively. P(1) in **7.1** deviates 0.018(5) Å from the plane compared to only -0.090(9) Å in **7.8**. The out-of-plane deviation of S(1) in **7.1** (0.136(5) Å), is within the range defined by

the copper-halide complexes, where **7.6** (0.101(9) Å) < **7.7** (0.112(10) Å) < **7.8** (0.186(9) Å). The Cu(1) sits ~1.6 Å out of the naphthalene plane in all three complexes.

Overall, in the copper complexes, the distortions of the angles near the *peri*-positions in the naphthalene backbone are minor and compare quite closely to the distortions in free (uncomplexed) **7.1**. However, the inner ring torsion angles in **7.6-7.8** are, for the most part, less distorted than in **7.1**.

7.5. Cumulative Discussion

Each metal center has distinct properties and characteristics that influence ligand binding. In the previous sections, a structural comparison of free ligand, **7.1**, to metal bound ligand was performed within a single metal series. Using the seven metal-halide compounds introduced in this chapter, the structural features around a small variety of metal centers- Pt(II), Ru(II), or Cu(I)- can be compared. This section contains a direct comparison of the geometric distortions and the physical properties of all of the complexes with **7.1**. The conclusions that can be inferred from the data point towards a general lack of geometric preference on the part of the Ru(II) and Cu(I) centers, but a determination on the part of the Pt(II) center to adopt and maintain a square planar geometry.

7.5.1. Metal center

Each metal center has distinct geometrical properties that can influence the geometry around it. The d^8 platinum(II) complexes presented in this study are square planar, the d^{10} copper(I) complexes are pseudo-tetrahedral (commonly observed in metals having filled or empty *d* shells), while the d^6 ruthenium complex adopts a previously observed "piano stool" geometry, which is in fact, a distorted octahedral. The typical ionic radius of the Pt(II) and Cu(I) ions are identical (0.74 Å).[18] The ionic radius for Ru(II) is not reported,.[18] It is useful to compare the M(1)-P(1) and M(1)-S(1) distances in each complex (Figure 7-11). Since both phosphines and thioethers are good sigma donors, but phosphines are better π-acceptors than thioethers, it is unsurprising that the M(1)-P(1) distance is

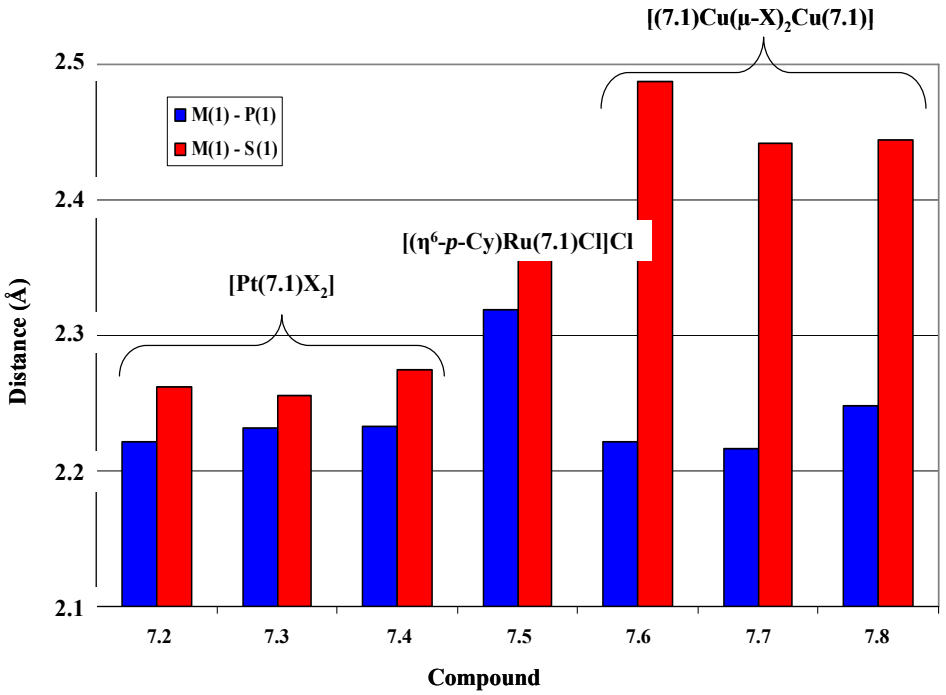

Figure 7-11. Graph of M(1)-P(1) and M(1)-S(1) distances for **7.2**-**7.8**.

shorter in every complex, than the M(1)-S(1) distance is. Further, the M(1)-P(1) distances are similar among the different metal centers, ranging from 2.217(2) Å to 2.248(2) Å in the Pt(II) and Cu(I) complexes and are slightly longer in the Ru(II) complex (2.319(2) Å. In the Pt(II) and Ru(II) complexes, the metal-sulfur distance is slightly (~0.03 Å, or ~10 %) longer than the metal-phosporus distance, but in the copper complexes, the Cu-S distance is relatively enormous compared to the Cu-P distance. The Cu-P distances are all very close to the distances in the complexes of the similarly sized Pt(II) ions, while the Cu-S distances are ~0.2 Å to 0.5 Å (~8 to 10 %) larger. Most simply, this could be due to the rather electron-rich nature of the Cu(I) ion and the very poor π-accepting nature of the thioether ligands, which renders that coordination relatively weak.

The P(1)-M(1)-S(1) angle in the platinum complexes (**7.2**-**7.4**) are relatively large, ranging from 90.41(18)° to 90.61(11)°. By comparison, in **7.5** the angle is 80.22(8)° and in the copper(I) complexes, the angle ranges from

81.51(7)° to 82.89(7)°. As will be shown, these distortions in the ligand bite angle are likely caused by the desire of platinum(II) to adopt the square planar geometry and the lack of geometric desire on the part of the other two metal centers. This same motivation is also suggested by the X(1)-Pt(1)-X(2) (ranging from 89.37(18)° to 90.163(15)°), which is much smaller than the X(1)-Cu(1)-X(2) angle. The X(1)-Cu(1)-X(2) angles drastically increases as the size of the halide ion increases, from 102.52(6)° (**7.6**) to 106.45(4)° (**7.7**) to 113.15(3)° (**7.8**).

Finally, the distance that the metal center gets displaced from the naphthalene plane depends on the metal ion. This displacement is minor in the platinum(II) complexes (~1 Å), increases in the single ruthenium(II) complex (-1.2837(136) Å) and further increases in the copper(I) complexes (~1.59 Å).

7.5.2. Ligand environment and geometry

The geometry of each of the complexes is controlled by a compromise between the preferred bite of the bidentate phospine/thioether ligand and the influence of the *d* orbitals at the metal center. A comparison of the P(1)…S(1) (*peri*) distances can shed light on where the geometric preference is coming from. Figure 7-12 shows the *peri*-distances of unbound ligand, **7.1**, and each of the complexes.

As the table shows, the P(1)…S(1) distance increases from the ruthenium complex to the free ligand to the copper complexes to the largest distance in the platinum complexes. This is logical since the Ru(II) complex has a slightly smaller P(1)-M(1)-S(1) bond angle (80.2^{o}) than the Cu(I) complexes (82.0^{o}), but slightly longer M(1)-P(1) and M(1)-S(1) bonds. Discarding the ligand, except for the P and the S atoms allows for a picture of the S-M-P unit as a scalene triangle with the P…S leg being the longest, it is reasonable that a slightly smaller angle combined with slightly longer bonds would give about the same P…S distance as a slightly narrower angle with slightly shorter bonds (Figure 7-13.) It is likewise logical that the Pt(II) complexes have the largest *peri*-distances since the bond distances are about the same as in the copper complexes but the P-Pt-S angle is significantly larger, around 90^{o}.

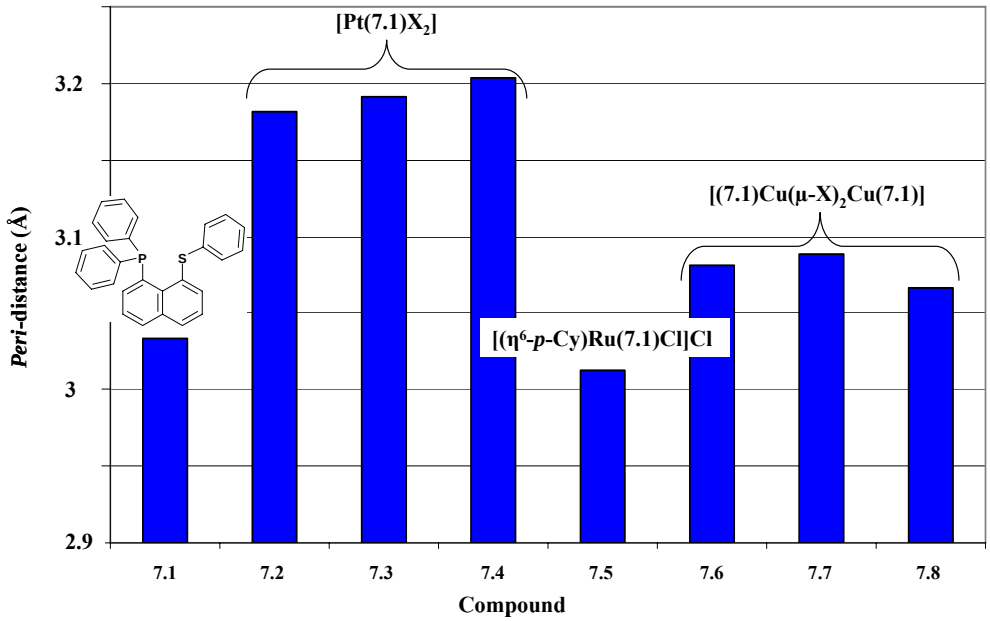

Figure 7-12. Graph of P(1)…S(1) *peri*-distances for **7.1** and **7.2**-**7.8**.

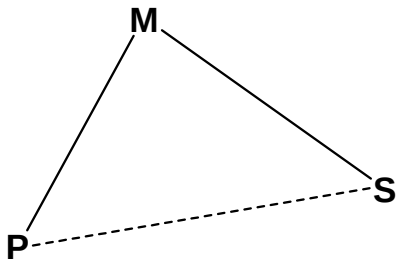

Figure 7-13. Scalene triangle of M-P-S, where M = Pt, Ru, or Pt. P and S are from **7.1**.

The "unconstrained" *peri*-distance (that of the free ligand, **7.1**, where the P and the S can presumably settle where they wish) is 3.10 Å. This falls between (and very close to) the analogous distance in the Ru and Cu complexes. This data suggests that the Ru(II) and Cu(I) complexes may be adopting the geometry they do because of constraints imposed by the ligand, since they change the free ligand very little in this respect. By contrast, Pt(II) coordination distorts the *peri*-distance of the ligand more than double than the Cu(I) or Ru(II) metal centers do. This

implies that the ligand is adopting a geometry enforced by the well-established energetic preferences of the *d* orbitals on the Pt(II) metal center. As shown in Figure 7-14, the ligand seems to benefit from the square planar arrangement in that it develops a weak π…π interaction with a phenyl ring on P(1) to a phenyl ring on S(1). This interaction is not seen in the other complexes (**7.5** to **7.8**) or the free ligand.

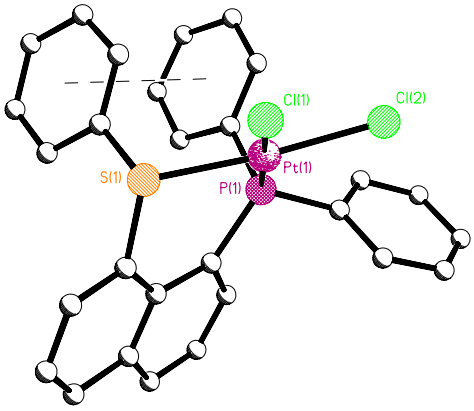

Figure 7-14. Possible π…π interaction of phenyl rings in **7.2**. This distance slightly increases as the size of the halide ion increases **7.2** (3.536(1) Å) < **7.3** (3.574(1) Å) < **7.4** (3.598(1) Å).

The in-plane distortions of the inner angles in the ligand (i.e. those angles that open up towards the metal center) should follow the same trend of greater distortions enforced by the geometry of the Pt(II) ion as the *peri*-distance does. A comparison of one of these angles, P(1)-C(1)-C(10), is shown in Figure 7-15. The P(1)-C(1)-C(10) angle is the most different from the free ligand in the Pt(II) complexes and decreases to near-similarity in the Ru(II) complex and is essentially identical in the Cu(I) complexes.

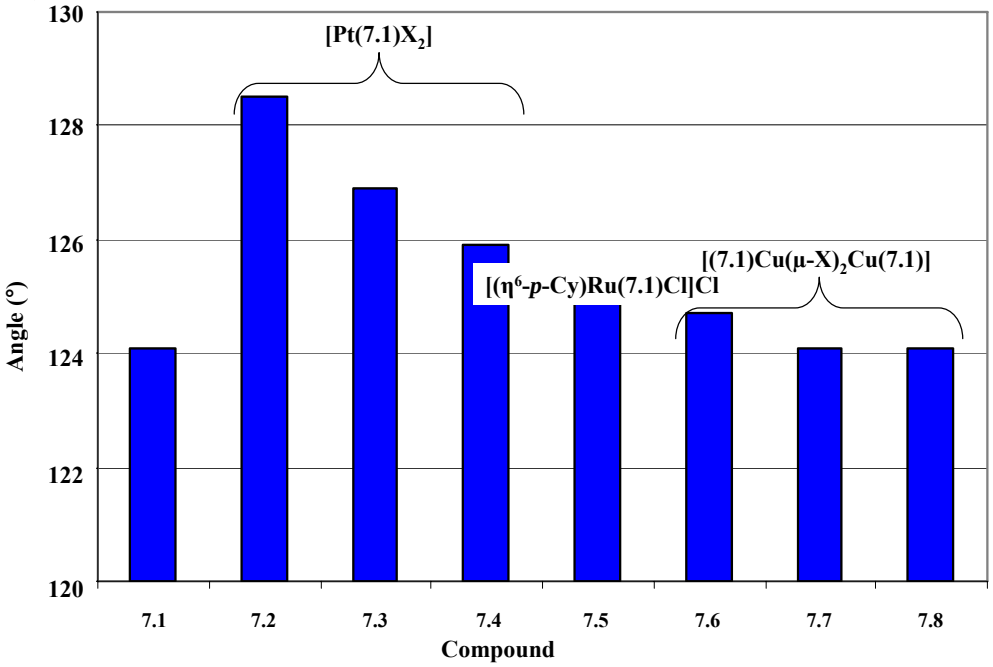

Figure 7-15. The P(1)-C(1)-C(10) angle for **7.1**-**7.8**.

One final distortion to compare in the ligand is the buckling of the naphthalene ring. Table 7-7 compares angles in unsubstituted naphthalene, the phospine/thioether containing naphthalene, and the ranges of angles found in the naphthalene containing metal complexes. While different from unsubstituted naphthalene, the C(2)-C(1)-C(10), C(10)-C(9)-C(8), and C(1)-C(10)-C(9) angles in all of the complexes occur in a range that is no more than one or two degrees away from the same angles in **7.1.** Since the deviations in the naphthalene backbone found in the bound ligand are similar to those present in the free ligand, it would seem that the vast majority of the stress on the backbone comes simply

Table 7-7. Selected naphthalene backbone angles(°).

Angle	Naphthalene	7.1	7.2-7.4	(7.5)	7.6-7.8
C(2)-C(1)-C(10)	120.6(1)	117.8(3)	115.0(18)-119.1(5)	118.7(9)	118.4(7)-119.1(7)
C(10)-C(9)-C(8)	120.5(1)	121.0(3)	120.5(11)-123.1(19)	122.9(9)	119.8(7)-121.8(7)
C(1)-C(10)-C(9)	121.7(1)	126.4(3)	125.4(18)-127.8(6)	127.7(9)	127.3(7)-129.1(7)

from *peri*-substitution and not from metal coordination. This holds true even for the Pt(II) metal center, which, while it does stress the *peri*-substituents, does not untowardly affect the naphthalene backbone.

The out of plane distortion of P(1) and S(1) in these complexes can be seen in Figure 7-16. In each case, except **7.4**, the P(1) and S(1) lie on opposite sides of the naphthalene plane and are more distorted than the parent ligand. It is interesting that the Pt-chloride (**7.2**) and Pt-bromide (**7.3**) complexes have the largest out-of-plane distortion of all the complexes while the Pt-iodide complex (**7.4**) has the smallest distortion. Not to mention that all three atoms (the Pt, P, and S) in the Pt-iodide complex (**7.4**) sit on the same side of the plane. In all of the complexes, except in the Pt-iodide and the Cu-iodide cases, the metal center sits on the same side of the plane as P(1). The general amount of distortion observed is presumably due to steric effects in the rather crowded binuclear copper complexes versus the less crowded mononuclear ruthenium complexes and the rather sterically open mononuclear platinum complexes.

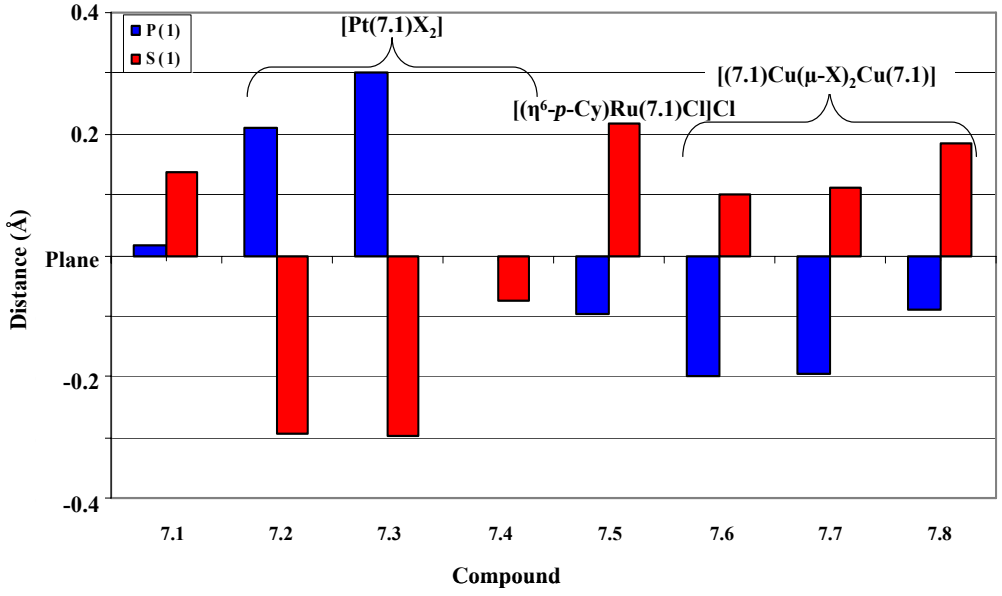

Figure 7-16. Out of plane distortions for P(1) (blue) and S(1) (red) in **7.1**-**7.8**.

7.6. Summary

In conclusion, the different geometries observed in the metal complexes discussed in this chapter are adopted for different reasons. In the copper and ruthenium complexes, the bidentate P/S ligand seems to dictate the selection of geometry around the metal center, keeping its most comfortable internal geometry, while also trying to stay as far away from any steric interference as it can. This leads to a distorted tetrahedral or octahedral geometry, respectively, in each case, which allows the metal center to adopt an energetically not-unfavorable geometry, while putting as few of the large bidentate ligands around the metal as possible. In the case of the platinum center, the energetic driving force to adopt a square planar geometry is strong enough to distort the ligand to fit into a square plane rather than allow the ligand to enforce a different geometry that stresses it less.

7.7. References

1. A. Bader and E. Lindner, *Coord. Chem. Rev.,* 1991, 108, 27-110.

2. J. C. Bayón, C. Claver and A. M. Masdeu-Bultó, *Coord. Chem. Rev.,* 1999, 193-195, 73-145.

3. J. R. Dilworth and N. Wheatley, *Coord. Chem. Rev.,* 2000, 199, 89-158.

4. A. R. Sanger, *Can. J. Chem.,* 1983, 61, 2214-2219.

5. P. Kapoor, K. Lövqvist and Å. Oskarsson, *J. Mol. Struct.,* 1998, 470, 39-47.

6. S. D. Toto, M. M. Olmstead, B. W. Arbuckle, P. K. Bharadwaj and W. K. Musker, *Inorg. Chem.,* 1990, 29, 691-699.

7. R. Malacea, L. Routaboul, E. Manoury, J. Daran and R. Poli, *J. Organomet. Chem.,* 2008, 693, 1469-1477.

8. Y. Jun, H. Dejian, L. Guangnian and Z. Liangfu, *Acta Chimica Sinca,* 1993, 51, 1145-1150.

9. A. Karaçar, M. Freytag, H. Thönnessen, J. Omelanczuk, P. G. Jones, R. Bartsch and R. Schmutzler, *Z. Anorg. Allg. Chem.,* 2000, 626, 2361-2372.

10. N. Taguchi, K. Kashiwabara, K. Nakajima, H. Kawaguchi and K. Tatsumi, *J. Organomet. Chem.,* 1999, 587, 290-298.

11. T. Suzuki, N. Taguchi and K. Kashiwabara, *Acta Cryst. C,* 1996, 52, 2982-2984.

12. K. D. Redwine and J. H. Nelson, *J. Organomet. Chem.,* 2000, 613, 177-199.

13. S. Burger, B. Therrien and G. Süss-Fink, *Inorg. Chim. Acta,* 2004, 357, 1213-1218.

14. O. G. Mancheno, R. G. Arrayas and J. C. Carretero, *J. Am. Chem. Soc.,* 2004, 126, 456-457.

15. O. G. Mancheno, R. G. Arrayas and J. C. Carretero, *Organometallics,* 2005, 24, 557-561.

16. O. N. Kataeva, I. A. Litvinov, V. A. Naumov, L. I. Kursheva and E. S. Batyeva, *Inorg. Chem.,* 1995, 34, 5171-5174.

17. T. S. Lobana, S. Khanna, R. J. Butcher, A. D. Hunter and M. Zeller, *Inorg. Chem.,* 2007, 46, 5826-5828.

18. J. E. Huheey, *Inorganic Chemistry: Principles of Structure and Reactivity*, HarperCollins College Publishers, 1993.

CHAPTER 8
THE X-RAY STRUCTURES OF SULFOXIDES

8.1. Introduction

A sulfoxide is a molecule with the general formula R-S(=O)-R', where R is an organic group. Structurally, these molecules display some interesting characteristics. There has been some debate over the nature of the S=O bond and a comparison with other well known molecules possessing the R(X=O)R' motif (where X = C or P) illustrates why the S=O bond in sulfoxides is debated.[1] In the carbon analog R(C=O)R', the carbon atom forms a typical *p-p* π bond with oxygen. In the sulfoxide or phosphine oxide ($O=PR_3$) molecules, however, it has been suggested that the oxygen contributes electrons from its unshared lone pairs from the 2*p* orbital to an empty 3*d* orbital of the central sulfur or phosphorus atom, *i.e.*, *d-p* π bonding.[1,2] However, there is some debate over the compatibility of the energy level overlap of the 3*d* orbital with the oxygen 2*p* orbital. The sulfoxide bond is probably best represented as being somewhere in between a double and a single bond, with significant ionic character.[3] This is represented by the two resonances structures in Figure 8-1.

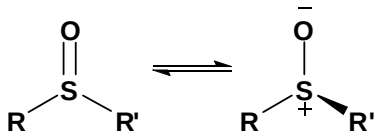

Figure 8-1. Two resonance structures of the sulfoxide bond.

Another important characteristic of sulfoxide molecules is their ability to be chiral. When sulfur is bound to three substituents, such as in a sulfoxide, the lone pair of electrons on the sulfur atom forces the substituents into a pyramidal geometry. Since the sulfur now has four unique arms, it is most similar to chiral

tertiary phosphine oxides (O=PRR'R'') (Figure 8-2). The Cahn-Ingold-Prelog priority rules are used when deciding the stereochemistry of chiral sulfoxide compounds, and the unpaired electrons are assigned as the lowest priority group.[3] Many reaction pathways have been investigated in attempts to synthesize a sulfoxide with specific chirality, including the use of inorganic, organic, and enzymatic catalysts.[4-6] Specific chirality enables sulfoxides to be used as catalysts to transfer their chirality to carbon compounds.[5] Sulfoxide chirality is also becoming increasingly important in pharmaceutical synthesis.[3]

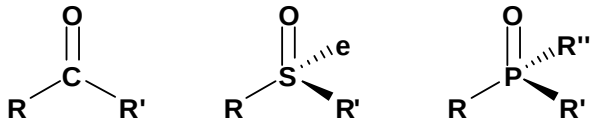

Figure 8-2. Geometric comparison of a carbonyl carbon, a sulfoxide, and a tertiary phosphine oxide.

Three classes of sulfoxide compounds have been previously described as having very specific hydrogen bonding interactions that enforce particular conformations in the molecule and influence crystal packing.[7] Here, we have investigated the structural properties of three types of sulfoxides where the R groups are alkyl-alkyl, alkyl-aryl, and aryl-aryl arms using X-ray crystallography. We discuss both intra- and intermolecular interactions that influence the packing of these compounds.

8.2. Experimental

8.2.1. General

Crystals of dibenzyl sulfoxide **8.1**, benzyl 4-chlorophenyl sulfoxide **8.2**, benzyl 4-methylphenyl sulfoxide **8.3**, benzyl phenyl sulfoxide **8.4**, di(*p*-tolyl) sulfoxide **8.5**, benzyl ethyl sulfoxide **8.6**, and 4-nitrobenzyl phenyl sulfoxide **8.7** were analyzed by X-ray crystallography. Crystallographic data for diphenyl sulfoxide ($SOPh_2$) were already determined.[8] Compounds **8.1** and **8.5** were purchased from Aldrich. Compounds **8.2-8.4**, **8.6**, and **8.7** were prepared by

oxidation of the relevant sulfides with $NaIO_4$ in aq. MeOH.[9-13] All compounds were recrystallized from a CH_2Cl_2/pentane solution.

8.2.2. X-ray Crystallography

Appendix 1 contains details of data collections and refinements for **8.1-8.7**. Data for **8.1**, **8.2**, **8.3**, **8.5**, and **8.7** were collected using a Rigaku SCX-Mini diffractometer (Mercury2 CCD) and **8.4** was collected using the St Andrews Robotic diffractometer (Saturn724 CCD) at either 125 or 293 K with graphite monochromated Mo-Kα radiation (λ = 0.71073 Å) whilst **8.6** was collected using a Rigaku MM007 RA/confocal optics and Mercury CCD at 93 K.[14-16] Intensity data were collected using ω (and ϕ for **8.7**) steps accumulating area detector images spanning at least a hemisphere of reciprocal space. All data were corrected for Lorentz polarization and long-term intensity fluctuations. Absorption effects were corrected on the basis of multiple equivalent reflections or by semi-empirical methods. Structures were solved by direct methods and refined by full-matrix least-squares against F^2 (SHELXL).[17] Hydrogen atoms were assigned riding isotropic displacement parameters and constrained to idealized geometries. Details are available from the Cambridge Crystallographic Data Centre CCDC 689268-689274.

8.3. Results and Discussion

8.3.1. Structural Analysis Around Sulfur

Structures from the single X-ray analysis of the sulfoxides **8.1-8.7** are shown in Figure 8-3. Compounds **8.1** and **8.6** have two alkyl arms attached to the sulfoxide moiety, **8.5** has two aryl groups attached, and **8.2**, **8.3**, **8.4**, and **8.7** have one alkyl (benzyl) and one aryl arm.

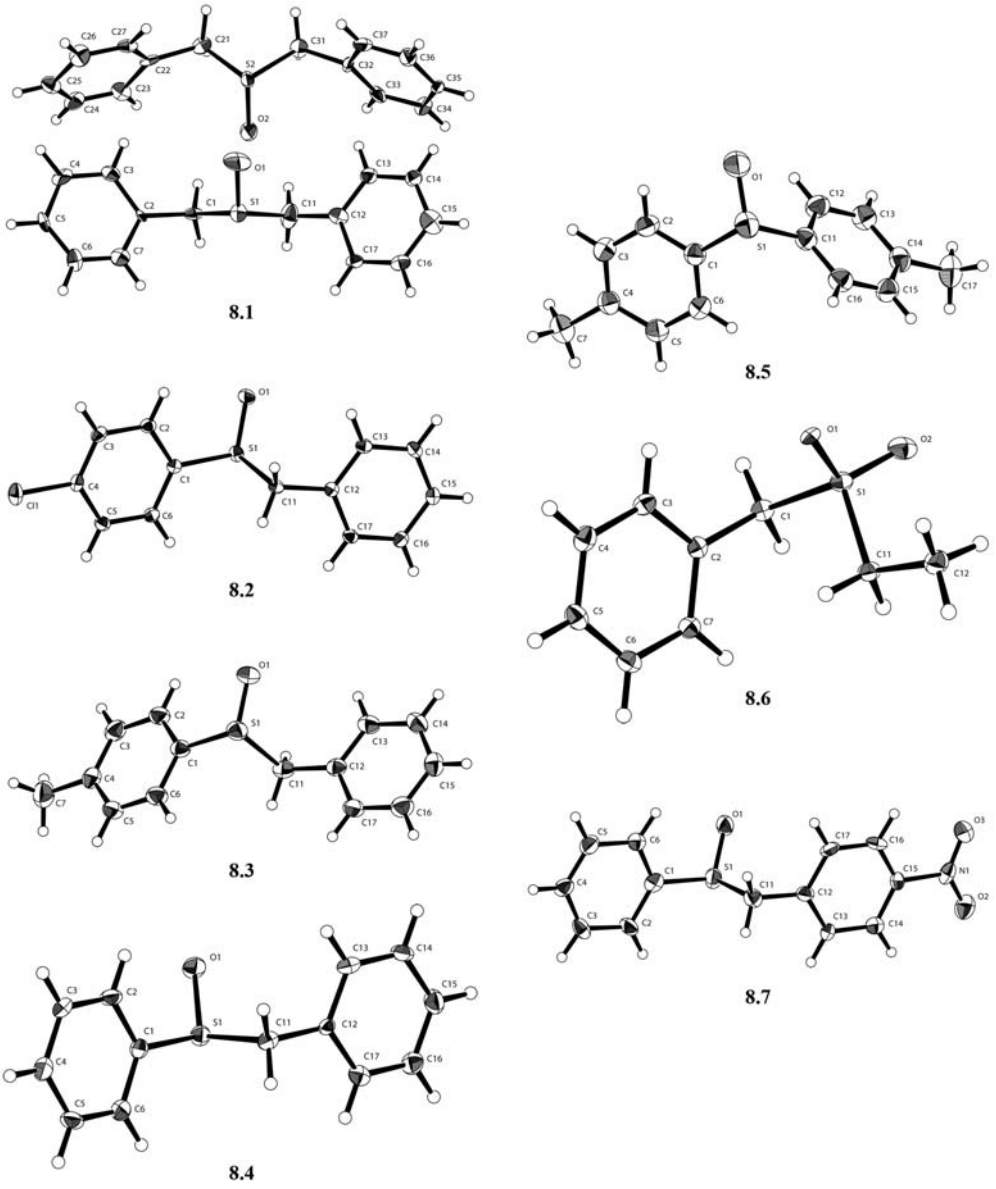

Figure 8-3. Thermal ellipsoid plots (30% probability ellipsoids) of **8.1**-**8.7**.

The bond lengths around the sulfur atom in **8.1**-**8.7** are shown in Table 8-1. These compounds have similar S-O bond distances ranging from 1.489(7) to 1.515(8) Å and are consistent with the reported average sulfoxide distance of 1.497(13) Å.[18] However, the S-C bond distances seem more sensitive to the substituents and range from 1.746(12) to 1.865(10) Å. There is a very slight difference in bond length depending on the organic group attached to the sulfur,

Table 8-1. Selected bond distances (Å) and bond angles (°) for $SOPh_2$[8] and **8.1-8.7**.

	$SOPh_2$		**8.1a**	**8.1b**	**8.2**	**8.3**	**8.4**	**8.5**		**8.6**		**8.7**
S(1)-O(1)	1.4953(12)		1.505(9)		1.5050(19)	1.5032(16)	1.501(4)	1.495(2)		1.489(2)		1.489(7)
S(1)-C(1)	1.781(1)		1.805(9)		1.801(2)	1.808(2)	1.803(6)	1.798(2)		1.811(2)		1.809(10)
S(1)-C(11)	1.779(1)		1.746(12)		1.831(2)	1.839(2)	1.822(6)	1.794(2)		1.792(3)		1.865(10)
S(1)-O(2)										1.488(7)		
S(2)-O(2)				1.515(8)								
S(2)-C(21)				1.809(10)								
S(2)-O(31)				1.815(10)								
O(1)-S(1)-C(1)	106.77(6)		105.8(4)		106.69(10)	107.42(10)	106.0(2)	106.17(12)		108.14(12)		108.5(4)
O(1)-S(1)-C(11)	106.39(5)		106.7(5)		106.52(10)	106.66(10)	107.3(2)	108.21(12)		106.51(13)		105.1(4)
C(1)-S(1)-C(11)	98.5(1)		95.1(5)		97.52(10)	96.98(10)	97.9(2)	99.00(10)		100.56(12)		98.4(4)
O(1)-S(1)-O(2)										119.1(3)		
O(2)-S(1)-C(1)										109.2(3)		
O(2)-S(1)-C(11)										111.7(3)		
O(2)-S(2)-C(21)				108.2(4)								
O(2)-S(2)-C(31)				105.7(4)								
C(31)-S(2)-C(21)				94.1(4)								
Intramolecular Interactions (Å) Angles (°).												
	$SOPh_2$		**8.1a**	**8.1b**	**8.2**	**8.3**	**8.4**	**8.5**		**8.6**		**8.7**
O…H_{aryl}	2.51	2.57			2.50	2.61	2.54	2.75	2.53			2.61
O-S-C-C	11.38(1)	11.70(1)			3.27(1)	8.16(1)	17.64(1)	32.37(1)	23.48(1)			19.57(1)
O-phenyl (distance out of plane)							0.142(3)	0.230(3)	0.464(6)	0.803(3)	0.462(3)	
	0.506(11)											
Intermolecular Interactions (Å) Angles (°).												
S…O	4.20(1)		3.58(1)	3.57(1)	4.31(1)	4.35(1)	4.02(1)	4.37(1)		3.99(1)		3.95(1)
										Ethyl	Benzyl	
O…H_{alkyl}			2.80[b]	2.77[b]	2.29	2.50	2.46			2.48	2.53	2.49
O…C			3.54(1) [b]	3.51(1)[b]	3.27(1)	3.44(1)	3.38(1)			3.37(1)	3.40(1)	3.37(1)
O…H-C angle			132.24[b]	132.72[b]	170.84	163.7	153.91			149.04	145.91	147.90

H_{aryl} refers to the ortho-proton on the aromatic ring, where H_{alkyl} refers to the benzyl proton.
1a and 1b refer to two independent molecules in the asymmetric unit.
[b]Average interaction from the two benzyl arms in each independent molecule

though the range is larger for the alkyl case. If the group is aromatic, the S-C distances have a tendency to be slightly shorter (ranging from 1.798(2) to 1.811(2) Å) than if the group is alkyl (ranging from 1.746(12) to 1.839(2) Å). This could be due to a very weak conjugation of the π-system in the aromatic ring with the S=O double bond. The average reported S-C bond distance is 1.818(1) Å.[18]

Selected bond angles around the sulfur atom are shown in Table 8-1. Due to the lone pair of electrons on the sulfur, it adopts a pyramidal structure. The O(1)-S-C bond angle for all seven structures vary from 105.1(4) to 108.5(4)°, with the two extremes being present in **8.7**. The C(1)-S(1)-C(11) bond angles are smaller, ranging from 94.1(4) to 100.56(12)°. This difference reflects the stereochemical impact of the lone pair of electrons on the sulfur atom. In **8.6**, the disorder in the oxygen atoms may be responsible for the larger O(2)-S-C bond angles of 109.2(3) and 111.7(3)°. The O(1)-S(1)-O(2) bond angle in **8.6** is 119.1(3)°.

8.3.2. O···H_{aryl} Intramolecular Interactions

When an aryl group is attached to the sulfur, not only is there the possibility of a weak conjugation of the double bonds, but it has been suggested that an intramolecular interaction can exist between the sulfoxide oxygen and the ortho-hydrogen (H_{aryl}) on a neighboring aromatic ring.[7] The strength of the O···H_{aryl} interaction influences how the aromatic ring is oriented in the molecule and will ultimately influence crystal packing. Three measures can be used to determine the strength of the O···H_{aryl} intramolecular interaction; (1) the distance between the oxygen and hydrogen atom, (2) the O-S-C-C torsion angle, and (3) the O atom deviation from the S-aryl ring plane. For example, a stronger interaction will result in a shorter O···H_{aryl} distance, a smaller torsion angle, and a smaller deviation of the oxygen atom from the S-aryl plane. These three values can be found in Table 8-1. Figure 8-4 illustrates the possible O···H_{aryl} interaction and the O-S-C-C torsion angle being measured.

Compounds **8.2**-**8.4** and **8.7** have one aryl group adjacent to the sulfoxide moiety enabling an intramolecular interaction to exist between the O and the H_{aryl}.

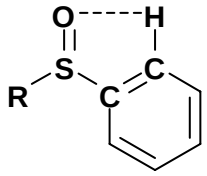

Figure 8-4. Possible intramolecular interactions between the O···H_{aryl} can be described by the O···H_{aryl} distance, the O-S-C-C torsion angle, and the oxygen deviation from the S-aryl plane.

The O···H_{aryl} distance in these compounds range from 2.50(1) to 2.61(1) Å. For the most part, as the O···H_{aryl} distance increases, the torsion angle also increases, reflecting the displacement of the O atom from the plane of the aromatic group. **8.2** has the shortest O···H interaction (2.50(1) Å), the smallest torsion angle (3.27(1)°), and the smallest oxygen deviation from the plane (0.142(3) Å). The O···H_{aryl} distance increases **8.2** < **8.4** < **8.3** ~ **8.7** whilst the O-S-C-C torsion angle and the mean deviation of the oxygen atom increases **8.2** < **8.3** < **8.4** < **8.7**. Compound **8.3** displays some interesting behavior, as it has the second longest O···H_{aryl} distance of the series (2.61(1) Å), but a very tight torsion angle (8.16(1)°).

Compound **8.5** does not fit into the previous structural group because it has two aryl arms attached to the sulfoxide. However, this compound can be compared to the well known compound diphenyl sulfoxide ($SOPh_2$). Both phenyl arms in $SOPh_2$ have similar O···H_{aryl} bond distances of 2.51(1) and 2.57(1) Å and similar O-S-C-C torsion angles of 11.38(1) and 11.70(1)°.[8] Compound **8.5** has two *p*-tolyl substituents. While these arms are structurally similar to the phenyl arms in $SOPh_2$, they display different structural characteristics. Only one O···H_{aryl} distance (2.53(1) Å) is similar to $SOPh_2$, while the other one is significantly longer (2.75(1) Å). The O-S-C-C torsion angles for the two arms are also much larger in **8.5** than in $SOPh_2$, twisting to 23.48(1) and 32.37(1)° (Figure 8-5).

Across the entire series, as the O···H_{aryl} distance increases, so does the torsion angle; **8.2** has the smallest O···H_{aryl} distance and the smallest torsion angle and **8.5** has the largest O···H_{aryl} distance and the largest torsion angle. There are

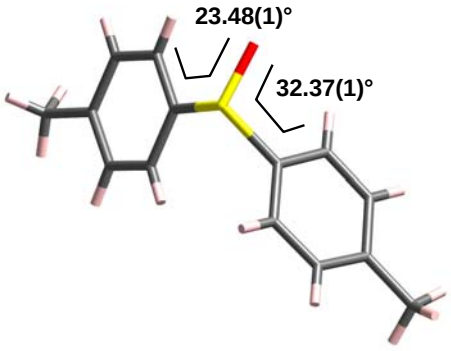

Figure 8-5. The X-ray structure of **8.5** showing the large O-S-C-C torsion angles.

only two exceptions to this trend: one arm of compound **8.5** and one arm of compound **8.3**. Interestingly enough, in both exceptions, it seems to be a *p*-tolyl substituent causing the deviations. However, a crystallographic example of (-)-(*S*)-4-aminophenyl *p*-tolyl sulfoxide is known (Figure 8-6).[19] The O···H_{aryl} distance of the *p*-tolyl group in this compound is 2.31(1) Å, which is much closer than the equivalent distance in **8.3** or **8.5**. The *p*-tolyl group also has a O-S-C-C torsion angle of -10.8(3)°, which is less than that of **8.5** and only slightly larger than that of **8.3**.

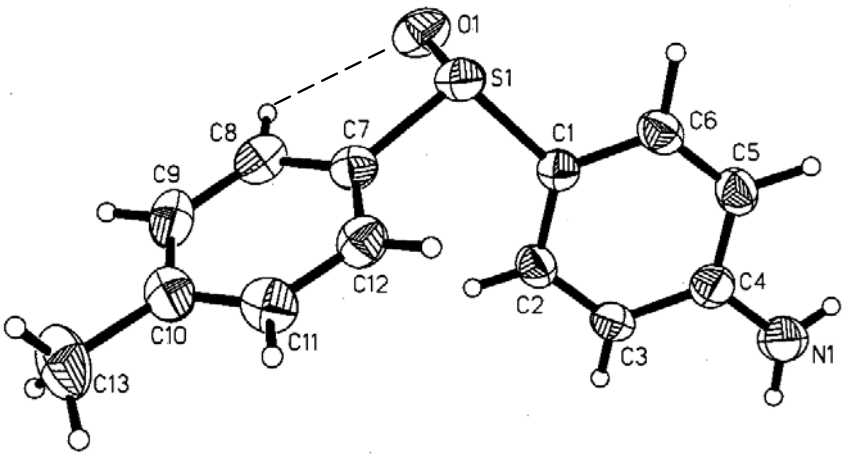

Figure 8-6. ORTEP drawing of (-)-(*S*)-4-aminophenyl *p*-tolyl sulfoxide: O1…H_{aryl} interaction is 2.31Å and O1-S1-C7-C8 torsion angle is -10.8(3)°.[19]

8.3.3. O···H_{methyl} Intramolecular Interactions

Compound **8.6** has two alkyl groups attached to the sulfoxide moiety, and it appears that an O···H_{methyl} intramolecular interaction could be present. In **8.6** there is a disordered oxygen atom, with 80% O(1) and 20% O(2) occupancy. Structurally there is a close contact between O(2) and C(12) (Figure 8-7). In addition, O(2) and one H_{methyl} are perfectly eclipsed with a distance of 2.93(1) Å. This orientation does not exist when looking at O(1). Even though the O(1)···H_{methyl} distance is slightly shorter (2.80(1) Å), the atoms are ~12° degrees out of alignment.

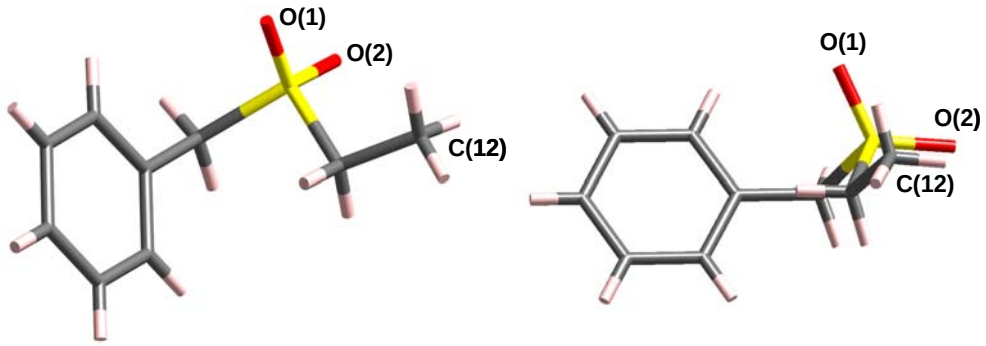

Figure 8-7. Left, X-ray structure of **8.6** showing the disorder in the oxygen atom (O(1), 80% and O(2), 20% occupancy). Right, **8.6** is rotated bringing the ethyl group forward to show the alignment of O(2) and H_{methyl}.

8.3.4. S, O Intermolecular Interactions

The sulfoxide bond has been described as a single bond with ionic character, with the sulfur bearing a formal positive charge and the oxygen bearing a formal negative charge.[1,3] The large dipole moments in these bonds allow unique intermolecular interactions in the packing of these molecules. The intermolecular S···O distances range from 3.57(1) to 4.37(1) Å. The shortest distance is in **8.1** and the longest is in **8.5** (Table 8-1). In **8.1**-**8.7** sulfur bound to alkyl groups tends to have a shorter intermolecular S···O distance than when

sulfur is bound to aromatic substituents. This could be due to one or a combination of several reasons. When aryl substituents are present, conjugation of the entire pi system in the molecule could reduce the positive dipole on the sulfur atom, lengthening the intermolecular S···O distance. Alternatively, alkyl groups could simply give more space for close approach of the oxygen atom. Thirdly, when alkyl substituents are present, any intermolecular O···H_{alkyl} interactions could help pull the S and O closer together.

8.3.5. O···H_{alkyl} Intermolecular Interactions

Sulfoxide compounds display some unique intermolecular interactions in their crystal packing. It has been suggested that a type of intermolecular O···H_{alkyl} interaction can occur in sulfoxides when the sulfur atom is flanked by a -CH_2-R group.[7] An interaction between the oxygen atom of one sulfoxide molecule and the hydrogen from the -CH_2-R group can be difficult to demonstrate because it is so weak. The O···H_{alkyl} distance, the O···C_{alkyl} distance, and the O···H-C angle can be used as evidence to help support or contradict this theory.

Significant intermolecular hydrogen bonding interactions are considered in these compounds if the O···H distances are <2.70 Å and the O···H-C angle is >120°.[7] Table 8-1 shows the O···H_{alkyl} distance, the O···C distance, and the O···H-C angle for compounds **8.1**-**8.7**. The weaker O···H-C interactions are longer than classical O···H-O hydrogen bond distances (~2.30 Å), and they are less sensitive to deviations from ideal geometries than stronger H-bonds.[20] Therefore, a larger O···H-C angle can deviate from linearity, but that doesn't necessarily mean the hydrogen bond is weaker.[7]

In this study, **8.1** and **8.6** have two alkyl arms adjacent to the sulfur. **8.1** has two benzyl groups (crystallizing with two independent molecules in the asymmetric unit cell, **8.1a** and **8.1b**). The values in Table 8-1 show the average interaction distances associated with each molecule. The average values for **8.1a** and **8.1b** are very close and are in most cases within experimental error of each other. Of all of the reported compounds, **8.1b** has the shortest S···O distance

(3.57(1) Å), but the longest O···H_{alkyl} distance (2.77(1) Å), and the O···H-C atoms form a 132.72(1)° angle (Figure 8-8).

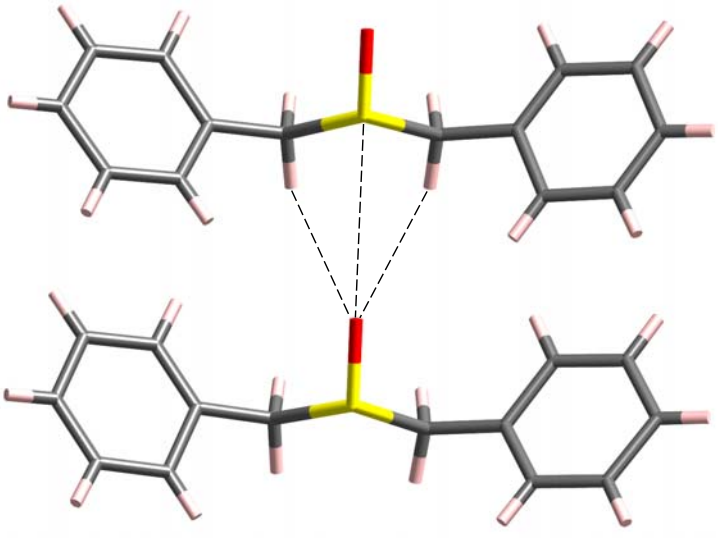

Figure 8-8. Possible intermolecular interactions in **8.1**.

In **8.6**, the sulfur is flanked by one benzyl group and one ethyl group. The S···O distance is 3.99(1) Å, which is longer than in **8.1**. Intermolecular O···H_{alkyl} interactions with the O···H-C of the benzyl arm are shorter and more linear than that of **8.1**. The O···H_{alkyl} distance in **8.6** is 2.53(1) Å and an O···C-H angle is 145.91(0)°. The ethyl arm shows an even shorter O···H_{alkyl} distance of 2.48(1) Å, with a more linear O···C-H angle of 149.04(1)°.

Given the benchmarks discussed earlier, if there is an O···H_{alkyl} interaction, it would have to be considered very weak. However, two weak O···H-C intermolecular interactions could pull the molecules closer together and decrease the O···S distance and decrease the O···H-C angle (Figure 8-9).

Compounds **8.2-8.4** and **8.7** have one alkyl and one aryl group. The S···O interactions in these molecules are slightly longer (range from 3.95(1) to 4.35(1) Å) than the compounds with two alkyl groups (**8.1**: 3.57(1) and 3.58(1) Å and **8.6**: 3.99(1) Å). **8.3** has the longest S···O distance of 4.35(1) Å. The O···H_{alkyl} distances range from 2.29(1) in **8.2** to 2.50(1) Å in **8.3**. The O···H_{alkyl}-C angles are more

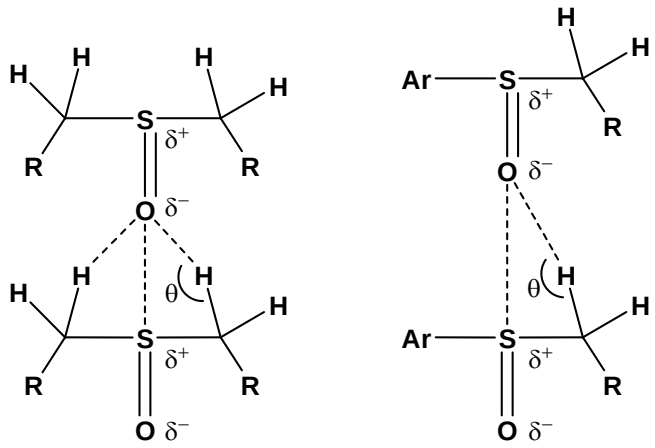

Figure 8-9. Simple depiction of intermolecular hydrogen bonding interactions in sulfoxide compounds with two alkyl arms (left) and an alkyl and aryl arms (right).

linear in these compounds than in the alkyl/alkyl compounds ranging from 147.90(1) in **8.7** to 170.84(1)° in **8.2**. Possible intermolecular interactions for **8.2** are shown in Figure 8-10. This could be due to having only one -CH_2-R arm available for O···H_{alkyl} intramolecular interaction, which would allow the molecules to align in a more linear fashion. It could also be due to the lengthening of the S···O interaction, which would also increase the O···H_{alkyl}-C angle (Figure 8-9). **8.5** is the only compound in this study containing two aryl groups and

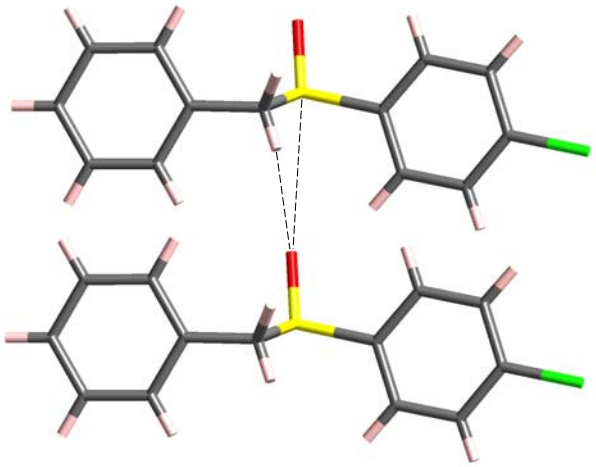

Figure 8-10. Possible intermolecular interactions in **8.2**.

unsurprisingly has the longest S···O intramolecular interaction (4.37(1) Å).

8.4. Conclusions

We have structurally characterized and investigated sulfoxide compounds **8.1**-**8.7**. The S=O bond distances in these compounds are all very similar ranging from 1.489(7) to 1.515(8) Å. In all seven structures, the O(1)-S-C bond angles vary from 105.1(4) to 108.5(4)° and the C(1)-S(1)-C(11) bond angles range from 94.1(4) to 100.56(12)°.

We find that compounds **8.1**-**8.7** contain unique intra- and intermolecular interactions depending on the groups attached to the sulfoxide moiety. The polarity of the sulfoxide bond in these compounds allows for an intramolecular S···O interaction to occur. When the sulfur is bound to alkyl groups, there tends to be a shorter S···O intermolecular distance than when the sulfur is bound to aromatic substituents. Additionally, if the sulfur is flanked by an aryl group, the S-C bond distance is slightly shorter than if flanked by an alkyl group. These distances suggest a possible interaction, which could be weak conjugation, $O\cdots H_{aryl}$ intramolecular interaction, or both. The strength of these combined interactions would also determine the amount of twisting the aryl group can undergo and would also influence the molecular packing. Furthermore, if the sulfur is flanked by an alkyl group, a CH_2 proton of S-CH_2-R can be properly oriented to participate in an intermolecular hydrogen bond with the sulfoxide oxygen of another molecule.

8.5. References

1. R. Thomas, C. B. Shoemaker and E. Klaas, *Acta Cryst.*, 1966, 21, 12-20.

2. L. Vandermeeren, T. Leyssens and D. Peeters, *J. Mol. Struct. (Theochem)*, 2007, 804, 1-8.

3. R. Bentley, *Chem. Soc. Rev.*, 2005, 34, 609-624.

4. K. Kaczorowska, Z. Kolarska, K. Mitka and P. Kowalski, *Tetrahedron*, 2005, 61, 8315-8327.

5. H. L. Holland, *Chem. Rev.,* 1988, 88, 473-485.

6. D. J. Procter, *J. Chem. Soc., Perkin Trans. 1*, 2000, 835-871.

7. F. Naso, C. Cardellicchio, M. A. M. Capozzi, F. Capitelli and V. Bertolasi, *New J. Chem.*, 2006, 30, 1782-1789.

8. D. Casarini, L. Lunazzi and A. Mazzanti, *Angew. Chem. Int. Ed.*, 2001, 40, 2536-2540.

9. N. G. Clark, J. E. Cranham, D. Greenwood, J. R. Marshall and H. A. Stevenson, *J. Sci. Fd. Agric.*, 1957, 8, 566-570.

10. E. Fromm, *Liebigs Ann. Chem.,* 1913, 396, 75-103.

11. R. Pummerer, *Ber. Dtsch. Chem. Ges.*, 1910, 43, 1401-1412.

12. H. Bohme, *Ber. Dtsch. Chem. Ges.*, 1936, 69, 1610-1615.

13. G. A. Russell and J. M. Pecoraro, *J. Org. Chem.*, 1979, 44, 3990-3991.

14. Rigaku, *CrystalClear 1.36*, 2004, Rigaku Corporation: 3-9-12 Akishima, Tokyo, Japan.

15. Rigaku, *SCXmini Benchtop Crystallography System software 1.0*, 2006,; Rigaku Americas Corp: 9009 New Trails Drive, The Woodlands, TX 77381-5209 USA.

16. Rigaku, *Crystalstructure, single crystal structure analysis 3.8*, 2006, Rigaku/MSC 9009 New Trails Drive, The Woodlands, TX 77381-5209 USA Rigaku Tokyo, 196-8666, Japan.

17. G. M. Sheldrick, *Acta Crystallogr. A*, 2008, 64, 112-122.

18. F. H. Allen, O. Kennard, D. G. Watson, L. Brammer, A. G. Orpen and R. Taylor, *J. Chem. Soc., Perkin Trans. 2*, 1987 S1-S19.

19. C. Reichardt, H. P. Erfurt, K. Harms and G. Schafer, *Eur. J. Org. Chem.*, 2002, 439-452.

20. J. E. Huheey, E. A. Keiter and R. L. Keiter, *Inorganic Chemistry: Principles of Structure and Reactivity*, HarperCollins College Publishers, 1993, p 301.

CHAPTER 9

DETERMINATION OF THE CHIRALITY AND THE ENANTIOMORPHIC EXCESS IN THE CRYSTAL STRUCTURES OF E_2Ph_2, (E = S, Se, OR Te) USING A ROBOTIC X-RAY DIFFRACTOMETER

9.1. Introduction

The word 'chiral' comes from the Greek word for hand (*cheir*). In chemistry, it is used to describe similar molecules whose only difference is in their 'handedness'. These molecules, called enantiomers, exist in two distinguishable mirror-image forms that cannot be super-imposed upon each other. While these enantiomers may look alike, they are not identical. This is important because seemingly small structural differences in molecular chirality can cause major changes in the molecular reactivity or the molecular properties of these compounds. There are five different types of chirality: point, axial, helical, planar, and surface all named according to the Cahn, Ingold, and Prelog rules.[1,2] Examples of the various types can be seen in Figure 9-1.

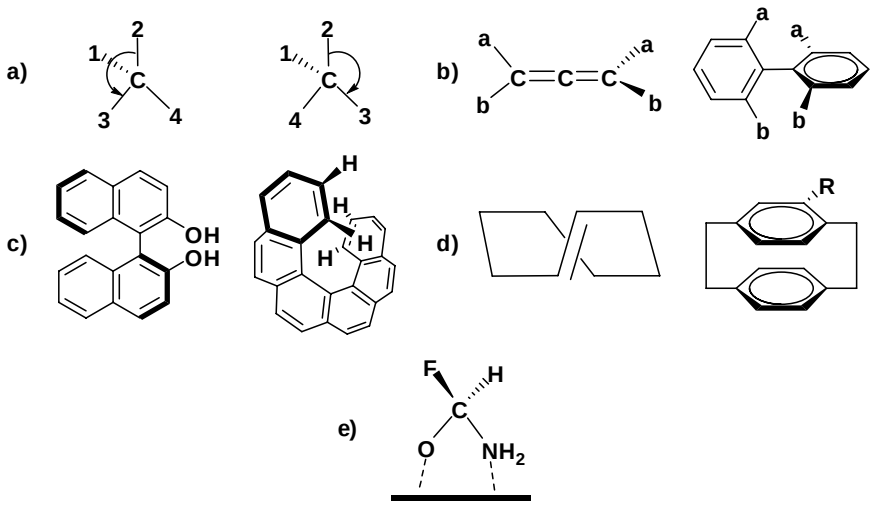

Figure 9-1. Examples of the five different types of chirality: a) Point - a tetra-substituted carbon in *S* and *R* configurations; b) Axial - allenes and biphenyls; c) Helical - binaphthol and (*M*)-hexahelicene; d) Planar - (*E*)-cyclooctene and monosubstituted paracyclophane; e) Surface - a chiral molecule binding specifically to a chiral surface.[1]

Homochirality, meaning "same handedness", occurs when chiral molecules all form with the same chirality. Homochirality forms the basis of biological chemistry. Simply stated, any molecular-based life could not exist without homochirality.[3] Chiral amino acids and sugar rings are some of the simplest building blocks of life. These homochiral molecules are used to make higher-order structures in which the chirality of the building block is conserved. For example, all biologically active amino acids (except glycine, which is not chiral) exist primarily as left-handed enantiomers. These amino acids, when linked, form chiral polypeptide chains, which then form the right-handed α-helices and the folds that give proteins their overall structures (Figure 9-2).[3]

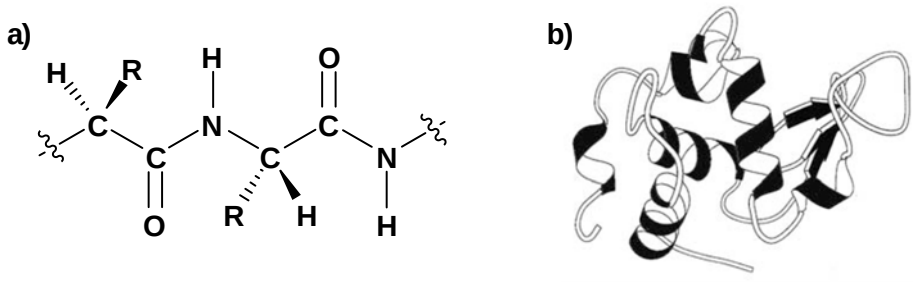

Figure 9-2. Examples of higher order structures composed of amino acids: a) the polypeptide backbone and b) a folded protein.[3]

The other principal homochiral biological building blocks are both the ribose-based and pyranose-based sugars. Most biologically relevant sugar rings are right-handed, being either *D*-deoxyribose or *D*-ribose. Nucleic acids consist of chains of deoxyribonucleosides (DNA) or ribonucleosides (RNA), which are chiral sugar rings connected by phosphodiester linkages.[3] The chains then make up the backbone of DNA, which leads directly to the right-handed turn of the β-type DNA double helix (Figure 9-3).[3]

Since homochirality is widespread throughout biology, chiral compounds often serve as substrates for highly selective enzymes in important biological reaction pathways. In these enzymes, it is impossible (or at least extremely difficult) for the wrong substrate isomer to react. Much like a right hand trying to

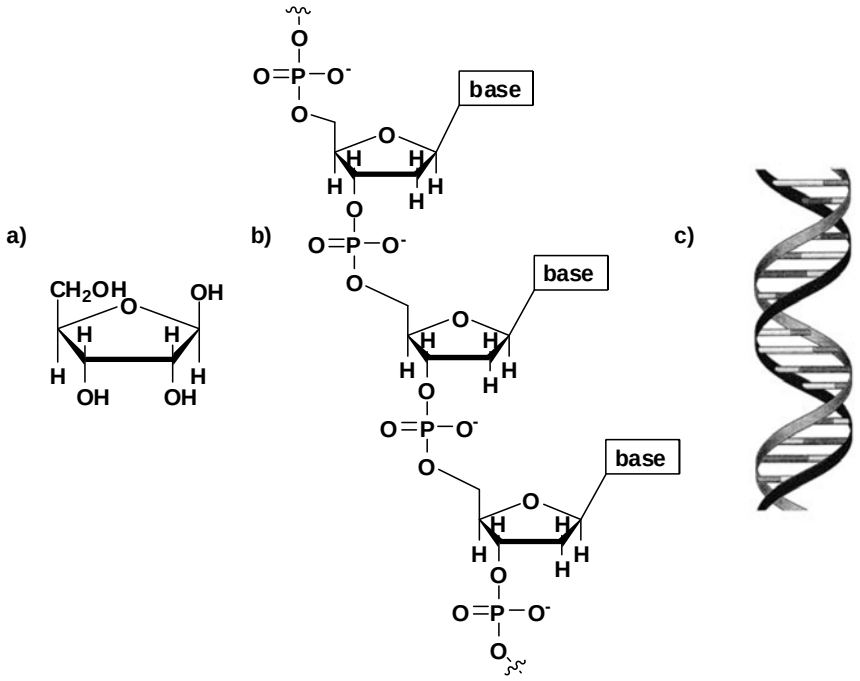

Figure 9-3. *D*-deoxyribose (a) forms the backbone of DNA (b) and is responsible for the right-handed twist in the DNA double helix (c).[3]

fit into a left-handed glove, a right-handed enantiomer simply won't fit into an enzyme active site designed for a left-handed enantiomer.

Even though it is generally agreed that homochirality is essential for efficient biochemical reactions, there are many suggestions (and strenuous debates) about its origin. One idea is that one enantiomer of a given compound may have a lower intrinsic energy than the other and would therefore form almost exclusively.[4]

By investigating the chiral properties of simple compounds, this theory can be more closely examined.[5-8] In solution, molecules can exist in two "enantiomorphous equienergetic" forms, meaning that both enantiomers exist in solution and they are equal in energy. Essentially their structures possess all the features necessary for chirality, but in solution the molecules are too flexible to be chiral.[6] When this type of molecule crystallizes there are two options; either both

enantiomers can crystallize, producing a solid racemate or, less commonly, only one enantiomer will occur in any given crystal, forming a conglomerate.

Enantiomerically pure crystals may form when the first few molecules to crystallize do so with a common chirality. The initial seed then acts as a template for other molecules to follow; creating a domino effect in that all of the following molecules crystallize with the same chirality as the first. This process is called autoseeding. From an engineering standpoint, the problem with autoseeding is that the chirality of the spontaneously formed crystals cannot be predicted. Furthermore, a pure enantiomorph forming on its own is unusual because more often than not, a mixture is formed.[6]

A practical problem arises when many individual crystals form a mixture of chiral enantiomers. When this happens, it is difficult to determine the overall chirality of the bulk sample. Experiments like circular dichroism (CD) or second harmonic generation (SHG) can be used to study the bulk sample or a single crystal from the bulk sample, but these methods have limitations.[6] Single crystal X-ray diffraction; however, can be used to unambiguously distinguish enantiomorphs in a suitable crystal.[9] This technique can also be applied to a vast range of compounds. Despite being a powerful tool, X-ray diffraction is time consuming for both the instrument and the crystallographer, making it daunting to perform repeated experiments on a bulk sample. Therefore, X-ray diffraction is normally used to collect data on one crystal to verify previous CD or SHG experiments. It is generally not used to determine the overall chirality in a bulk sample.[10]

Our group aimed to study the chiral properties of simple molecules. Diphenyl dichalcogenides (E_2Ph_2, where E = S, Se, or Te) are compounds that can undergo homochiral crystallization (Figure 9-4).

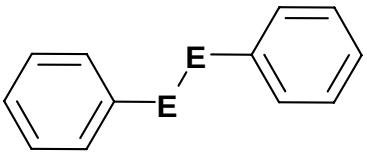

Figure 9-4. Drawing of diphenyl dichalcogenide; E = S, Se, or Te.

In solution, free rotation around the E-E and E-C bonds creates a racemic mixture because the rings can be in an infinite number of conformations with respect to each other. Figure 9-5 depicts Newman projections of four examples of these possible confirmations. As these compounds crystallize, the phenyl rings get locked into a specific position resulting in a helical twist in the crystalline molecule.

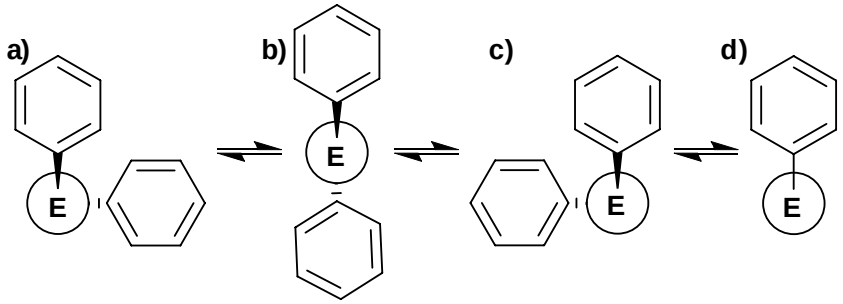

Figure 9-5. Newman projections, looking down the E-E bond, of only four different confirmations of E_2Ph_2 that can exist in solution.

Helical chirality, or helicity, refers to the chirality of a helical, propeller, or screw-shaped molecule. It is governed by the direction in which the propeller or helix turns and, as in other types of chirality, the direction of the turn is designated using the Cahn, Ingold, and Prelog rules. In a molecule with a helix, if the helix rotates to the left the chirality is termed minus (*M*-), but if the helix rotates to the right the chirality is termed plus (*P*-) (Figure 9-6).[2]

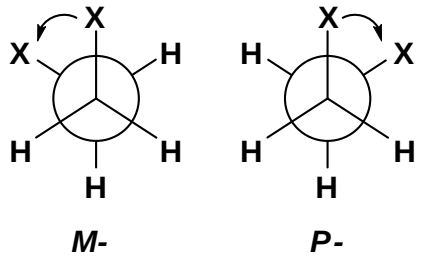

Figure 9-6. Newman Projection drawings demonstrating a helical rotation to the left (*M*-) and rotation to the right (*P*-).

The crystal structures of the diphenyl dichalcogenides have been known for over 30 years, with Se_2Ph_2 being the first of this series to be reported (1969), followed by S_2Ph_2 (1969) and Te_2Ph_2 (1978).[11-13] Despite crystallizing in the space group $P2_12_12_1$, the chirality of the crystalline compounds was not mentioned in these initial publications. It wasn't until 2001, that Shimizu *et al*. reported investigations into the chiral behavior of these solid diphenyl dichalcogenides.[14] In their research, eight or nine vials per E_2Ph_2 sample (~27 total samples) were recrystallized and CD experiments were performed on KBr pellets made from individual crystals of E_2Ph_2. In their crystallization vials, S_2Ph_2 and Se_2Ph_2 underwent homochiral crystallization, with seven out of nine vials of S_2Ph_2 and seven out of eight vials of Se_2Ph_2 forming the *P*-enantiomer. Te_2Ph_2 formed a racemic mixture containing both enantiomers. They also found that they could seed a crystallization vial and regardless of E (S, Se, or Te) or of the chirality of the seed crystal, all crystals (ten were measured) from that vial produced the same CD spectrum as the seed crystal. They only reported X-ray data for the *P*-S_2Ph_2 enantiomer.[14]

The research of Shimizu is empirical and there are not many points in their data sets. However, their data raises some intriguing questions. For instance, is there an underlying structural or energetic reason why the *P*-enantiomer was preferred in these simple E_2Ph_2 molecules? Could this tendency to form *P*-E_2Ph_2

be a key to understanding biological homochirality? Statistically, could there be a real preference for the *P*-enantiomer?

We were intrigued by these questions. Since single crystal X-ray diffraction is the most powerful experiment used to distinguish enantiomers, we decided to use it to investigate the diphenyl dichalcogenides.[9] The **St And**rews **A**utomated **R**obotic **D**iffractometer (**STANDARD**) has provided us with the opportunity to use X-ray diffraction as it has never been used before - to analyze numerous crystals, one after another, quickly, efficiently, and non-stop, 24 hours per day. The E_2Ph_2 series are particularly advantageous since they are readily available and contain heavier elements, which we anticipated would make determining absolute structures reasonably straightforward. Not only with this methodology were we able to compare the molecular structures between the enantiomers, but we were also able to collect enough individual crystal structure data to adequately support our conclusions on a statistically significant basis.

9.2. Results and Discussion

As a starting point, a structural investigation of both enantiomers was performed in order to investigate if there is an underlying molecular reason for a preference of one enantiomer over the other in E_2Ph_2 molecules. We have crystallographically characterized both *M*- and *P*-enantiomers of each compound in the E_2Ph_2 series, where *P*-S_2Ph_2 (**9.1**), *M*-S_2Ph_2 (**9.1a**), *P*-Se_2Ph_2 (**9.2**), *M*-Se_2Ph_2 (**9.2a**), *P*-Te_2Ph_2 (**9.3**), and *M*-Te_2Ph_2 (**9.3a**) (Figure 9-7). Refinement data is in Appendix 1 and the bond lengths and angles are shown in Table 9-1.

Unsurprisingly, the E-E bond lengths increase as the chalcogen size increases, from S (2.022(2) Å, 2.0289(7) Å) to Se (2.3066(7) Å, 2.3073(10) Å) to Te (2.7089(7) Å, 2.7073(5) Å), and are statistically indistinguishable between the *P*- and *M*- enantiomers of the same chalcogen. Logically enough, as the chalcogen atom size increases, the E-C bond distance also increases and again, a negligible difference is seen between the enantiomers.

The E-E-C angles decrease across the series from S to Se to Te, however there is a slight difference between the E(2)-E(1)-C(1) angle, which in every

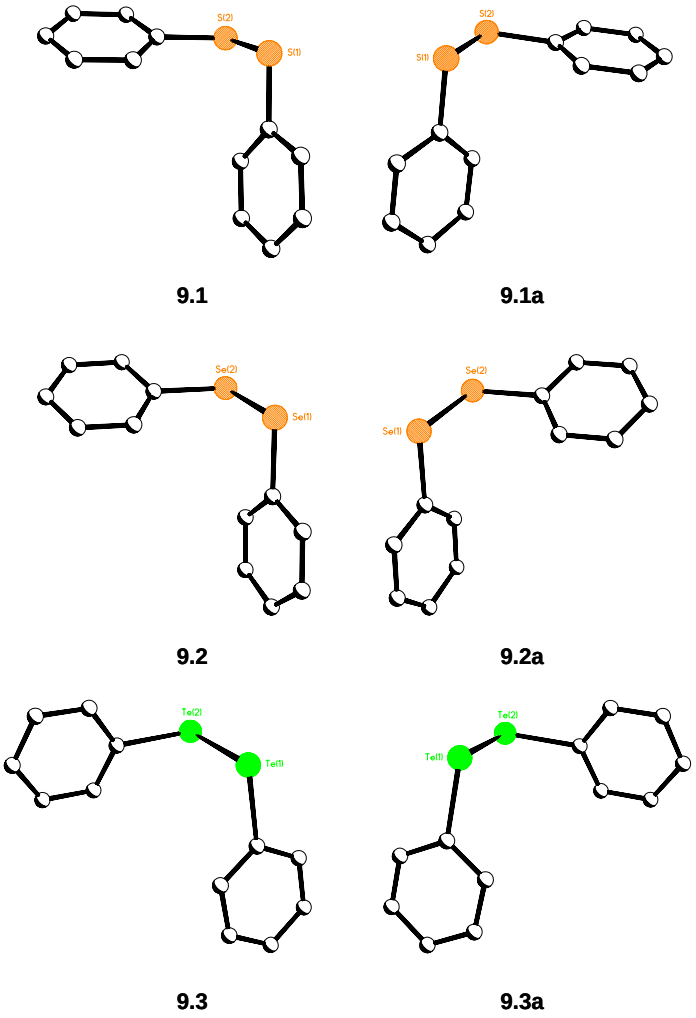

Figure 9-7. (*P*)-E_2Ph_2 on the left and (*M*)-E_2Ph_2 on the right, where E = S (**9.1**, **9.1a**); Se (**9.2**, **9.2a**); or Te (**9.3**, **9.3a**).

molecule is ~1° to 3° larger than the E(1)-E(2)-C(7) angle. In S_2Ph_2 and Se_2Ph_2, the similar E(1)-C(1)-C(2) and E(2)-C(7)-C(12) are much smaller than the E(1)-C(1)-C(6) and E(2)-C(7)-C(8) angles. In Te_2Ph_2, all four of these angles are similar. Finally, the torsion angles C(1)-E(1)-E(2)-C(7) in both *P*- and *M*-Te_2Ph_2 are 90.7(3)° and -90.5(2)°, respectively. The same torsion angles in the other compounds are slightly smaller (~ 5°).

With the knowledge that these compounds are structurally indistinguishable, other than the direction of their helicity, we decided to

Table 9-1. Table of bond lengths (Å) and angles (°) for **9.1**-**9.3a**.

	9.1	**9.1a**	**9.2**	**9.2a**	**9.3**	**9.3a**
E(1)-E(2)	2.022(2)	2.0289(7)	2.3066(7)	2.3073(10)	2.7089(7)	2.7073(5)
E(1)-C(1)	1.785(6)	1.787(2)	1.933(5)	1.933(6)	2.143(7)	2.132(5)
E(2)-C(7)	1.796(6)	1.788(2)	1.947(5)	1.937(6)	2.126(7)	2.115(5)
C(1)-C(2)	1.395(8)	1.392(3)	1.392(8)	1.401(10)	1.382(11)	1.383(8)
C(1)-C(6)	1.368(8)	1.386(3)	1.382(7)	1.377(10)	1.388(12)	1.396(8)
C(2)-C(3)	1.369(9)	1.393(3)	1.404(8)	1.402(10)	1.393(12)	1.377(8)
C(3)-C(4)	1.373(9)	1.381(3)	1.374(8)	1.366(10)	1.355(13)	1.375(9)
C(4)-C(5)	1.380(9)	1.383(3)	1.395(8)	1.415(10)	1.366(12)	1.380(9)
C(5)-C(6)	1.391(9)	1.387(3)	1.381(8)	1.383(10)	1.384(12)	1.385(8)
C(7)-C(8)	1.390(8)	1.385(3)	1.385(7)	1.393(9)	1.398(11)	1.400(8)
C(7)-C(12)	1.395(9)	1.390(3)	1.384(7)	1.382(10)	1.372(10)	1.395(7)
C(8)-C(9)	1.392(8)	1.383(3)	1.374(7)	1.381(9)	1.406(12)	1.385(9)
C(9)-C(10)	1.366(9)	1.381(3)	1.383(8)	1.368(11)	1.376(12)	1.390(8)
C(10)-C(11)	1.393(10)	1.381(3)	1.366(9)	1.378(12)	1.401(11)	1.391(8)
C(11)-C(12)	1.379(9)	1.385(3)	1.389(7)	1.393(10)	1.383(11)	1.378(8)
E(2)-E(1)-C(1)	106.2(2)	106.19(8)	103.49(17)	103.5(2)	100.5(2)	100.74(16)
E(1)-E(2)-C(7)	104.5(2)	104.97(7)	102.41(15)	102.7(2)	97.4(2)	97.69(14)
E(1)-C(1)-C(2)	116.0(4)	115.70(17)	115.4(4)	115.7(5)	119.8(5)	120.1(4)
E(1)-C(1)-C(6)	124.3(4)	124.07(17)	123.8(4)	124.6(5)	119.6(5)	120.0(4)
C(2)-C(1)-C(6)	119.6(6)	120.2(2)	120.8(5)	119.7(6)	120.4(7)	119.6(5)
C(1)-C(2)-C(3)	119.9(5)	119.5(2)	118.6(5)	119.2(6)	118.3(8)	120.2(6)
C(2)-C(3)-C(4)	121.1(6)	120.2(2)	120.5(5)	121.2(6)	122.1(8)	121.1(6)
C(3)-C(4)-C(5)	119.0(6)	120.1(2)	120.2(5)	119.3(7)	118.8(8)	118.5(5)
C(4)-C(5)-C(6)	120.6(5)	120.3(2)	119.8(5)	119.5(6)	121.6(8)	121.8(6)
C(1)-C(6)-C(5)	119.8(5)	119.7(2)	120.1(5)	121.1(6)	118.8(8)	118.7(5)
E(2)-C(7)-(8)	124.3(4)	124.28(16)	123.2(3)	123.1(5)	120.5(5)	121.3(4)
E(2)-C(7)-C(12)	115.0(4)	115.59(16)	115.5(3)	116.4(5)	120.2(5)	120.4(4)
C(8)-C(7)-C(12)	120.6(5)	120.1(2)	121.2(4)	120.5(6)	119.3(7)	118.2(5)
C(7)-C(8)-C(9)	117.8(5)	119.7(2)	118.9(5)	119.3(6)	119.4(7)	120.6(5)
C(8)-C(9)-C(10)	121.8(6)	120.5(2)	120.6(5)	120.3(6)	120.5(7)	120.6(5)
C(9)-C(10)-C(11)	120.4(6)	119.7(2)	120.0(5)	120.8(7)	119.6(7)	118.8(5)
C(10)-C(11)-C(12)	118.9(6)	120.4(2)	120.7(5)	119.7(7)	119.4(7)	120.7(5)
C(7)-C(12)-C(11)	120.5(6)	119.6(2)	118.6(5)	119.3(6)	121.7(7)	121.0(5)
E(2)-E(1)-C(1)-C(2)	-179.3(4)	-179.42(15)	-179.2(3)	179.2(4)	94.3(6)	-94.9(5)
E(2)-E(1)-C(1)-C(6)	-2.5(5)	0.8(2)	-0.5(4)	-0.6(6)	-90.3(6)	90.2(4)
C(1)-E(1)-E(2)-C(7)	84.6(2)	-84.13(10)	85.4(2)	-85.5(3)	90.7(3)	-90.5(2)
E(1)-E(2)-C(7)-C(8)	-19.4(5)	19.6(2)	-23.3(4)	22.9(6)	-95.2(6)	95.2(4)
E(1)-E(2)-C(7)-C(12)	163.5(4)	-163.02(15)	159.6(3)	-159.7(5)	84.7(6)	-84.0(4)

investigate energetic differences between the conformations. Rotational barrier calculations were performed on Se_2Ph_2 to determine if one conformation is in fact, more energetically favorable than the other. The calculations resulted in one minimum where the molecule has C_2 symmetry (the *M*- or *P*-enantiomer), as well as two transition states for rotation, with *syn*- and *anti*- conformations of the two phenyl groups (Figure 9-8). Both DFT and MP2 calculations predict a barrier on the order of 5-6 kcal/mol for the lower of the two transition states. This value is consistent with a previously calculated rotational barrier of 12 kcal/mol (at 204 K) for a bis(2,4,6-tri-*tert*-butylphenyl) diselenium derivative.[15] For Te_2Ph_2, a smaller rotational barrier than Se_2Ph_2 is expected, and the conversion barrier in the bis(2,4,6-tri-*tert*-butylphenyl) ditellurium derivative is 9.4 kcal/mol.[15] In all cases, there was a single energy minimum, indicating, as predicted, no energy difference between the two enantiomers.

Our structural and computational studies suggest that these enantiomers are indistinguishable. This is reasonable but vexing, since previous data (although

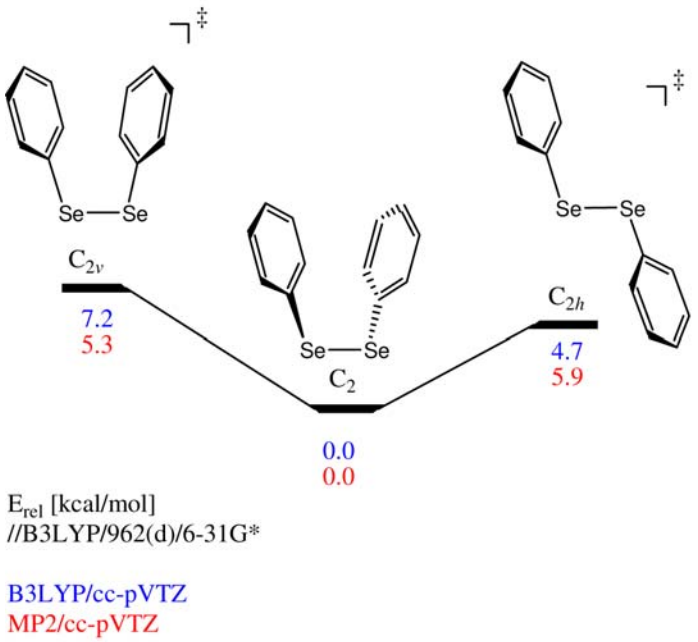

Figure 9-8. Results from Se_2Ph_2 rotational barrier calculations.

limited) suggested that there could be a preference.[14] Since nature doesn't always "play by the rules" of computation, we wanted to test actual crystals to see if there is an empirical relationship.

To produce statistically significant data in our experiments, we needed a large number of randomly chosen crystals and completely unbiased crystallization methods. Because homochiral crystallization has been found to occur in small pot crystallizations, we thought that growing crystals would bias the sample.[14] Therefore, crystals of commercially available samples from either Alfa Aesar or Sigma Aldrich were used. Since crystals of the *M*- and *P*- enantiomers are structurally and computationally indistinguishable, we believed that both enantiomers would be present in the bulk pre-packaged bottles, just in an unknown ratio.

Forty-nine single crystals of S_2Ph_2 were taken from a 50 g bottle purchased from Alfa Aesar and were analyzed by X-ray crystallography. After data collection and integration, the structures were solved using direct methods. The structures were refined anisotropically and the Flack parameter was closely examined. Of the 49 samples, 35 had Flack parameters and *R* factors of an appropriate value to be viable for the determination of chirality. An analysis of these 35 samples showed that 18 crystals were the *M*-enantiomer.

The estimated proportion of *M*-S_2Ph_2 in the sample bottle, $\hat{p}$, can be found by using Equation 9-1, where M is the total number of *M*-enantiomers and X is the total number of experiments. The estimated proportion of *M*-S_2Ph_2 in our sample bottle is 0.51. This near 50:50 ratio of *M*-:*P*- is consistent with the structural and computational data for these compounds.

$$\hat{p} = \frac{M}{X} \qquad \text{Eqn. 9-1.}$$

Unfortunately, Se_2Ph_2 was delivered as a powder. Two recrystallizations were performed, one in CH_2Cl_2, the other in CH_3NO_2. Evaporation of a concentrated CH_2Cl_2 solution of Se_2Ph_2 yielded yellow crystals, of which 24 single crystals were analyzed by X-ray diffraction. Out of the 24 crystals, 17

produced suitable data sets, all of these solved as the *M*-enantiomer. It seems that this sample, like those of Shimizu *et al.*, underwent homochiral crystallization.

An additional curiosity arose from our investigations. We observed that a concentrated CH_3NO_2 solution of Se_2Ph_2, upon exposure to open air for several days, precipitated white crystals. These crystals were analyzed by X-ray crystallography and elemental analysis and were found to be SeO(OH)Ph (**9.4),** an oxidized derivative of the starting material (Scheme 9-1). Although this molecule is known, it has only been reported to form when Se_2Ph_2 is treated with concentrated hydrogen peroxide and then acid. This synthesis was reported as early as 1919, but the crystal structure was first reported in 1954. [16-18]

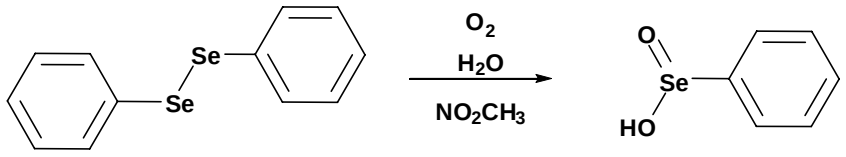

9.2 **9.4**

Scheme 9-1. Product (**9.4**) from the oxidation of Se_2Ph_2 in NO_2CH_3.

Finally, sixty-five single crystals of Te_2Ph_2 were chosen from a 1 g bottle purchased from Sigma Aldrich and were analyzed by X-ray crystallography. Of the 65 samples, 46 had suitable Flack parameters and *R* factors to be statistically viable for chirality determination. Out of 46 samples, 33 were *M*-Te_2Ph_2. Using Equation 9-1, the estimated proportion of *M*-enantiomers in our sample bottle is 0.72. This result suggests there is an enantiomeric preference for *M*-Te_2Ph_2, but the error in the experiment needs to be found.

The error associated with the estimate, $\hat{p}$, is found through calculating a 95% confidence interval (CI_{95}). CI_{95} gives a range within which we are 95% certain that the true proportion of *M*-E_2Ph_2 in the sample bottle will lie. Since we have proportion data, a binomial distribution is used to calculate CI_{95} (Equation 9-2). A binomial distribution usually applies when an experiment is repeated a fixed number of times. Each trial has one of two outcomes - success or failure, or in this case - *M*-E_2Ph_2 or not. The probability of success is the same for each trial and the

trials are statistically independent of each other. A summary of the results for the confidence intervals are shown in Table 9-2 (Figure 9-9).

$$CI_{95} = \hat{p} \pm 1.96 * \sqrt{\frac{\hat{p}(1-\hat{p})}{X}} \qquad \text{Eqn. 9-2.}$$

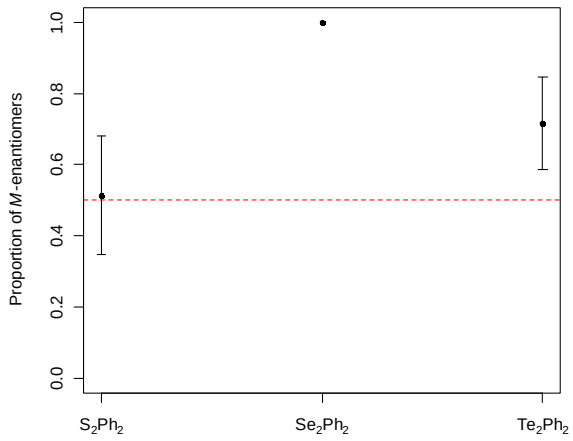

Figure 9-9. Graph of the estimated proportion of *M*-E_2Ph_2 in each sample with corresponding CI_{95}.

The CI_{95} for *M*-S_2Ph_2 is 0.51 ± 0.17 (Figure 9-9). These results, as we expected from our structural and computational studies, suggest that in the sample bottle, crystals of S_2Ph_2 crystallize indiscriminately as either the *M*- or the *P*-enantiomer. This agrees with the calculations, which predicted there would be no preference for either enantiomer.

Te_2Ph_2 has proven to be different to the other two diphenyl dichalcogenides. In Shimizu *et al.*'s experiments, this compound did not undergo homochiral crystallization and when comparing rotational barrier calculations for similar compounds, the barriers are smaller for Te analogues. We thought that because of these two facts, this compound would have a higher propensity to form 50:50 *M*- and *P*- enantiomers; however, in our bottle, there seems to be a distinct

preference for the *M*-enantiomer. The CI_{95} for *M*-Te_2Ph_2 is 0.72 ± 0.13, suggesting that there is a 95% chance that the true proportion of *M*-Te_2Ph_2 in our sample bottle is within the interval 0.59 - 0.85. Most remarkably, we appear able to crystallize the selenium compound entirely as one isomer.

9.3. Conclusions

The diphenyl dichalcogens (E_2Ph_2, where E = S, Se, or Te) are molecules that are racemic in solution and can undergo homochiral crystallization. We calculated rotational barriers of Se_2Ph_2 and determined that although the *M*- and *P*- forms are the most stable conformation for these molecules, there is no apparent preference for one form over the other.

Experimentally, we investigated unbiased commercially available sample crystals by X-ray crystallography. We solved a large number of crystal structures, narrowed our results to contain only suitable data, and then calculated confidence intervals to 95% based on our results. Table 9-2 is a summary of this experiment.

Table 9-2. Summary of CI_{95} for E_2Ph_2 experiment

	Total	**Suitable**	**%*P*-**	**%*M*-**	**CI_{95}**
S_2Ph_2	49	35	0.49	0.51	± 0.17
Se_2Ph_2*	24	17	0	100	
Te_2Ph_2	65	46	0.28	0.72	± 0.13

*Se_2Ph_2 was obtained as a powder and was recrystallized. We believe it underwent homochiral crystallization.

We found that in our sample bottles, S_2Ph_2 formed the *P*- and *M*-enantiomers equally, while there was a definite preference for the *M*-enantiomer in Te_2Ph_2. Without a large-batch crystallization of Se_2Ph_2, we were unable to draw firm conclusions on a general enantiomeric preference because our crystallizations underwent homochiral crystallization. We did find it interesting that Se_2Ph_2 oxidized in air to form **9.4**.

Our experiment suggests that there could be an enantiomeric preference in Te_2Ph_2, and if so, this could lead to further investigations with these simple achiral compounds to help better understand biological homochirality.

9.4. Experimental

Crystals of S_2Ph_2 were chosen from a 50 g bottle purchased from Alfa Aesar. Crystals of Te_2Ph_2 were chosen from a 1 g bottle purchased from Sigma Aldrich. Se_2Ph_2 was ordered, but arrived as a power and wasrecrystallized from either CH_2Cl_2 or NO_2CH_3. Elemental Analysis data for **9.4** is calc'd: C 38.11 H 3.20; found: C 38.19 H 2.90.

9.5. References

1. B. Bhatia and D. S. Sholl, *Angew. Chem. Int. Ed.*, 2005, 44, 7761-7764.

2. R. S. Cahn, C. Ingold, and V. Prelog, *Angew. Chem. Int. Ed.*, 1966, 5, 385-415.

3. L. Barron, *Space Science Reviews*, 2008, 135, 187-201.

4. Lahav, M. *Orig. Life Evol. Biosph.* 2007, *37*, 371-377.

5. T. Kawasaki, K. Suzuki, K. Hatase, M. Otsuka, H. Koshima, and K. Soai, *Chem. Commun.*, 2006, 1869-1871.

6. M. Sakamoto, *J. Photochem. Photobio. C: Photochem. Rev.*, 2006, 7, 183-196.

7. K. Penzien and G. M. J. Schimidt, *Angew. Chem. Int. Ed.I,* 1969, 8, 608-609.

8. B. S. Green, M. Lahav and D. Rabinovich, *Acc. Chem. Res.*, 1979, 12, 191-197.

9. H. D. Flack and G. Bernardinelli, *Chirality*, 2008, 20, 681-690.

10. H. D. Flack and G. Bernardinelli, *Acta Cryst. A*, 2005, 61, C316.

11. J. D. Lee and M. W. R. Bryant, *Acta Cryst.*, 1969, 25, 2094-2101.

12. R. Marsh, *Acta Cryst.*, 1952, 5, 458-462.

13. G. Llabres, O. Dideberg and L. Dupont, *Acta Cryst.*, 1972, 28, 2438-2444.

14. T. Shimizu, H. Isono, M. Yasui, F. Iwasaki and N. Kamigata, *Org. Lett.*, 2001, 3, 3639-3641.

15. B. M. Pinto, R. Y. N. Leung, R. D. Sharma, *Magn. Reson. Chem.*, 1988, 26, 729-734.

16. J. D. McCullough and E. S. Gould, *J. Am. Chem. Soc.*, 1949, 71, 674-676.

17. F. L. Pyman, *J. Chem. Soc, Trans.*, 1919, 115, 166.

18. J. H. Bryden and J. D. McCullough, *Acta Cryst.*, 1954, 7, 833-838.

APPENDIX

APPENDIX 1

CRYSTAL DATA AND REFINEMENT

Contents **Page**

Table 1. Compound **3.1**

EXPERIMENTAL DETAILS	FKDW95-2
Empirical Formula	$C_{22}H_{16}S_2$
Formula Weight	344.49
Temperature (°C)	-148(1)
Crystal Color, Habit	colorless, chunk
Crystal Dimensions (mm^3)	0.15 X 0.15 X 0.09
Crystal System	Monoclinic
Lattice Parameters	a = 8.330(3) Å b = 19.401(7) Å c = 10.544(4) Å β = 90.910(8)°
Volume ($Å^3$)	V = 1703.9(10)
Space Group	$P2_1/c$
Z value	4
Dcalc (g/cm^3)	1.343
F000	720
μ(MoKα) (cm^{-1})	3.114
No. of Reflections Measured	9305
Rint	0.058
Min and Max Transmissions	0.953 - 0.972
Independent Reflections	2979
Observed Reflection (No. Variables)	2662 (218)
Reflection/Parameter Ratio	13.67
Residuals: R_1 (I>2.00σ(I))	0.0658
Residuals: R (All reflections)	0.0794
Residuals: wR_2 (All reflections)	0.1856
Goodness of Fit Indicator	1.25
Flack Parameter	—
Maximum peak in Final Diff. Map	0.40 e /$Å^3$
Minimum peak in Final Diff. Map	-0.41 e /$Å^3$

Table 2. Compound **3.2**

EXPERIMENTAL DETAILS	FKDW112-1
Empirical Formula	$C_{22}H_{16}SSe$
Formula Weight	391.39
Temperature (°C)	-148(1)
Crystal Color, Habit	colorless, block
Crystal Dimensions (mm^3)	0.27 X 0.09 X 0.09
Crystal System	Orthorhombic
Lattice Parameters	a = 21.150(5) Å b = 5.7154(12) Å c = 14.421(3) Å β = 90°
Volume ($Å^3$)	V = 1743.3(7)
Space Group	$Pca2_1$
Z value	4
Dcalc (g/cm^3)	1.491
F000	792
μ(MoKα) (cm^{-1})	22.731
No. of Reflections Measured	6528
Rint	0.063
Min and Max Transmissions	0.397 - 0.815
No. Observations (All reflections)	2368
Independent Reflections	2217 (218)
Reflection/Parameter Ratio	10.86
Residuals: R_1 (I>2.00σ(I))	0.0593
Residuals: R (All reflections)	0.0655
Residuals: wR_2 (All reflections)	0.1574
Goodness of Fit Indicator	1.140
Flack Parameter	0.07(2)
Maximum peak in Final Diff. Map	0.67 e /$Å^3$
Minimum peak in Final Diff. Map	-0.68 e /$Å^3$

Table 3. Compound **3.3**

EXPERIMENTAL DETAILS	FKDW98-0-8
Empirical Formula	$C_{22}H_{16}STe$
Formula Weight	440.03
Temperature (°C)	-148(1)
Crystal Color, Habit	yellow, prism
Crystal Dimensions (mm^3)	0.18 X 0.15 X 0.12
Crystal System	Triclinic
Lattice Parameters	a = 9.997(2) Å
	b = 11.2364(18) Å
	c = 17.928(3) Å
	α = 74.309(18)°
	β = 87.24(2)°
	γ = 66.344(13)°
Volume ($Å^3$)	V = 1771.7(6)
Space Group	*P*-1
Z value	4
Dcalc (g/cm^3)	1.65
F000	864
μ(MoKα) (cm^{-1})	17.962
No. of Reflections Measured	19899
Rint	0.032
Min and Max Transmissions	0.718 - 0.806
No. Observations (All reflections)	7014
Independent Reflections	6663 (434)
Reflection/Parameter Ratio	16.16
Residuals: R_1 (I>2.00σ(I))	0.0566
Residuals: R (All reflections)	0.0599
Residuals: wR_2 (All reflections)	0.1714
Goodness of Fit Indicator	1.099
Flack Parameter	—
Maximum peak in Final Diff. Map	1.64 e /$Å^3$
Minimum peak in Final Diff. Map	-1.86 e /$Å^3$

Table 4. Compound **3.4**

EXPERIMENTAL DETAILS	FKDW164-3
Empirical Formula	$C_{22}H_{12}Br_4S_2$
Formula Weight	660.07
Temperature (°C)	-148(1)
Crystal Color, Habit	yellow, prism
Crystal Dimensions (mm^3)	0.12 X 0.06 X 0.06
Crystal System	Monoclinic
Lattice Parameters	a = 32.535(13) Å b = 5.4833(18) Å c = 27.215(9) Å β = 92.729(11)°
Volume ($Å^3$)	V = 4850(3)
Space Group	*C*2/*c*
Z value	8
Dcalc (g/cm^3)	1.808
F000	2528
μ(MoKα) (cm^{-1})	68.368
No. of Reflections Measured	13347
Rint	0.068
Min and Max Transmissions	0.406 - 0.664
No. Observations (All reflections)	4268
Independent Reflections	3398 (254)
Reflection/Parameter Ratio	16.8
Residuals: R_1 (I>2.00σ(I))	0.0866
Residuals: R (All reflections)	0.1144
Residuals: wR_2 (All reflections)	0.2732
Goodness of Fit Indicator	1.206
Flack Parameter	—
Maximum peak in Final Diff. Map	2.78 e /$Å^3$
Minimum peak in Final Diff. Map	-1.00 e /$Å^3$

Table 5. Compound **3.5**

EXPERIMENTAL DETAILS	FKDW173-1
Empirical Formula	$C_{22}H_{16}Br_4SSe$
Formula Weight	711
Temperature (°C)	-148(1)
Crystal Color, Habit	orange, platelet
Crystal Dimensions (mm^3)	0.18 X 0.12 X 0.06
Crystal System	Monoclinic
Lattice Parameters	a = 13.555(2) Å b = 9.2381(13) Å c = 18.663(3) Å β = 103.009(3)°
Volume ($Å^3$)	V = 2277.0(6)
Space Group	$P2_1/c$
Z value	4
Dcalc (g/cm^3)	2.074
F000	1352
μ(MoKα) (cm^{-1})	87.882
No. of Reflections Measured	12771
Rint	0.064
Min and Max Transmissions	0.294 - 0.590
Independent Reflections	3971
Observed Reflection (No. Variables)	3489 (254)
Reflection/Parameter Ratio	15.63
Residuals: R_1 (I>2.00σ(I))	0.0699
Residuals: R (All reflections)	0.0813
Residuals: wR_2 (All reflections)	0.1938
Goodness of Fit Indicator	1.15
Flack Parameter	—
Maximum peak in Final Diff. Map	2.33 e /$Å^3$
Minimum peak in Final Diff. Map	-1.18 e /$Å^3$

Table 6. Compound **3.6**

EXPERIMENTAL DETAILS	FKDW195A-1
Empirical Formula	$C_{22}H_{16}Br_2STe$
Formula Weight	599.84
Temperature (°C)	-148(1)
Crystal Color, Habit	yellow, prism
Crystal Dimensions (mm^3)	0.21 X 0.03 X 0.03
Crystal System	Monoclinic
Lattice Parameters	a = 18.873(10) Å b = 15.452(7) Å c = 13.922(6) Å β = 100.423(11)°
Volume ($Å^3$)	V = 3993(3)
Space Group	*C*2/*c*
Z value	8
Dcalc (g/cm^3)	1.995
F000	2288
μ(MoKα) (cm^{-1})	56.13
No. of Reflections Measured	10797
Rint	0.082
Min and Max Transmissions	0.542 - 0.845
Independent Reflections	3510
Observed Reflection (No. Variables)	2992 (236)
Reflection/Parameter Ratio	14.87
Residuals: R_1 (I>2.00σ(I))	0.0696
Residuals: R (All reflections)	0.0876
Residuals: wR_2 (All reflections)	0.1808
Goodness of Fit Indicator	1.261
Flack Parameter	—
Maximum peak in Final Diff. Map	1.50 e /$Å^3$
Minimum peak in Final Diff. Map	-1.67 e /$Å^3$

Table 7. Compound **3.7**

EXPERIMENTAL DETAILS	FKDW157B-3
Empirical Formula	$C_{22}H_{16}I_2Se_2$
Formula Weight	692.1
Temperature (°C)	-148(1)
Crystal Color, Habit	orange, prism
Crystal Dimensions (mm^3)	0.12 X 0.12 X 0.06
Crystal System	Triclinic
Lattice Parameters	a = 10.003(3) Å
	b = 10.453(2) Å
	c = 11.749(3) Å
	α = 64.218(18)°
	β = 84.68(3)°
	γ = 80.05(2)°
Volume ($Å^3$)	V = 1089.3(5)
Space Group	*P*-1
Z value	2
Dcalc (g/cm^3)	2.11
F000	644
μ(MoKα) (cm^{-1})	62.337
No. of Reflections Measured	11727
Rint	0.036
Min and Max Transmissions	0.486 - 0.688
Independent Reflections	3715
Observed Reflection (No. Variables)	3557 (236)
Reflection/Parameter Ratio	15.74
Residuals: R_1 (I>2.00σ(I))	0.0302
Residuals: R (All reflections)	0.0359
Residuals: wR_2 (All reflections)	0.1262
Goodness of Fit Indicator	1.28
Flack Parameter	—
Maximum peak in Final Diff. Map	1.44 e /$Å^3$
Minimum peak in Final Diff. Map	-1.77 e /$Å^3$

Table 8. Compound **4.1**

EXPERIMENTAL DETAILS	AFDW14off
Empirical Formula	$C_{18}H_{22}Se_2$
Formula Weight	396.29
Temperature (°C)	-148(1)
Crystal Color, Habit	orange, block
Crystal Dimensions (mm^3)	0.55 x 0.40 x 0.30
Crystal System	Orthorhombic
Lattice Parameters	a = 11.333(11) Å b = 12.079(11) Å c = 12.029(11) Å β = 90°
Volume ($Å^3$)	V = 1647(3)
Space Group	*Pcca*
Z value	4
Dcalc (g/cm^3)	1.598
F000	792
μ(MoKα) (cm^{-1})	44.807
No. of Reflections Measured	13383
Rint	0.032
Min and Max Transmissions	0.130-0.261
Independent Reflections	1508
Observed Reflection (No. Variables)	1314 (94)
Reflection/Parameter Ratio	16.04
Residuals: R_1 (I>2.00σ(I))	0.385
Residuals: R (All reflections)	0.0444
Residuals: wR_2 (All reflections)	0.1011
Goodness of Fit Indicator	1.093
Flack Parameter	—
Maximum peak in Final Diff. Map	0.83 e /$Å^3$
Minimum peak in Final Diff. Map	-0.55 e /$Å^3$

Table 9. Compound **4.3**

EXPERIMENTAL DETAILS	FKDW168A-2
Empirical Formula	$C_{14}H_{14}Br_2Se_2$
Formula Weight	499.99
Temperature (°C)	-148(1)
Crystal Color, Habit	red, prism
Crystal Dimensions (mm^3)	0.09 X 0.06 X 0.06
Crystal System	Monoclinic
Lattice Parameters	a = 9.638(7) Å b = 7.112(5) Å c = 10.499(8) Å β = 94.263(15)°
Volume ($Å^3$)	V = 717.6(8)
Space Group	$P2_1/m$
Z value	2
Dcalc (g/cm^3)	2.314
F000	472
μ(MoKα) (cm^{-1})	107.166
No. of Reflections Measured	4132
Rint	0.039
Min and Max Transmissions	0.373 - 0.526
Independent Reflections	1362
Observed Reflection (No. Variables)	1267 (115)
Reflection/Parameter Ratio	11.84
Residuals: R_1 (I>2.00σ(I))	0.0452
Residuals: R (All reflections)	0.0499
Residuals: wR_2 (All reflections)	0.1072
Goodness of Fit Indicator	1.181
Flack Parameter	—
Maximum peak in Final Diff. Map	0.66 e /$Å^3$
Minimum peak in Final Diff. Map	-0.99 e /$Å^3$

Table 10. Compound **5.1**

EXPERIMENTAL DETAILS	AFDW25
Empirical Formula	$C_{46}H_{36}O_6Se_2P_2Pt$
Formula Weight	1099.74
Temperature (°C)	-148(1)
Crystal Color, Habit	orange, block
Crystal Dimensions (mm^3)	0.22 X 0.15 X 0.07
Crystal System	Orthorhombic
Lattice Parameters	a = 13.3431(5) Å b = 13.5580(5) Å c = 22.8535(8) Å β = 90°
Volume ($Å^3$)	V = 4134.3(3)
Space Group	$P2_12_12_1$
Z value	4
Dcalc (g/cm^3)	1.767
F000	2144
μ(MoKα) (cm^{-1})	52.68
No. of Reflections Measured	43187
Rint	0.095
Min and Max Transmissions	0.398 - 0.692
Independent Reflections	9468
Observed Reflection (No. Variables)	8094 (515)
Reflection/Parameter Ratio	18.38
Residuals: R_1 (I>2.00σ(I))	0.048
Residuals: R (All reflections)	0.0629
Residuals: wR_2 (All reflections)	0.061
Goodness of Fit Indicator	1.051
Flack Parameter	-0.006(5)
Maximum peak in Final Diff. Map	2.59 e /$Å^3$
Minimum peak in Final Diff. Map	-1.02 e /$Å^3$

Table 11. Compound **5.2**

EXPERIMENTAL DETAILS	AFDW27
Empirical Formula	$PtC_{51}H_{46}O_6P_2Se_2Cl_2$
Formula Weight	1240.78
Temperature (°C)	-148(1)
Crystal Color, Habit	yellow, platelet
Crystal Dimensions (mm^3)	0.41 X 0.14 X 0.10
Crystal System	Monoclinic
Lattice Parameters	a = 17.1347(5) Å b = 26.5360(8) Å c = 11.0032(3) Å β = 102.4922(8)
Volume ($Å^3$)	V = 4884.6(2)
Space Group	*Cc*
Z value	4
Dcalc (g/cm^3)	1.687
F000	2440
μ(MoKα) (cm^{-1})	45.75
No. of Reflections Measured	25442
Rint	0.041
Min and Max Transmissions	0.304 - 0.633
Independent Reflections	11089
Observed Reflection (No. Variables)	9956 (578)
Reflection/Parameter Ratio	19.19
Residuals: R_1 (I>2.00σ(I))	0.0345
Residuals: R (All reflections)	0.042
Residuals: wR_2 (All reflections)	0.0543
Goodness of Fit Indicator	0.987
Flack Parameter	0.001(3)
Maximum peak in Final Diff. Map	1.54 e /$Å^3$
Minimum peak in Final Diff. Map	-0.70 e /$Å^3$

Table 12. Compound **5.3**

EXPERIMENTAL DETAILS	Alex34
Empirical Formula	$C_{62}H_{50}Cl_4O_6P_2Pt_2Se_4$
Formula Weight	1800.78
Temperature (°C)	-180(1)
Crystal Color, Habit	yellow, prism
Crystal Dimensions (mm^3)	0.20 x 0.20 x 0.20
Crystal System	Monoclinic
Lattice Parameters	a = 12.0039(15) Å b = 20.430(2) Å c = 25.009(3) Å β = 99.836(3)°
Volume ($Å^3$)	V = 6043.1(13)
Space Group	*Cc*
Z value	4
Dcalc (g/cm^3)	1.979
F000	3440
μ(MoKα) (cm^{-1})	73.15
No. of Reflections Measured	19245
Rint	0.0453
Min and Max Transmissions	0.7102-1.0000
Independent Reflections	8754
Observed Reflection (No. Variables)	7937 (722)
Reflection/Parameter Ratio	12.12
Residuals: R_1 (I>2.00σ(I))	0.0362
Residuals: R (All reflections)	0.0414
Residuals: wR_2 (All reflections)	0.0705
Goodness of Fit Indicator	0.874
Flack Parameter	-0.005(7)
Maximum peak in Final Diff. Map	1.744 e /$Å^3$
Minimum peak in Final Diff. Map	-1.424 e /$Å^3$

Table 13. Compound **5.4**

EXPERIMENTAL DETAILS	AFDW31
Empirical Formula	$C_{146}H_{124}O_{18}P_6Pt_3Se_6Cl_4$
Formula Weight	3553.26
Temperature (°C)	-148(1)
Crystal Color, Habit	orange, block
Crystal Dimensions (mm^3)	0.52 X 0.10 X 0.06
Crystal System	Monoclinic
Lattice Parameters	a = 61.179(3) Å b = 11.9162(4) Å c = 18.9059(9) Å β = 98.6466(18)°
Volume ($Å^3$)	V = 13626.1(11)
Space Group	*C*2/*c*
Z value	4
Dcalc (g/cm^3)	1.732
F000	6960
μ(MoKα) (cm^{-1})	48.776
No. of Reflections Measured	52775
Rint	0.329
Min and Max Transmissions	0.383 - 0.746
Independent Reflections	11981
Observed Reflection (No. Variables)	7175 (826)
Reflection/Parameter Ratio	14.5
Residuals: R_1 (I>2.00σ(I))	0.125
Residuals: R (All reflections)	0.1953
Residuals: wR_2 (All reflections)	0.3989
Goodness of Fit Indicator	1.145
Flack Parameter	—
Maximum peak in Final Diff. Map	6.56 e /$Å^3$
Minimum peak in Final Diff. Map	-10.18 e /$Å^3$

Table 14. Compound **5.5**

EXPERIMENTAL DETAILS	Alex31
Empirical Formula	$C_{60}H_{50}O_6P_2Pt_2Se_4$
Formula Weight	1634.96
Temperature (°C)	-180(1)
Crystal Color, Habit	yellow, prism
Crystal Dimensions (mm^3)	0.10 x 0.03 x 0.03
Crystal System	Triclinic
Lattice Parameters	a = 10.1847(12) Å
	b = 13.7001(16) Å
	c = 20.338(2) Å
	α = 83.840(7)°
	β = 82.868(7)°
	γ = 85.896(8)°
Volume ($Å^3$)	V = 2794.7(6)
Space Group	*P*-1
Z value	2
Dcalc (g/cm^3)	1.943
F000	1560
μ(MoKα) (cm^{-1})	77.13
No. of Reflections Measured	18111
Rint	0.0470
Min and Max Transmissions	0.6118 - 1.0000
Independent Reflections	9897
Observed Reflection (No. Variables)	7534 (688)
Reflection/Parameter Ratio	14.39
Residuals: R_1 (I>2.00σ(I))	0.0453
Residuals: R (All reflections)	0.0670
Residuals: wR_2 (All reflections)	0.0726
Goodness of Fit Indicator	0.975
Flack Parameter	—
Maximum peak in Final Diff. Map	1.807 e /$Å^3$
Minimum peak in Final Diff. Map	-1.542 e /$Å^3$

Table 15. Compound **6.1**/**7.1**

EXPERIMENTAL DETAILS	FKDW99-0-3
Empirical Formula	$C_{28}H_{21}PS$
Formula Weight	420.51
Temperature (°C)	-148(1)
Crystal Color, Habit	colorless, platelet
Crystal Dimensions (mm^3)	0.21 X 0.09 X 0.03
Crystal System	Monoclinic
Lattice Parameters	a = 11.145(2) Å b = 8.9552(16) Å c = 21.541(4) Å β = 91.341(5)°
Volume ($Å^3$)	V = 2149.2(7)
Space Group	$P2_1/c$
Z value	4
Dcalc (g/cm^3)	1.299
F000	880
μ(MoKα) (cm^{-1})	2.376
No. of Reflections Measured	13566
Rint	0.076
Min and Max Transmissions	0.951 - 0.993
Independent Reflections	3760
Observed Reflection (No. Variables)	3367 (272)
Reflection/Parameter Ratio	13.82
Residuals: R_1 (I>2.00σ(I))	0.0774
Residuals: R (All reflections)	0.0895
Residuals: wR_2 (All reflections)	0.1399
Goodness of Fit Indicator	1.250
Flack Parameter	—
Maximum peak in Final Diff. Map	0.28 e /$Å^3$
Minimum peak in Final Diff. Map	-0.29 e /$Å^3$

Table 16. Compound **6.2**

EXPERIMENTAL DETAILS	FKDW20(ox)-1
Empirical Formula	$C_{29}H_{23}OPSCl_2$
Formula Weight	521.44
Temperature (°C)	-148(1)
Crystal Color, Habit	colorless, prism
Crystal Dimensions (mm^3)	0.09 X 0.09 X 0.09
Crystal System	Triclinic
Lattice Parameters	a = 9.2265(17) Å
	b = 11.6406(16) Å
	c = 13.239(3) Å
	α = 102.74(2)°
	β = 98.54(2)°
	γ = 112.23(2)°
Volume ($Å^3$)	V = 1240.7(5)
Space Group	*P*-1
Z value	2
Dcalc (g/cm^3)	1.396
F000	540
μ(MoKα) (cm^{-1})	4.313
No. of Reflections Measured	12814
Rint	0.041
Min and Max Transmissions	0.961 - 0.962
Independent Reflections	4275
Observed Reflection (No. Variables)	3896 (308)
Reflection/Parameter Ratio	13.88
Residuals: R_1 (I>2.00σ(I))	0.0508
Residuals: R (All reflections)	0.061
Residuals: wR_2 (All reflections)	0.1469
Goodness of Fit Indicator	1.203
Flack Parameter	—
Maximum peak in Final Diff. Map	0.51 e /$Å^3$
Minimum peak in Final Diff. Map	-0.51 e /$Å^3$

Table 17. Compound **6.3**

EXPERIMENTAL DETAILS	FKDW122-1-9
Empirical Formula	$C_{28}H_{21}S_2P$
Formula Weight	452.57
Temperature (°C)	-148(1)
Crystal Color, Habit	colorless, platelet
Crystal Dimensions (mm^3)	0.18 X 0.12 X 0.06
Crystal System	Monoclinic
Lattice Parameters	a = 9.3241(13) Å b = 17.769(2) Å c = 13.7930(19) Å β = 97.328(3)°
Volume ($Å^3$)	V = 2266.6(5)
Space Group	$P2_1/n$
Z value	4
Dcalc (g/cm^3)	1.326
F000	944
μ(MoKα) (cm^{-1})	3.191
No. of Reflections Measured	12358
Rint	0.054
Min and Max Transmissions	0.943 - 0.981
Independent Reflections	3948
Observed Reflection (No. Variables)	3521 (281)
Reflection/Parameter Ratio	14.05
Residuals: R_1 (I>2.00σ(I))	0.0582
Residuals: R (All reflections)	0.0694
Residuals: wR_2 (All reflections)	0.123
Goodness of Fit Indicator	1.201
Flack Parameter	—
Maximum peak in Final Diff. Map	0.29 e /$Å^3$
Minimum peak in Final Diff. Map	-0.36 e /$Å^3$

Table 18. Compound **6.4**

EXPERIMENTAL DETAILS	FKDW111D-2
Empirical Formula	$C_{28}H_{21}PSSe$
Formula Weight	499.47
Temperature (°C)	-148(1)
Crystal Color, Habit	yellow, block
Crystal Dimensions (mm^3)	0.15 X 0.12 X 0.12
Crystal System	Monoclinic
Lattice Parameters	a = 9.432(4) Å b = 17.849(6) Å c = 13.701(4) Å β = 96.511(7)°
Volume ($Å^3$)	V = 2291.8(13)
Space Group	$P2_1/n$
Z value	4
Dcalc (g/cm^3)	1.447
F000	1016
μ(MoKα) (cm^{-1})	18.131
No. of Reflections Measured	12375
Rint	0.04
Min and Max Transmissions	0.757 - 0.804
Independent Reflections	4012
Observed Reflection (No. Variables)	3694 (281)
Reflection/Parameter Ratio	14.28
Residuals: R_1 (I>2.00σ(I))	0.0427
Residuals: R (All reflections)	0.0504
Residuals: wR_2 (All reflections)	0.1537
Goodness of Fit Indicator	1.231
Flack Parameter	—
Maximum peak in Final Diff. Map	0.56 e /$Å^3$
Minimum peak in Final Diff. Map	-0.53 e /$Å^3$

Table 19. Compound **6.5**

EXPERIMENTAL DETAILS	FKDW20
Empirical Formula	$C_{28}H_{21}O_{1.6}PS$
Formula Weight	446.11
Temperature (°C)	-146(1)
Crystal Color, Habit	colorless, prism
Crystal Dimensions (mm^3)	0.18 X 0.06 X 0.06
Crystal System	Triclinic
Lattice Parameters	a = 8.7904(11) Å
	b = 9.0993(11) Å
	c = 5.006(2) Å
	α = 75.107(14)°
	β = 81.857(16)°
	γ = 70.161(12)°
Volume ($Å^3$)	V = 1089.1(3)
Space Group	*P*-1
Z value	2
Dcalc (g/cm^3)	1.36
F000	465.6
μ(MoKα) (cm^{-1})	2.439
No. of Reflections Measured	11957
Rint	0.048
Min and Max Transmissions	0.957 - 0.985
Independent Reflections	3799
Observed Reflection (No. Variables)	3602 (290)
Reflection/Parameter Ratio	13.1
Residuals: R_1 (I>2.00σ(I))	0.0561
Residuals: R (All reflections)	0.0613
Residuals: wR_2 (All reflections)	0.1284
Goodness of Fit Indicator	1.187
Flack Parameter	—
Maximum peak in Final Diff. Map	0.26 e /$Å^3$
Minimum peak in Final Diff. Map	-0.37 e /$Å^3$

Table 20. Compound **6.6**

EXPERIMENTAL DETAILS	FKDW53-2
Empirical Formula	$C_{28}H_{21}PSeO$
Formula Weight	483.41
Temperature (°C)	-148(1)
Crystal Color, Habit	colorless, chunk
Crystal Dimensions (mm^3)	0.30 X 0.15 X 0.12
Crystal System	Monoclinic
Lattice Parameters	a = 10.1430(16) Å b = 10.6578(17) Å c = 10.6907(19) Å β = 100.935(4)°
Volume ($Å^3$)	V = 1134.7(3)
Space Group	$P2_1$
Z value	2
Dcalc (g/cm^3)	1.415
F000	492
μ(MoKα) (cm^{-1})	17.43
No. of Reflections Measured	6648
Rint	0.029
Min and Max Transmissions	0.588 - 0.811
Independent Reflections	3674
Observed Reflection (No. Variables)	3611 (281)
Reflection/Parameter Ratio	13.07
Residuals: R_1 (I>2.00σ(I))	0.0374
Residuals: R (All reflections)	0.0406
Residuals: wR_2 (All reflections)	0.1131
Goodness of Fit Indicator	1.203
Flack Parameter	0.022(13)
Maximum peak in Final Diff. Map	0.69 e /$Å^3$
Minimum peak in Final Diff. Map	-0.67 e /$Å^3$

Table 21. Compound **6.7**

EXPERIMENTAL DETAILS	FKDW119-1-3
Empirical Formula	$C_{28}H_{21}PSeS$
Formula Weight	499.47
Temperature (°C)	-148(1)
Crystal Color, Habit	colorless, block
Crystal Dimensions (mm^3)	0.15 X 0.15 X 0.15
Crystal System	Monoclinic
Lattice Parameters	a = 9.3748(15) Å b = 17.820(3) Å c = 13.847(2) Å β = 97.820(5)°
Volume ($Å^3$)	V = 2291.7(6)
Space Group	$P2_1/n$
Z value	4
Dcalc (g/cm^3)	1.448
F000	1016
μ(MoKα) (cm^{-1})	18.132
No. of Reflections Measured	13337
Rint	0.034
Min and Max Transmissions	0.756 - 0.762
Independent Reflections	4607
Observed Reflection (No. Variables)	4279 (281)
Reflection/Parameter Ratio	16.4
Residuals: R_1 (I>2.00σ(I))	0.0431
Residuals: R (All reflections)	0.0486
Residuals: wR_2 (All reflections)	0.087
Goodness of Fit Indicator	1.14
Flack Parameter	—
Maximum peak in Final Diff. Map	0.41 e /$Å^3$
Minimum peak in Final Diff. Map	-0.45 e /$Å^3$

Table 22. Compound **6.8**

EXPERIMENTAL DETAILS	FKDW146A-2
Empirical Formula	$C_{28}H_{21}PSe_2$
Formula Weight	546.37
Temperature (°C)	-148(1)
Crystal Color, Habit	yellow, prism
Crystal Dimensions (mm^3)	0.18 X 0.15 X 0.09
Crystal System	Monoclinic
Lattice Parameters	a = 9.4797(12) Å b = 17.844(2) Å c = 13.7175(16) Å β = 96.789(3)°
Volume ($Å^3$)	V = 2304.1(5)
Space Group	$P2_1/n$
Z value	4
Dcalc (g/cm^3)	1.575
F000	1088
μ(MoKα) (cm^{-1})	32.93
No. of Reflections Measured	12528
Rint	0.051
Min and Max Transmissions	0.543 - 0.744
Independent Reflections	4046
Observed Reflection (No. Variables)	3691 (281)
Reflection/Parameter Ratio	14.4
Residuals: R_1 (I>2.00σ(I))	0.0553
Residuals: R (All reflections)	0.065
Residuals: wR_2 (All reflections)	0.1585
Goodness of Fit Indicator	1.291
Flack Parameter	—
Maximum peak in Final Diff. Map	0.71 e /$Å^3$
Minimum peak in Final Diff. Map	-0.67 e /$Å^3$

Table 23. Compound **6.9**

EXPERIMENTAL DETAILS	FKDW15(ox)-8
Empirical Formula	$C_{24}H_{21}OPS$
Formula Weight	388.46
Temperature (°C)	-148(1)
Crystal Color, Habit	colorless, prism
Crystal Dimensions (mm^3)	0.21 X 0.21 X 0.03
Crystal System	Monoclinic
Lattice Parameters	a = 12.851(3) Å b = 10.384(3) Å c = 29.473(8) Å β = 91.689(8)°
Volume ($Å^3$)	3931.5(18)
Space Group	*C*2/*c*
Z value	8
Dcalc (g/cm^3)	1.312
F000	1632
μ(MoKα) (cm^{-1})	2.57
No. of Reflections Measured	10443
Rint	0.044
Min and Max Transmissions	0.946 - 0.992
Independent Reflections	3418
Observed Reflection (No. Variables)	3044 (246)
Reflection/Parameter Ratio	13.89
Residuals: R_1 (I>2.00σ(I))	0.0677
Residuals: R (All reflections)	0.0844
Residuals: wR_2 (All reflections)	0.2324
Goodness of Fit Indicator	1.183
Flack Parameter	—
Maximum peak in Final Diff. Map	0.75 e /$Å^3$
Minimum peak in Final Diff. Map	-0.84 e /$Å^3$

Table 24. Compound **6.10**

EXPERIMENTAL DETAILS	FKDW147A-1
Empirical Formula	$C_{24}H_{21}PS_2$
Formula Weight	404.52
Temperature (°C)	-148(1)
Crystal Color, Habit	colorless, prism
Crystal Dimensions (mm^3)	0.21 X 0.18 X 0.15
Crystal System	Monoclinic
Lattice Parameters	a = 11.652(2) Å b = 9.6047(18) Å c = 18.293(3) Å β = 92.268(5)°
Volume ($Å^3$)	V = 2045.6(6)
Space Group	$P2_1/c$
Z value	4
Dcalc (g/cm^3)	1.313
F000	848
μ(MoKα) (cm^{-1})	3.446
No. of Reflections Measured	12018
Rint	0.06
Min and Max Transmissions	0.928 - 0.950
Independent Reflections	3571
Observed Reflection (No. Variables)	3334 (246)
Reflection/Parameter Ratio	14.52
Residuals: R_1 (I>2.00σ(I))	0.0658
Residuals: R (All reflections)	0.0735
Residuals: wR_2 (All reflections)	0.1767
Goodness of Fit Indicator	1.274
Flack Parameter	—
Maximum peak in Final Diff. Map	0.46 e /$Å^3$
Minimum peak in Final Diff. Map	-0.42 e /$Å^3$

Table 25. Compound **6.11**

EXPERIMENTAL DETAILS	FKDW150B-6
Empirical Formula	$C_{24}H_{21}PSSe$
Formula Weight	451.42
Temperature (°C)	-148(1)
Crystal Color, Habit	colorless, prism
Crystal Dimensions (mm^3)	0.12 X 0.09 X 0.06
Crystal System	Monoclinic
Lattice Parameters	a = 13.622(3) Å b = 9.3562(18) Å c = 17.224(4) Å β = 112.028(4)°
Volume ($Å^3$)	V = 2034.9(8)
Space Group	$P2_1/n$
Z value	4
Dcalc (g/cm^3)	1.473
F000	920
μ(MoKα) (cm^{-1})	20.33
No. of Reflections Measured	11654
Rint	0.075
Min and Max Transmissions	0.779 - 0.885
Independent Reflections	3570
Observed Reflection (No. Variables)	3162 (246)
Reflection/Parameter Ratio	14.51
Residuals: R_1 (I>2.00σ(I))	0.069
Residuals: R (All reflections)	0.0808
Residuals: wR_2 (All reflections)	0.1172
Goodness of Fit Indicator	1.209
Flack Parameter	—
Maximum peak in Final Diff. Map	0.49 e /$Å^3$
Minimum peak in Final Diff. Map	-0.51 e /$Å^3$

Table 26. Compound **6.12**

EXPERIMENTAL DETAILS	SPDW25
Empirical Formula	$C_{23}H_{19}OP$
Formula Weight	342.38
Temperature (°C)	-148(1)
Crystal Color, Habit	colorless, chunk
Crystal Dimensions (mm^3)	0.36 X 0.32 X 0.19
Crystal System	Triclinic
Lattice Parameters	a = 8.8248(8) Å
	b = 10.7137(10) Å
	c = 11.1950(10) Å
	α = 102.816(3)°
	β = 112.641(3)°
	γ = 103.520(3)°
Volume ($Å^3$)	V = 890.62(14)
Space Group	*P*-1
Z value	2
Dcalc (g/cm^3)	1.277
F000	360
μ(MoKα) (cm^{-1})	1.613
No. of Reflections Measured	7630
Rint	0.047
Min and Max Transmissions	0.942 - 0.970
Independent Reflections	3138
Observed Reflection (No. Variables)	2463 (228)
Reflection/Parameter Ratio	13.76
Residuals: R_1 (I>2.00σ(I))	0.0631
Residuals: R (All reflections)	0.0878
Residuals: wR_2 (All reflections)	0.1355
Goodness of Fit Indicator	1.122
Flack Parameter	—
Maximum peak in Final Diff. Map	0.44 e /$Å^3$
Minimum peak in Final Diff. Map	-0.37 e /$Å^3$

Table 27. Compound **6.13**

EXPERIMENTAL DETAILS	FKDW140-3
Empirical Formula	$C_{23}H_{19}OPS$
Formula Weight	374.44
Temperature (°C)	-148(1)
Crystal Color, Habit	colorless, prism
Crystal Dimensions (mm^3)	0.15 X 0.09 X 0.09
Crystal System	Triclinic
Lattice Parameters	a = 9.7972(12) Å
	b = 11.7887(18) Å
	c = 17.681(3) Å
	α = 86.043(13)°
	β = 77.168(12)°
	γ = 71.227(10)°
Volume ($Å^3$)	V = 1885.1(5)
Space Group	*P*-1
Z value	4
Dcalc (g/cm^3)	1.319
F000	784
μ(MoKα) (cm^{-1})	2.653
No. of Reflections Measured	19723
Rint	0.073
Min and Max Transmissions	0.960 - 0.976
Independent Reflections	6507
Observed Reflection (No. Variables)	5702 (472)
Reflection/Parameter Ratio	13.79
Residuals: R_1 (I>2.00σ(I))	0.0788
Residuals: R (All reflections)	0.0925
Residuals: wR_2 (All reflections)	0.1353
Goodness of Fit Indicator	1.235
Flack Parameter	—
Maximum peak in Final Diff. Map	0.27 e /$Å^3$
Minimum peak in Final Diff. Map	-0.31 e /$Å^3$

Table 28. Compound **6.14**

EXPERIMENTAL DETAILS	FKDW155-1
Empirical Formula	$C_{23}H_{19}OPSe$
Formula Weight	421.34
Temperature (°C)	-148(1)
Crystal Color, Habit	colorless, prism
Crystal Dimensions (mm^3)	0.15 X 0.15 X 0.15
Crystal System	Triclinic
Lattice Parameters	a = 9.8572(17) Å b = 11.841(3) Å c = 17.750(5) Å α = 85.944(19)° β = 77.638(18)° γ = 71.454(16)°
Volume ($Å^3$)	V = 1918.6(8)
Space Group	*P*-1
Z value	4
Dcalc (g/cm^3)	1.459
F000	856
μ(MoKα) (cm^{-1})	20.494
No. of Reflections Measured	21068
Rint	0.037
Min and Max Transmissions	0.729 - 0.735
Independent Reflections	6645
Observed Reflection (No. Variables)	6211 (472)
Reflection/Parameter Ratio	14.08
Residuals: R_1 (I>2.00σ(I))	0.0386
Residuals: R (All reflections)	0.045
Residuals: wR_2 (All reflections)	0.1372
Goodness of Fit Indicator	1.152
Flack Parameter	—
Maximum peak in Final Diff. Map	0.57 e /$Å^3$
Minimum peak in Final Diff. Map	-0.75 e /$Å^3$

Table 29. Compound **7.2**

EXPERIMENTAL DETAILS	FKDW54-1
Empirical Formula	$C_{29}H_{22}Cl_5PPtS$
Formula Weight	805.88
Temperature (°C)	-148(1)
Crystal Color, Habit	colorless, prism
Crystal Dimensions (mm^3)	0.10 X 0.05 X 0.03
Crystal System	Monoclinic
Lattice Parameters	a = 13.524(6) Å b = 15.311(7) Å c = 14.029(6) Å β = 102.103(9)°
Volume ($Å^3$)	V = 2840(2)
Space Group	$P2_1/n$
Z value	4
Dcalc (g/cm^3)	1.884
F000	1560
μ(MoKα) (cm^{-1})	55.392
No. of Reflections Measured	22810
Rint	0.087
Min and Max Transmissions	0.570 - 0.847
Independent Reflections	4928
Observed Reflection (No. Variables)	4650 (335)
Reflection/Parameter Ratio	14.71
Residuals: R_1 (I>2.00σ(I))	0.0987
Residuals: R (All reflections)	0.1044
Residuals: wR_2 (All reflections)	0.2505
Goodness of Fit Indicator	1.169
Flack Parameter	—
Maximum peak in Final Diff. Map	5.58 e /$Å^3$
Minimum peak in Final Diff. Map	-2.23 e /$Å^3$

Table 30. Compound **7.3**

EXPERIMENTAL DETAILS	FKDW20-10-8a
Empirical Formula	$C_{29}H_{23}Br_2PPtSCl_2$
Formula Weight	860.34
Temperature (°C)	-148(1)
Crystal Color, Habit	colorless, platelet
Crystal Dimensions (mm^3)	0.12 X 0.12 X 0.03
Crystal System	Monoclinic
Lattice Parameters	a = 12.8977(13) Å b = 15.5520(14) Å c = 14.5122(15) Å β = 103.571(3)°
Volume ($Å^3$)	V = 2829.7(5)
Space Group	$P2_1/n$
Z value	4
Dcalc (g/cm^3)	2.019
F000	1640
μ(MoKα) (cm^{-1})	81.09
No. of Reflections Measured	15702
Rint	0.069
Min and Max Transmissions	0.493 - 0.784
Independent Reflections	5127
Observed Reflection (No. Variables)	4639 (326)
Reflection/Parameter Ratio	15.73
Residuals: R_1 (I>2.00σ(I))	0.0677
Residuals: R (All reflections)	0.0774
Residuals: wR_2 (All reflections)	0.1637
Goodness of Fit Indicator	1.255
Flack Parameter	—
Maximum peak in Final Diff. Map	1.10 e /$Å^3$
Minimum peak in Final Diff. Map	-1.61 e /$Å^3$

Table 31. Compound **7.4**

EXPERIMENTAL DETAILS	FKDW20-7-2
Empirical Formula	$C_{29}H_{23}I_2PPtSCl_2$
Formula Weight	954.34
Temperature (°C)	-148(1)
Crystal Color, Habit	yellow, prism
Crystal Dimensions (mm^3)	0.21 X 0.21 X 0.03
Crystal System	Monoclinic
Lattice Parameters	a = 15.053(4) Å b = 11.559(3) Å c = 17.567(4) Å β = 108.385(5)°
Volume ($Å^3$)	V = 2900.7(12)
Space Group	$P2_1/c$
Z value	4
Dcalc (g/cm^3)	2.185
F000	1784
μ(MoKα) (cm^{-1})	72.769
No. of Reflections Measured	18781
Rint	0.042
Min and Max Transmissions	0.475 - 0.804
Independent Reflections	5877
Observed Reflection (No. Variables)	5732 (326)
Reflection/Parameter Ratio	18.03
Residuals: R_1 (I>2.00σ(I))	0.0394
Residuals: R (All reflections)	0.041
Residuals: wR_2 (All reflections)	0.1146
Goodness of Fit Indicator	1.223
Flack Parameter	—
Maximum peak in Final Diff. Map	2.32 e /$Å^3$
Minimum peak in Final Diff. Map	-2.25 e /$Å^3$

Table 32. Compound **7.5**

EXPERIMENTAL DETAILS	FKDW20-1-8 Take2
Empirical Formula	$C_{41}H_{41}Cl_2OPRuS$
Formula Weight	784.78
Temperature (°C)	-148(1)
Crystal Color, Habit	orange, block
Crystal Dimensions (mm^3)	0.21 X 0.09 X 0.03
Crystal System	Monoclinic
Lattice Parameters	a = 9.829(3) Å b = 22.199(6) Å c = 17.506(5) Å β = 106.021(6)°
Volume ($Å^3$)	V = 3671.4(18)
Space Group	$P2_1/n$
Z value	4
Dcalc (g/cm^3)	1.42
F000	1616
μ(MoKα) (cm^{-1})	7.045
No. of Reflections Measured	16039
Rint	0.083
Min and Max Transmissions	0.861 - 0.979
Independent Reflections	6381
Observed Reflection (No. Variables)	5505 (430)
Reflection/Parameter Ratio	14.84
Residuals: R_1 (I>2.00σ(I))	0.1126
Residuals: R (All reflections)	0.1311
Residuals: wR_2 (All reflections)	0.1848
Goodness of Fit Indicator	1.3
Flack Parameter	—
Maximum peak in Final Diff. Map	0.93 e /$Å^3$
Minimum peak in Final Diff. Map	-0.57 e /$Å^3$

Table 33. Compound **7.6**

EXPERIMENTAL DETAILS	FKDW26off
Empirical Formula	$C_{56}H_{42}Cl_2Cu_2P_2S_2$
Formula Weight	1039.01
Temperature (°C)	-148(1)
Crystal Color, Habit	yellow, block
Crystal Dimensions (mm^3)	0.24 X 0.14 X 0.11
Crystal System	Triclinic
Lattice Parameters	a = 10.184(8) Å
	b = 10.366(8) Å
	c = 11.668(9) Å
	α = 77.52(2)
	β = 81.46(3)
	γ = 75.24(2)
Volume ($Å^3$)	V = 1157.2(15)
Space Group	*P*-1
Z value	1
Dcalc (g/cm^3)	1.491
F000	532
μ(MoKα) (cm^{-1})	12.33
No. of Reflections Measured	10019
Rint	0.078
Min and Max Transmissions	0.709 - 0.873
Independent Reflections	4062
Observed Reflection (No. Variables)	2819 (290)
Reflection/Parameter Ratio	14.01
Residuals: R_1 (I>2.00σ(I))	0.0857
Residuals: R (All reflections)	0.1176
Residuals: wR_2 (All reflections)	0.259
Goodness of Fit Indicator	1.067
Flack Parameter	—
Maximum peak in Final Diff. Map	2.17 e /$Å^3$
Minimum peak in Final Diff. Map	-0.73 e /$Å^3$

Table 34. Compound **7.7**

EXPERIMENTAL DETAILS	FKDW107A-1
Empirical Formula	$C_{56}H_{42}Br_2Cu_2P_2S_2$
Formula Weight	1127.92
Temperature (°C)	-148(1)
Crystal Color, Habit	yellow, platelet
Crystal Dimensions (mm^3)	0.09 X 0.09 X 0.03
Crystal System	Triclinic
Lattice Parameters	a = 10.218(2) Å b = 10.400(3) Å c = 11.690(3) Å α = 76.18(2)° β = 80.20(2)° γ = 74.909(18)°
Volume ($Å^3$)	V = 1156.9(5)
Space Group	*P*-1
Z value	1
Dcalc (g/cm^3)	1.619
F000	568
μ(MoKα) (cm^{-1})	28.502
No. of Reflections Measured	12396
Rint	0.068
Min and Max Transmissions	0.768 - 0.918
Independent Reflections	3998
Observed Reflection (No. Variables)	3527 (290)
Reflection/Parameter Ratio	13.79
Residuals: R_1 (I>2.00σ(I))	0.0858
Residuals: R (All reflections)	0.0985
Residuals: wR_2 (All reflections)	0.149
Goodness of Fit Indicator	1.212
Flack Parameter	—
Maximum peak in Final Diff. Map	1.44 e /$Å^3$
Minimum peak in Final Diff. Map	-0.81 e /$Å^3$

Table 35. Compound **7.8**

EXPERIMENTAL DETAILS	FKDW107B-1
Empirical Formula	$C_{56}H_{42}Cu_2I_2P_2S_2$
Formula Weight	1221.92
Temperature (°C)	-148(1)
Crystal Color, Habit	yellow, block
Crystal Dimensions (mm^3)	0.12 X 0.12 X 0.09
Crystal System	Triclinic
Lattice Parameters	a = 10.3416(17) Å
	b = 10.6256(13) Å
	c = 11.988(2) Å
	α = 73.87(2)°
	β = 77.76(2)°
	γ = 73.326(18)°
Volume ($Å^3$)	V = 1199.6(3)
Space Group	*P*-1
Z value	1
Dcalc (g/cm^3)	1.691
F000	604
μ(MoKα) (cm^{-1})	23.658
No. of Reflections Measured	13313
Rint	0.052
Min and Max Transmissions	0.578 - 0.808
Independent Reflections	4756
Observed Reflection (No. Variables)	4431 (290)
Reflection/Parameter Ratio	16.4
Residuals: R_1 (I>2.00σ(I))	0.0684
Residuals: R (All reflections)	0.0741
Residuals: wR_2 (All reflections)	0.1592
Goodness of Fit Indicator	1.257
Flack Parameter	—
Maximum peak in Final Diff. Map	1.12 e /$Å^3$
Minimum peak in Final Diff. Map	-1.38 e /$Å^3$

Table 36. Relevant crystal data and refinement parameters for **8.1-8.7**.

EXPERIMENTAL DETAILS	**8.1**	**8.2**	**8.3**	**8.4**	**8.5**	**8.6**	**8.7**
Empirical Formula	$C_{14}H_{14}OS$	$C_{13}H_{11}ClOS$	$C_{14}H_{14}OS$	$C_{13}H_{12}OS$	$C_{14}H_{14}OS$	$C_9H_{12}OS$	$C_{13}H_{11}O_3NS$
Formula Weight	230.32	250.74	230.32	216.30	230.32	168.25	261.29
Temperature (°C)	-148(1)	-148(1)	20(1)	-148(1)	20(1)	-180(1)	-148(1)
Crystal Color, Habit	colorless, platelet	colorless, prism	colorless, prism	colorless, platelet	colorless, prism	colorless, prism	colorless, block
Crystal Dimensions (mm^3)	0.25 X 0.20 X 0.05	0.35 X 0.21 X 0.18	0.33 X 0.21 X 0.21	0.15 X 0.15 X 0.03	0.22 X 0.20 X 0.18	0.20 X 0.15 X 0.15	0.24 X 0.16 X 0.15
Crystal System	orthorhombic	monoclinic	orthorhombic	orthorhombic	orthorhombic	orthorhombic	monoclinic
Lattice Parameters	a = 17.653(5) Å b = 53.153(14) Å c = 10.071(3) Å	a = 7.894(13) Å b = 5.653(10) Å c = 27.02(5) Å β = 97.347(15)°	a = 5.7569(6) Å b = 12.2139(12) Å c = 17.5974(18) Å	a = 8.256(4) Å b = 5.470(3) Å c = 23.995(13) Å	a = 5.848(4) Å b = 7.568(5) Å c = 27.650(17) Å	a = 10.0569(15) Å b = 9.9403(16) Å c = 17.843(3) Å	a = 13.217(4) Å b = 5.3766(14) Å c = 8.370(2) Å β = 90.673(6)°
Volume ($Å^3$)	V = 9449.2(41)	V = 1196(3)	V = 1237.3(2)	V = 1083.6(10)	V = 1223.7(14)	V = 1783.8(5)	V = 594.8(3)
Space Group	*Fdd*2	$P2_1/c$	$P2_12_12_1$	$Pca2_1$	$P2_12_12_1$	*Pbca*	*Pc*
Z value	32	4	4	4	4	8	2
Dcalc (g/cm^3)	1.295	1.392	1.236	1.326	1.250	1.253	1.459
F000	3904	520	488	456	488	720	272
μ(MoKα) (cm^{-1})	2.485	4.673	2.372	2.662	2.398	3.028	2.707
Diffractometer	Rigaku Mercury2	Rigaku Mercury2	Rigaku Mercury2	Rigaku Saturn	Rigaku Mercury2	Rigaku Mercury	Rigaku Mercury2
No. of Reflections Measured	Total: 16183	Total: 6986	Total: 10501	Total: 3884	Total: 10334	Total: 10735	Total: 4652
Unique	4143	2122	2171	1396	2142	1577	2053
Rint	0.128	0.053	0.031	0.073	0.042	0.051	0.131
Friedel pairs	1940	—	884	443	857	—	1008
Min and Max Transmissions	0.939, 0.988	0.847, 0.919	0.923, 0.951	0.960, 0.992	0.884, 0.958	0.940, 0.956	0.936, 0.960
No. Observations (All reflections)	4143	2122	2171	1396	2142	1577	2053
No. Variables	290	147	146	137	146	110	164
Reflection/Parameter Ratio	14.29	14.44	14.87	10.19	14.67	14.34	12.52
Residuals: R_1 (I>2.00σ(I))	0.1122	0.0469	0.0364	0.068	0.0405	0.0602	0.1102
Residuals: R (All reflections)	0.1883	0.0547	0.043	0.0724	0.0490	0.0671	0.1816
Residuals: wR_2 (All reflections)	0.3320	0.1158	0.0852	0.1404	0.1077	0.1789	0.2638
Goodness of Fit Indicator	1.045	1.056	1.069	1.161	1.084	1.134	1.020
Flack Parameter	0.1(2)	—	0.07(9)	0.4(2)	-0.01(10)	—	-0.1(2)
Maximum peak in Final Diff. Map	1.24 e /$Å^3$	0.29 e /$Å^3$	0.21 e /$Å^3$	0.36 e /$Å^3$	0.14 e /$Å^3$	0.82 e /$Å^3$	0.60 e /$Å^3$
Minimum peak in Final Diff. Map	-0.49 e /$Å^3$	-0.29 e /$Å^3$	-0.12 e /$Å^3$	-0.28 e /$Å^3$	-0.15 e /$Å^3$	-0.70 e /$Å^3$	-0.33 e /$Å^3$

Table 37. Compound **9.1**

EXPERIMENTAL DETAILS	S-61
Empirical Formula	$C_{12}H_{10}S_2$
Formula Weight	218.33
Temperature (°C)	-148(1)
Crystal Color, Habit	colorless, platelet
Crystal Dimensions (mm^3)	0.15 X 0.12 X 0.06
Crystal System	Orthorhombic
Lattice Parameters	a = 5.5401(11) Å b = 8.0864(18) Å c = 23.478(5) Å β = 90°
Volume ($Å^3$)	V = 1051.8(4)
Space Group	$P2_12_12_1$
Z value	4
Dcalc (g/cm^3)	1.379
F000	456
μ(MoKα) (cm^{-1})	4.593
No. of Reflections Measured	3634
Rint	0.062
Min and Max Transmissions	0.511 - 0.973
Independent Reflections	2051
Observed Reflection (No. Variables)	1773 (128)
Reflection/Parameter Ratio	16.02
Residuals: R_1 (I>2.00σ(I))	0.0723
Residuals: R (All reflections)	0.0851
Residuals: wR_2 (All reflections)	0.172
Goodness of Fit Indicator	1.108
Flack Parameter	-0.1(2)
Maximum peak in Final Diff. Map	0.46 e /$Å^3$
Minimum peak in Final Diff. Map	-0.50 e /$Å^3$

Table 38. Compound **9.1a**

EXPERIMENTAL DETAILS	S-23
Empirical Formula	$C_{12}H_{10}S_2$
Formula Weight	218.33
Temperature (°C)	-148(1)
Crystal Color, Habit	colorless, prism
Crystal Dimensions (mm^3)	0.24 X 0.15 X 0.12
Crystal System	Orthorhombic
Lattice Parameters	a = 5.5363(7) Å b = 8.0793(11) Å c = 23.483(3) Å β = 90°
Volume ($Å^3$)	V = 1050.4(2)
Space Group	$P2_12_12_1$
Z value	4
Dcalc (g/cm^3)	1.381
F000	456
μ(MoKα) (cm^{-1})	4.599
No. of Reflections Measured	3422
Rint	0.024
Min and Max Transmissions	0.894, 0.946
Independent Reflections	1753
Observed Reflection (No. Variables)	1719 (128)
Reflection/Parameter Ratio	13.7
Residuals: R_1 (I>2.00σ(I))	0.0293
Residuals: R (All reflections)	0.0301
Residuals: wR_2 (All reflections)	0.0646
Goodness of Fit Indicator	1.073
Flack Parameter	0.11(9)
Maximum peak in Final Diff. Map	0.18 e /$Å^3$
Minimum peak in Final Diff. Map	-0.19 e /$Å^3$

Table 39. Compound **9.2**

EXPERIMENTAL DETAILS	Se9
Empirical Formula	$C_{12}H_{10}Se_2$
Formula Weight	312.13
Temperature (°C)	-148(1)
Crystal Color, Habit	yellow, prism
Crystal Dimensions (mm^3)	0.21 X 0.06 X 0.03
Crystal System	Orthorhombic
Lattice Parameters	a = 5.5699(19) Å b = 8.238(3) Å c = 23.826(7) Å β = 90°
Volume ($Å^3$)	V = 1093.3(6)
Space Group	$P2_12_12_1$
Z value	4
Dcalc (g/cm^3)	1.896
F000	600
μ(MoKα) (cm^{-1})	67.202
No. of Reflections Measured	4088
Rint	0.032
Min and Max Transmissions	0.522, 0.817
Independent Reflections	2083
Observed Reflection (No. Variables)	2028 (128)
Reflection/Parameter Ratio	16.27
Residuals: R_1 (I>2.00σ(I))	0.0334
Residuals: R (All reflections)	0.0359
Residuals: wR_2 (All reflections)	0.1014
Goodness of Fit Indicator	1.224
Flack Parameter	0.06(2)
Maximum peak in Final Diff. Map	0.90 e /$Å^3$
Minimum peak in Final Diff. Map	-0.92 e /$Å^3$

Table 40. Compound **9.2a**

EXPERIMENTAL DETAILS	Se26
Empirical Formula	$C_{12}H_{10}Se_2$
Formula Weight	312.13
Temperature (°C)	-148(1)
Crystal Color, Habit	yellow, prism
Crystal Dimensions (mm^3)	0.21 X 0.15 X 0.06
Crystal System	Orthorhombic
Lattice Parameters	a = 5.5878(11) Å b = 8.2521(17) Å c = 23.907(5) Å β = 90°
Volume ($Å^3$)	V = 1102.4(4)
Space Group	$P2_12_12_1$
Z value	4
Dcalc (g/cm^3)	1.881
F000	600
μ(MoKα) (cm^{-1})	66.647
No. of Reflections Measured	3843
Rint	0.042
Min and Max Transmissions	0.313, 0.670
Independent Reflections	1920
Observed Reflection (No. Variables)	1812 (128)
Reflection/Parameter Ratio	15
Residuals: R_1 (I>2.00σ(I))	0.0408
Residuals: R (All reflections)	0.045
Residuals: wR_2 (All reflections)	0.0806
Goodness of Fit Indicator	1.146
Flack Parameter	0.03(3)
Maximum peak in Final Diff. Map	0.54 e /$Å^3$
Minimum peak in Final Diff. Map	-0.62 e /$Å^3$

Table 41. Compound **9.3**

EXPERIMENTAL DETAILS	Te9a
Empirical Formula	$C_{12}H_{10}Te_2$
Formula Weight	409.41
Temperature (°C)	-148(1)
Crystal Color, Habit	orange, prism
Crystal Dimensions (mm^3)	0.20 X 0.20 X 0.20
Crystal System	Orthorhombic
Lattice Parameters	a = 5.1563(8) Å b = 8.5809(13) Å c = 26.784(4) Å β = 90°
Volume ($Å^3$)	V = 1185.1(3)
Space Group	$P2_12_12_1$
Z value	4
Dcalc (g/cm^3)	2.294
F000	744
μ(MoKα) (cm^{-1})	48.828
No. of Reflections Measured	3511
Rint	0.03
Min and Max Transmissions	0.363, 0.377
Independent Reflections	1971
Observed Reflection (No. Variables)	1936 (128)
Reflection/Parameter Ratio	15.4
Residuals: R_1 (I>2.00σ(I))	0.031
Residuals: R (All reflections)	0.033
Residuals: wR_2 (All reflections)	0.1032
Goodness of Fit Indicator	1.124
Flack Parameter	0.01(9)
Maximum peak in Final Diff. Map	1.10 e /$Å^3$
Minimum peak in Final Diff. Map	-1.24 e /$Å^3$

Table 42. Compound **9.3a**

EXPERIMENTAL DETAILS	Te10a
Empirical Formula	$C_{12}H_{10}Te_2$
Formula Weight	409.41
Temperature (°C)	-148(1)
Crystal Color, Habit	orange, prism
Crystal Dimensions (mm^3)	0.25 X 0.20 X 0.20
Crystal System	Orthorhombic
Lattice Parameters	a = 5.1523(14) Å b = 8.571(3) Å c = 26.799(7) Å β = 90°
Volume ($Å^3$)	V = 1183.5(6)
Space Group	$P2_12_12_1$
Z value	4
Dcalc (g/cm^3)	2.298
F000	744
μ(MoKα) (cm^{-1})	48.895
No. of Reflections Measured	3841
Rint	0.025
Min and Max Transmissions	0.284, 0.376
Independent Reflections	2239
Observed Reflection (No. Variables)	2195 (128)
Reflection/Parameter Ratio	17.49
Residuals: R_1 (I>2.00σ(I))	0.0253
Residuals: R (All reflections)	0.0261
Residuals: wR_2 (All reflections)	0.0603
Goodness of Fit Indicator	1.104
Flack Parameter	0.07(6)
Maximum peak in Final Diff. Map	0.87 e /$Å^3$
Minimum peak in Final Diff. Map	-0.57 e /$Å^3$

APPENDIX 2

CRYSTAL STRUCTURES DETERMINED DURING PHD STUDIES, NOT DISCUSSED IN THIS THESIS

Experiment performed on

BS2-2

P-1

a = 7.9837(16) Å
b = 9.5070(12) Å
c = 9.624(2) Å
α = 74.156(16)°
β = 87.847(19)°
γ = 70.251(16)°
V = 660.2(2) Å^3

R_1 = 0.0580

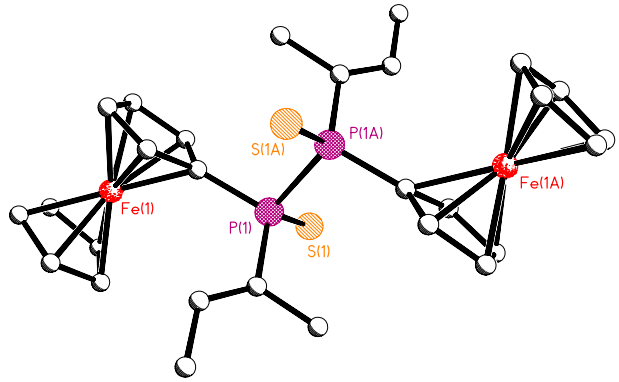

BS3-2

*C*2/*c*

a = 35.455(9) Å
b = 8.4972(17) Å
c = 23.776(6) Å
α = 90°
β = 123.354(4)°
γ = 90°
V = 5983(2) Å^3

R_1 = 0.0747

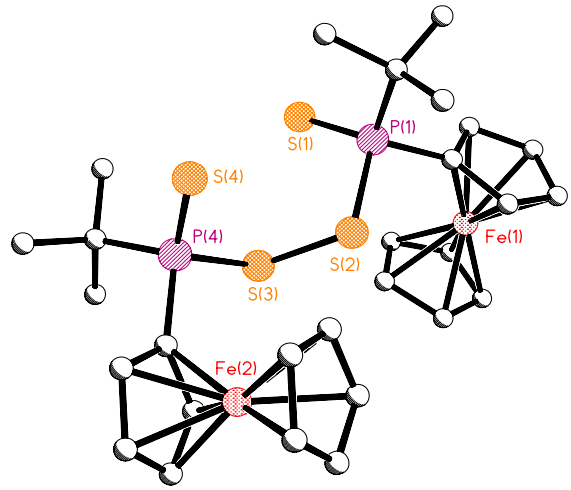

BS4-2C

*C*2/*c*

a = 25.838(7) Å
b = 12.338(3) Å
c = 2.740(3) Å
α = 90°
β = 111.293(5)°
γ = 90°
V = 3784.1(15) Å^3

R_1 = 0.0828

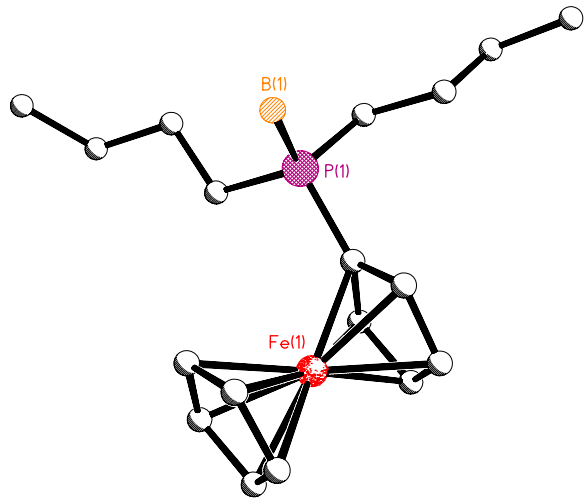

DKDX2-3

*P*2$_1$/*c*

a = 9.862(8) Å
b = 27.549(2) Å
c = 27.387(2) Å
α = 90°
β = 92.957(2)°
γ = 90°
V = 660.2(2) Å^3

R_1 = 0.1124

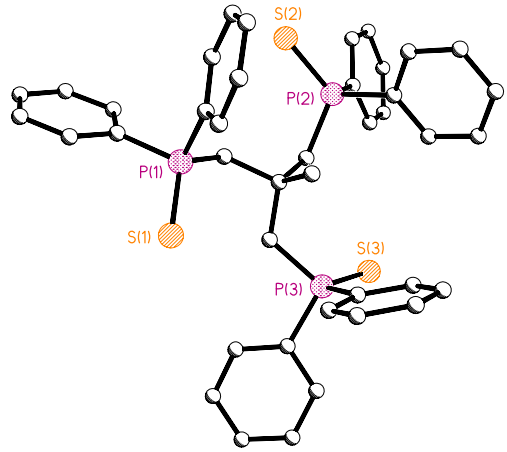

DUTTA-3-7

*P*2$_1$/*c*

a = 9.9477(9) Å
b = 27.857(2) Å
c = 27.559(3) Å
α = 90°
β = 92.837(3)°
γ = 90°
V = 7627.5(12) Å^3

R_1 = 0.0885

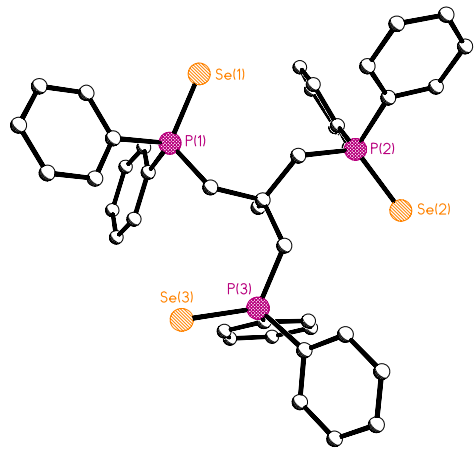

DUTTA-4-1

P-1

a = 11.2418(15) Å
b = 13.061(2) Å
c = 13.9967(15) Å
α = 109.550(13)°
β = 113.430(13)°
γ = 92.985(18) °
V = 1735.8(5) Å^3

R_1 = 0.0786

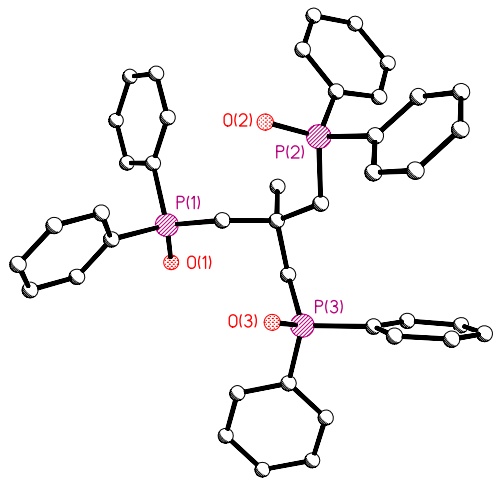

DUTTA-5-3

P-1

a = 8.490(4) Å
b = 8.549(4) Å
c = 10.672(4) Å
α = 112.73(5)°
β = 98.82(6)°
γ = 101.47(6)°
V = 677.1(7) Å^3

R_1 = 0.0748

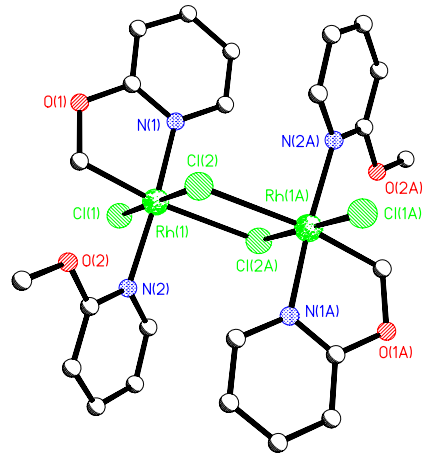

DUTTA-7-4t

*C*2/*c*

a = 7.865(3) Å
b = 10.976(4) Å
c = 15.342(4) Å
α = 76.12(2)°
β = 75.16(2)°
γ = 89.66(3)°
V = 1240.7(8) Å^3

R_1 = 0.0648

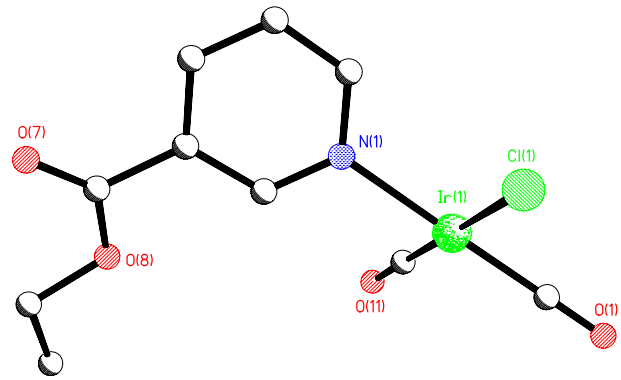

Two independent molecules in the unit cell

DUTTA-8-3

P-1

a = 9.851(4) Å
b = 12.342(6) Å
c = 19.093(8) Å
α = 107.184(7)°
β = 90.537(6)°
γ = 108.817(13)°
V = 2085.1(16) Å^3

R_1 = 0.0422

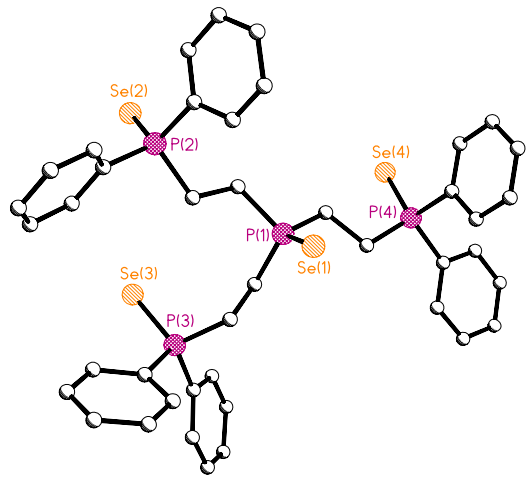

DUTTA-9-2

*P*2$_1$/*n*

a = 14.6003(10) Å
b = 16.8562(9) Å
c = 14.7687(10) Å
α = 90°
β = 103.7937(17)°
γ = 90°
V = 3529.8(4) Å^3

R_1 = 0.0324

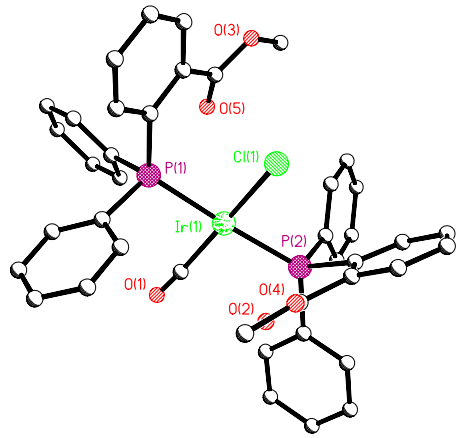

DUTTA-14-1

P-1

a = 7.4380(17) Å
b = 9.085(2) Å
c = 19.727(6) Å
α = 83.253(19)°
β = 83.933(20)°
γ = 67.325(17)°
V = 1218.8(6) Å^3

R_1 = 0.0546

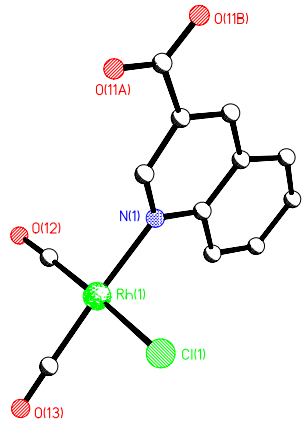

Two independent molecules in the unit cell
Disordered aldehyde O11B:60% O11B:40%

FKDW73-2

P-1

a = 10.094(4) Å
b = 11.2590(19) Å
c = 18.122(8) Å
α = 73.66(4)°
β = 87.13(4)°
γ = 67.06(3)°
V = 1815.9(13) Å^3

R_1 = 0.0646

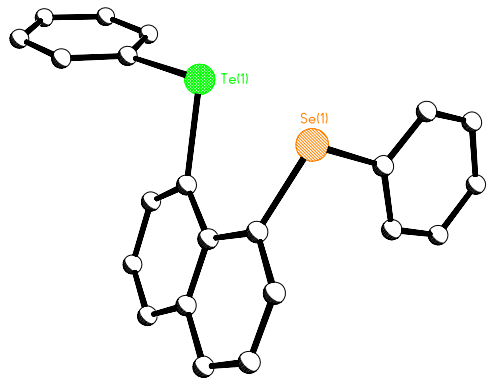

Two independent molecules in the unit cell

FKDW74-5-2

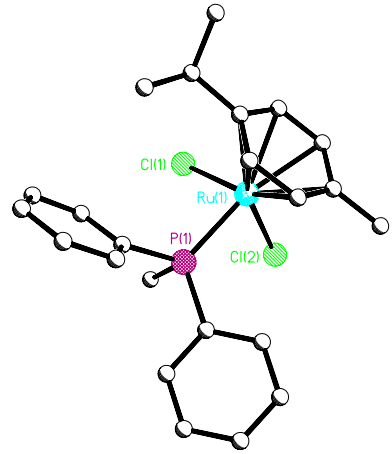

*P*2$_1$/*c*

a = 10.365(3) Å
b = 11.888(4) Å
c = 17.513(7) Å
α = 90°
β = 98.367(8)°
γ = 90°
V = 2135.0(12) Å^3

R$_1$ = 0.0689

FKDW77

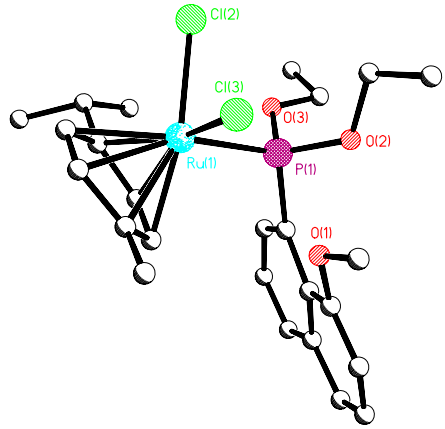

P-1

a = 9.916(4) Å
b = 10.349(4) Å
c = 13.298(7) Å
α = 88.26(3)°
β = 89.46(3)°
γ = 68.07(2)°
V = 1265.3(10) Å^3

R$_1$ = 0.0482

FKDW84-3-2

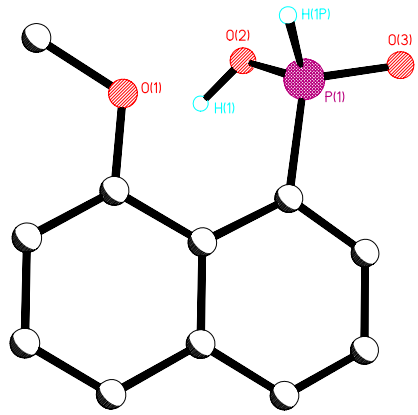

*P*2$_1$/*c*

a = 8.264(5) Å
b = 13.302(8) Å
c = 9.374(7) Å
α = 90°
β = 104.014(15)°
γ = 90°
V = 999.8(11) Å^3

R$_1$ = 0.0704

FKDW84-3-6

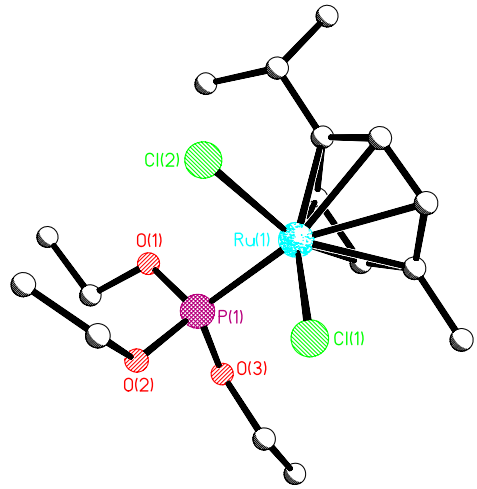

P2_1/*c*

a = 15.581(5) Å
b = 7.255(2) Å
c = 17.747(6) Å
α = 90°
β = 98.299(9)°
γ = 90°
V = 1985.2(11) Å^3

R_1 = 0.0419

FKDW92-0-2

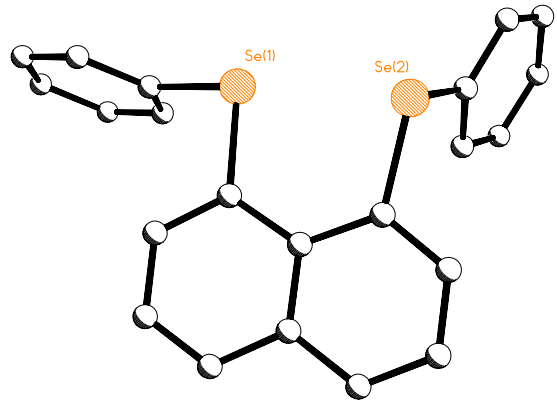

Pca2_1

a = 21.353(5) Å
b = 5.6814(12) Å
c = 14.424(4) Å
α = 90°
β = 90°
γ = 90°
V = 1749.9(7) Å^3

R_1 = 0.0473

FKDW111C-1

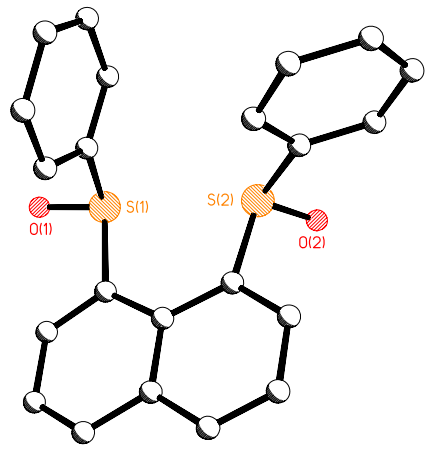

*C*2/*c*

a = 17.275(9) Å
b = 15.216(7) Å
c = 13.59(7) Å
α = 90°
β = 105.593(11)°
γ = 90°
V = 3441(3) Å^3

R_1 = 0.0675

FKDW123-1

Pbca

a = 7.768(2) Å
b = 20.971(6) Å
c = 13.735(4) Å
α = 90°
β = 90°
γ = 90°
V = 2237.5(12) Å^3

R_1 = 0.0435

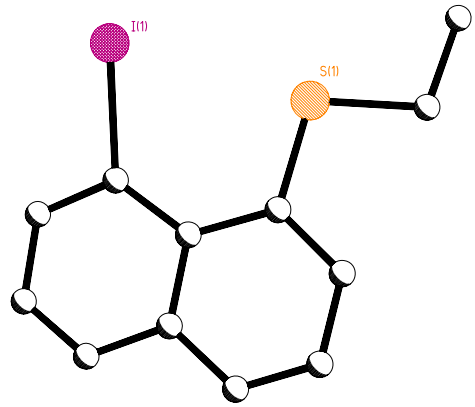

FKDW126-3

Pbca

a = 9.0074(15) Å
b = 16.221(3) Å
c = 17.386(3) Å
α = 90°
β = 90°
γ = 90°
V = 2540.2(8) Å^3

R_1 = 0.0764

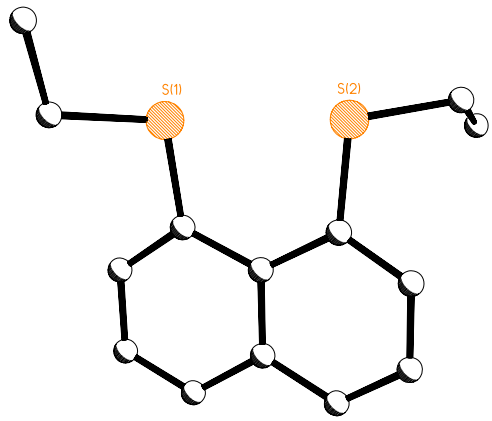

FKDW157A-2

P2_1/*n*

a = 9.293(3) Å
b = 14.082(5) Å
c = 17.212(6) Å
α = 90°
β = 97.177(9)°
γ = 90°
V = 2234.8(13) Å^3

R_1 = 0.0435

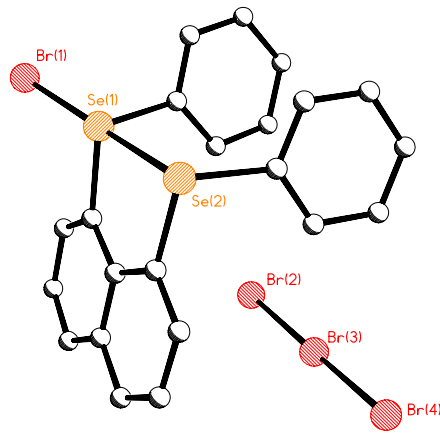

FKDW157B-3

P-1

a = 10.003(3) Å
b = 10.453(2) Å
c = 11.749(3) Å
α = 64.218(18)°
β = 84.68(3)°
γ = 80.05(2)°
V = 1089.3(5) Å^3

R_1 = 0.0302

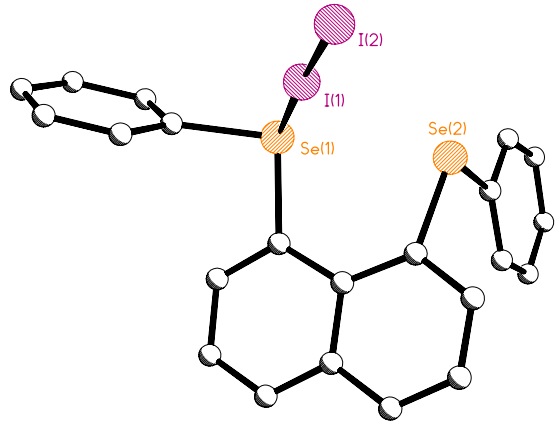

FKDW157BI-3

P-1

a = 9.6503(18) Å
b = 11.3357(16) Å
c = 11.8269(16) Å
α = 65.996(10)°
β = 82.763(14)°
γ = 83.206(14)°
V = 1169.3(3) Å^3

R_1 = 0.0483

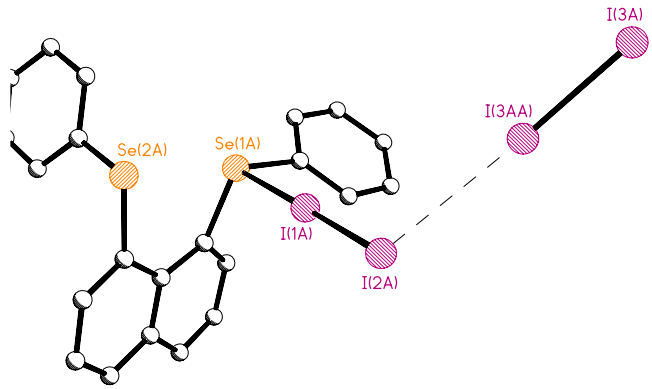

FKDW157c-3

*P*2$_1$/*c*

a = 11.652(5) Å
b = 20.240(10) Å
c = 8.544(3) Å
α = 90°
β = 93.874(14)°
γ = 90°
V = 2010.4(16) Å^3

R_1 = 0.0989

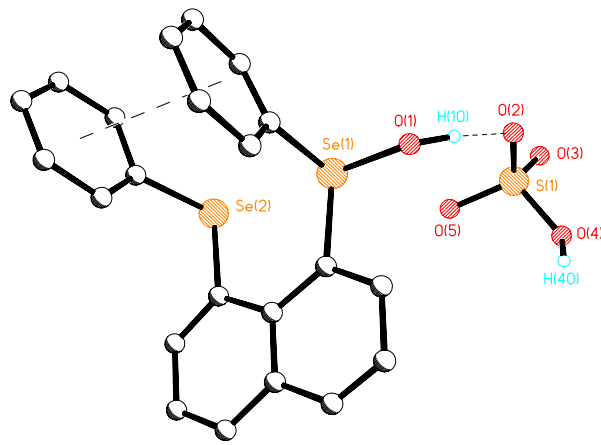

FKDW158-5

P-1

a = 7.726(4) Å
b = 13.613(5) Å
c = 14.352(4) Å
α = 70.93(3)°
β = 82.44(4)°
γ = 88.61(4)°
V = 1413.9(10) Å^3

R_1 = 0.0550

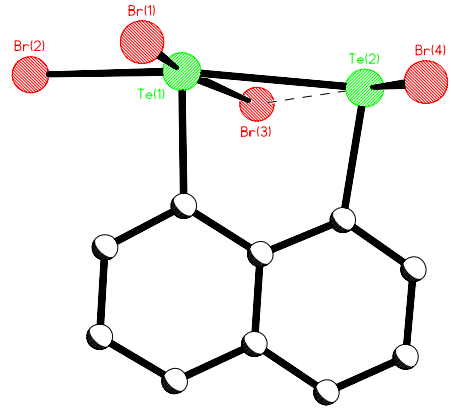

Two independent molecules in the unit cell

FKDW161-2

*Pca*2$_1$

a = 8.4839(18) Å
b = 12.041(2) Å
c = 15.592(3) Å
α = 90°
β = 90°
γ = 90°
V = 1592.8(5) Å^3

R_1 = 0.0461

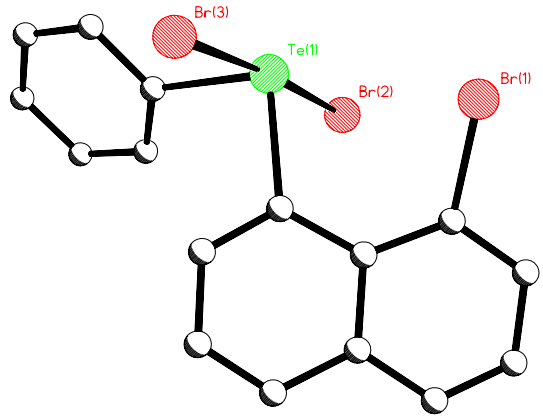

FKDW182-1

*P*2$_1$/*c*

a = 12.556(3) Å
b = 8.0136(16) Å
c = 14.803(4) Å
α = 90°
β = 111.945(4)°
γ = 90°
V = 1381.5(6) Å^3

R_1 = 0.0483

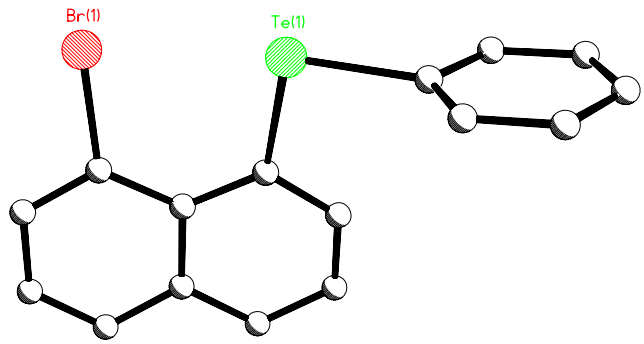

FKDW195B-1

*C*2/*c*

a = 18.909(4) Å
b = 15.954(3) Å
c = 14.282(3) Å
α = 90°
β = 99.994(5)°
γ = 90°
V = 4243.1(15) Å^3

R_1 = 0.0361

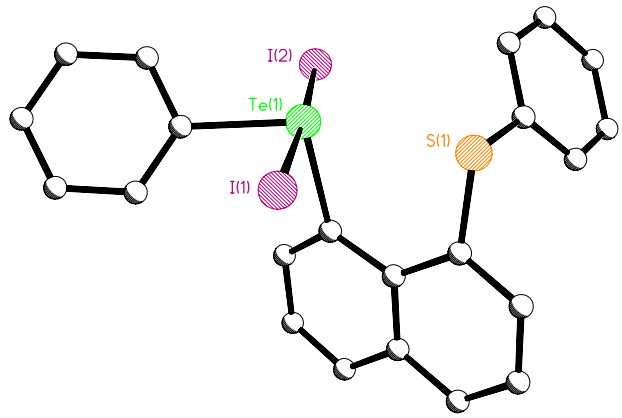

FKDW205-2

*P*2$_1$/*c*

a = 12.437(8) Å
b = 8.174(4) Å
c = 14.694(10) Å
α = 90°
β = 110.305(14)°
γ = 90°
V = 1400.9(15) Å^3

R_1 = 0.0356

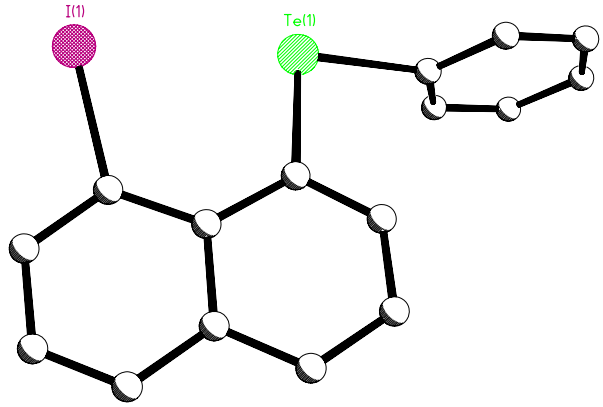

FKDW211A-2

*P*2$_1$/*c*

a = 10.139(5) Å
b = 15.379(6) Å
c = 11.579(6) Å
α = 90°
β = 111.083(15)°
γ = 90°
V = 1684.0(14) Å^3

R_1 = 0.0693

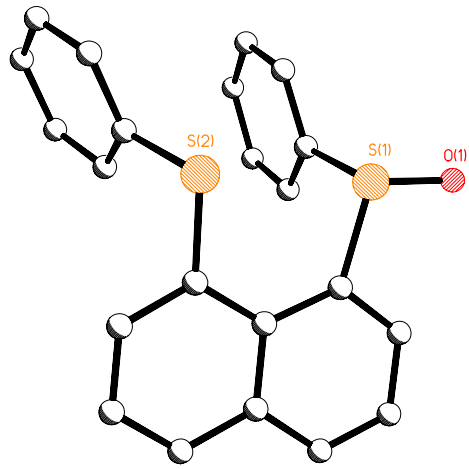

FKDW217A-1

P-1

a = 9.6066(17) Å
b = 11.2528(14) Å
c = 11.8080(14) Å
α = 65.855(9)°
β = 82.839(14)°
γ = 83.443(14)°
V = 1152.9(3) Å^3

R_1 = 0.0429

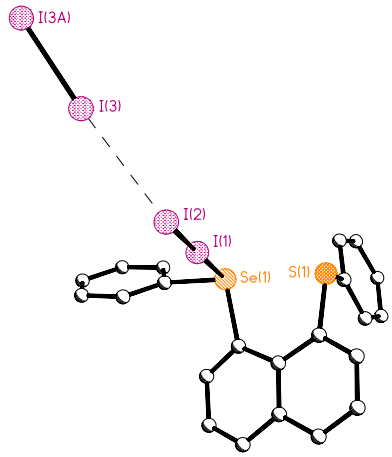

FKDW219B-1

P-1

a = 8.221(2) Å
b = 9.639(3) Å
c = 11.613(3) Å
α = 105.274(8)°
β = 90.454(4)°
γ = 102.945(9)°
V = 863.0(4) Å^3

R_1 = 0.0373

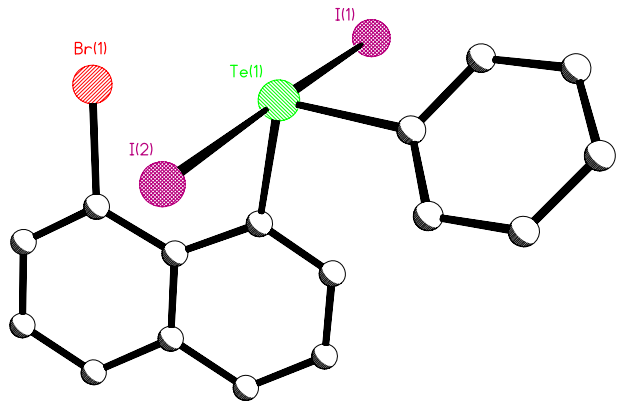

FKDW223A-1

*Pca*2$_1$

a = 8.5238(18) Å
b = 12.165(3) Å
c = 15.780(3) Å
α = 90°
β = 90°
γ = 90°
V = 1636.3(6) Å^3

R_1 = 0.0313

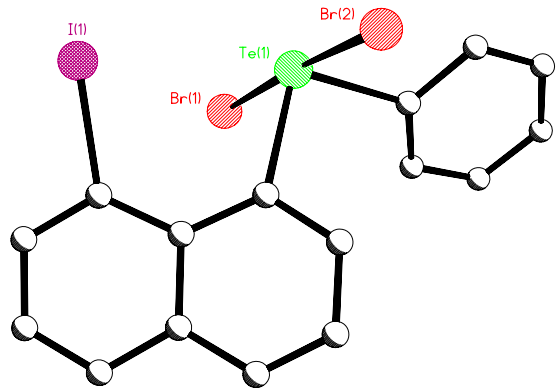

Hua27-9rm2

*P*2/*c*

a = 19.176(6) Å
b = 7.535(2) Å
c = 13.005(4) Å
α = 90°
β = 109.888(8)°
γ = 90°
V = 1767.1(9) Å^3

R_1 = 0.0351

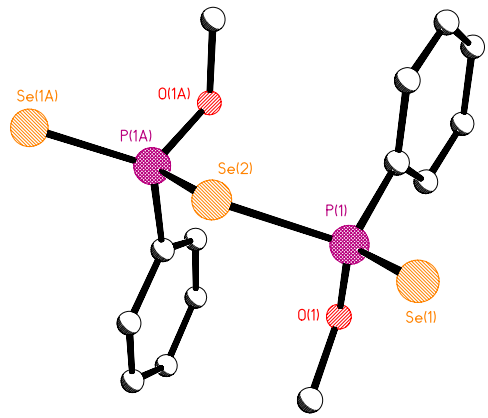

Two independent molecules in the unit cell

Hua30a-2

*P*2$_1$2$_1$2

a = 9.615(8) Å
b = 14.132(13) Å
c = 3.991(3) Å
α = 90°
β = 90°
γ = 90°
V = 542.4(8) Å^3

R_1 = 0.0548

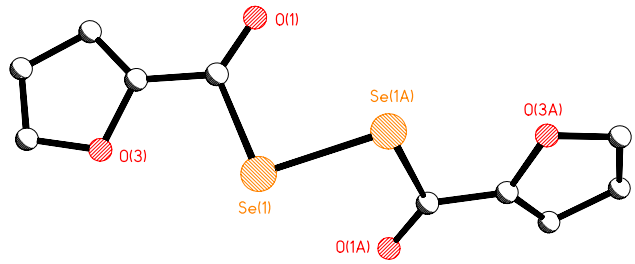

Hua45-1

*P*2$_1$/*c*

a = 11.060(3) Å
b = 11.767(3) Å
c = 15.528(4) Å
α = 90°
β = 108.299(7)°
γ = 90°
V = 1918.7(9) Å^3

R_1 = 0.0429

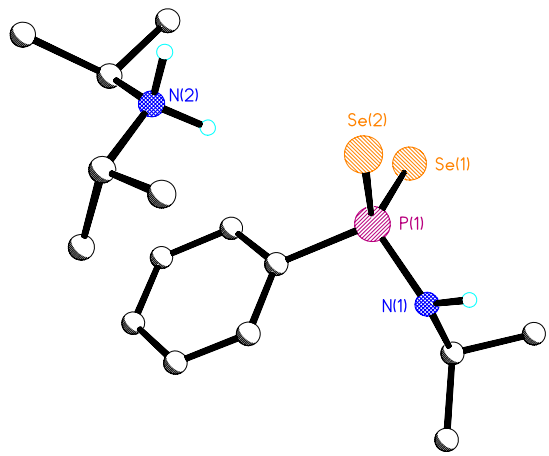

Hua341a

*P*2$_1$/*c*

a = 13.178(5) Å
b = 5.4838(18) Å
c = 16.197(6) Å
α = 90°
β = 99.119(7)°
γ = 90°
V = 1155.7(7) Å^3

R_1 = 0.0738

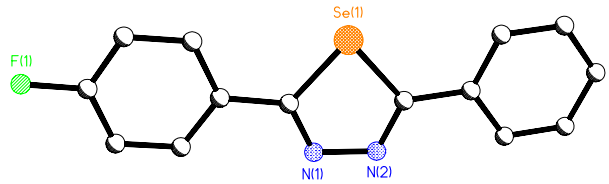

Hua423-1-1

P-1

a = 8.456(3) Å
b = 11.254(3) Å
c = 14.314(3) Å
α = 113.115(19)°
β = 103.79(2)°
γ = 93.41(3)°
V = 1198.6(6) Å^3

R_1 = 0.0736

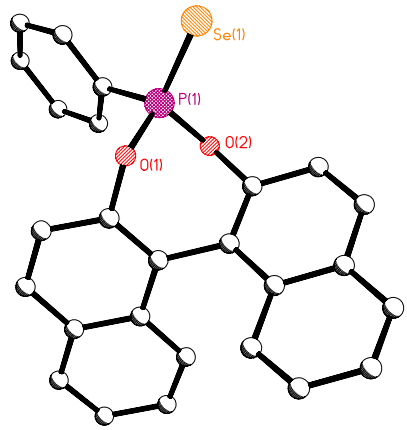

Hua423-1-3

P-1

a = 11.1149(11) Å
b = 11.617(2) Å
c = 14.254(3) Å
α = 87.692(14)°
β = 70.506(11) °
γ = 74.158(12)°
V = 1666.5(5) Å^3

R_1 = 0.0706

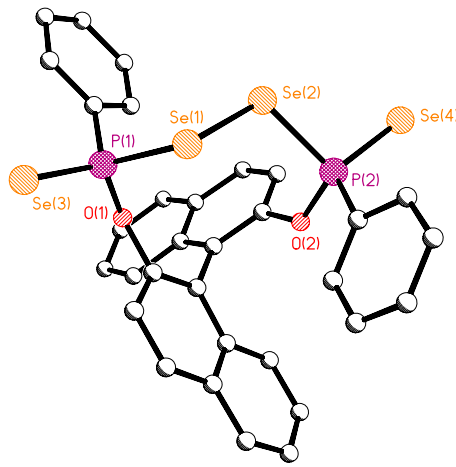

Hua427-5

$P2_1/n$

a = 9.6007(16) Å
b = 11.5387(18) Å
c = 29.679(5) Å
α = 90°
β = 94.742(4)°
γ = 90°
V = 3276.6(9) Å^3

R_1 = 0.0402

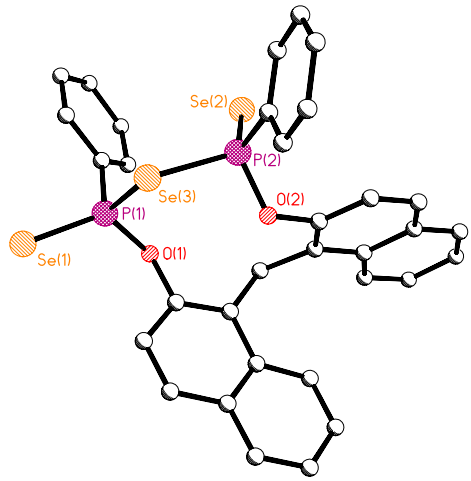

Hua428-2-5

$P2_1/c$

a = 13.065(3) Å
b = 19.737(3) Å
c = 11.192(2) Å
α = 90°
β = 112.234(4)°
γ = 90°
V = 2671.4(9) Å^3

R_1 = 0.0659

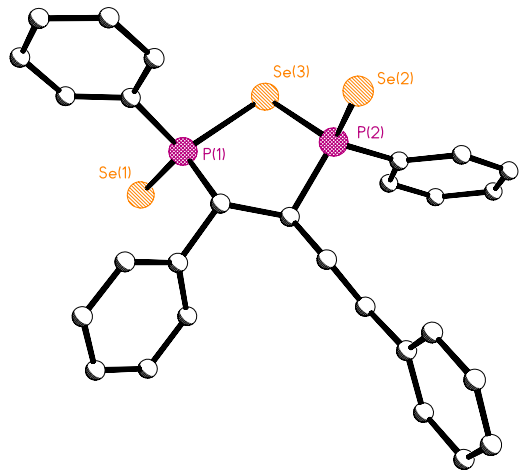

Hua439-3-3

$P2_1/n$

a = 9.1244(15) Å
b = 8.6606(13) Å
c = 20.178(3) Å
α = 90°
β = 102.065(4)°
γ = 90°
V = 1559.3(4) Å^3

R_1 = 0.0382

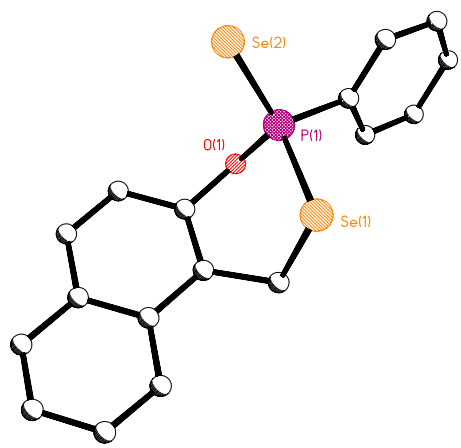

Hua441-1-1

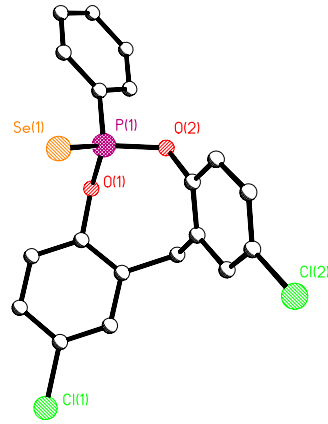

*P*2$_1$/*c*

a = 11.868(3) Å
b = 7.585(2) Å
c = 21.097(6) Å
α = 90°
β = 104.045(6)°
γ = 90°
V = 1842.3(9) Å^3

R_1 = 0.0637

Hua441-3-11

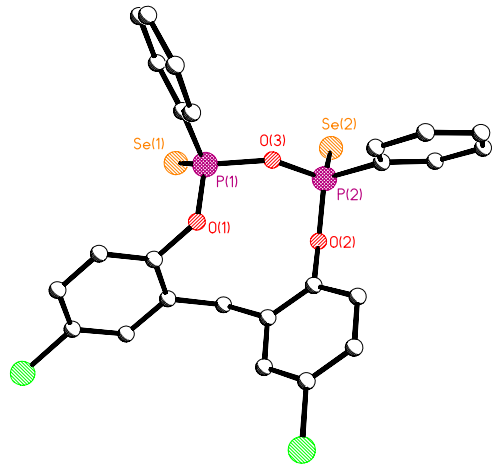

P-1

a = 12.990(5) Å
b = 13.829(5) Å
c = 16.436(5) Å
α = 94.306(3)°
β = 107.147(6)°
γ = 108.060(9)°
V = 2636.8(17) Å^3

R_1 = 0.0779

Hua445-1-3

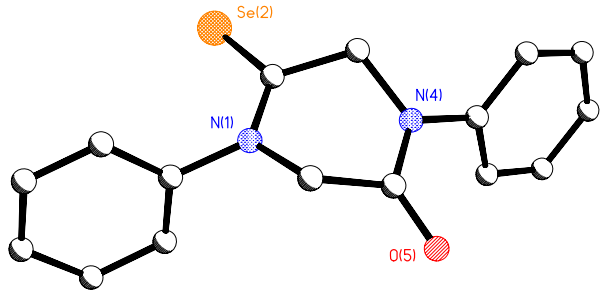

P-1

a = 4.9903(9) Å
b = 11.6672(16) Å
c = 12.945(2) Å
α = 70.153(14)°
β = 82.324(16)°
γ = 78.543(17)°
V = 693.01(19) Å^3

R_1 = 0.0489

Hua445-1-4

P-1

a = 7.053(4) Å
b = 9.998(5) Å
c = 11.277(6) Å
α = 107.697(14)°
β = 92.283(4)°
γ = 103.980(14)°
V = 729.6(7) Å^3

R_1 = 0.0637

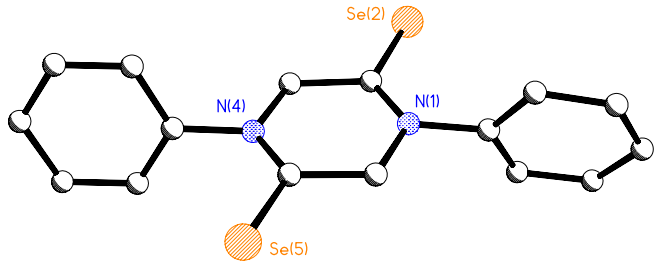

Hua447-1-1

*P*2$_1$/*n*

a = 5.5306(15) Å
b = 21.964(5) Å
c = 6.2566(17) Å
α = 90°
β = 111.047(6)°
γ = 90°
V = 709.3(3) Å^3

R_1 = 0.0619

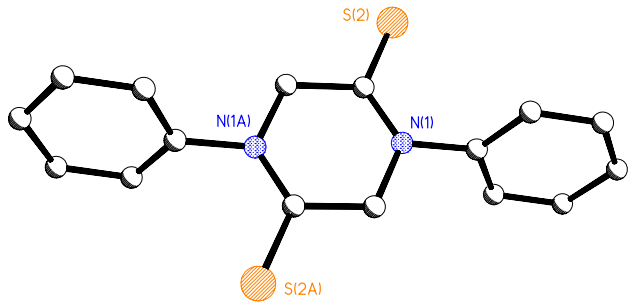

Hua447-2-2

*P*2$_1$/*c*

a = 11.118(5) Å
b = 11.604(5) Å
c = 9.640(4) Å
α = 90°
β = 95.828(11)°
g = 90°
V = 1237.3(9) Å^3

R_1 = 0.1745

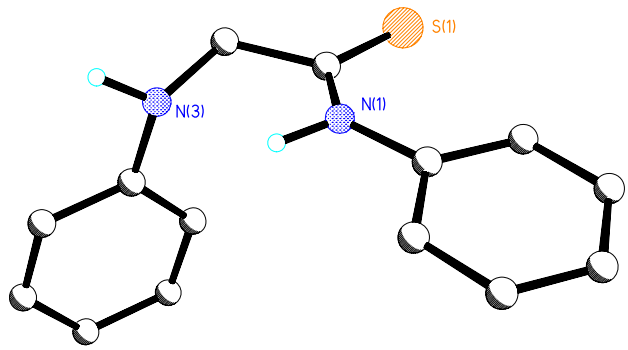

Hua448-2-2

*P*2$_1$/*c*

a = 13.391(7) Å
b = 5.727(3) Å
c = 7.530(4) Å
α = 90°
β = 93.652(15)°
γ = 90°
V = 576.3(5) Å^3

R$_1$ = 0.0851

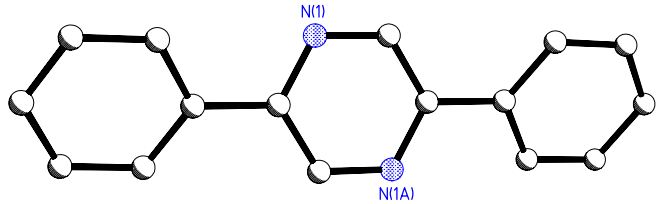

Hua452-2-3

*P*2$_1$/*c*

a = 20.158(10) Å
b = 5.509(3) Å
c = 7.846(4) Å
α = 90°
β = 98.765(12)°
γ = 90°
V = 861.1(8) Å^3

R$_1$ = 0.0628

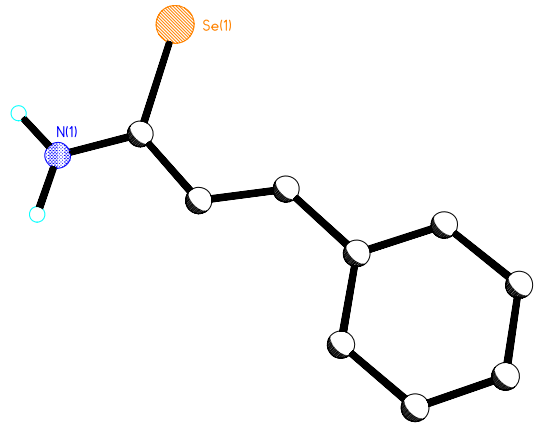

Hua457-3

P-1

a = 10.766(3) Å
b = 11.096(4) Å
c = 13.174(4) Å
α = 97.431(9)°
β = 94.454(8)°
γ = 91.879(9)°
V = 1554.4(9) Å^3

R$_1$ = 0.0964

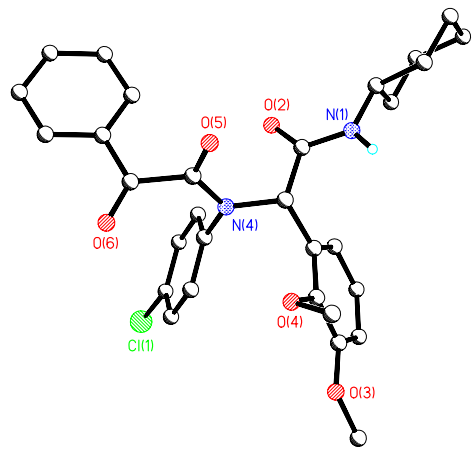

Hua459-3

P$2_1/c$

a = 10.745(3) Å
b = 11.551(3) Å
c = 21.504(5) Å
α = 90°
β = 102.304(6)°
γ = 90°
V = 2607.7(11) Å^3

R_1 = 0.0784

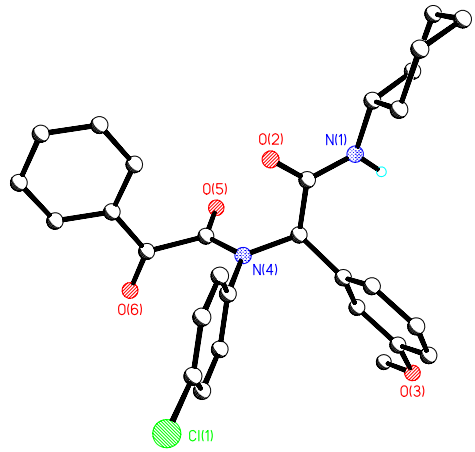

Hua469-1-1

P-1

a = 8.785(4) Å
b = 9.7406(19) Å
c = 19.590(11) Å
α = 76.22(4)°
β = 87.46(5)°
γ = 69.26(4)°
V = 1521.2(11) Å^3

R_1 = 0.0515

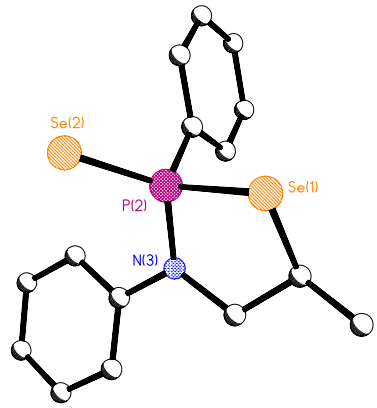

Hua473-1

Cmca

a = 6.754(8) Å
b = 15.116(17) Å
c = 14.086(15) Å
α = 90°
β = 90°
γ = 90°
V = 1438(3) Å^3

R_1 = 0.0760

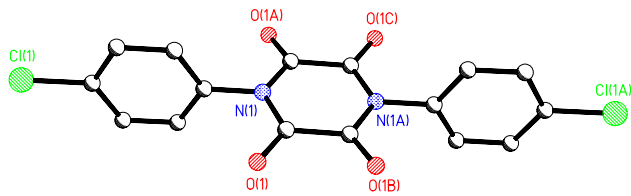

Oxygen is at 50% occupancy

HuaHD4-1

P-3

a = 21.605(2) Å
b = 21.605(2) Å
c = 12.9024(14) Å
α = 90°
β = 90°
γ = 120°
V = 5215.5(9) Å^3

R_1 = 0.0838

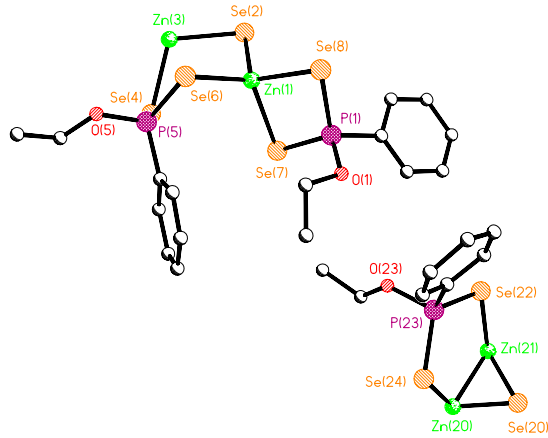

Before symmetry expansion

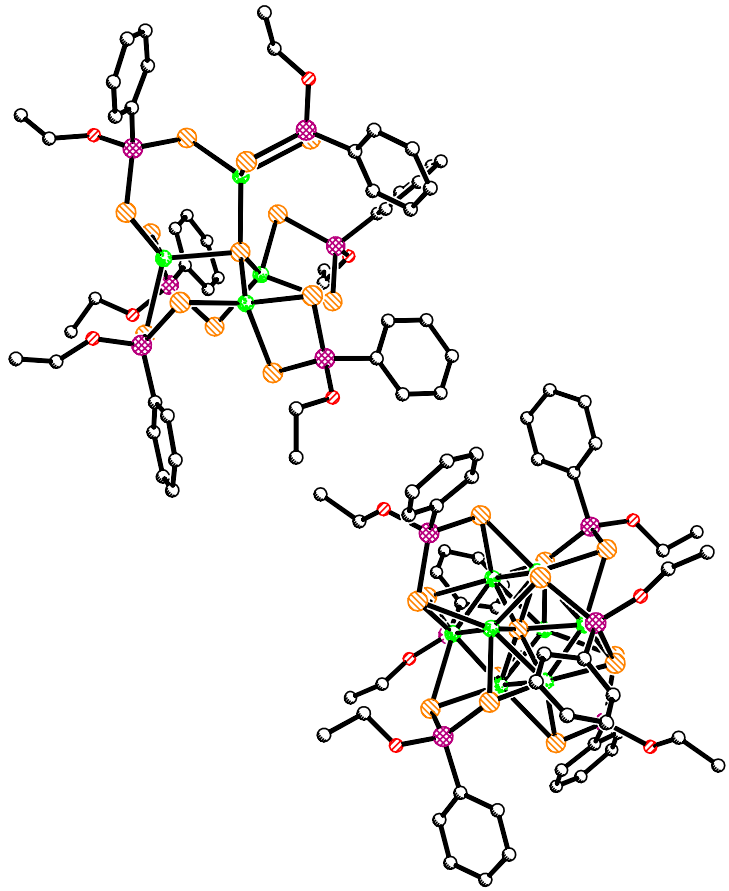

Two different molecules in the unit cell.
A disordered tetrahedral geometry (Zn atoms) around a selenium atom.

Hua-HP-0314-2

$P2_1/n$

a = 10.873(3) Å
b = 9.002(2) Å
c = 15.714(4) Å
α = 90°
β = 106.102(6)°
γ = 90°
V = 1477.9(6) Å^3

R_1 = 0.0452

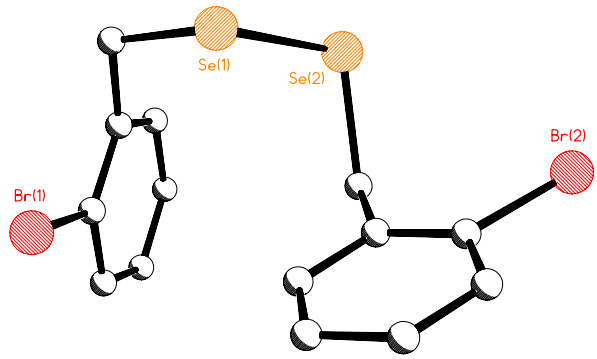

Ken1-5

$P2_1/c$

a = 8.157(8) Å
b = 19.112(17) Å
c = 10.133(10) Å
α = 90°
β = 105.44(2)°
γ = 90°
V = 1523(2) Å^3

R_1 = 0.1785

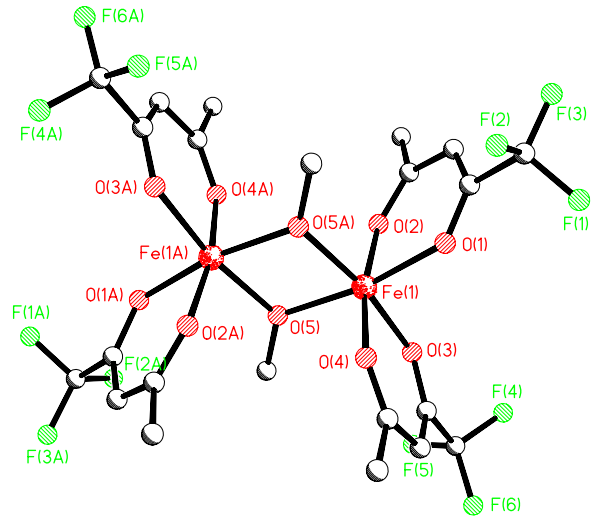

PWMC2-1

$P2_1/c$

a = 13.997(4) Å
b = 4.4831(14) Å
c = 28.092(10) Å
α = 90°
β = 93.734(8)°
γ = 90°
V = 1759.1(10) Å^3

R_1 = 0.0864

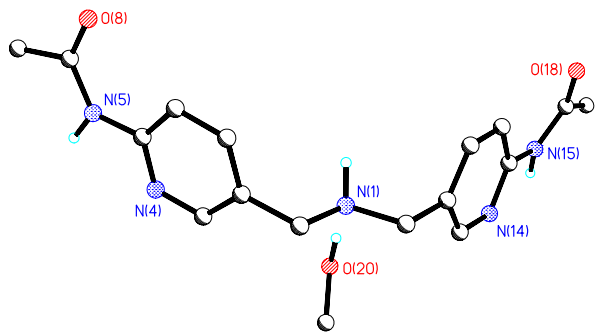

PWMC3-1r

*C*2/*c*

a = 14.870(12) Å
b = 4.015(3) Å
c = 23.080(19) Å
α = 90°
β = 96.97(2)°
γ = 90°
V = 1367.7(19) Å^3

R_1 = 0.0670

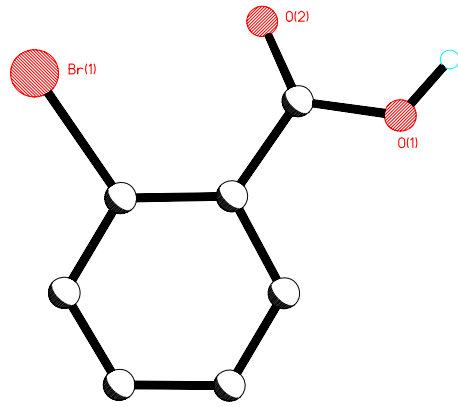

PWPK-12

P-1

a = 9.529(3) Å
b = 12.311(3) Å
c = 13.562(4) Å
α = 97.508(9)°
β = 109.413(8)°
γ = 92.039(3)°
V = 1482.4(8) Å^3

R_1 = 0.0461

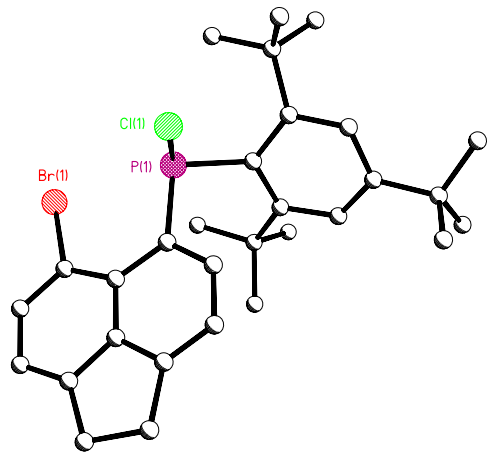

PWPK-33

P-1

a = 8.246(2) Å
b = 9.802(3) Å
c = 10.3580(18) Å
α = 72.500(18)°
β = 73.004(19)°
γ = 89.73(2)°
V = 760.4(3) Å^3

R_1 = 0.0417

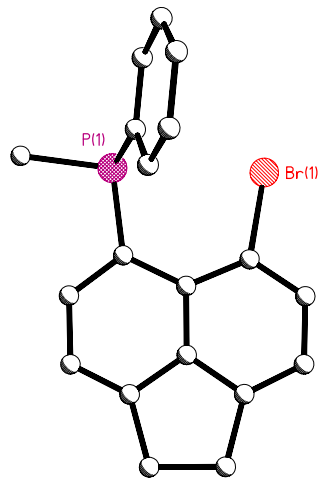

PWPK-36

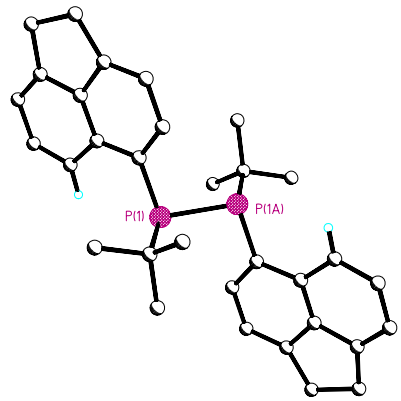

P$2_1/c$

a = 11.493(3) Å
b = 9.933(2) Å
c = 11.929(3) Å
α = 90°
β = 106.759(7)°
γ = 90°
V = 1304.0(5) Å^3

R_1 = 0.0865

PWPK-46

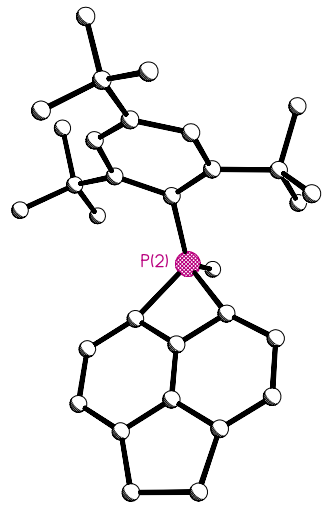

P-1

a = 11.2391(16) Å
b = 11.8953(12) Å
c = 18.116(3) Å
α = 74.273(20)°
β = 80.28(2)°
γ = 63.267(14)°
V = 2079.0(6) Å^3

R_1 = 0.0733

PWPK-49

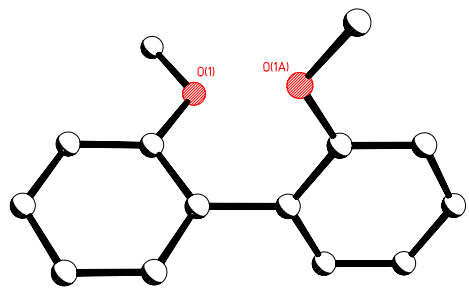

P4_32_12

a = 7.3875(11) Å
b = 7.3875(11) Å
c = 20.134(3) Å
α = 90°
β = 90°
γ = 120°
V = 1098.8(3) Å^3

R_1 = 0.0348

PWPK-59

P-1

a = 10.1940(18) Å
b = 11.392(3) Å
c = 11.6907(18) Å
α = 83.197(11)°
β = 73.623(11)°
γ = 89.315(15)°
V = 1293.1(5) Å^3

R_1 = 0.0638

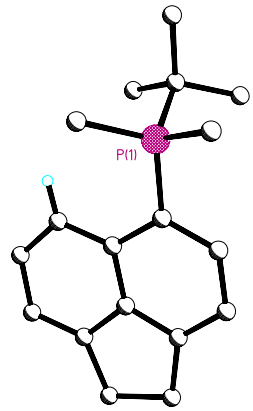

PWPK-61

*P*2$_1$/*c*

a = 11.941(2) Å
b = 9.651(2) Å
c = 26.695(6) Å
α = 90°
β = 99.359(6)°
γ = 90°
V = 3035.7(11) Å^3

R_1 = 0.0954

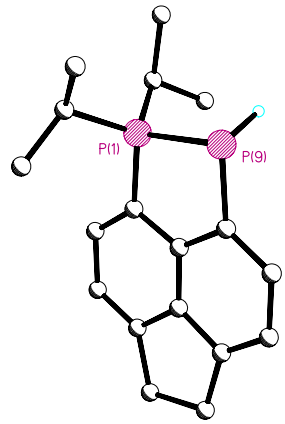

PWPK-51

P-1

a = 7.776(4) Å
b = 9.007(4) Å
c = 10.234(4) Å
α = 107.536(8)°
β = 90.349(6)°
γ = 111.484(9)°
V = 630.5(5) Å^3

R_1 = 0.0792

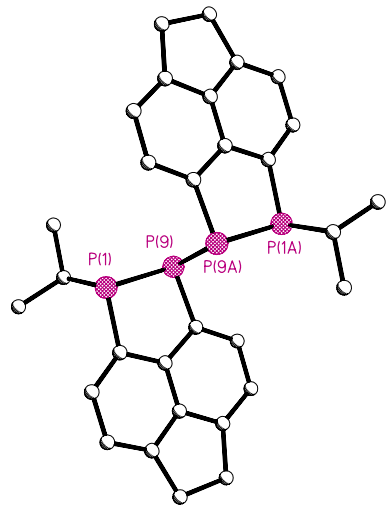

PWPK-66-1

*Fdd*2

a = 12.670(2) Å
b = 24.173(4) Å
c = 12.465(2) Å
α = 90°
β = 90°
γ = 90°
V = 3817.6(11) Å^3

R_1 = 0.0382

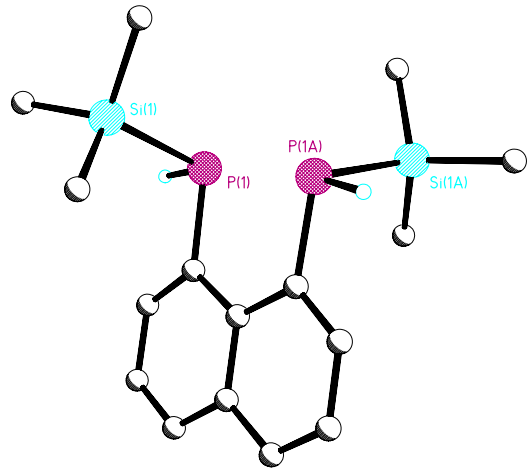

PWPK-68-2

*P*2$_1$/*n*

a = 10.421(2) Å
b = 7.5169(16) Å
c = 19.287(5) Å
α = 90°
β = 104.317(5)°
γ = 90°
V = 1463.9(6) Å^3

R_1 = 0.0528

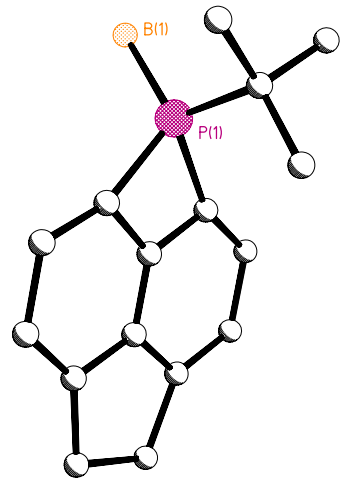

Tim29-1

*P*2$_1$/*c*

a = 12.853(2) Å
b = 16.533(3) Å
c = 11.839(2) Å
α = 90°
β = 107.119(5)°
γ = 90°
V = 2404.2(7) Å^3

R_1 = 0.0762

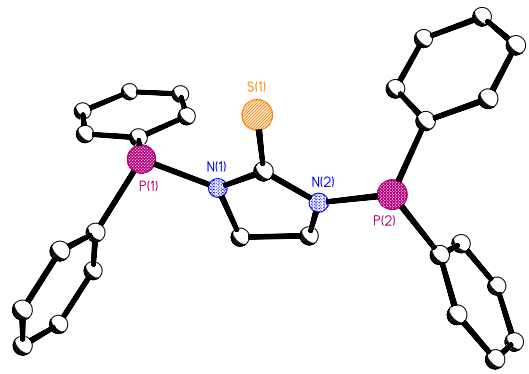

Tim29-7

*C*2/*c*

a = 17.331(6) Å
b = 14.704(4) Å
c = 11.237(4) Å
α = 90°
β = 99.521(8)°
γ = 90°
V = 2824.1(15) Å^3

R_1 = 0.0747

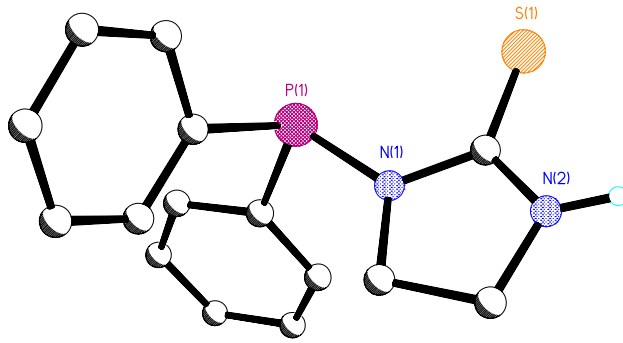

Tim43-1

*C*2/*c*

a = 29.135(7) Å
b = 9.746(2) Å
c = 11.269(2) Å
α = 90°
β = 96.034(6)°
γ = 90°
V = 3182.2(12) Å^3

R_1 = 0.0816

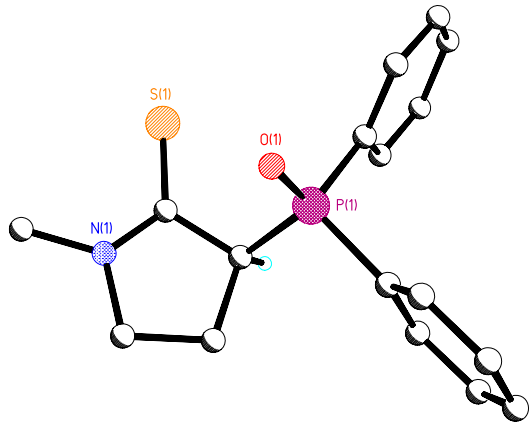

Tim47-4

P-1

a = 9.408(7) Å
b = 9.727(7) Å
c = 11.765(10) Å
α = 100.46(2)°
β = 105.453(14)°
γ = 92.67(2)°
V = 1015.3(14) Å^3

R_1 = 0.0912

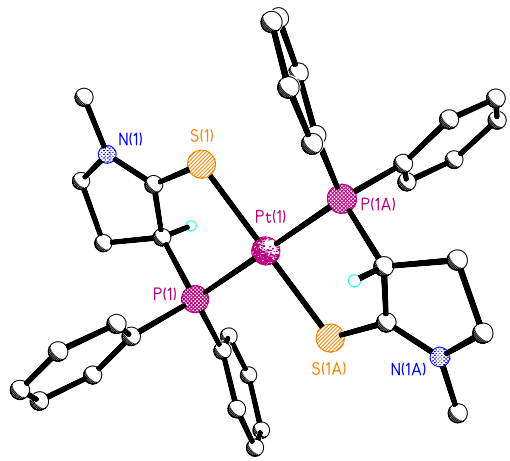

Tim49-1

Pc

a = 12.011(2) Å
b = 9.4381(15) Å
c = 24.013(5) Å
α = 90°
β = 104.209(5)°
γ = 90°
V = 2638.9(8) Å^3

R_1 = 0.0944

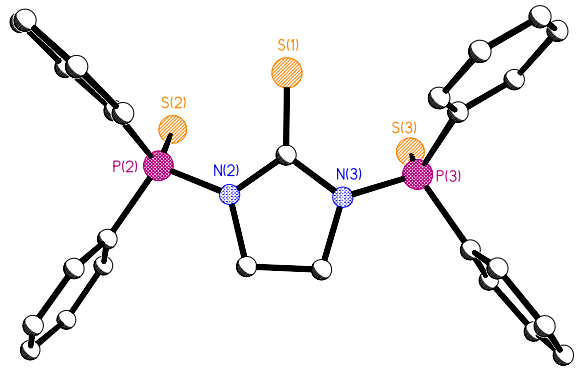

Two independent molecules in the unit cell

Tim61-2

P-1

a = 8.964(2) Å
b = 9.691(3) Å
c = 10.376(2) Å
α = 81.46(3)°
β = 65.144(20)°
γ = 78.49(3)°
V = 799.3(4) Å^3

R_1 = 0.0391

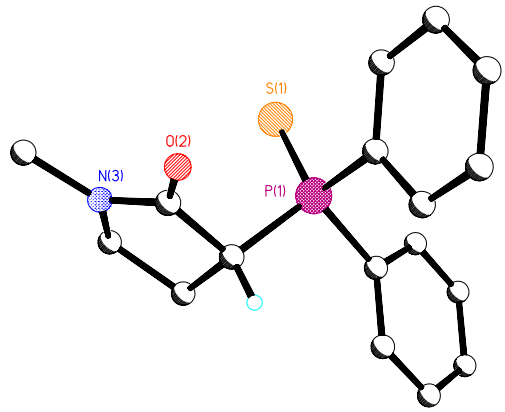

Tim61-5

*P*3$_2$

a = 9.502(3) Å
b = 9.502(3) Å
c = 14.784(4) Å
α = 90°
β = 90°
γ = 120°
V = 1155.9(6) Å^3

R_1 = 0.0927

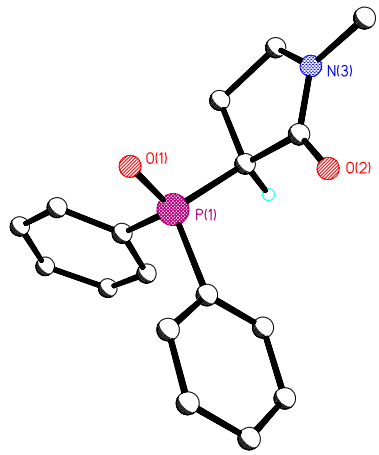

Tim63-1

P-1

a = 9.0034(14) Å
b = 9.7474(17) Å
c = 10.4596(18) Å
α = 82.02(2)°
β = 65.022(14)°
γ = 79.04(2)°
V = 815.1(3) Å^3

R_1 = 0.0337

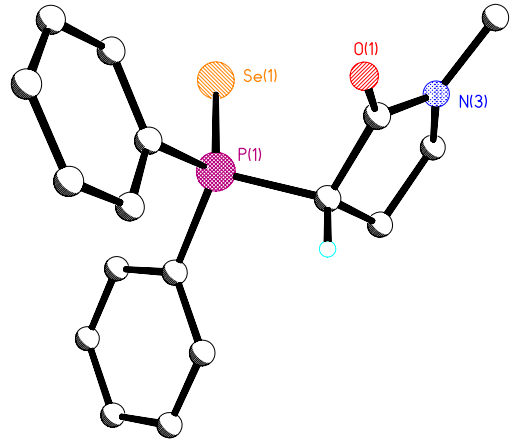

Tim-19-4

*P*2$_1$/*c*

a = 8.111(2) Å
b = 19.283(4) Å
c = 12.521(3) Å
α = 90°
β = 97.041(6)°
γ = 90°
V = 1943.6(8) Å^3

R_1 = 0.0471

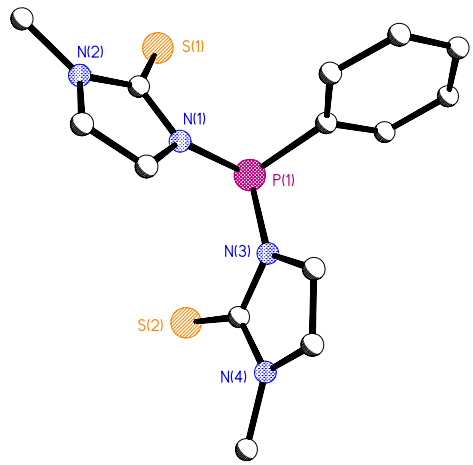

Tim-26-2

*C*2/*c*

a = 22.210(7) Å
b = 6.402(2) Å
c = 17.817(7) Å
α = 90°
β = 95.713(10)°
γ = 90°
V = 2520.9(15) Å^3

R_1 = 0.0681

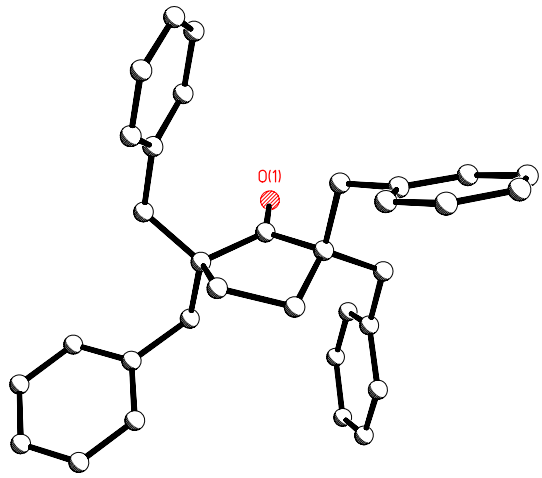

Upu-1-3

$P2_12_12_1$

a = 10.0816(13) Å
b = 11.2562(15) Å
c = 17.755(3) Å
α = 90°
β = 90°
γ = 90°
V = 2014.8(5) Å^3

R_1 = 0.0575

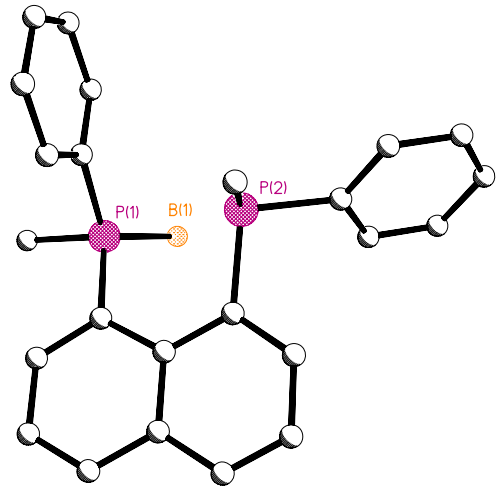

AFDW23

*Pna*2$_1$

a = 7.2317(12) Å
b = 15.270(3) Å
c = 7.9780(14) Å
α = 90°
β = 90°
γ = 90°
V = 881.0(3) Å^3

R_1 = 0.0882

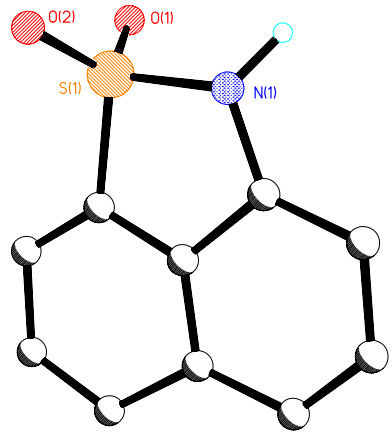

AFDW28

P-1

a = 6.8825(6) Å
b = 8.0514(7) Å
c = 8.8857(8) Å
α = 63.904(2)°
β = 76.979(2)°
γ = 87.447(3)°
V = 429.99(7) Å^3

R_1 = 0.0431

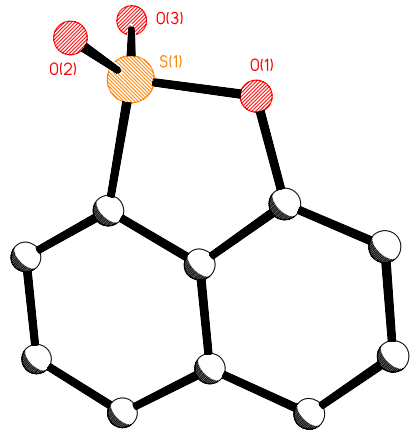

FKDW7

P-1

a = 7.8388(7) Å
b = 8.1008(7) Å
c = 11.9491(10) Å
α = 98.5504(19)°
β = 108.8828(18)°
γ = 98.007(2)°
V = 695.57(10) Å^3

R_1 = 0.0445

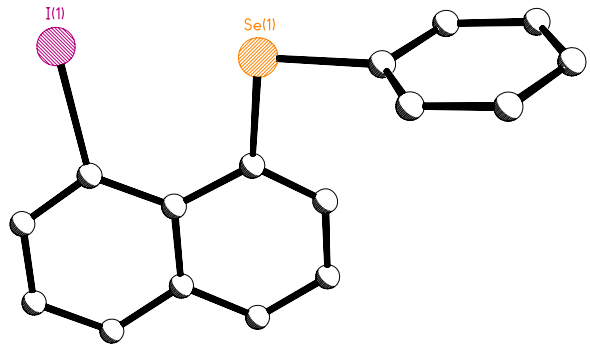

FKDW8

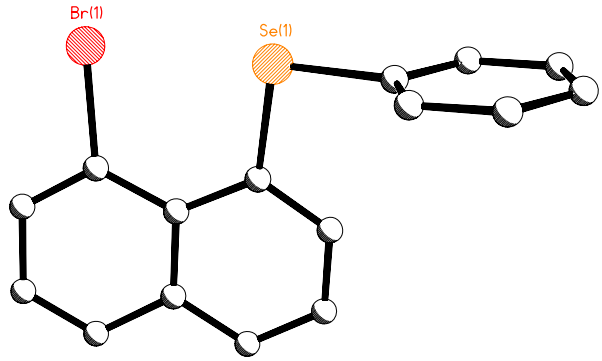

*P*2$_1$/*c*

a = 12.2378(6) Å
b = 7.8921(4) Å
c = 14.7367(8) Å
α = 90°
β = 110.9800(13)°
γ = 90°
V = 1328.94(12) Å^3

R_1 = 0.0393

FKDW15e

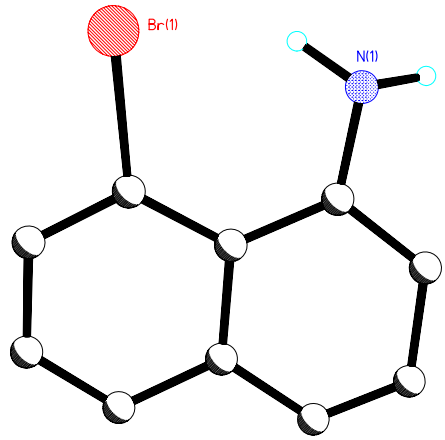

*P*2$_1$/*n*

a = 13.6692(14) Å
b = 4.1579(4) Å
c = 15.8256(16) Å
α = 90°
β = 109.941(3)°
γ = 90°
V = 845.52(15) Å^3

R_1 = 0.0512

Hua15

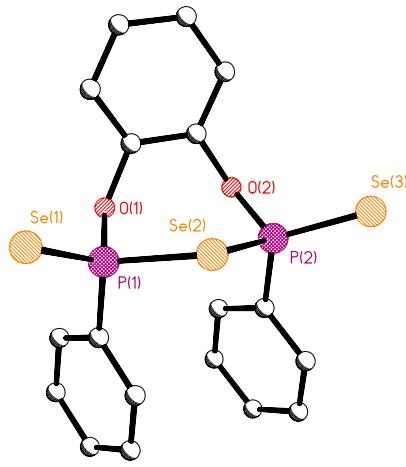

P-1

a = 8.3203(4) Å
b = 9.6324(4) Å
c = 13.5237(6) Å
α = 103.2960(14)°
β = 91.4965(15)°
γ = 115.0917(13)°
V = 945.81(7) Å^3

R_1 = 0.0256

Hua16

*P*2$_1$/*c*

a = 8.5293(6) Å
b = 9.9922(7) Å
c = 18.1201(12) Å
α = 90°
β = 94.3449(13)°
γ = 90°
V = 1539.87(18) Å^3

R_1 = 0.0465

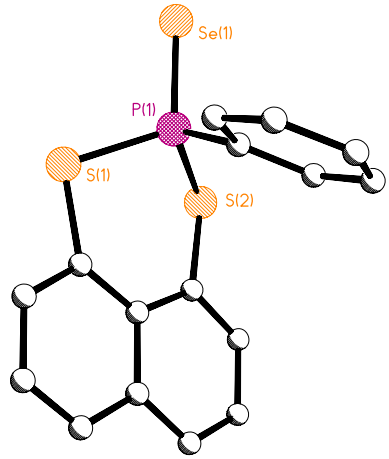

PWPK1-alexfs

*C*2/*c*

a = 16.284(2) Å
b = 10.1866(15) Å
c = 11.5029(17) Å
α = 90°
β = 90.294(4)°
γ = 90°
V = 1908.1(5) Å^3

R_1 = 0.0776

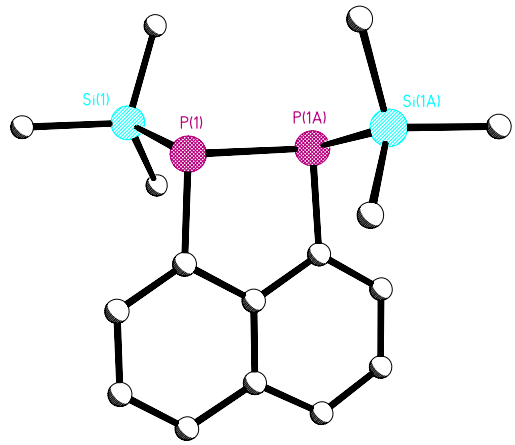

SINHA9

*C*2/*c*

a = 19.0665(16) Å
b = 14.7176(13) Å
c = 12.8185(11) Å
α = 90°
β = 125.0891(18)°
γ = 90°
V = 2943.3(4) Å^3

R_1 = 0.0751

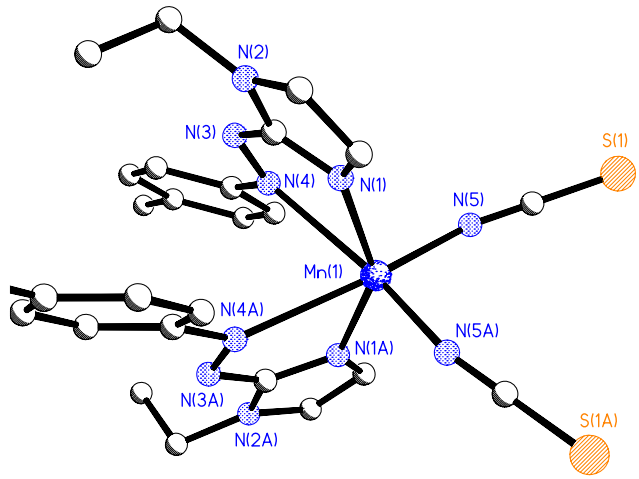

SPDW21

$P2_1/c$

a = 7.9079(6) Å
b = 15.0393(10) Å
c = 15.7616(11) Å
α = 90°
β = 94.3009(17)°
γ = 90°
V = 1869.2(2) Å^3

R_1 = 0.0626

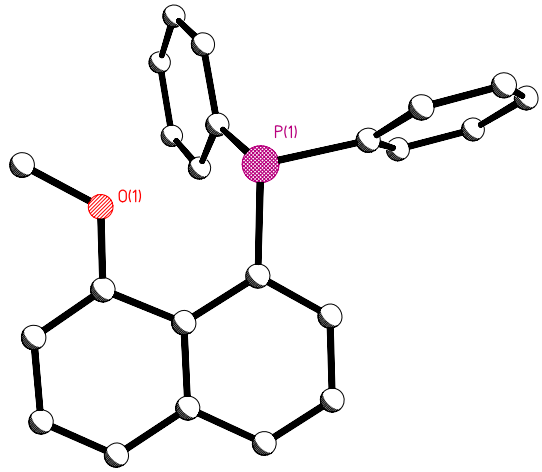

Tim3

$P2_1/c$

a = 8.0969(7) Å
b = 19.3312(16) Å
c = 12.4941(10) Å
α = 90°
β = 97.086(2)°
γ = 90°
V = 1940.7(3) Å^3

R_1 = 0.0512

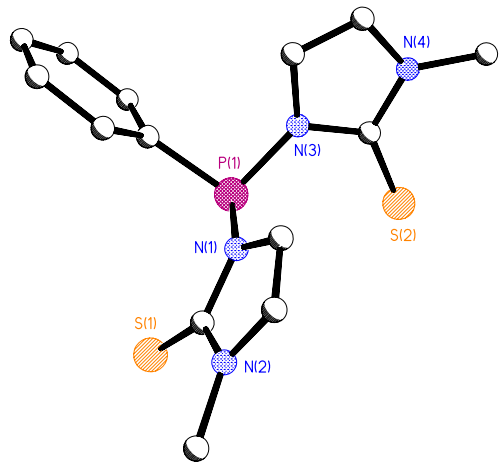

AFDW30-Alex

P$2_1/c$

a = 17.262(10) Å
b = 15.172(9) Å
c = 25.750(15) Å
α = 90°
β = 108.418(10)°
γ = 90°
V = 6399(6) Å^3

R_1 = 0.1458

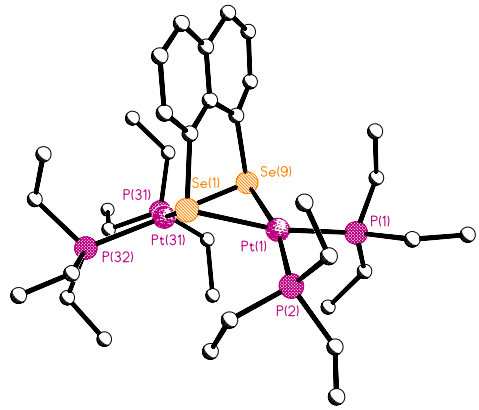

Crystallizes with three Cl^- counter-ions and six H_2O (water protons weren't refined).

AFDW37-Alex

Pbca

a = 11.0438(5) Å
b = 23.6199(13) Å
c = 33.8528(19) Å
α = 90°
β = 90°
γ = 90°
V = 8830.6(8) Å^3

R_1 = 0.0460

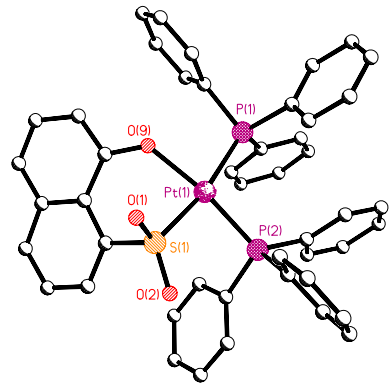

Crystallizes with two CH_2Cl_2.

Amy2-Alex

P-1

a = 10.558(3) Å
b = 12.130(3) Å
c = 13.774(4) Å
α = 96.555(14)°
β = 101.522(12)°
γ = 107.629(11)°
V = 1618.2(8) Å^3

R_1 = 0.0625

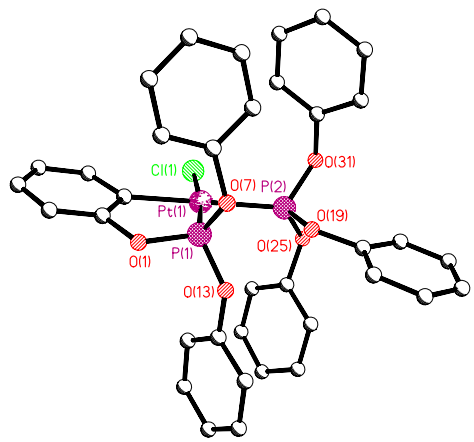

APPENDIX 3

CRYSTAL STRUCTURE EXPERIMENTAL

Data for all compounds in chapters 3-7 and 9, excluding **4.1**, **5.1**-**5.5**, **6.12**, and **7.6** were collected using the St Andrews robotic diffractometer (Rigaku ACTOR-SM, Saturn 724 CCD) at -148(1)°C, data for **4.1**, **5.1**, **5.2**, **5.4**, **6.12**, and **7.6** were collected at -148(1)°C on a Rigaku SCXmini (Mercury 2 CCD) and data for **5.3** and **5.5** were collected at -180(1)°C using a Rigaku MM007 rotating anode/confocal optics and Mercury CCD. All data was collected with graphite monochromated Mo-Kα radiation (λ = 0.71073 Å) and corrected for Lorentz and polarization effects. The data for all of the compounds were collected and processed using CrystalClear (Rigaku).[1] The structures were solved by direct methods[2] and expanded using Fourier techniques[3]. The non-hydrogen atoms were refined anisotropically. Hydrogen atoms were refined using the riding model. All calculations were performed using the CrystalStructure[4] crystallographic software package and SHELXL-97[5]. See Appendix 1 for crystallographic data.

References

1. CrystalClear 1.6: Rigaku Corporation, 1999. CrystalClear Software User's Guide, Molecular Structure Corporation, (c) 2000. J.W. Pflugrath *Acta Cryst.*, 1999, D55, 1718-1725.

2. SIR97: A. Altomare, M. Burla, M. Camalli, G. Cascarano, C. Giacovazzo, A. Guagliardi, A. Moliterni, G. Polidori, and R. Spagna, *J. Appl. Cryst.*, 1999, 32, 115-119.

3. DIRDIF99: P. T. Beurskens, G. Admiraal, G. Beurskens, W. P. Bosman, R. de Gelder, R. Israel and J. M. M. Smits, (1999). The DIRDIF-99 program system, Technical Report of the Crystallography Laboratory, University of Nijmegen, The Netherlands.

4. CrystalStructure 3.8.1: Crystal Structure Analysis Package, Rigaku and Rigaku/MSC (2000-2006). 9009 New Trails Dr. The Woodlands, TX 77381 USA.

5. G. M. Sheldrick, *Acta Cryst. A*, 2008, 64, 112-122.

APPENDIX 4

PUBLICATIONS TO DATE

F. R. Knight, **A. L. Fuller**, A. M. Z. Slawin, and J. D. Woollins, "Controlling Cu···Cu distances using halides: (8-phenylthionaphth-1-yl)diphenylphosphine copper halide dimmers" *Dalton Trans.* 2009, 40, 8476.

P. Wawrzyniak, A. M. Z. Slawin, **A. L. Fuller**, J. D. Woollins, and P. Kilian, "Phosphorus peri-bridged acenaphthenes: efficient syntheses, characterisation and quaternization reactions" *Dalton Trans.* 2009, 38, 7883.

P. Wawrzyniak, **A. L. Fuller**, A. M. Z. Slawin, and P. Kilian, "Intramolecular Phosphine-Phosphine Donor-Acceptor Complexes" *Inorg. Chem.* 2009, 48, 6, 2500-2506.

G. Hua, Y. Li, **A. L. Fulle**r, A. M. Z. Slawin, and J. D. Woollins, "Facile Synthesis and Structure of Novel 2,5-Disubstituted 1,3,4-Selenadiazoles" *Eur. J. Org. Chem.* 2009, 10, 1612–1618.

A. L. Fuller, R. A. Aitken, B. M. Ryan, A. M. Z. Slawin, J. D. Woollins, "The X-Ray Structures of Sulfoxides," *J. Chem. Crystallogr.* 2009, 39, 6, 407-415.

A. L. Fuller, F. R. Knight, A. M. Z. Slawin, and J. D. Woollins, "8-Bromonaphthalen-1-amine" *Acta Cryst*. 2008, E64, o977.

P. Kilian, S. Parveen, **A. L. Fuller**, "Structure and reactivity of phosphorus-selenium heterocycles with peri-substituted naphthalene backbones," *Dalton Trans.* 2008, 1908-1916.

A. L. Fuller, F. R. Knight, A. M. Z. Slawin, and J. D. Woollins, "1-Bromo-8-(ethylsulfanyl)naphthalene" *Acta Cryst*. 2007, E63, 3957.

A. L. Fuller, F. R. Knight, A. M. Z. Slawin, and J. D. Woollins, "1-Bromo-8-(phenylulfanyl)naphthalene" *Acta Cryst*. 2007, E63, 3855.

A. L. Fuller, R. W. Watkins, A. M. Arif, and L. M. Berreau, "Synthesis and Characterization of a Series of N_3O-ligated Mononuclear Mn(II) Halide Complexes" *Inorg. Chim. Acta* 2006, *359*, 1282-1290.

A. L. Fuller, R. W. Watkins, K. R. Dunbar, A. V. Prosvirin, A. M. Arif, and L. M. Berreau, "Manganese(II) Chemistry of a New N_3O-donor Chelate Ligand: Synthesis, X-ray Structures, and Magnetic Properties of Solvent- and Oxalate-bound Complexes" *Dalton Trans.* 2005, 1891-1896.

E. Szajna, P. Dobrowolski, **A. L. Fuller**, A. M. Arif, and L. M. Berreau, "NMR Studies of Mononuclear Octahedral Ni(II) Complexes of Tris((2-pyridyl)methyl)amine-type Ligands" *Inorg. Chem.* 2004, *43*, 3988-3997.

K. J. Tubbs, **A. L. Fuller**, B. Bennett, A. M. Arif, L. M. Berreau, "Mononuclear N_3S(thioether)-Ligated Copper(II) Methoxide Complexes: Synthesis, Characterization, and Hydrolytic Reactivity" *Inorg. Chem.* 2003, *42*, 4790-4791.

K. J. Tubbs, **A. L. Fuller**, B. Bennett, A. M. Arif, M. M. Makowska-Grzyska, L. M. Berreau, "Evaluation of the Influence of a Thioether Substituent on the Solid State and Solution Properties of N_3S-ligated Copper(II) Complexes" *Dalton Trans.* 2003, 3111-3116.

APPENDIX 5

STRUCTURE CODES FOR ALL COMPOUNDS

Compound	Code
3.1	FKDW95-2
3.2	FKDW112-1
3.3	FKDW98-0-8
3.4	FKDW164-3
3.5	FKDW173-1
3.6	FKDW195A-1
3.7	FKDW157B-3
4.1	AFDW14off
4.3	FKDW168A-2
5.1	AFDW25
5.2	AFDW27
5.3	Alex34
5.4	AFDW31-processed on robot
5.5	Alex31
6.1	FKDW99-0-3
6.2	FKDW20(ox)-1
6.3	FKDW122-1-9
6.4	FKDW111D-2
6.5	FKDW20
6.6	FKDW53-2
6.7	FKDW119-1-3
6.8	FKDW146A-2
6.9	FKDW15(ox)-8
6.10	FKDW147A-1
6.11	FKDW150B-6
6.12	SPDW25
6.13	FKDW140-3

6.14	FKDW155-1
7.1	FKDW99-0-3
7.2	FKDW54-1
7.3	FKDW20-10-8a
7.4	FKDW20-7-2
7.5	FKDW20-1-8
7.6	FKDW26off
7.7	FKDW107A-1
7.8	FKDW107B-1
8.1	AFDW22
8.2	AFDW6off
8.3	AMDW1
8.4	SOBenz-1
8.5	AFDW3b
8.6	AFDW18
8.7	AFDW55
9.1	S-61
9.1a	S-23
9.2	Se9
9.2a	Se26
9.3	Te9a
9.3a	Te10a